To: Conmy, Robyn[Conmy.Robyn@epa.gov]
Cc: CJ.Beegle-Krause@sintef.no[CJ.Beegle-Krause@sintef.no]; Brooks, Rebecca J LT[Rebecca.J.Brooks@uscg.mil]
From: Maghini, Monica K CIV
Sent: Thur 3/23/2017 7:34:41 PM
Subject: For attention: IOSC paper comments
IOSC paper Conmy.docx

Good afternoon Robyn,

I had the honor of reviewing your IOSC paper. I found it interesting and relatively easy to follow. I have a few comments for your consideration which I am including here in track changes. Please let me know if any of my comments are unclear. Keep what you want, chuck what you don't.

Regards,
Monica

Monica K. Rusk Maghini
CG-MER-3 Interagency Coordination
O: 202-372-2253
C: 802-751-9177

United States Coast Guard
2703 Martin Luther King Jr Ave SE
Washington, DC 20593-7516

Oil plume simulations: Tracking oil droplet size distribution and fluorescence within high-pressure release jets

R.N. Conmy[1], B. Robinson [2], T. King [2], M. Boufadel[3], S. Ryan[2], C. McIntyre[2], M. I. Abercrombie[4], K. Lee [2,5]

[1]U.S. Environmental Protection Agency, Office of Research and Development, 26 MLK Drive West, Cincinnati, OH 45255, USA

[2] Bedford Institute of Oceanography, Fisheries and Oceans Canada, 1 Challenger Dr, Dartmouth, NS, B2Y 4A2, Canada

[3] New Jersey Institute of Technology, Department of Civil and Environmental Engineering, University Heights, Newark, NJ 07102, USA

[4]University of South Florida, College of Marine Science, 140 7th Ave South, St. Petersburg, FL 33701, USA

[5] Commonwealth Scientific and Industrial Research Organisation, Oceans and Atmosphere Flagship, PO Box 1130, Bentley WA 6102, Australia

ABSTRACT

Optical measurements have been used during oil spill response for more than three decades to determine oil presence in slicks and plumes. Oil surveillance approaches range from simple (human eyeball) to the sophisticated (sensors on AUVs, aircraft, satellites). *In situ* fluorometers and particle size analyzers were deployed during the Deepwater Horizon (DWH) Gulf of Mexico oil spill to track shallow and deep subsea plumes. Uncertainties regarding instrument specifications and capabilities during DWH necessitated performance testing of sensors exposed to simulated, dispersed oil plumes. Seventy two wave tank experiments were conducted at the Bedford Institute of Oceanography. Simulated were oil releases with varying parameters such as oil release rate, oil temperature (reservoir temp ~ 80 ^{o}C), water temperature (<8 ^{o}C and >15 ^{o}C), oil type, dispersant type (Corexit 9500 and Finasol OSR52) and dispersant to oil ratio (DOR). Plumes of Alaskan North Slope Crude, South Louisiana Crude and IFO-120

oils were tracked using *in situ* fluorescence, droplet size distribution (DSD), total petroleum hydrocarbons (TPH) and benzene-toluene-ethylbenzene-xylene (BTEX). Results offer valuable information on the behavior and dispersibility of oils over a range of viscosity, DOR and environmental conditions. Findings have implications for fate and transport models, where DSD, chemistry and fluorescence are all impacted by release variables. This research was supported by the Bureau of Safety and Environmental Enforcement.

INTRODUCTION

The 2010 *Deepwater Horizon* (DWH) oil spill highlighted the pressing need for a better understanding of the interaction of chemical dispersants and crude oil at ocean depth. Early in the blowout release, partial emulsification of oil and heterogeneous slicks were observed as it rose to the surface from 1500-m depth (JAG report, 2010). As a countermeasure, Sub-Sea Dispersant Injection (SSDI) was used, where dispersants were injected directly at the release point as a possible means to increase dispersion efficiency and to potentially reduce the amount of dispersant needed if applied at the air-sea interface (CRRC Report, 2010). Potential advantages of this application during a continuous oil release included the fact that the fresh (unweathered) oil was considered well suited for dispersion, operators were able to inject the dispersant directly into the oil stream thereby maximizing dispersant/oil contact, sufficient control of DOR (Dispersant-to-Oil Ratio) could be maintained, injection may minimize the need for surface application because of reduced oil surfacing, and optimized subsurface application would likely promote formation of smaller and stable oil droplets, enhancing biodegradation (Lee et al., 2009). The Unified Area Command (UAC) coordinated a large-scale environmental monitoring program to track and characterize dispersed subsurface oil plumes based on field data and transport modeling outputs. Oil Droplet Size Distribution (DSD) and fluorescence intensity

from submersible sensors were used as an indication of Dispersion Effectiveness (DE) onboard vessels, where concentrations were monitored to evaluate oil dispersion (presence of small droplets $\leq$ 70 μm) based on previous studies for surface dispersant applications (Li et al., 2009a). Monitoring provided sound evidence of the presence of oil-bearing small particles both in surface waters and in the subsurface plume (JAG Report, 2010). SSDI correlated with a higher proportion of low molecular weight compounds in subsea waters compared to surface, suggesting that SSDI may have promoted the formation of small oil droplets in the deep sea and thus would have the potential for enhancing the weathering and dissolution of oil in the water column.

Uncertainties still exist, however, regarding the effectiveness of this application. For example, assumptions of the optimal DOR are based on empirical data mostly obtained from bench-scale experiments designed for testing at standard temperatures and pressures (STP), whereas conditions at a wellhead on the ocean floor or anywhere along a riser could be significantly different. Hence, DOR for direct injection needs to be better understood. Although theoretical analyses and experiments suggest that oil jet breakup is insensitive to the absolute value of hydrostatic pressure for incompressible liquid-liquid systems (Masutani and Adams 2000), the effects of several ambient environmental factors on SSDI, including high release pressure, high oil temperature, low water temperature, and the presence of methane and suspended sediments in the oil plume and/or surrounding water column remain to be clarified. Improved understanding on the influence of these factors and the interaction of oil and chemical dispersant under a range of turbulent regimes at depth is required for informed decision-making for future SSDI use.

For evaluating DE, standard laboratory tests are inherently limited in simulating operational performance under realistic environmental conditions in part due to space constraints that are critical for transport and dilution efficiency (NRC, 2005). Meso-scale tanks capable of generating waves and flume flows to simulate ocean conditions help to address this issue. One such tank facility at the Bedford Institute of Oceanography (BIO; Dartmouth, Nova Scotia) has been used previously to assess chemical dispersant effectiveness for various oil types as a function of energy dissipation rate and particle size distribution (Li et al. 2009b) and demonstrated that the effectiveness of a dispersant is strongly dependent on wave conditions, dispersant type, and oil type (Wickley-Olsen et al. 2007; Li et al. 2008; Lee et al. 2009). A strong correlation has been established between dispersion effectiveness and *in situ* DSD within the hydrodynamic regime, particularly energy dissipation rate, under a variety of wave conditions (Li et al. 2008; Li et al. 2009b), where flume mode can simulate the effects of underwater currents on dispersion and dilution of oil (Li et al. 2009a; Li et al. 2010). Experiments have also shown the reliability of fluorescence intensity as a proxy for oil concentration within oil dispersions (Conmy et al., 2014).

Presented here are results from a series of high pressure jet releases of oil within the BIO flume tank to assess the operational performance of SSDI. DSD and fluorescence intensity were used as a proxy for dispersion efficiency for treatments with (chemically-enhanced dispersion) and without (physical dispersion) chemical dispersants. The objective of this work was to evaluate the effects of water temperature and dispersant-to-oil ratio on DE of three oils at high reservoir temperatures. Findings help (1) to determine the applicability of existing *in situ* monitoring technologies for SSDI and (2) inform efforts to integrate DSD into deepwater blowout plume formation models that enable prediction of the dispersed oil droplets under high-

flow subsurface release velocities. DWH spill monitoring program DSD and fluorescence data played a significant role in supporting emergency response operations, fate and transport modeling, and impact assessment. Findings from this study have implications for efforts in support of future deep-water spill preparedness.

METHODS

Flume Tank Description - Oil dispersion experiments were conducted using Alaska North Slope crude oil (ANS), South Louisiana Crude (SLC) and Intermediate Fuel Oil 120 (IFO 120) with Corexit 9500 and Finasol OSR 52 chemical dispersants in the 32m long flow-through carbon steel flume tank (31,000 L) at BIO. Seawater was pulled from the Bedford Basin (50cm below surface) via two smaller centrifugal pumps (110 gpm), and filtered through high-flow polypropylene bag filters (5 and 25 μm) to a fiberglass holding tank (25,000 L) that supplies seawater for the system to ensure that a constant flow rate is maintained. Two high-flow centrifugal pumps (600 gpm) provided flow to generate horizontal water currents in the tank, where flow gauges on influent and effluent pipes were monitored and valve adjustments made to obtain a balanced flow rate throughout experiments. Water current velocities were measured in the tank using an ADV (Nortek Vectrino) to maintain consistent horizontal water current velocities (3.5 cm/s) at all measured depths. At the completion of experiments, oil absorbent pads removed oil from the water surface. Effluent wastewater was filtered over layers of polypropylene PomPom Oil-Mops to remove insoluble oil from the water prior to discharging, where effluent samples were collected and PomPom's were changed if oil concentrations exceed the minimum guidelines (10 ppm) for wastewater discharge in Canada.

Subsurface Oil Injection System - A custom subsurface oil injection system was used to generate dispersed oil plumes in the tank (Figure 1), consisting of a 2 L stainless steel pressure

vessel and a series of valves and pressure gauges, fastened to the outer wall of the tank. Inside the tank, a fitting connects the outer assembly to a nozzle (2.4 mm), which extends mid-width perpendicular to the tank wall (9 m downstream from the influent pipe) and is angled at the tip to direct the discharge plume downstream and use horizontal length of the tank to capture the plume movement. For each experiment, oil or oil/dispersant premix is added to the pressure vessel in order to reduce the influence of any additional confounding factor of mixing effectiveness. Copper coil within the pressure vessel connects to a water bath to permit oil heating to 80°C, and then pressurized (40 psi for ANS and SLC; 60 psi for IFO 120) with compressed Nitrogen. A ball valve connected to the vessel controls the oil release through the subsurface nozzle into the tank. Release time and total volume (determined by mass) of oil injected are recorded. After each experiment, the subsurface injector system was cleaned by flushing with toluene, acetone and fresh water.

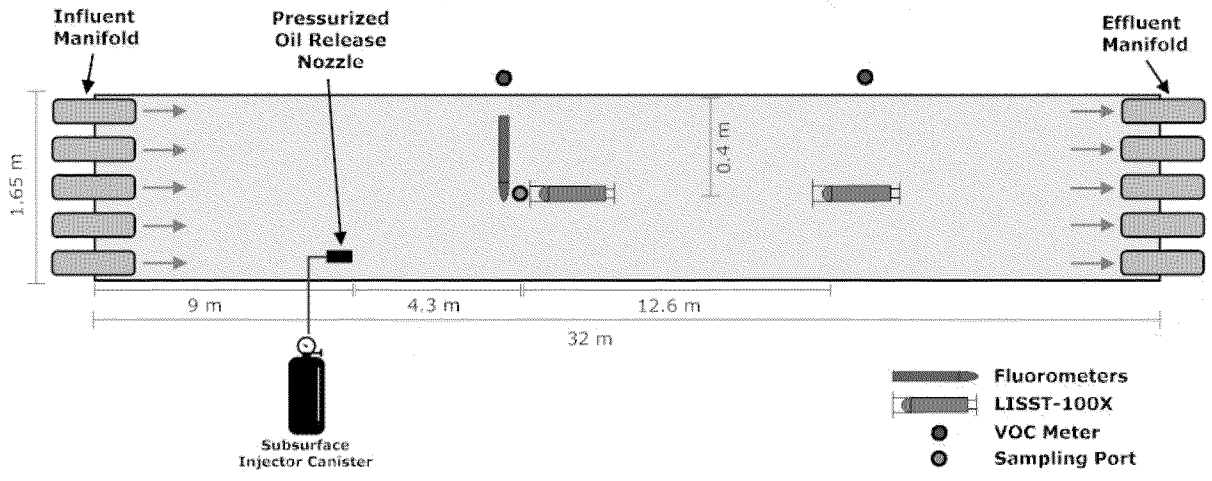

Figure 1. Schematic diagram showing the location of the subsurface injector and *in situ* instrumentation submerged within the tank.

Submersible Sensor Deployment - Sensors were mounted on an aluminum frame located 4.3 m from the oil release point with their pressure windows and at a depth of 0.4 m. The instruments were attached to a crosspiece support bar, so that they were all located the same distance downstream from the oil release point with the pressure window pointed directly towards the bottom of the tank. Data acquisition systems were used to control and collect data with real-time displays from the *in situ* fluorometers. A total of six *in situ* hydrocarbon fluorometers were evaluated during this study; Chelsea Technologies Group UV Aquatrackas - Refined and Crude models, Turner Designs Group Cyclops - Fine and Crude models, Sea Bird – Wet Labs Inc ECO-FLU, and GmBH Trios. Sampling rates and units of signal intensity varied for each instrument with one reading every 5 seconds for GmBH (µg/L PAH), every 3 seconds for Cyclops (auto-gain feature; mV), and every 1 second for the ECO and Aquatrackas (µg/L QSDE, µg/L perylene and µg/L carbazole, respectively. Oil droplet size was measured *in situ* using two LISST-100X (Laser *in-situ* Scattering and Transmissometry) particle size analyzers (Sequoia Scientific, Inc), measuring particle size from 2.5 – 500 µm. The first LISST (upstream LISST) was located immediately after the fluorometer package support frame at a distance of 5.1 m from the oil release point and the second LISST (downstream LISST) was located at 16.9 m from the oil release point and both at a depth of 0.4 m (Figure 1). Placement was informed by the numerical modeling efforts conducted previously in the tank to maximize oil droplet detection without saturating the instrument. Real-time data was provided by LISST-SOP data acquisition software (ver. 5) with a sample acquisition rate of one measurement every 3 seconds. Underwater video of oil droplets and the transport of the plume were captured using a GoPro Hero4 digital camera, as well as a Sony RX100 III digital camera with underwater housing.

Submersible Sensor Data Processing - LISST data files were processed using a statistically-based quality control script written using the R statistical package. This script identifies and removes "Over Range" samples (defined as 0 μL/L) and outliers. Outliers are defined as any reading that is greater than the moving mean (5 data points before and after the targeted time point) of the dataset multiplied by four times the standard deviation (over the same interval as the moving mean). Due to the potential for one or more extreme outliers to skew both the moving mean and standard deviation calculations for points around them, this outlier detection routine is run iteratively, excluding previously flagged points, until no more outliers are detected. The script then calculates the Total Particle Concentration (TPC), Volume Mean Diameter (VMD), and Particle Size Concentration (PSC). It then detects the plume curve (if present) and time-normalizes the data based on that location. Data are presented as Droplet Size Distribution (DSD). Plots presented include data 2 minutes before and 8 minutes after the start of the plume curve. Data from the Downstream LISST were normalized so that the plume began at t = 5 min in order to visually convey that the plume was detected in the tank roughly 3 min after detection by the LISST further upstream near point of injection release. Similar to the LISST data, a script was used to detect outliers in the fluorometry data. Curve detection was performed and the data was time-normalized to include 2 minutes of data before, and 8 minutes of data after the start of the plume curve. The baseline of the plume curve was calculated using data points observed in the first minute preceding the start of the curve and this baseline was subtracted from the data. Finally, factory calibration factors were applied to the data.

Experimental Design -. Seawater temperature and salinity in the tank were recorded using a handheld probe (YSI Incorporated, Yellow Springs, OH). Prior to experiments, the tank was operated in recirculation mode (10 minutes) to allow current flow to stabilize. Five minutes

prior to oil injection, data-logging on all instruments was started and background seawater samples were collected. After oil injection, the real-time readout of the fluorometer signal was monitored for the first spike in signal intensity (usually after 2 minutes), and bottle chemistry sample collection began. The experiments ran for 12 minutes and the tank was cleaned using Big Orange Degreaser, to prevent any potential contamination between experiments. Instrument windows were cleaned using disposable alcohol wipes. Water samples were returned to the lab and stored at 4°C.

Discrete Chemistry Samples - Water samples for chemical analysis were collected at various time points throughout the experiments. Three ¼" stainless steel tubes were attached to the aluminum fluorometer frame, so that the end of the tube was located at the same depth as the instrument pressure windows (0.4 m). These were attached via silicon tubing to a digital peristaltic pump with a 120 mL/min flow rate. Samples were analyzed for Total Petroleum Hydrocarbon (TPH) using a method developed by DFO in-house (Cole et al., 2007; King et al., 2015) for Gas Chromatograph (GC) - Flame Ionization Detector (FID) analysis. An eight point calibration was generated using standards prepared from the appropriate crude oil stock that was used to generate the TPH samples (e.g. ANS, IFO 120 and SLC). Peak quantification was performed using relative response factors. Samples were analyzed for benzene, toluene, ethylbenzene and xylene (BTEX) using EPA Method 8240 (purge and trap), modified by running a GC - Mass Spectrometer (MS) in selected ion monitoring mode to include ethylbenzene. BTEX standards were prepared in 40 mL purge and trap vials; and samples and standards were analyzed using this method, along with sample blanks and duplicate samples. TPH and BTEX results are not shown here in detail but can be found in the EPA 600/F-16/250 Report (2016).

RESULTS & DISCUSSION

A total of 72 experiments were conducted in replicate, where water ranged in temperature from 4.9 - 20.3 $_{o}$C, with 11 $_{o}$C serving as the cut off between warm and cold water tests. Previous experiments within the BIO flume tank facility have assessed dispersion effectiveness as a function of energy dissipation rate and particle size distribution (Li et al. 2009a) and demonstrated that DE is strongly dependent on wave conditions, dispersant type, and oil type (Lee et al. 2009) and highly correlated with *in-situ* droplet size distribution (Li et al. 2008; Li et al. 2009a). Here, DE was evaluated via response monitoring tools (fluorescence and particle size analyzers) during high-pressure subsurface injection experiments.

Dispersant-to-Oil Ratio (DOR) Effects- Addition of either Corexit 9500 or Finasol OSR 52 chemical dispersants to Alaskan North Slope (ANS), IFO 120 and South Louisiana Crude (SLC) oils resulted in a decrease in the Volume Mean Diameter (VMD) and shifted the Droplet Size Distribution (DSD) to smaller droplets for warm water treatments (Figure 2). For ANS, dispersions created without chemical dispersants or Dispersant-to-oil ratio (DOR) = 1:100 yielded VMD > 70 μm and exhibited unimodal DSD. Dispersions created with DOR = 1:20 yielded VMD < 70 μm size range with a bimodal DSD. SLC oil was more dispersible compared to ANS for treatments with and without chemical dispersant. Bimodal distribution was observed during DOR = 1:20 and some DOR = 1:100 experiments indicating that the jet release of this particular oil into warm water produced smaller droplets than the ANS. During the DWH spill, droplets ≤ 70μm were considered small enough to remain in suspension and were monitored as a proxy for evaluating oil dispersion efficiency. This suggests that produced SLC droplets from a DOR = 1:20 or 1:100 dispersant injection, and ANS droplets at DOR = 1:20 would likely remain dispersed in the presence of mixing energy given the larger proportion of small droplet sizes observed. In general, Corexit 9500 produced slightly smaller

droplets compared to Finasol OSR 52 for warm water treatments. The addition of Corexit 9500 or Finasol OSR 52 to IFO 120 during warm temperature experiments resulted in a shift in DSD and a decrease in VMD; however bimodal distribution was not achieved and even DOR = 1:20 did not yield VMD less than 70 µm in most cases. This suggests that dispersant addition to this oil at warm temperatures would not yield droplet sizes that would likely remain in suspension.

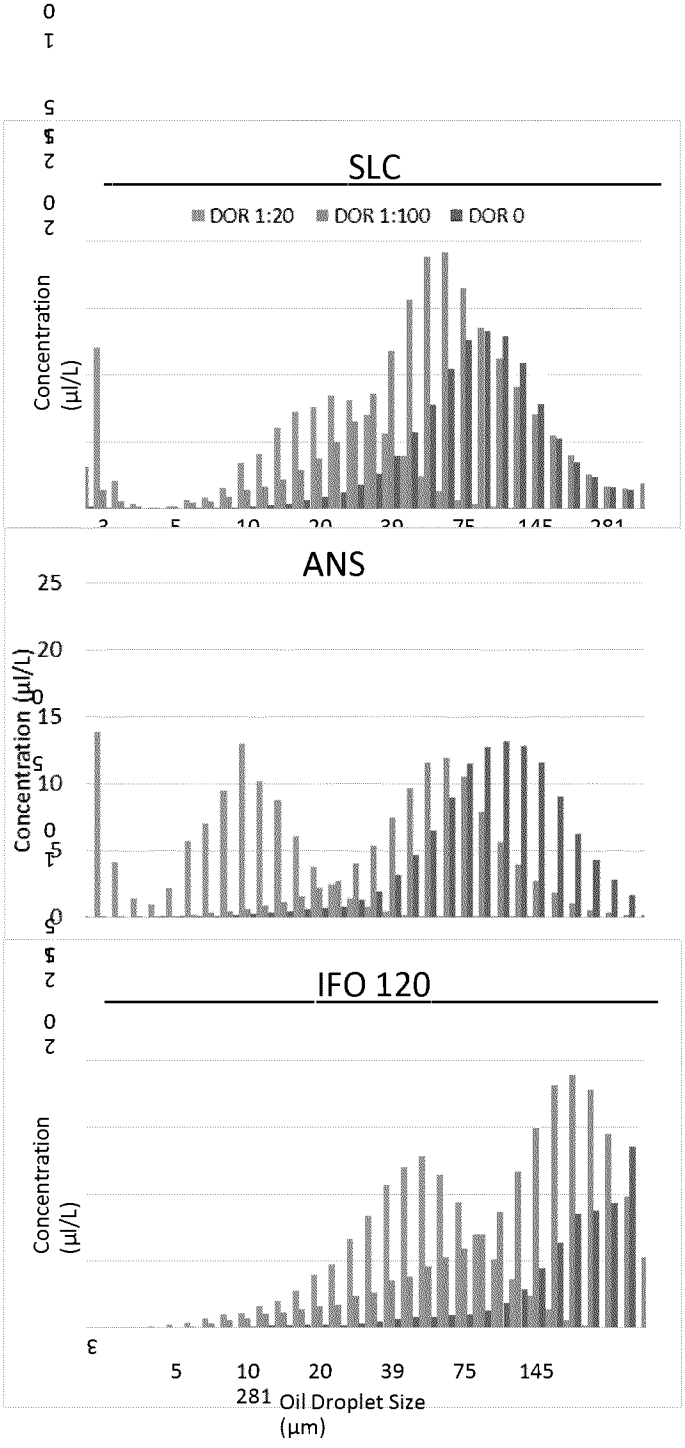

Figure 2. LISST DSD for SLC, ANS and IFO 120 with Corexit 9500 at three DOR treatments in warm water. Histograms represent averages obtained at the 2 minute time stamp during each experiment.

Water Temperature Effects - For ANS, dispersion with < 70 μm droplet VMD was observed for the DOR = 1:20 treatments at both cold and warm water temperatures (Figure 3). Water temperature did not appear to influence the DSD or VMD for this lighter crude oil. However, a temperature effect was observed on the Total Particle Concentration (TPC), where lower temperatures coincided with fewer particles dispersed within the plume for a given volume of oil injected. This may be due to enhanced density differences between the oil and water at colder temperatures, thus quicker rise time of the produced droplets. For the addition of Corexit 9500 or Finasol OSR 52 to IFO 120 at cold water temperatures, smaller droplet sizes were not observed, where DOR = 1:20 remained above 200 μm. This suggests that dispersant addition to this oil at cold temperatures would not yield droplet sizes that would likely remain in suspension.

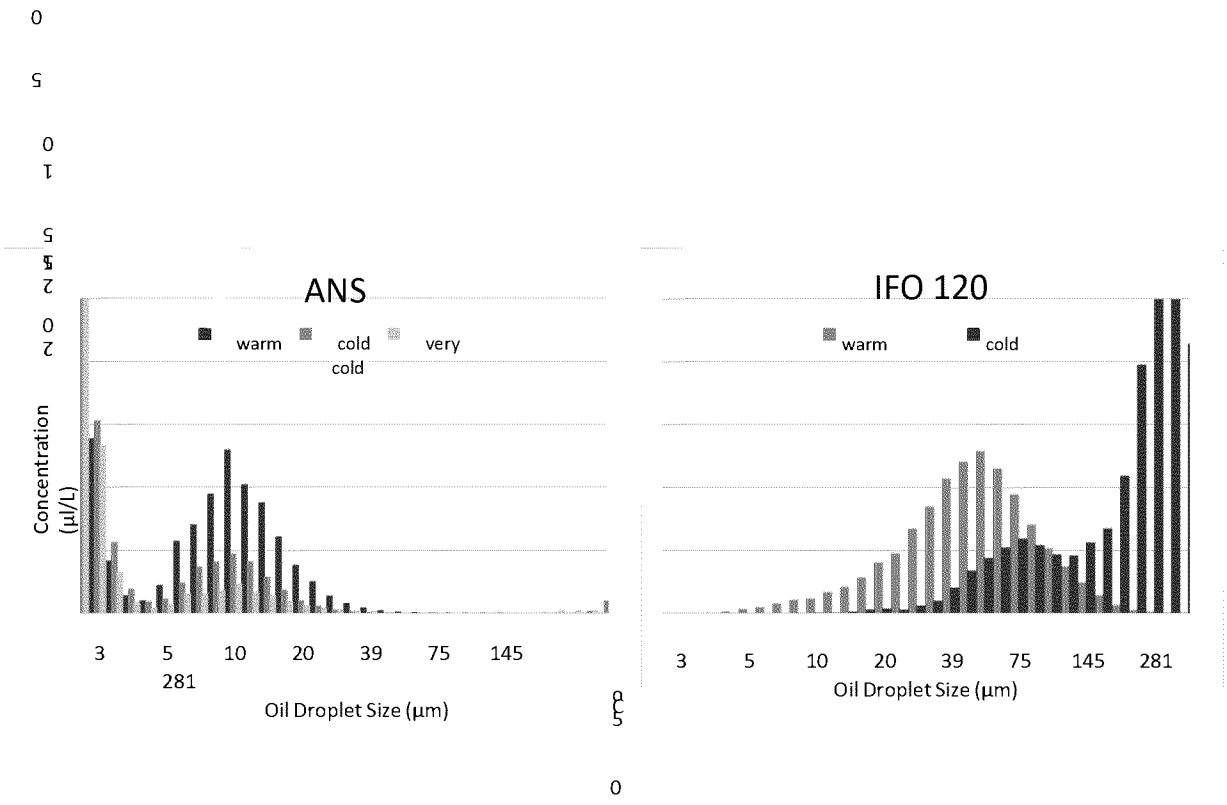

Figure 3. LISST DSD for ANS and IFO 120 with Corexit 9500 at DOR = 1:20 and varying water temperature.

For experiments conducted at water temperatures < 5 ^{o}C, the LISST particle size analyzer yielded unexpected DSD where even a unimodal distribution was not measured. Chemistry and *in situ* fluorescence data indicate that the oil was in fact dispersed adequately. This suggests potential operational problems of the LISST at < 5 ^{o}C, even though it is within the operating temperature (manufacturer manual). Additional testing of cold water temperature limits is recommended.

Upstream and Downstream Particle Fractionation - Histograms representing the particle concentration for a given size class from the upstream and downstream LISSTs suggest dilution and fractionation of particles within the plume. The downstream LISST positioned further from the jet release serves as an indication of plume evolution through the tank. For all oil and DOR treatments, dilution in particles (decrease in TPC) within the plume expectedly occurred. Also evident is a shift to smaller particles for all DOR treatments as the plume

moves through the tank, where size fractionation was dependent on DOR treatment (Figure 4). Physical dispersion (DOR 0) treatments for lighter oils were found to have the largest shift in DSD and VMD between the upstream and downstream LISSTs suggesting the largest effect of particle fractionation in the plume. Where the decrease in TPC suggests plume dilution in the tank, the DSD shift to smaller particles suggests that within each experiment larger droplets were removed from the plume within 6 minutes of the oil release, most likely rising to the surface of the tank. The effect was least observed in the DOR 1:20 treatments where dilution occurred but the presence of smaller droplets (with lower rise times) at the point of release most likely didn't allow for fractionation. The effects of fractionation were observed in warm and cold treatments.

Time series particle size data allows for evaluating plume dynamics over the duration of the experiments. Figure 5 depicts time series contour plots of the plume, where colored contours represent the particle concentration (normalized to max value for comparison purposes) for given droplet sizes through time. These plots allow for ascertaining how the DSD shifts over the duration of the release as the plume moves in the horizontal direction in the tank. For ANS, data suggest that the leading edge of the plume, as detected by the upstream LISST, exhibited a wide range in DSD during the first few minutes after release. As the plume advances down the tank, the DSD becomes narrower with a shift in the VMD for the DOR = 1:100 and 0 treatments. DSD remained similar for the DOR = 1:20 treatment. Warm and cold water treatments exhibit similar trends.

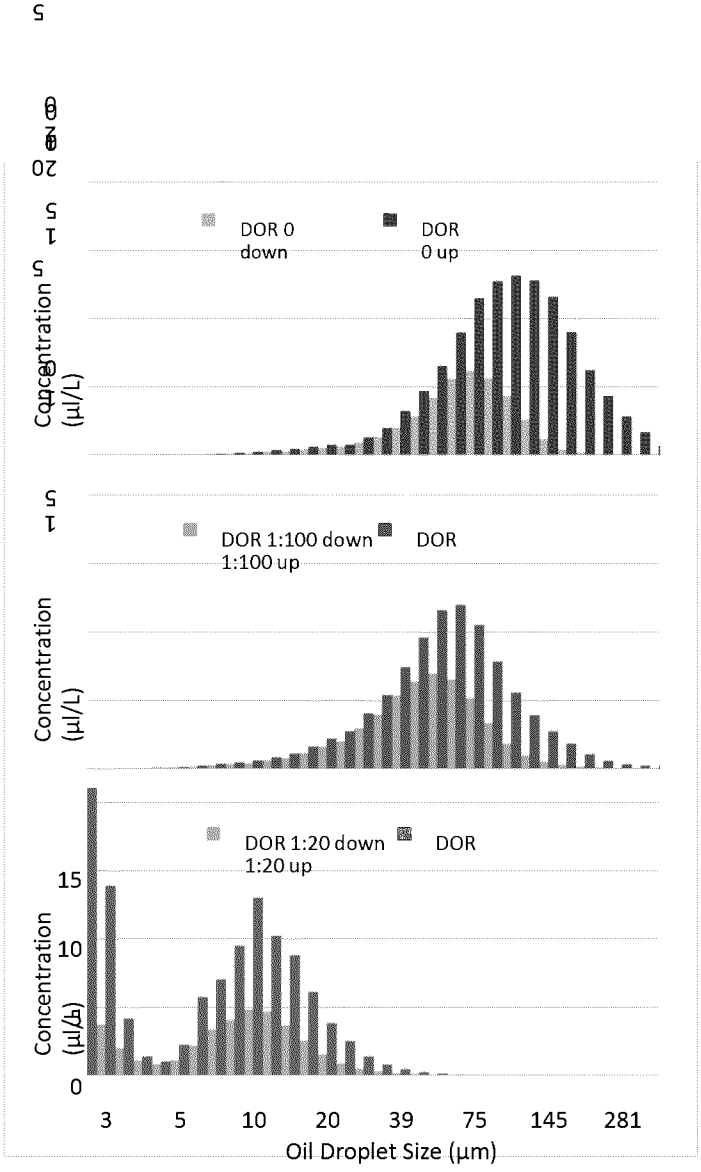

Figure 4. Upstream and downstream LISST Droplet Size Distribution and particle concentration for ANS with Corexit 9500 during warm water treatments.

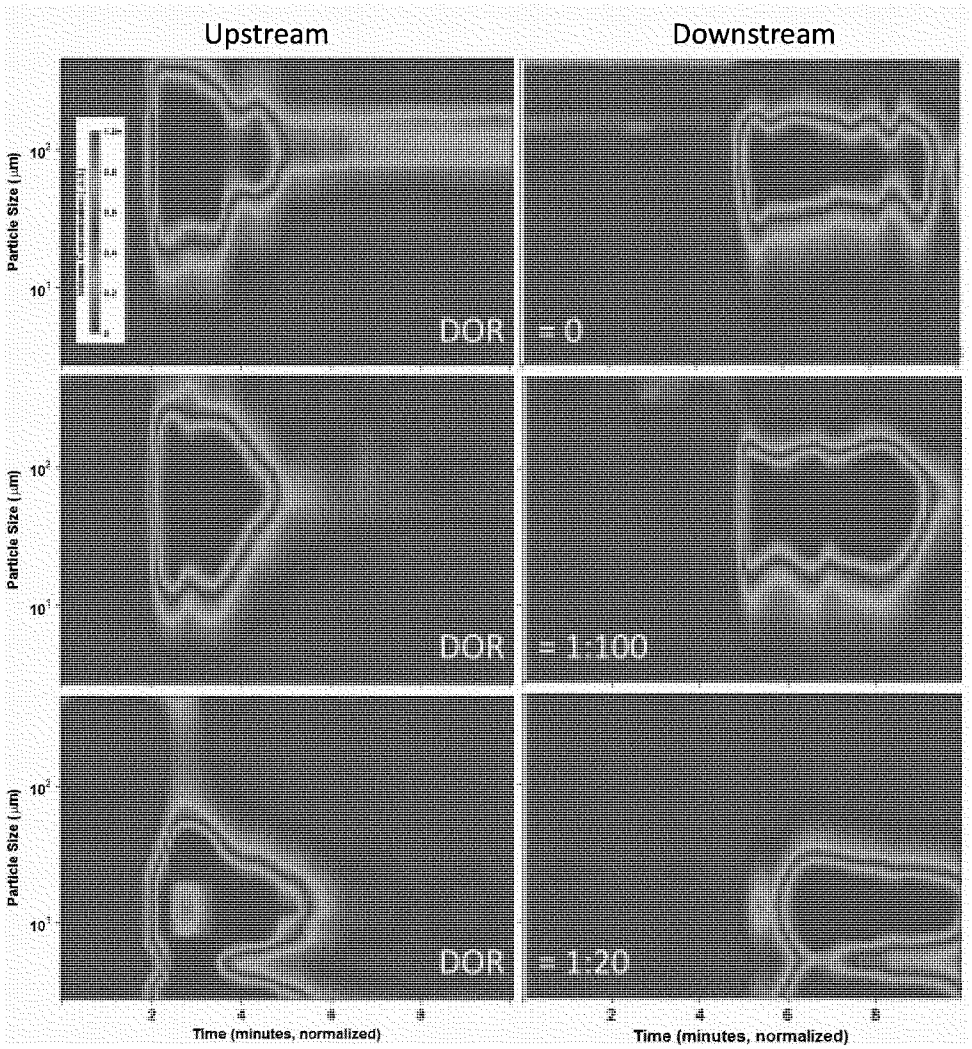

Figure 5. Time series contours of droplet size distribution and particle concentration from the upstream (left panels) and downstream (right panels) LISSTs for ANS with Corexit 9500 during warm water treatments.

Plume Fluorescence Intensity – In addition to the plume transport of particles (oil droplets), dissolved hydrocarbons were also measured via discrete samples and by proxy using fluorescence intensity. The reliability of *in situ* fluorescence measurements as a proxy for oil concentration within physically and chemically dispersed oil has been demonstrated previously within the tank (Conmy et al., 2014). Here, *in situ* fluorescence serves as a good proxy for oil

concentration during the subsurface injection experiments. However, heterogeneity of the produced plumes and the short time scale of experiments (~10 min) led to difficulties in correlations between the plume particle size analyses and chemistry results. This is in part due to discrete samples representing 15 second averages as opposed to instantaneous measures given by fluorometers and particle size analyzers. Thus, although general trends were similar, exact matchups between *in situ* data streams and discrete samples proved to be challenging (Figure 6). Given the experimental design, fluorescence was found to be better suited for correlation with total particle concentration (Figure 7). Depicted are the in situ fluorescence and TPC data during a warm water experiment of ANS with (left) and without (right) Corexit 9500. When exposed to dispersant, fluorescence estimates of dissolved hydrocarbons was higher compared to oil alone treatments, and signal persisted for longer periods of time. Whereas a sharper decay in the fluorescence intensity and the TPH values were observed for the physically dispersed oil.

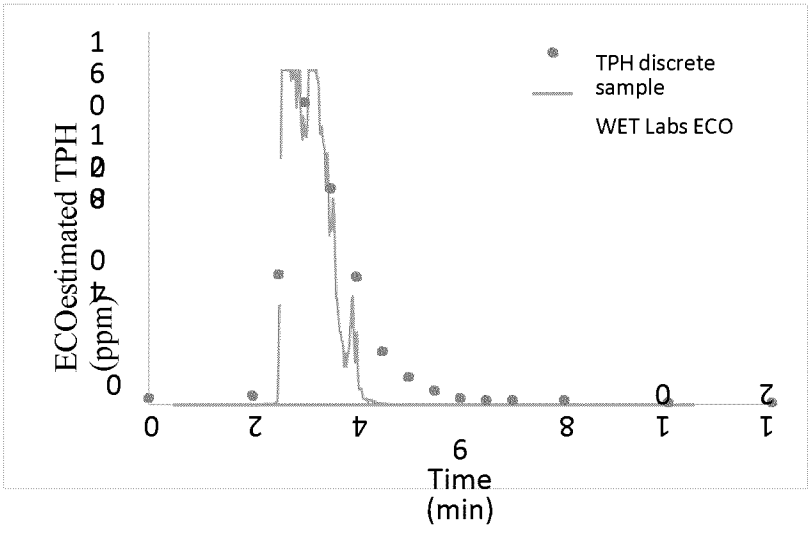

Figure 6. Fluorescence intensity and TPH samples for a warm water treatment using SLC at DOR = 1:20.

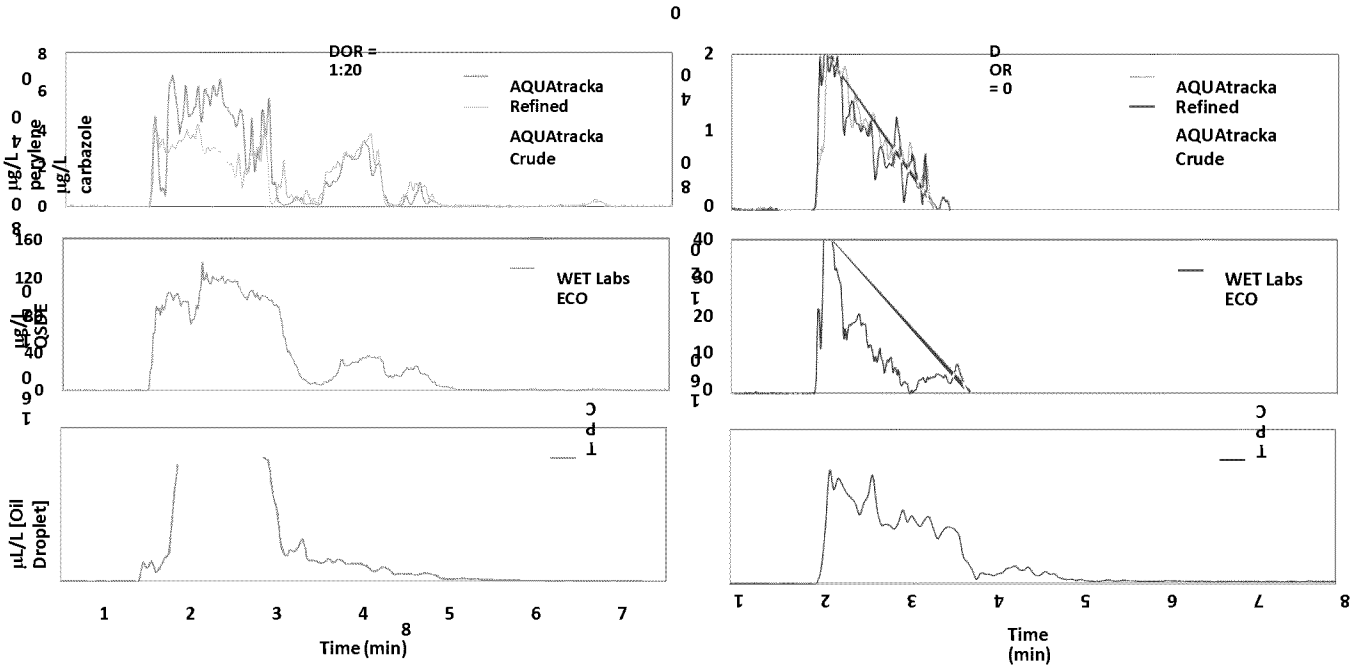

Figure 7. Fluorescence intensity and TPC as a function of time for ANS warm water treatment.

CONCLUSIONS

In situ oil droplet size distribution, particle concentration and fluorescence data from this study are essential for better understanding dispersion effectiveness and for refining droplet formation and trajectory models, such as modified Weber Number technique (Johansen et al., 2013) and the VDROP-J model (Zhou et al., 2014). Thus, findings from this study have implications for predicting the behavior of oil and plume formation, decision-making pertaining to SSDI as a countermeasure, and assessing the transport and fate of slicks and subsurface plumes in support of emergency response operations during any future deepwater spills.

REFERENCES

Conmy, R. N., et al. (2014) Submersible Optical Sensors Exposed to Chemically Dispersed Crude Oil: Wave Tank Simulations for Improved Oil Spill Monitoring. Environ. Sci. Technol. 48(3): 1803-1810.

Cole, M.G., T. King, K. Lee (2007) Analytical technique for extracting hydrocarbons from water using sample container as extraction vessel in combination with a roller apparatus. Anal. Chem., 77: 2210-17.

CRRC Report (2010) Coastal Response Research Center Deepwater Horizon Dispersant USE Meeting Report, May 26-27, 2010, 108 pp.

EPA 600/F-16/250 Federal Report (2016) Dispersant Effectiveness, In-Situ Droplet Size Distribution and Numerical Modeling to Assess Subsurface Dispersant Injection as a Deepwater Blowout Oil Spill Response Option *and* Evaluation of Oil Fluorescence Characteristics to Improve Forensic Response Tools; IAA No. E12PG00037 for DOI BSEE, 144 pp.

Joint Analysis Group Report (2010) Review of Data to Examine Subsurface Oil in the Vicinity of DWH MC-252, May 19-June 19, 2010; 29 pp.

Johansen, O., et al. (2013) Droplet breakup in subsea oil releases - Part 2: Predictions of droplet size distributions with and without injection of chemical dispersants. Mar. Poll. Bull. 73(1): 327-335.

Lee, K., Li, Z., Boufadel, M.C., Venosa, A.D. and Scott Miles, M. (2009) Wave tank studies on dispersant effectiveness as a function of energy dissipation rate and particle size distribution. Final report submitted to NOAA/CRRC/UNH, 67 pp.

Li, Z., Lee, K., King, T., Boufadel, M.C. and Venosa, A.D., (2008) Oil droplet size distribution

as a function of energy dissipation rate in an experimental wave tank 2008 International Oil

Spill Conference. American Petroleum Institute, Washington D.C., Savannah, GA, pp. 621-626.

Li, Z., Lee, K., King, T., Boufadel, M.C. and Venosa, A.D., (2009a) Evaluating crude oil chemical dispersion efficacy in a flow-through wave tank under regular non-breaking wave and breaking wave conditions. Mar. Poll. Bull., 58: 735-744.

Li, Z., Lee, K., King, T., Boufadel, M.C. and Venosa, A.D., (2009b) Evaluating Chemical Dispersant Efficacy in an Experimental Wave Tank: 2, Significant Factors Determining *In Situ* Oil Droplet Size Distribution. Environ. Engin. Sci., 26(9): 1407-1418.

Li, Z., Lee, K., King, T., Boufadel, M.C. and Venosa, A.D., (2010) Effects of temperature and wave conditions on chemical dispersion efficacy of heavy fuel oil in an experimental flow-through wave tank. Mar. Poll. Bull., 60(9): 1550-9.

NRC Report (2005) National Research Council Oil Spill Dispersants: Efficacy and Effects, Washington, DC, 400 pp.

Wickley-Olsen, E., Boufadel, M.C., King, T., Li, Z., Lee, K., Venosa, A.D. (2007) Regular and breaking waves in wave tank for dispersion effectiveness testing. In: Proceedings of the 30th Arctic and Marine Oil spill Program (AMOP) Technical Seminar, Edmonton, AB, Canada. Environment Canada, Ottawa, Ontario, Canada, pp. 161–187.

Zhao, L., et al. (2014). Evolution of droplets in subsea oil and gas blowouts: Development and validation of the numerical model VDROP-J. Mar. Poll. Bull., 83(1): 58-69.

To: Craig Watts[craig@hydrosphere.net]; Holder, Edith[holder.edith@epa.gov]; Conmy, Robyn[Conmy.Robyn@epa.gov]
Cc: Peter Meyer[pmeyer@hydrosphere.net]; Cris Griffin[cgriffin@hydrosphere.net]
From: Barron, Mace
Sent: Tue 10/4/2016 3:39:32 PM
Subject: RE: Final report for recent round of toxicity tests

I have completed my technical review of the report on Finasol, and confirm its technical adequacy.

Guys, thank you for another job well done.

Mace

From: Craig Watts [mailto:craig@hydrosphere.net]
Sent: Tuesday, October 04, 2016 10:23 AM
To: Barron, Mace <Barron.Mace@epa.gov>; Holder, Edith <holder.edith@epa.gov>; Conmy, Robyn <Conmy.Robyn@epa.gov>
Cc: Peter Meyer <pmeyer@hydrosphere.net>; Cris Griffin <cgriffin@hydrosphere.net>
Subject: Final report for recent round of toxicity tests

To all,

Below is a DropBox link to the final report for the Finasol testing. I believe this catches us up for now. We have nothing in-house to test for you. Please let us know if you plan on sending us any more products or oils so that we can plan accordingly.

https://www.dropbox.com/s/f0aejbht8lmwgsz/16156.pdf?dl=0

Mace – I will send you the survival spreadsheets in a separate email.

Regards,

Craig

Providing Environmental & Product Toxicity Testing since 1986

Craig Watts, Lab Director

Hydrosphere Research

11842 Research Circle

Alachua, FL 32615-6817

T (386) 462-7889

www.hydrosphere.net

To: Barron, Mace[Barron.Mace@epa.gov]; Holder, Edith[holder.edith@epa.gov]; Conmy, Robyn[Conmy.Robyn@epa.gov]
Cc: Peter Meyer[pmeyer@hydrosphere.net]; Cris Griffin[cgriffin@hydrosphere.net]
From: Craig Watts
Sent: Tue 10/4/2016 3:22:33 PM
Subject: Final report for recent round of toxicity tests

To all,

Below is a DropBox link to the final report for the Finasol testing. I believe this catches us up for now. We have nothing in-house to test for you. Please let us know if you plan on sending us any more products or oils so that we can plan accordingly.

https://www.dropbox.com/s/f0aejbht8lmwgsz/16156.pdf?dl=0

Mace – I will send you the survival spreadsheets in a separate email.

Regards,

Craig

Hydrosphere research

Providing Environmental & Product Toxicity Testing since 1986

Craig Watts, Lab Director

Hydrosphere Research

11842 Research Circle

Alachua, FL 32615-6817

T (386) 462-7889

www.hydrosphere.net

To: Conmy, Robyn[Conmy.Robyn@epa.gov]
From: Holder, Edith
Sent: Wed 3/25/2015 8:06:09 PM
Subject: FW: Dispersant samples request

Robyn,

I think answering these questions is your bailiwick!

Thanks,

Edie

Edith Holder

Pegasus Technical Services, Inc.

On-Site Contractor to the U.S. EPA

ORD/NRMRL/LRPCD

26 W. Martin Luther King Dr.

Cincinnati, OH 45268

Phone: 513-569-7178

Email: holder.edith@epa.gov

From: Bryan, Elisha
Sent: Wednesday, March 25, 2015 3:58 PM
To: Holder, Edith
Subject: Fw: Dispersant samples request
Importance: High

Happy Wednesday!

Would you like to answer all these questions that Ms. Theriot has? She also wants to know why we are doing these test since testing of their product has already been done. I thought the link explained everything, but I guess I was wrong.

Elisha Bryan

Pegasus Technical Services, Inc.

On-Site Contractor to the U.S. EPA

ORD/NRMRL/LRPCD

26 W. Martin Luther King Dr.

Cincinnati, OH 45268

Phone: 513-965-4805

Email: bryan.elisha@epa.gov

From: Theriot, Debby <Debby.Theriot@nalco.com>
Sent: Wednesday, March 25, 2015 1:12 PM
To: Bryan, Elisha
Subject: FW: Dispersant samples request

Hello Bryan,

Thank you for your interest in COREXIT brand products. Please provide a letter stating the below items, including the lab contact details and shipment address for the sample to be sent.

- What do you plan to do with the products and test results?
- What are the details of your testing specifics?

- Will you disclose formula test results to anyone?

Once we have these details in a letter I can forward your request through the proper route to obtain samples.

Much appreciated,

Debby Theriot

Nalco Environmental Solutions LLC

7705 Highway 90-A

Sugar Land, TX 77478

281.263.7709 ofc

832.851.5164 cell

debby.theriot@nalco.com

www.nalcoesllc.com

NALCO
Environmental
Solutions LLC

From: Bryan, Elisha [mailto:Bryan.Elisha@epa.gov]
Sent: Friday, March 20, 2015 8:02 AM
To: Russell, Linda
Subject: Dispersant samples request

Good Morning,

I had emailed you last year about SWA research the EPA are conducting, thanks again for your quick response. We will also be conducting a series of Dispersant Efficacy experiments using the newly proposed Baffled Flask Test for inclusion in the 40 CFR Appendix C to Part 300 Subpart J.

As your product is listed on the U.S. EPA National Contingency Plan Product Schedule, we would like to include your product in our research and are interested in procuring a small quantity. I am contacting all manufacturers listed so that we can take into consideration the different characteristics of the dispersants.

This research will not change the current status of your product on the Product Schedule. More information on the proposed revisions and who to contact for comments can be found here: https://www.federalregister.gov/articles/2015/01/22/2015-00544/national-oil-and-hazardous-substances-pollution-contingency-plan#h-44.

Unfortunately, I am not authorized to sign a NDA. Please let me know if you are interested in sending samples of COREXIT® EC9500A, COREXIT® EC9500B, and COREXIT® EC9527A.

Have a nice day,

Elisha Bryan

Pegasus Technical Services, Inc.

On-Site Contractor to the U.S. EPA

ORD/NRMRL/LRPCD

26 W. Martin Luther King Dr.

Cincinnati, OH 45268

Phone: 513-965-4805

Email: bryan.elisha@epa.gov

To: Conmy, Robyn[Conmy.Robyn@epa.gov]
From: Chris Barker
Sent: Mon 3/20/2017 7:54:53 PM
Subject: AMOP papers to review
Fingas Model of Chemical Oil Spill Dispersion AMOP 2017.pdf
Instructions to reviewers for AMOP papers.doc
Reviewers Check Sheet for AMOP Papers 2017.doc
Spaulding-DispersantTreatment.docx

Hi Robyn,
I'd appreciate your review of the enclosed papers:

We're hoping to get reviews back by the end of the month.

Thanks!

-Chris

--

Christopher Barker, Ph.D.
Oceanographer

Emergency Response Division
NOAA/NOS/OR&R (206) 526-6959 voice
7600 Sand Point Way NE (206) 526-6329 fax
Seattle, WA 98115 (206) 526-6317 main reception

Chris.Barker@noaa.gov

Development of a Model of Chemical Oil Spill Dispersion

Merv Fingas
Spill Science, 1717 Rutherford Point
Edmonton, Alberta, T6W 1J6 fingasmerv@shaw.ca

Abstract

The aim of this paper is to describe a new model of oil spill dispersion. A model was constructed utilizing four basic processes. Initial dispersion was calculated using the Delvigne equation adjusted to chemical dispersion, then the dispersion was distributed over the mixing depth, as predicted by the wave height. Then the droplets rise to the surface according to Stokes' law. Oil on the surface, from the rising oil and that undispersed, is re-dispersed. The droplets in the water column are subject to coalescence as governed by the Smoluchowski equation. A loss or portion of the amount dispersed, is input to account for the production of small droplets that rise slowly and are not re-integrated with the main surface slick. This is the amount taken as 'permanently' dispersed.

More than 1000 runs were carried out with variations of the models. The runs show that the most important factor to the time to extinction of the surface slick, is the mixing depth of the sea as predicted from wind speed. The second most important factor is the viscosity of the starting oil. The model predicts the maximum viscosity that would be dispersed given wind and wave conditions. Variations of the model were developed to enable inputs of only wind speed and oil viscosity. A simplified prediction model was created using regression.

The model outputs illustrate the time history of oil-in-water emulsions and the various influences on this time history. The long-term fate of the oil is not modeled.

1 Introduction

Consideration of water-in-oil dispersion is a concern for oil spill countermeasures. It is known that oil spill dispersions are sometimes temporary and re-surfaced slicks can appear (Fingas, 2010). Further the amount of oil entering the water has been shown to be highly variable and this has also been observed to be related to the oil properties and the sea energy (Guyomarch et al., 2012; Fingas, 2011). An important facet of the problem is the slow rise and coalescence of droplets to the surface after dispersion. Modeling these phenomena can provide useful insight into the oil spill dispersion process.

Gravitational separation is the most important force in the resurfacing of oil droplets from crude oil-in-water emulsions such as dispersions and is therefore the most important destabilization mechanism (Rosen and Punjappu, 2012). Droplets in an emulsion tend to move upwards when their density is lower than that of water. This is true for all crude oil and petroleum dispersions that have droplets with a density lower than that of the surrounding water. The rate at which oil droplets will rise due to gravitational forces is dependent on the difference in density of the oil droplet and the water, the size of the droplets (Stokes' Law), and the rheology of the continuous phase. The rise rate is also influenced by the hydro-dynamic and colloidal interactions between droplets, the physical state of the droplets, the rheology of the dispersed phase, the electrical charge on the droplets, and the nature of the interface.

Creaming is the destabilization process that is simply described by the appearance of the starting dispersed phase at the surface, without the processes in the intervening spaces being described. It is basically a prime example of gravitational separation. In the oil spill world, creaming is the process that might be described as resurfacing.

Coalescence is another important destabilization process, which has been studied in oil-in-water emulsions (Sterling, 2004). Two droplets that interact as a result of close proximity or collision can form a new larger droplet. The end result is to increase the droplet size and thus the rise rate, resulting in accelerated destabilization of the emulsion. Studies show that coalescence increases with increasing turbidity as collisions between particles become significantly more frequent. Temperature is also a factor in emulsion stability as a change in temperature causes changes in interfacial tension between the two phases. Temperature can cause differential changes in other factors such as the relative solubility of the surfactant in the two phases and in the diffusion rate. Emulsifying agents are usually most effective when near the point of minimum solubility in the solvent in which they are dissolved because at this point they are most surface-active. Since the solubility of the emulsifying agent usually changes with temperature, the emulsion stability also changes with temperature. The classic equation to describe this phenomenon is by Smoluchowski (Rosen and Punjappu, 2012):

$$\frac{dn}{dt} = 4\pi D r n^2 \qquad (1)$$

where $\frac{dn}{dt}$ is the rate of diffusion-controlled coalescence,
D is the diffusion,
r is the collision radius (distance between centres when coalescence begins), and
n is the number of particles per cm^3.

The first publication describing the modeling of oil spill dispersion was by Mackay et al. (1984). They proposed a model:

$$F = 1 - \exp(-K_e K_o K_d R) \qquad (2)$$

where: F is the fraction of oil dispersed,
R = an effective dispersant-to-oil ratio,
K_e = a constant determined by the turbulence conditions,
K_o = a constant related to the oil, mostly viscosity, and
K_d = a constant determined by the dispersant.

The data are all based on initial testing of the Mackay dispersant apparatus. The values were set at: $K_o = 1$, K_d was set at a value to correspond to results with Corexit 9527 (a chemical oil spill dispersant), being 0.77 and K_e set to the pressure drop in the apparatus, typically 100. Initial tests of this model against 13 data points showed good correlation between the predicted and observed dispersion. Comparison to other dispersion test results required changing of the constants to achieve reasonable correlation. It should be noted that there was no specific oil composition in this model.

Mackay (1985) subsequently published another model based on different parameters than those noted above. This new model presumed that a fraction of oil is dispersed by the dispersant according to the dispersant-to-oil ratio applied and then some of this rises, depending on the size of the droplet produced. There is no input for oil type or composition. Three steps were defined. The first was the mathematical statement of the dispersant dosage to the thick portion and the sheen of the oil slick. It is assumed that the dispersant dose applied to the sheen has little effect, but that the dispersant applied to the thick oil would disperse oil completely given high dosage. The second step of the model process was to calculate the oil initially dispersed into the water.

This was calculated only on the basis of the information obtained in the first step and the turbulence and oil slick thickness. The third step was to calculate the resurfacing rate of the dispersion. This was based on Stokes' law and the estimated droplet size of the dispersion calculated in step 2. The final output is the amount that remains in the water column, presuming a given time (not specified) had passed. This newer Mackay model (1985) was published along with the code for the model. It did not include specific oil composition data and was not used subsequently.

Reed et al. (2002, 2004) included a model of dispersion in the OSCAR spill model:

$$dm/dt = m(1-0.5^{\Delta t/t_{1/2}})\, f\, (W^2/W_{ref}^2) \quad (3)$$

where: m is the mass of the oil in the slick,
Δt is the time step,
$t_{1/2}$ is the half time for survival of fully treated slicks at the reference wind speed,
f is the ratio of dispersant to oil achieved,
W is the wind speed, and
W_{ref} is the reference wind speed which is set to the 7 m/sec time.

All parameters were based on the Haltenbanken experiments off Norway. The 'f' is the actual application achieved. The model presumes 100% efficiency at full treatment and that effectiveness is based on dispersant dosage. This model does not include any oil properties nor does it include a droplet rising component.

Fingas et al. (2003) collected chemical properties and dispersant effectiveness data on several oils and correlated these to form an empirical model of dispersion based on regression of these data. A total of 29 properties were correlated with the Corexit 9500 dispersibility in a laboratory apparatus. The highest correlation parameters were achieved with the content of nC12, naphthalenes, inversely with C26, the PAHs and the sum of C12 to C18 hydrocarbons. This is highly indicative that the smaller aliphatic hydrocarbons up to C18 and the PAHs are the most dispersible components of oil. Further, aliphatic hydrocarbons greater than C20 correlate inversely with the dispersant effectiveness indicating that these hydrocarbons suppress dispersion. The correlations provided a unique insight into dispersant effectiveness. Thirteen models were constructed to predict the chemical dispersibility of oils. The best model was with a regression coefficient of 0.998:

Dispersibility (%) = -11.1 -3.19(ln(C12 content) +0.00361(naphthalene content in ppm) - 7.62(PAH content)^2 + 0.115(C12 to C18 content)^2 + 0.785(%fraction oil boiling below 250 °C) (4)

If only the density and viscosity was used, the regression coefficient was 0.71. The model became: Dispersibility (%) = $-77.6 + 214e^{-density} + 60/viscosity^{0.5}$ (5)

The empirical dispersion models discussed above were calculated to give a dispersion effectiveness with time (about one-half hour) and did not consider rise time. It should be noted that the empirical data for equation (4) are difficult to obtain and would not be available for almost all oils.

Detailed chemical composition can yield good models with high correlation coefficients, however, these data are almost never available. Viscosity is a data point that is often available and can provide some indication of an oil's dispersibility (Zeinstra, et al., 2015a). There has been much discussion in recent years about 'limiting viscosity' to effect dispersion (Zeinstra et al.,

2015b). Some proposed 2000 mPa.s and others up to 20,000 mPa.s. However, the amount of dispersion predicted using viscosity as an indicator, also depends on sea energy and this in fact, may override the effect of viscosity. Further the amount of dispersion is also an important criterion here, if one sets it at 0.5% versus 10%, the difference certainly makes a difference.

Fingas (2010) constructed a model utilizing four basic processes. Initial dispersion was an input, then the dispersion was distributed over the mixing depth, as predicted by the wave height. Then the droplets rise to the surface according to Stokes' law. Oil on the surface, from the rising oil and that undispersed, is re-dispersed. The droplets in the water column were subject to coalescence as governed by the Smoluchowski equation. Given this coalescence, and the re-dispersion effectiveness, the dispersion in the water column decreases at an exponential rate with dispersion half-lives ranging from 120 to 250 minutes. Runs using the model showed that the most important factor to both the residual dispersion effectiveness and the half-life, is the mixing depth of the sea, and the droplet size. The second most important factor is the initial dispersion effectiveness assigned and then the re-dispersion effectiveness assigned. It was noted that many dispersion destabilising processes were not included because these processes are poorly understood, sub-models could not be found.

In summary, models to date have been somewhat primitive and did not include many factors, only a few have included the all-important factor of droplet size, coalescence and rising of dispersed droplets which is governing in terms of the overall resulting dispersion into the sea. Only a few models included oil properties.

Droplet size distribution is an important facet in understanding oil spill dispersions (Rosen and Punjappu, 2012). First, these distributions are wide, often reaching 2 orders-of-magnitude in droplet sizes. Second, these are characterized by a parameter known as VMD or volume mean diameter which is the average volume size or the median size when considering cubic droplet volume. VMD or Sauter mean diameter is the size of droplet that represents half of the volume distribution of the droplets. The VMD of a typical dispersed oil ranges from about 10 to 20 μm, and sometimes up to 35 μm (Mukherjee et al., 2012; Li et al., 2008, 2009, 2010). This VMD represents about half the volume of the droplets with many small droplets of lesser size and few of greater size. Figure 1 illustrates such a distribution. The rise time of the droplets is a large factor in that the very small droplets take a very long time to rise. Because of this, rise time can be considered to be a limiting value of oil spill dispersions (Fingas, 2010). The rise time of micron-sized droplets has been calculated and is shown in Figure 2. This shows a logarithmic-like effect of rise time dependent on droplet size. Figure 2 also shows that droplets greater than about 50 μ rise so fast that they are not useful in considering oil spill dispersions.

Sea energy is a major factor in dispersion (Zeinstra et al., 2015a; Delvigne and Sweeney, 1988). There have been several indications of sea energy that have been used in oil spill modeling including: wave height, wave steepness, wave period, wind speed, etc. (Parsa et al., 2016). Wave height has been used extensively in calculations. Studies have shown that steepness is an important parameter as well as, if the wave is breaking (Zeinstra et al., 2015b; Delvigne and Sweeney, 1988). Studies have shown that wave height is equivalent to a plunging stream and therefore could be used as an indicator of sea energy (Zeinstra et al., 2015b; Parsa et al., 2016). Breaking waves are much more likely to disperse oil and non-breaking waves, in fact the increase may be up to 25% (Zeinstra et al., 2015b). Some researchers have noted poor dispersion in non-breaking waves (Zeinstra et al., 2015b). Turbulence is obviously a good indicator of sea energy, however, values of turbulence are not available to spill modellers except in wave tanks

(Wang and Zhang, 2012; Li and Garrett, 1998; Pan et al., 2016). It has been noted that there is low dispersion when winds are low, in fact no dispersion was seen in one sea trial where the winds were below 5 m/s (Zeinstra et al., 2012b).

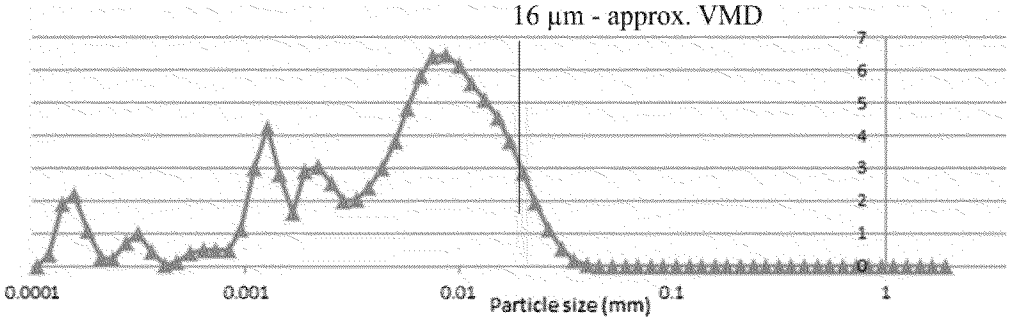

Figure 1 A particle size distribution of a chemically-dispersed oil showing that the main volume is centered at about 16 µm. (Figure courtesy of Robert Faragher, Environment Canada)

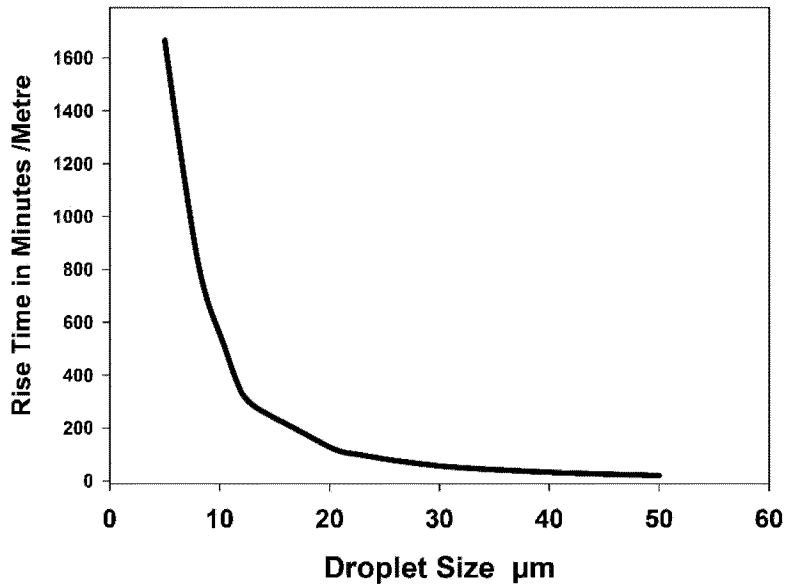

Figure 2 The rise time of droplets of various sizes in the <50 µm range. This shows that droplets larger than about 50 µm do not reside in the water column for very long.

The effect of oil layer thickness has been studied by researchers (Zeinstra et al, 2015b, 2016, Mackay, 1985). One group found that the dispersion rate or entrainment rate was directly proportional to the oil layer thickness. Despite this persuasive argument of including oil layer thickness, no current model has included oil thickness in calculations, simply because it is not a parameter that is available to the spill responder. Zeinstra-Helfrich et al. (2016) conducted experiments with plunging jets and measured large droplets (in millimeter size range). These experiments showed that the amount of oil entrained (in large droplets) did depend on oil layer thickness. This entrainment was increased by the application of dispersants. However, the fact

that small droplets in the micron range were not measured, may not make these experiments relevant to this work.

The distribution of the oil through the water column has been measured by some researchers (Parsa et al., 2016). This group found that the mid-depth concentrations in their flume were 44 to 77 % of the surface concentrations at the surface and that concentrations near the flume bed were 12 to 33% of the mid-depth concentrations. A simplification has appeared in other literature that the concentration is equally spread out to 1.5 times the wave height (Delvigne and Sweeney, 1988). This relationship will be used in this model.

Rising droplets which appear behind the main slick may not be visible or may appear as a tail to the slick giving it the appears of a comet (Zeinstra et al., 2015). The subsequent horizontal and vertical diffusion and movement is not modelled here but is included in most spill models which focus on trajectory prediction.

2 Model Development

The present model was constructed utilizing five basic processes. Initial dispersion was input using a modified Delvigne equation, then the droplet dispersion was distributed over the mixing depth as predicted by the wave height. The droplets rise to the surface according to Stokes' law. The droplets in the water column are subject to coalescence as governed by the Smoluchowski equation. Some oil is 'lost' in the process as a wide spectrum of droplet sizes are created. Very small droplets will rise only very slowly and may not be subject to re-dispersion. Oil on the surface, from the rising oil and that undispersed, is re-dispersed.

The starting point is the work of Delvigne carried out originally for natural dispersion (Delvigne, 1994; Delvigne and Sweeney, 1988: Fingas, 2013a; Johansen et al., 2015). This work was based on extensive experimental work in flumes large and medium-sized. It is important in that it incorporates several important factors such as wind speed, wave height and wave period. Fingas (2013a) worked on this relationship and converted constants in the equation to units of viscosity:

$$F_{(d)} = 6.3x10^{-4}/\rho^{1.5} (34.4 H^2_{rms})^{0.57} (0.032 (U - 5) / T_w) \qquad (6)$$

Where: $F_{(d)}$ Is the fraction of entrained mass rate of droplet sizes in the interval around from 10 to 30 μm - given in fraction/hour,
ρ is the viscosity of the oil in cSt or mPa.s,
H_{rms} is the r.m.s. value of the wave height (m),
U is the wind speed in m/s, and
T_w is the wave period, s.

This is required to be adjusted to chemical dispersion, so setting the optimal conditions for chemical dispersion at optimal conditions of 20 m/sec wind, 8 m wave height, wave period of 11 s and oil viscosity of 100 mPa.s so that the dispersion at these conditions becomes 95% per hour, the constant in the equation becomes 284. This represents an increase of about one half of a million. The equation becomes:

$$F_{(d)} = 284/\rho^{1.5} (34.4 H^2_{rms})^{0.57} (0.032 (U - 5) / T_w) \qquad (7)$$

Where: $F_{(d)}$ Is the fraction of entrained mass rate of droplet sizes in the interval from 10 to 30 μm - given in /hour,

ρ is the viscosity of the oil in cSt or mPa.s,
H_{rms} is the r.m.s. value of the wave height (m),
U is the wind speed in m/s, and
T_w is the wave period, s.

This equation inputs wind speed, wave height and wave period. As there is a relationship among these components in a fully arisen sea (equilibrium between wind and wave conditions), the equation can be simplified (Pierson and Moskowitz, 1964, Wikipedia, 2016). To achieve a fully arisen sea, the conditions in Table 1 apply:

Table 1 Conditions to Achieve a Fully Arise Sea (Wikipedia, 2016)

Wind Speed	Fetch	Wind Duration	Average Wave Height	Wave Length	Wave Period
19 km/h (12 mph)	19 km (12 mi)	2 hr	0.27 m (0.89 ft)	8.5 m (28 ft)	3.0 sec 9.3 ft/sec
37 km/h (23 mph)	139 km (86 mi)	10 hr	1.5 m (4.9 ft)	33.8 m (111 ft)	5.7 sec 19.5 ft/sec
56 km/h (35 mph)	518 km (322 mi)	23 hr	4.1 m (13 ft)	76.5 m (251 ft)	8.6 sec 29.2 ft/sec
74 km/h (46 mph)	1,313 km (816 mi)	42 hr	8.5 m (28 ft)	136 m (446 ft)	11.4 sec 39.1 ft/sec
92 km/h (57 mph)	2,627 km (1,632 mi)	69 hr	14.8 m (49 ft)	212.2 m (696 ft)	14.3 sec 48.7 ft/sec

These conditions can then be used to develop relationships among wind speed, wave height and wave period be using regression and choosing a simple and appropriate model. This is applicable to a fully arisen sea of the specified duration. The following relationships are obtained:

$$\text{Wave height} = 0.0045\ \text{Wind}^{2.5} \quad (8)$$

$$\text{Wave period} = 0.55\ \text{Wind} \quad (9)$$

Where the wave height is in m, Wind is wind speed in m/s and wave period in s.

Substituting these in equation (7) one derives the dispersion equation in wind speed and oil viscosity only. Further the equation is multiplied by 100 to yield the output in percentage.

$$\text{Dispersion (\%)} = 449 * \text{Wind}^{2.85} * (0.58 - 0.29/\text{Wind}) * 1/\rho^{1.5} \quad (10)$$

Where Dispersion is the percent dispersed per hour.
Wind is the wind speed in m/s, and

ρ is the viscosity of the oil in cSt or mPa.s.

One of the factors that becomes important in the above relationship is that of oil viscosity. Oil viscosity increases with weathering. This typically varies with oil type (Guyomarch, et al., 2012). In order to provide an estimate of the change in viscosity of oils, weathering data on several oils (Alaska North Slope, Louisiana, and Alberta Sweet Mixed) were combined and were correlated with time (Fingas, 2013b). This yielded the following simplified relationship (r^2 = 0.76):

New viscosity = 7 + (starting viscosity)*0.3*(hours weathered) (11)

This relationship can then be used to correct oil viscosity for weathering before the dispersion process starts. The longer the oil sits on the water before the dispersion process starts, the more viscous it becomes.

The depth that droplets are injected into the water becomes an important factor (Parsa et al., 2016). Delvigne (1984) experimentally measured droplet injection and found that it was 1 ½ times the wave height over a broad spectrum. This 1.5 factor will then be used to predict how deep droplets are injected with wave height.

The coalescence occurring in the water column is described by Smoluchowski (Rosen and Kunjappu, 2012):

$$\frac{dn}{dt} = 4\pi Drn^2 \qquad (12)$$

Where: $\frac{dn}{dt}$ is the rate of diffusion-controlled coalescence,

D is the diffusion,
r is the collision radius (distance between centres when coalescence begins), and
n is the number of particles per cm^3.

Combining this equation with diffusion equations yields an expression for particle coalescence rate and thus for emulsion stability (Fingas, 2010):

$$\frac{d\bar{V}}{dt} = \frac{4}{3}\frac{Vkt}{\eta}e^{-E/kT} = Ae^{-E/kt} \qquad (13)$$

where $\frac{d\bar{V}}{dt}$ is the rate of the coalescence of droplets or the stability of the emulsion,
V is the volume of the dispersed phase, e.g., volume per unit volume,
k is Boltzmann constant,
T is the absolute temperature,
E is the energy barrier to coalescence,
η is the viscosity of the liquid continuous phase, and
A is the collision factor as defined by the left portion of the equation.

This is the most important equation in describing the stability of oil-in-water emulsions as it shows that the volume and viscosity of the continuous phase (e.g. water), are limiting parameters in describing stability or increased coalescence. In other words, oil spill dispersions in water will always have low stability because water viscosity is low.

Filling in the variables for the CGS system of units and using the values from Sterling (2004) for a system such as this:

$$Droplet\,size = ODS + 0.686(ODS^{0.715}) \qquad (14)$$

Where the droplet size is new droplet size in μm, for one hour and for typical turbulence conditions,
and ODS is the previous droplet size in μm.

The rise of the droplets through the water column to the surface is limiting and is governed by the Stokes rise time (Rosen and Kunjappu, 2012). This is classically given by:

$$s = \frac{2\Delta\rho g a^2}{9\Delta\eta} \qquad (15)$$

where s is the rise rate,
$\Delta\rho$ is the density difference between the disperse and droplet phases,
g is the gravitational constant,
a is the droplet radius, and
$\Delta\eta$ is the difference between the viscosity of the disperse and droplet phases.
Solving equation (7) for cgs units and typical oil densities:

$$S = 3.20\ e^{-07}\ (a)^2 \qquad (16)$$

Where:
S is the rise rate in m/sec
a is the droplet diameter value of the droplet size in μm.
The starting droplet size chosen for this study is 16 μm as this is the typical size for a chemical dispersion (Lehr et al, 2014; Khelifa et al., 2011; Fingas, 2010).

The effect of the droplet size and the increase in droplet size is summarized in Table 2:

Table 2 - Droplet Size and Rise Rate

Hour	Droplet Size VMD (μm)	Rise Rate (M/hour)
0	16	0.3
1	21	0.51
2	27	0.84
3	34	1.33
4	43	2.13
5	53	3.24
6	65	4.87
7	79	7.2
8	95	10.4

An important piece of information is the loss of oil and dispersed oil during the dispersion process (Fingas, 2010; Li et al., 2010). An important loss is the formation of very small oil droplets which rise only slowly and when resurfaced appear some distance away from the main slick. This present model, as do most models, look only at the VMD or volume mean diameter, which is the mean of the cubic volume of droplets. This represents the diameter of the particle of the average volume of the mixture. The VMD lies close to the largest diameter of particles which are in the mixture. Typically, there are many smaller particles and often particles that are one or two orders of magnitude smaller than that of the VMD sizes. These particles will rise to the surface in hours and not minutes and thus are far from the main slick. These droplets might be considered as those 'permanently' dispersed. Several estimates of this loss average range from 2 to 10% (Fingas, 2010; Li et al., 2010). These are the values which will be used in this study.

A summary of the typical and extent of inputs appears in Table 3.

Table 3 Inputs to Modelling

Input to model	Units	Use	Range
Starting oil viscosity	mPa.s (or cSt)	Delvigne Eqn.	20 to 1000
Hours oil on water	hours	to recalculate viscosity	1 to 30
Wave height	m	Depth of Penetration	calculated from wind
Wind speed	m/s	Delvigne Eqn.	5 to 20
Period	s	Delvigne Eqn.	calculated from wind
Loss Rate	%	The loss be hour cycle	2 to 10 %
Length of time to model	hours	When to terminate model	1 to 96

3 Practical Calculations

The conditions set down are fairly extensive and do not enable a simple calculation of dispersion with time. Certain simplifications are necessary to implement a practical model. First, a simplification of the droplet rise calculation will be implemented. Manually plotting a matrix of rise time for various depths using Table 2, one finds that one can simplify and using regression calculate the cycles of rise in hours by using the empirical plot matrices as input. The resulting equation is:

$$\text{Number of hours} = -.388 + 2.51*\text{Depth}^{1/2} \qquad (17)$$

Where the Number of hours is the time that the droplets would arrive at the surface,

Depth is the depth of injection in metres, which can also be calculated from the wind as shown in equation (8).

This result simplifies the calculations and the inclusion of the coalescence in the rise time. The number of cycles/hour is given by 1/number of hours.

The second simplification step is to simplify the major calculation of the oil in the water column at each step. The first step is to calculate the rise time in hours using equation (17). This value then indicates what fraction of the oil rise with each hourly step. The reciprocal of the rise time gives the number of cycles. Table 4 illustrates this calculation. These calculations were performed for more than 600 combinations of inputs of wind speed, oil viscosity, time and loss percent. The outputs chosen are the loss percent (final after considering rise through the water column) and the amount of oil that is still dispersible (on surface or near surface).

The results of the calculations were subjected to regression analysis to yield a simple formula that can be used to estimate the desired outputs without proceeding through a complete tedious calculation as illustrated in Table 4. In addition to regression, the total errors were minimized by adjust the constants. The resulting R^2s are 0.55. The resulting equations are:

$$\text{Loss} = -8 + 1.51*\text{Time} + 0.0031*\text{Wind}^{2.85} - 1.36*\rho^{0.5} + 1.75*\text{Input Loss} \quad (18)$$

$$\text{Dispersible} = 102 + -1.51*\text{Time} - 0.0031*\text{Wind}^{2.85} - 1.82*\rho^{0.5} - 1.74*\text{Input Loss} \quad (19)$$

Where **Loss** is the total loss percent over the time of calculation, this is the oil that is truly dispersed and the values should be limited to values of 0 to 100,
Time is time in hours or fractions thereof,
Wind is the wind speed in m/s,
Input loss is the predetermined fixed percentage estimated that is lost per cycle, typically 2 to 10%, this also can be given by the percentage of droplets below a certain size,
ρ is the viscosity of the oil in cSt or mPa.s,
Dispersible is the amount of oil that remains on the surface or near surface that is still dispersible, 100 less the dispersible is the amount dispersed (loss) at a point in time, Dispersible values should be limited to 0 to 100.

Equations (18) and (19) provide a rapid method of estimating outputs with all four inputs of time, wind speed, oil viscosity and input loss. While the accuracy is less than the detailed matrix calculation, estimations can be obtained in rapid order.

Detailed calculation steps are given in Table 5.

Table 4 - Example of Exact Matrix Calculation						
Values						
A	Dispersion % applicable - calculated by equation (10)					
B	Fraction Dispersed per hour = reciprocal of value from equation (17)					
C	Loss - an input value between 2 to 10%					
D	Interim sum of values dispersed					
E	Sum of all losses to point					
	Example Matrix					
Hour	Dispersed					
1	A					
2	B*A - C*A				Sum row	D1
3	B*D1 - C*D1	B*D1 - C*D1			Sum row	D2
4	B*D2 - C*D2	B*D2 - C*D2	B*D2 - C*D2		Sum row	D3
5	B*D3 - C*D3	B*D3 - C*D3	B*D3 - C*D3	B*D3 - C*D3	Sum row	D4
6	B*D4 - C*D4	B*D4 - C*D4	B*D4 - C*D4	B*D4 - C*D4	Sum row	D5
7	B*D5 - C*D5	B*D5 - C*D5	B*D5 - C*D5	B*D5 - C*D5	Sum row	D6
	Sum of losses				Total sum of losses -	
note this is an example where there are 4 rise portions, B						

Table 5 Detailed Calculation Steps

Step	Procedure		Units
1	Collect input values		
	ρ	Starting oil viscosity	mPa.s (or cSt)
	t	Hours oil on water	hours
	Wind	Wind speed	m/s
	Wave Height	Calculate from wind using eqn. (8)	
	Time	Length of time to model	hours
	Input Loss	Estimate % loss or tiny droplets	%
2	Adjust oil viscosity to time of model start		ρ
	use equation (11)		
3	Calculate the starting maximum dispersion		%
	use equation (10)		
4	Estimate the number of cycles until oil resurfaces		
	use equation (17) to find time to resurface		hours
	then 1/hours is the cycles per hour		cycles
	the fraction returning each hour then is 1/cycles		
	(the equation (17) also includes the effect of coalesence)		
5	Set up a matrix as shown in Table 4		
	calculate the resulting dispersion and loss		

until the desired time

6 A less accurate way, but simpler would be to use equation (18)

4 Model Assessment

It would be useful to compare the predicted dispersion with and without the injection and rising of droplets into and from the water column. Figure 3 shows the dispersion of oil using equation (10) which does not include the effect of droplet injection and rising. Figure 4 shows a similar graph with the effect of droplet injection and rising. A comparison of these shows that dispersion percent is far less when droplet injection and rising are considered. The comparison made does not consider time and fixed loss percent as shown in Figure 3.

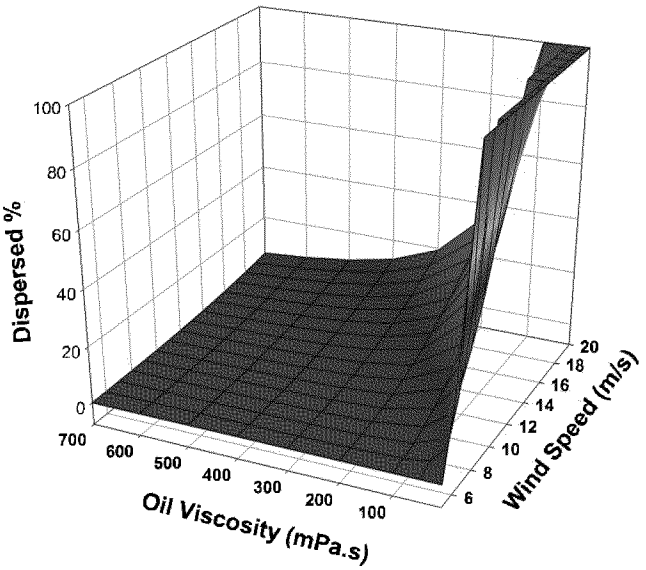

Figure 3 Graph of the percent dispersion with oil viscosity and wind speed without the effect of droplet injection and rising.

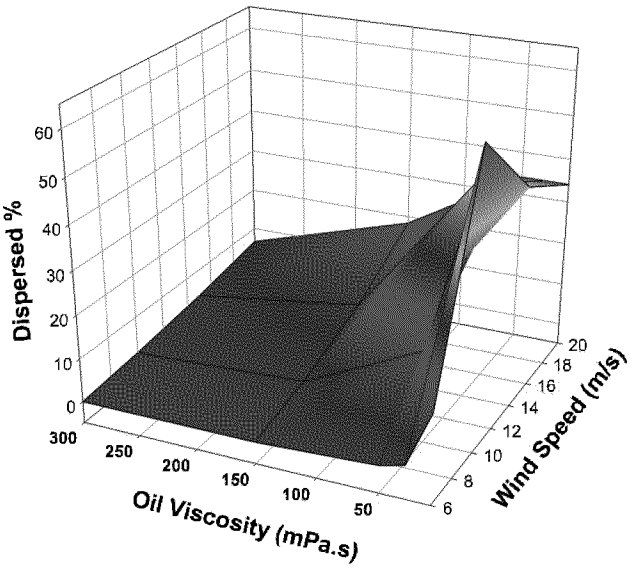

Figure 4 Graph of the percent dispersion including the effect of dispersant rising. This graph shows the effect at 15 hours and with a pre-established loss of 5%. At 15 hours, the peak dispersion is 60% compared to 100% without the effect of droplet injection, rising and coalescence.

As can be seen by a comparison of Figures 3 and 4, there is a major difference between the two graphs. The effect of dispersion at 50 hours only reaches a maximum effectiveness of about 60% while that without the effect of injection and droplet rising as shown in Figure 3 shows an effectiveness of about 100% maximum. This is also because dispersion in the new model includes only the droplets that do not rise rapidly. The effect of time after dispersion is evident in the new dispersion model. This time effects both the amount dispersed and the cumulative loss. Figure 5 and Figure 6 show the effect of time with a given set of conditions.

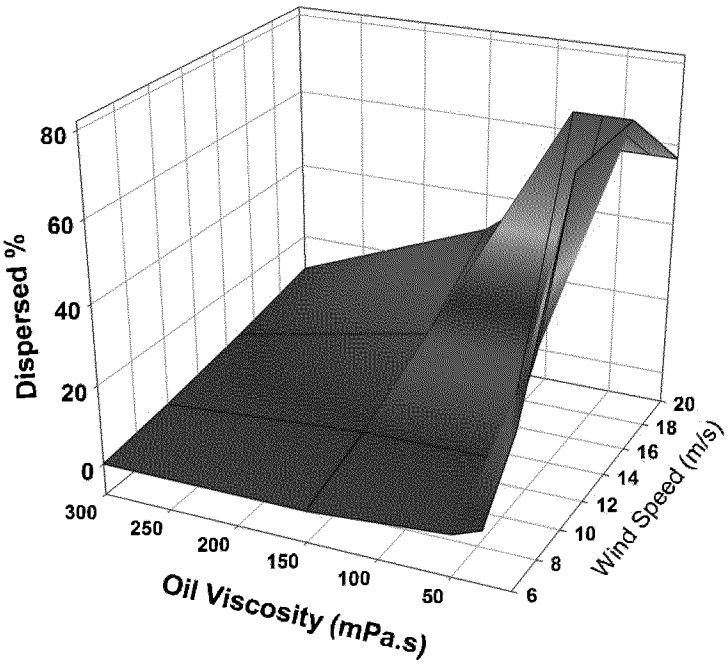

Figure 5 Graph of the percent dispersion including the effect of dispersant rising. This graph shows the effect at 20 hours and with a pre-established loss of 10%.

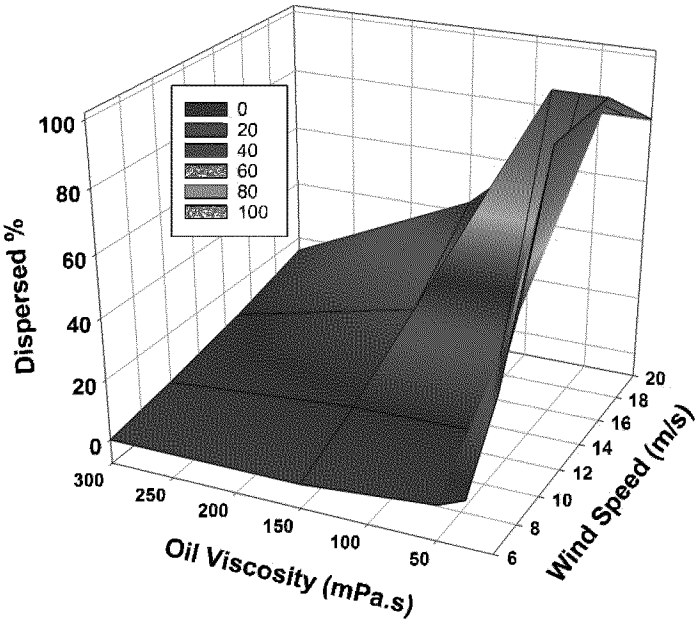

Figure 6 Graph of the percent dispersion including the effect of dispersant rising. This graph shows the effect at 30 hours and with a pre-established loss of 10%.

Figures 5 and 6 show the effect of time on dispersant rising. The length of time increases the amount that is actually lost. Thus, time can compensate somewhat for oil viscosity and wind speed. The difference between 20 and 30 hours shows a maximum effectiveness difference of

about 20% (between 80 and 100%). Figure 7 shows the effect of time that is isolated from other effects.

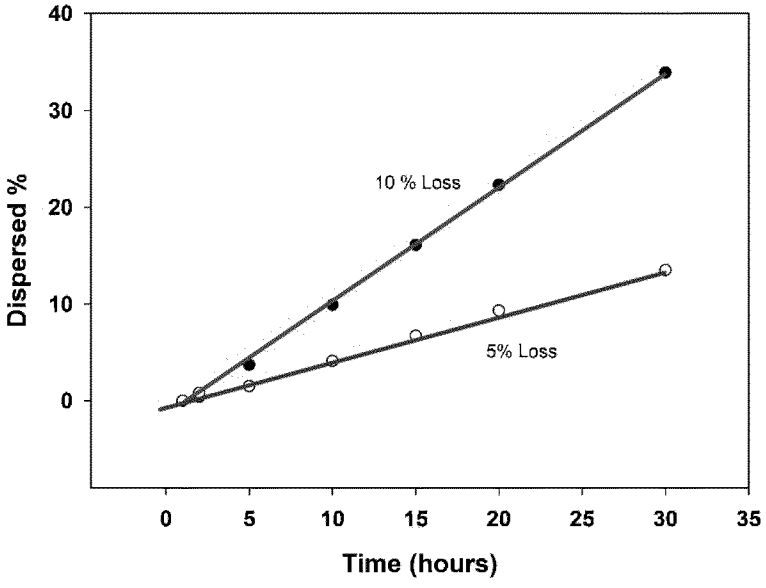

Figure 7 Graph of the dispersion show the effects of time after dispersion at two different pre-set loss rates. This shows that the dispersion approximately doubles every half day or 12 hours. This will end when the maximum amount or 100% is reached.

Figure 7 shows that dispersion is compensated for during time when considering only the small droplets (input loss) as being actually dispersed. This is further illustrated in Figures 8 and 9.

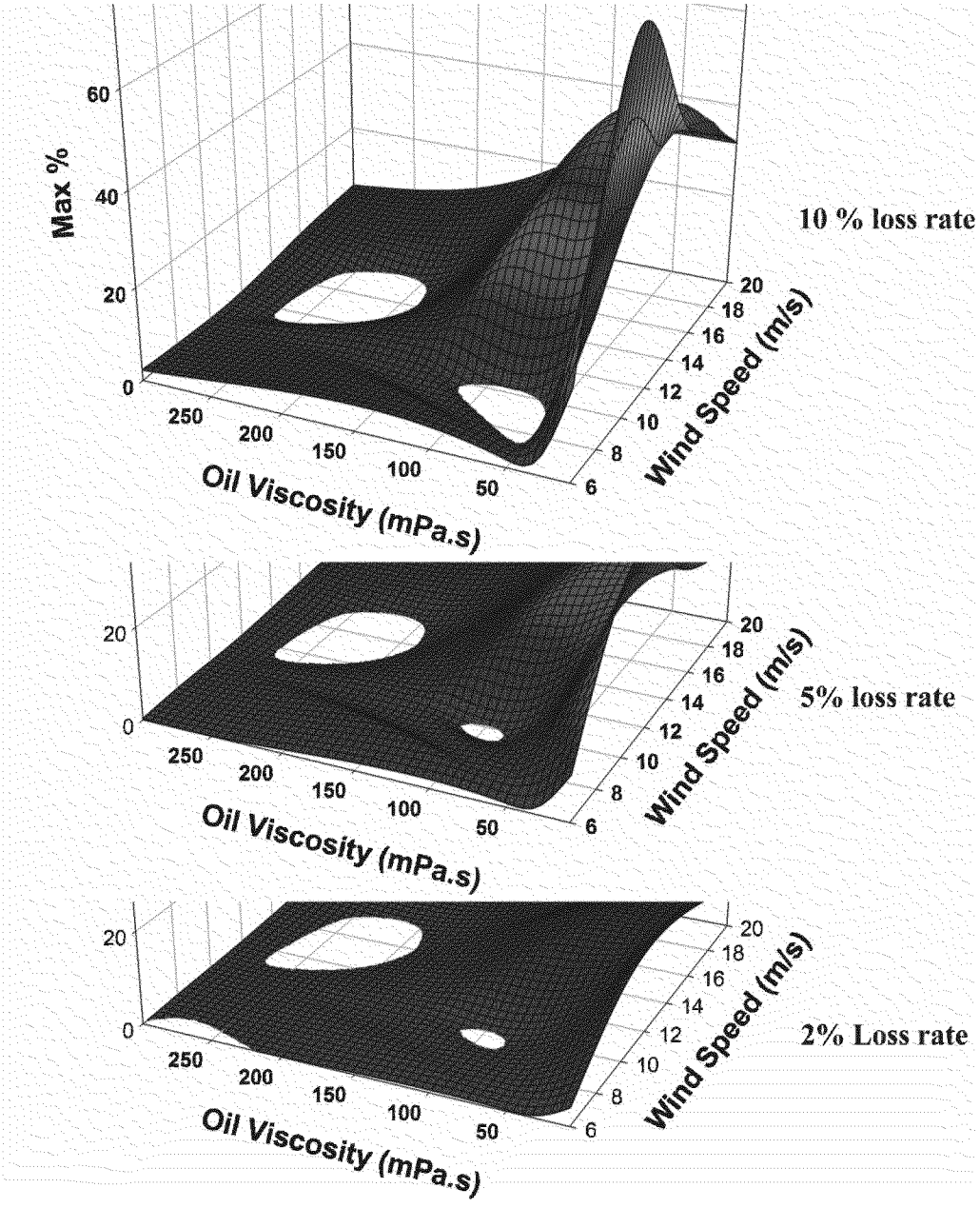

Figure 8 Graph of the maximum total loss (permanently dispersed) percentage with viscosity and wind speed inputs at various input loss rates and at 10 hours after initial dispersion.

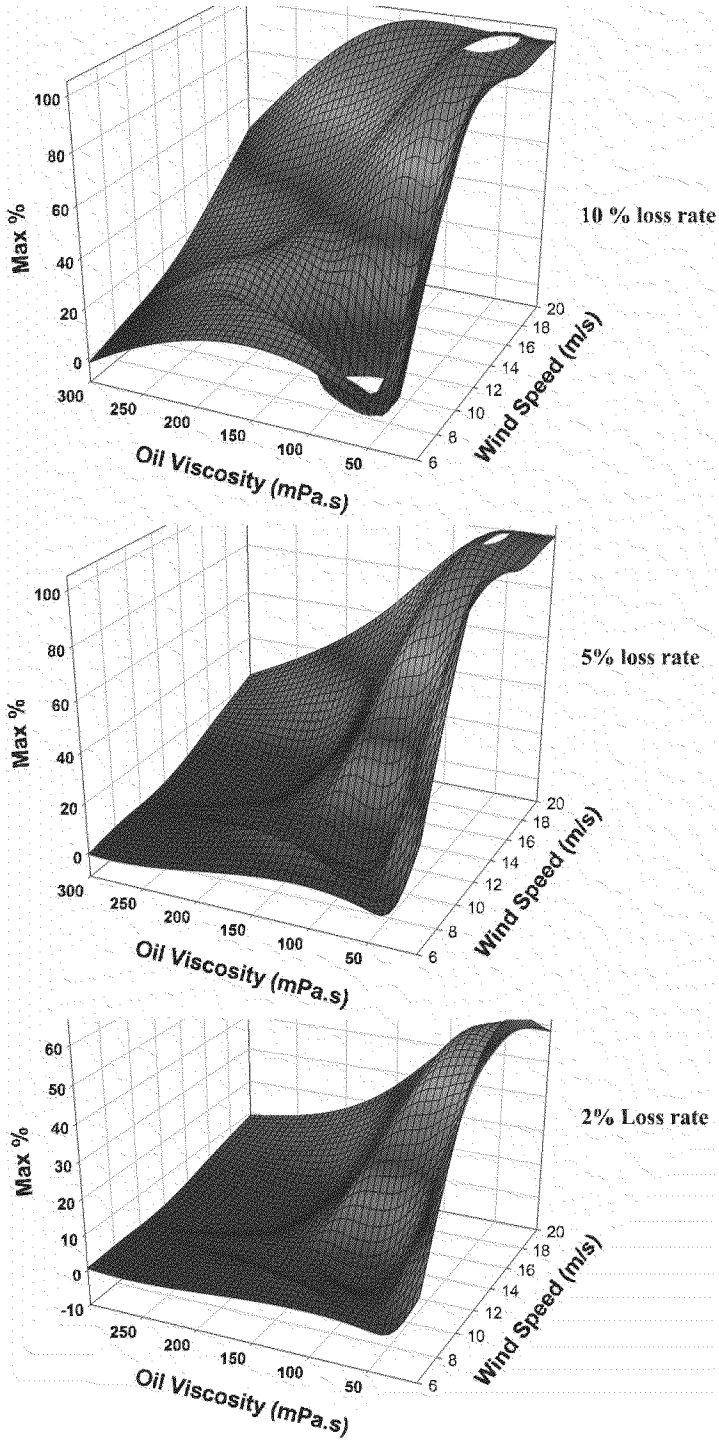

Figure 9 Graph of the maximum total loss (permanently dispersed) percentage with viscosity and wind speed inputs at various input loss rates and at 30 hours after initial dispersion.

Another model of chemical dispersion was recently published by Johansen et al. (2015). The model was developed from a theoretical point of view and then fit to experimental data from a wave tank experiment. A simplified version of this was developed as well:

$$\frac{dC_s}{dt} = -\alpha C_s \qquad (20)$$

Where: $\frac{dC_s}{dt}$ is the rate of mass disappearance (Kg/s),

C_s is the starting mass, kg, and

$$\alpha = p\ WCC/Tm \qquad (21)$$

Where in turn, p is the volume fraction of oil contained in oil droplets smaller than the limiting diameter D*, here taken as 0.00054,

WCC is the white cap coverage, which as suggested by Johansen et al as:

$WCC(\%) = 3.18 \times 10^{-3} (U-3.7)^3$ (for wind speeds between 3.7 and 11.25 m/s) (22)

$WCC(\%) = 4.82 \times 10^{-4} (U+1.98)^3$ (for wind speeds between 9.25 and 23.1 m/s) (23)

Tm is the wave period, which can be given as equation (9) or 0.55*Wind.

Equation 20 can be solved by converting it into percentage by multiplying C_s by 100. Similarly dividing by 3600 will convert the equation into % per hour to be consistent with the values used in this paper. The following equations result:

$C = 0.636 * (U-3.7)^3 / 0.55U$ (for wind speeds between 3.7 and 11.25 m/s) (24)

$C = 0.0964 * (U+1.98)^4 / 0.55U$ (for wind speeds between9.25 and 23.1 m/s) (25)

Where: C is the percent dispersed per hour,

U is the wind speed in m/s.

This model is compared with the results of the current model as shown in Figure 10. This figure shows that the Johansen et al. model results in very similar results to the modified Delvigne model as presented in equation (10). The addition of droplet and injection considerations reduces the amount dispersed, however, with time these increase slowly.

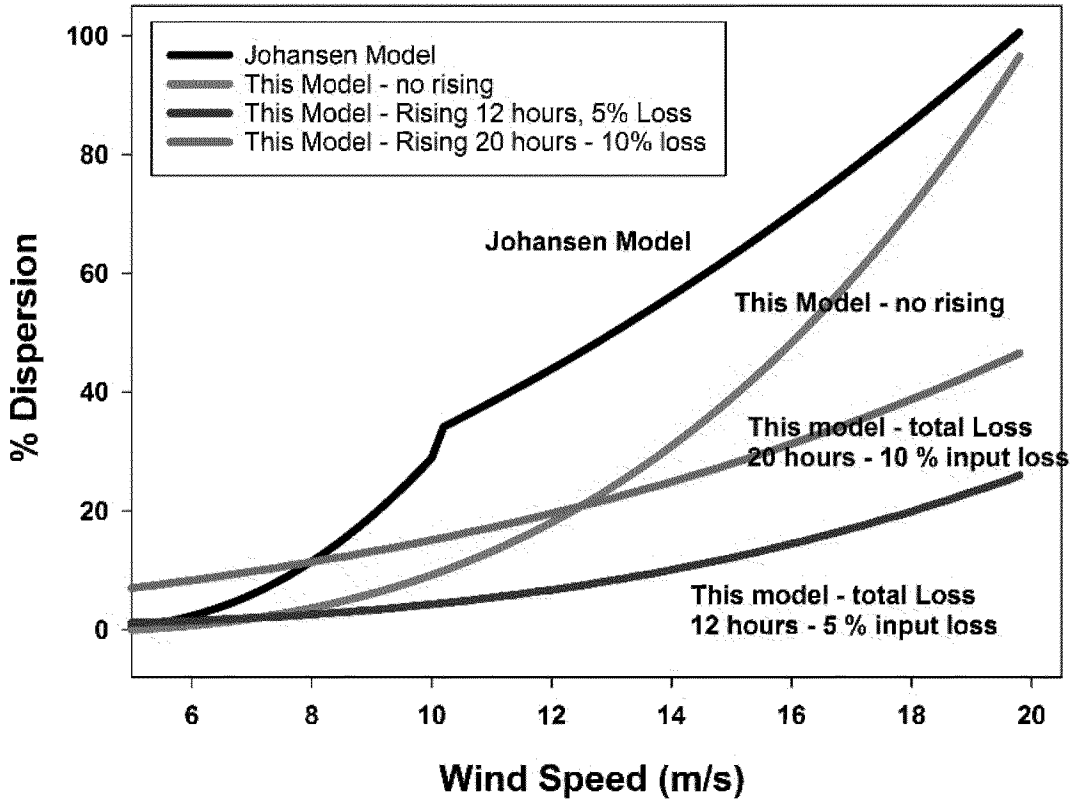

Figure 10 A comparison of four models over a range of winds, the Johansen model, this paper's model without injection-rising effects, and two instances of models from this paper with the effects of injection and rising of droplets. The parameters for this paper's models were set as oil with 100 mPa.s viscosity, and those with the injection-rising effect were taken at 12 and 20 hours, and input loss rates of 5 and 10 % respectively. The parameters for the latter two models were calculated using equation (18).

5. Results and Discussion

A new model for predicting the chemical dispersion was developed using an empirical model by Delvigne. This natural dispersion model was first modified by substituting oil viscosity for constants in the equation with the same units. Second the model was calibrated to a chemical dispersant situation by adjusting the equation to yield 100% initial dispersant effectiveness for a 100 mPa.s oil. This adjustment involves about 500,000 times adjustment to the equation's constant. The essential feature of the model is that it considers the injection of droplets, the subsequent rising and coalescence of these droplets to the surface. Since dispersion involves a wide spectrum of droplet sizes, it is calculated here that the very small droplets (probably less than about 1 μm) do not rise sufficiently to reform slicks and thus may be 'permanently' dispersed. Droplets are injected one and a half times the significant wave height into the water column. The droplets that are rising are subject to coalescence as predicted by the Smoluchowski equation. This effect is included in the calculations. The coalescence effect is profound and

results in almost 50% increase in droplet size per hour and nearly a logarithmic decrease in their rise time.

This new model includes the properties of the oil (viscosity), droplet size, as well as wave conditions and wind conditions. This is the only model that also considers the injection and rising of the droplets as well as the coalescence that occurs among the droplets. The results compared to conventional dispersion models shows that considering the injection, rise and coalescence of droplets results in lower dispersion at given times, however over time this amount dispersed does increase. At some time, however, the practicality of the particular dispersion may be limited. Perhaps consideration should not extend past 12 to 24 hours.

Comparison of the new model with another model (Johansen et al., 2015) shows that the base model yields very similar results, without the consideration of injection, rise and coalescence of the droplets in the water column. Once these water column considerations are included, the comparison is less consistent. The inclusion of water column considerations decreases the amount dispersed at a given point in time because only the smaller droplets are considered to be 'permanently' dispersed and because there is still oil rising in the water column. The new model also has the effect of stretching out the time scale at which dispersion occurs.

There are a number of considerations that could not be included in the model, because of lack of information. There is a net loss of surfactant in dilute emulsions such as oil spill dispersions. This net loss is caused by the tendency of the surfactants to equilibrate between the water bulk phase and the oil droplet interface. As crude oil emulsions are continually being diluted, surfactant desorption from the interface to achieve equilibrium constitutes a loss of surfactant to the system. This loss of surfactant accelerates emulsion destabilization. This basically was not modeled, although the coalescence was modeled by the Smoluchowski equation. Another consideration that was not modeled was the specific oil-dispersant effectiveness. It is known that other properties of the oil, other than viscosity, play a role in the dispersant process. This effect might be included by varying parameters in the initial model dependent on specific oil-dispersant tests. The terminal time that the dispersion is effective is relevant, was not evaluated as there is no data. It is not known if dispersion would be relevant at 12, 20 or even 30 hours, as modelled here. Effects as such dispersant loss from droplets may end effective dispersion.

References

Delvigne, G.A.L., "Natural and Chemical Dispersion of Oil," *Journal of Advanced Marine Technology Conference*, Vol. 11, pp. 23-40, 1994.

Delvigne, G.A.L. and C.E. Sweeney, "Natural Dispersion of Oil," *Oil and Chemical Pollution*, Vol. 4, pp. 281-310, 1988.

Fingas, M.F., Z. Wang, B. Fieldhouse, and P. Smith, "The Correlation of Chemical Characteristics of an Oil to Dispersant Effectiveness," in *Proceedings of the Twenty-Sixth Arctic and Marine Oil Spill Program Technical Seminar*, Environment Canada, Ottawa, Ontario, pp. 679-730, 2003.

Fingas, M., "Models of Oil Spill Dispersion Stability," in *Proceedings of the Thirty-third Arctic and Marine Oil Spill Program Technical Seminar*, Environment Canada, Ottawa, Ontario, pp. 555-586, 2010.

Fingas, M., "A Review of Natural Dispersion Models," in *Proceedings of the Thirty-Sixth Arctic and Marine Oil Spill Program Technical Seminar*, Environment Canada, Ottawa, Ontario, pp. 207-233, 2013a

Fingas, M., "Modeling Oil and Petroleum Evaporation," *Journal of Petroleum Science Research,* (JPSR), Volume 2, Issue 3, July, 2013b.

Fingas, M., "Oil Spill Dispersants: A Technical Summary," Chapter 15, in *Oil Spill Science and Technology*, M. Fingas, Editor, Gulf Publishing Company, NY, NY, pp. 435-582, 2011.

Guyomarch, J., S. Le Floch, and R. Jezequel, "Oil Weathering, Impact Assessment and Response Options Studies at the Pilot Scale: Improved Methodology and Design of a New Dedicated Flume Test," *Proceedings of the 35th AMOP Technical Seminar on Environmental Contamination and Response*, pp. 1001-1017, 2012.

Johansen, T., M. Reed, and M.R. Bodsberg, "Natural Dispersion Revisited," *Marine Pollution Bulletin*, 93 (1-2), pp. 20-26, 2015.

Khelifa, A., D.M. Charron, T.-S. Tong, and N.R. Singh, "Effects of Chemical Dispersants on Oil-brine Interfacial Tension and Droplet Formation: New Results Using New High Resolution Imaging Setup and Weathered Oils," P*roceedings of the 34th AMOP Technical Seminar on Environmental Contamination and Response*, pp. 865-879, 2011.

Lehr, W., D. Simecek-Beatty, A. Aliseda, and M. Boufadel, "Review of Recent Studies on Dispersed Oil Droplet Distribution," *Proceedings of the 37th AMOP Technical Seminar on Environmental Contamination and Response*, pp. 1-8, 2014.

Li, M., and C. Garrett, "The Relationship Between Oil Droplet Size and Upper Ocean Turbulence," *Marine Pollution Bulletin*, 36 (12), pp. 961-970, 1998.

Li, Z., K. Lee, T. King, M.C. Boufadel, and A.D. Venosa, "Oil Droplet Size Distribution as a Function of Energy Dissipation Rate in An Experimental Wave Tank," Proceedings *of the International Oil Spill Conference - IOSC 2008*, pp. 621-626, 2008.

Li, Z., K. Lee, T. King, M.C. Boufadel, and A.D. Venosa, "Evaluating Chemical Dispersant Efficacy in An Experimental Wave Tank: 2-Significant Factors Determining In-situ Oil Droplet Size Distribution," *Environmental Engineering Science*, 26 (9), pp. 1407-1418, 2009.

Li, Z., K. Lee, T. King, M.C. Boufadel, and A.D. Venosa," Effects of Temperature and Wave Conditions on Chemical Dispersion Efficacy of Heavy Fuel Oil in an Experimental Flow-through Wave Tank," *Marine Pollution Bulletin*, 60 (9), pp. 1550-1559, 2010.

Mackay, D., A. Chau, K. Hossain, and M. Bobra, "Measurement and Prediction of the Effectiveness of Oil Spill Chemical Dispersants," in *Oil Spill Chemical Dispersants: Research, Experience and Recommendations*, T.E. Allen (ed.), STP 840, American Society for Testing and Materials, Philadelphia, Pennsylvania, pp. 38-54, 1984.

Mackay, D., "Chemical Dispersion: A Mechanism and a Model," in *Proceedings of the Eighth Arctic Marine Oilspill Program Technical Seminar*, Environment Canada, Ottawa, Ontario, pp. 260-268, 1985.

Mukherjee, B., B.A. Wrenn, and P. Ramachandran, "Relationship Between Size of Oil Droplet Generated During Chemical Dispersion of Crude Oil and Energy Dissipation Rate: Dimensionless, Scaling, and Experimental Analysis," *Chemical Engineering Science*, 68 (1), pp. 432-442, 2012.

Pan, Z., L. Zhao, M.C. Boufadel, T. King, B. Robinson, R. Conmy, and K. Lee, "Impact of Mixing Time and Energy on the Dispersion Effectiveness and Droplets Size of Oil," *Chemosphere*, 166, pp. 246-254, 2017.

Parsa, R., M. Kolahdoozan, and M.R.A Moghaddam, "Vertical Oil Dispersion Profile under Non-Breaking Regular Waves, *Environmental Fluid Mechanics*, 16 (4), pp. 833-844, 2016.

Pierson, W.J., Jr. and L.A. Moskowitz, "Proposed Spectral Form for Fully Developed Wind Seas Based on the Similarity Theory of S. A. Kitaigorodskii," *Journal of Geophysical Researc*h, Vol. 69, p.5181-5190, 1964.

Reed, M., *Technical Description and Verification Tests of OSCAR2000, A Multi-Component 3-Dimensional Oil Spill Contingency and Response Model*, SINTEF Report, 2002.

Reed, M., P. Daling, A. Lewis, M.K. Ditlevsen, B. Brørs, J. Clark, and D. Aurand, "Modelling of Dispersant Application to Oil Spills in Shallow Coastal Waters," *Environmental Modelling and Software*, 19 (7-8), pp. 681-690, 2004.

Rosen, M.J. and J.T. Kunjappu, *Surfactants and Interfacial Phenomena, Fourth Edition*, Wiley Interscience, NY, 2012.

Sterling, M.C., J.S. Bonner, A.N.S. Ernest, C.A. Page, and R.L. Autenreith, "Chemical Dispersant Effectiveness Testing: Influence of Droplet Coalescence," *Marine Pollution Bulletin*, Vol. 48, pp. 969-977, 2004.

Wang, J.-H., and J.-S Zhang, "Specification of Turbulent Diffusion by Random Walk Method for Oil Dispersion Modeling," *Applied Mechanics and Materials*, 212-213, pp. 1161-1167, 2012.

Wikipedia, "Wind Wave," Wikipedia, Accessed November, 2016.

Zeinstra-Helfrich, M., W. Koops, and A.J. Murk, "The NET Effect of Dispersants - A Critical Review of Testing and Modelling of Surface Oil Dispersion," *Marine Pollution Bulletin*, 100 (1), pp. 102-111, 2015a.

Zeinstra-Helfrich, M., W. Koops, K. Dijkstra, and A.J. Murk, "Quantification of the Effect of Oil Layer Thickness on Entrainment of Surface Oil," *Marine Pollution Bulletin*, 96 (1-2), pp. 401-409, 2015b.

Zeinstra-Helfrich, M., W. Koops, and A.J. Murk, "How Oil Properties and Layer Thickness Determine the Entrainment of Spilled Surface Oil," *Marine Pollution Bulletin*, 110 (1), pp. 184-193, 2016.

Impact of Subsurface Dispersant Treatment on Deepwater Horizon (DWH) Spill: May 10-12, 2010 Treatment Event

Malcolm L. Spaulding[1], Deborah French-McCay[2], and Deborah Crowley[2]
[1] Ocean Engineering, University of Rhode Island, Narragansett, RI 02882 USA,
spaulding@egr.uri.edu
[2] RPS ASA, 55 Village Square Drive, South Kingstown, RI 02879 USA,
Debbie.McCay@rpsgroup.com, Deborah.Crowley@rpsgroup.com

Abstract

To experimentally assess the impact of subsurface dispersant treatment on surface oiling during the Deepwater Horizon spill, subsurface dispersant application was suspended from May 5 to 10, 2010, restarted late in the day on May 10, continued for a period of about 24 hrs, and then suspended again late in the day on May 11 through May 14 and restarted on May 15. Aerial imagery at the spill site during this period shows the presence, disappearance, and then reappearance of thick oil at the surface. An evaluation was performed to determine whether this temporal variation in thick oil could be explained by changes in surface entrainment due to breaking waves or surface or subsurface application of dispersants. Breaking wave induced entrainment was ruled out as the causative factor, since the wind speeds and wave heights measured at a nearby buoy did not indicate large changes correlated with the dramatic changes in observed surface oil volume. Surface dispersant treatment was also ruled out since the flight paths for aerial dispersant applications during this period were well to the east of the spill site. Application of the OILMAP DEEP blowout and SIMAP, spill transport and fate, models showed that the subsurface application of dispersants and its impact on droplet size distributions qualitatively explains the change in amount of oil at the sea surface during the May 10 to 12, 2010 treatment event and gives results that are fully consistent with the observations.

1. Background

To assess the impact of subsurface dispersant treatment on surface oiling during the Deepwater Horizon spill, dispersant application was halted from May 5, 2010 until 4:30 AM CDT (Central Daylight Time) on May 10, 2010; dispersant treatment then resumed until 4:30 AM CDT on May 11, 2010, and then halted again until May 15, 2010. Ocean Imaging Inc. (OI) used aerial imagery taken during this time period to develop estimates of the area covered and oil thicknesses in the immediate vicinity of the spill site (Svejkovsky et al, 2012; Svejkovsky and Hess, 2012). Analyses were performed for images available on May 10, 2010 at 8:30 AM (CDT) and 5:05 PM (CDT); May 11, 2010 at 9:15 AM (CDT); and May 12, 2010 at 8:35 AM (CDT) (Figure 1). The images have a spatial resolution of 2.7 m. The circles shown in the lower panel of the figure have a diameter of approximately 10 km. The star denotes the location of the wellhead. Table 1 (provided by Ocean Imaging) summarizes the area within each thickness class for each date. The volume of oil was estimated using the mean value from thickness ranges recommended by Ocean Imaging (Mark Hess, personal communication, August 7, 2013) (Table 2).

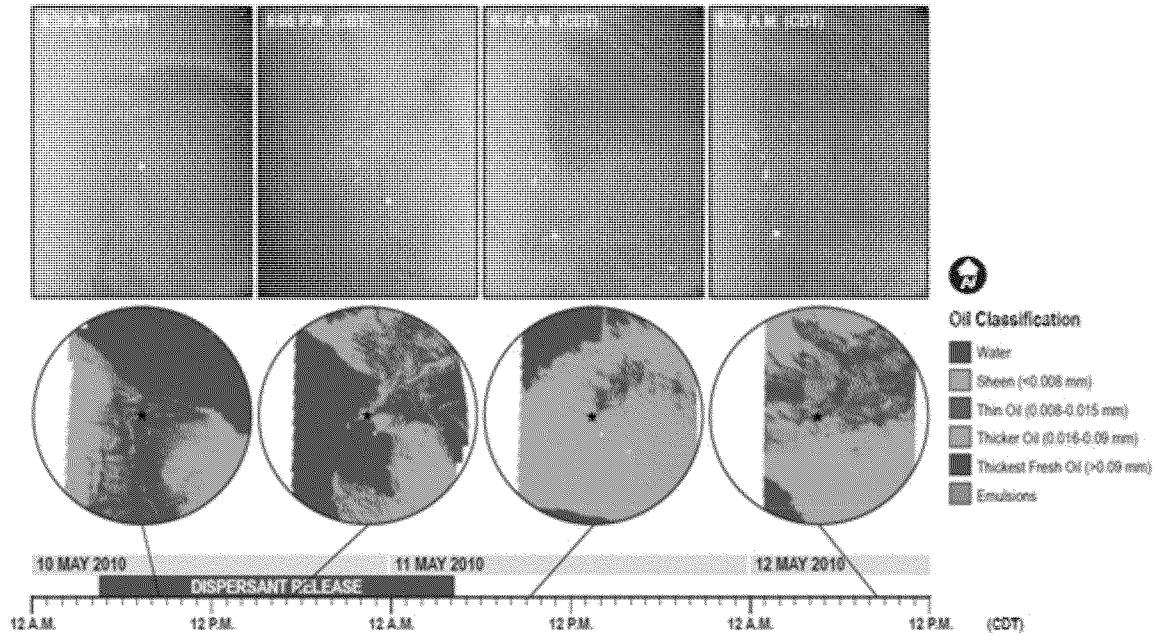

Figure 1. Areal images (upper panel) and estimated thickness contours (mid panel) in the vicinity of the DWH spill site for May 10 to 12, 2010. The spill site is noted by the black star in the center of each image. The lower panel shows the timeline (all times in CDT) for the observations and the subsurface dispersant application. Figure courtesy of Ocean Imaging.

The areal imagery data shows evidence of thick oil emanating from the vicinity of the spill site (red streak) for the images on the morning of May 10 and from May 11 and 12 (Figure 1). In contrast, imagery on May 10 at 5:05 PM still shows oil emanating from the spill site but at a much lower rate since the slick thickness is reduced from thick fresh oil (red) to a thin sheen (green). The winds were toward the S and SW at 5 to 6 m/sec early on May 10 and switched directions toward the NW later in the day on May 10 and through May 12, with similar wind speeds. The wind speed and direction, obtained from NOAA NDBC buoy #42040, are shown in Figure 2 from May 9 to 14, 2010 (CDT). The times of the images, shown in Figure 1, are noted by the vertical lines. The thick fresh oil distribution ribbon oriented NNW to SSE at 8:30 AM on May 10 is clearly observed in approximately the same orientation but advected (~2.5 km) to the ENE later in the day at 5:05 PM.

Figure 3 shows the estimated volume of oil on the sea surface for each thickness class and the total amount for each observation date. This analysis shows a substantial decrease in the total volume of oil and the volumes in the thick and thicker classes late in the day on May 10, 2010, with higher values prior to, and after this time. The total volume begins at 689 m^3, declines to 370 m^3 at the low point, and then increases to 1100 m^3 during the last two measurements. The volumes of the oil sheen and emulsion classes remain almost unchanged while the thin oil disappears late in the day on May 10, but returns to earlier volume levels after this date. While the exact volumes are sensitive to the assumed values for thicknesses (See Table 2) (+/- 50 % change in volumes for upper and lower bound thickness estimates) the trends of the loss of oil from thick and thicker classes late in the day on May 10 are clear; no matter what values are selected. A review of Figure 1 shows that the origin of the thick and thicker oil is immediately

above the spill site (black star in the middle panel of the figure) for the May 10 (morning) and May 11 and 12 images but detached from the spill site for the May 10 (late in day) image.

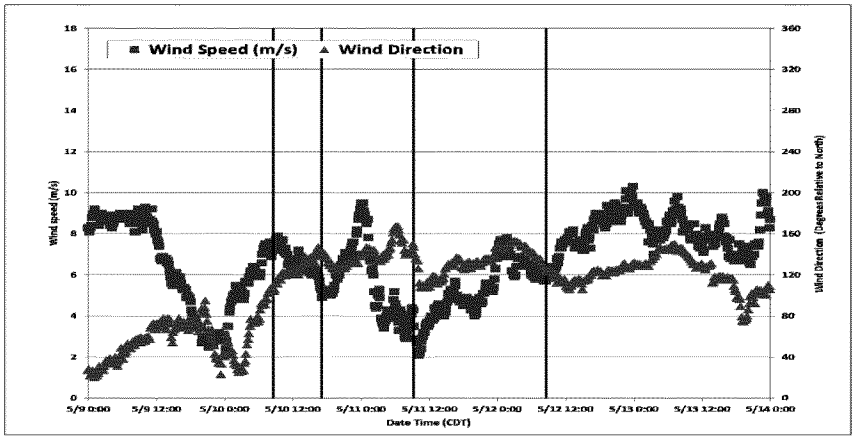

Figure 2 **Time series of wind speed and direction from NOAA NDBC Buoy 42040 from May 9 to May 14, 2010 (CDT). The vertical lines denote the times when the images shown in Figure 1 were available from Svejkovsky and Hess (2012). (Wind direction is from which the winds are blowing).**

The oil release rate during this period was estimated to be constant at 60,000 barrels per day or 9,534 m^3/day. The remotely sensed image on May 10, 8:30 AM CDT shows a linear thread of thick oil emanating from the spill site directed to the south. This linear feature has been advected to the east north east (ENE) by the time of the next image on May 10, 5:05 PM CDT. Note there is no thick oil observed at the spill site at this time. The advection rate appears to be 0.3 km/hr (transport of 2.5 km between 8:30 AM and 5:05 PM; approximately 8.5 hr). If the surface oil is assumed to have a residence time of approximately 16.6 hr (5 km divided by 0.3 km/hr = 16.6 hr) within the 10 km diameter observation circle, then the percent of the oil released from the blowout and observed at the surface is 10.4% on the morning of May 10, 5.6 % later in the afternoon on May 10, and 16.7% on May 11 and 12.

The question is what caused the dramatic decrease in surface oiling in the immediate vicinity of the spill site during this period. Can it be attributed to entrainment of oil due to breaking waves or to dispersant application either at the surface or applied subsurface at the blowout release site, all of which would remove oil from the sea surface for a short period of time? Each possibility is explored in more depth in Section 3. Study conclusions are provided in Section 4 and references in Section 5.

Table 1: **DWH - Ocean Imaging DMSC-derived oil thickness class area within 5 km radius from well head location.**

Date	Time	Class	Area (km^2)	Thickness assumed (mm)	Volume (m^3)
5/10/2010	**13:07-14:00 UTC**	No Data	8.3	-	-
		Water	25.9	-	-

		Sheen	25.1	0.004	100.4
		Thin	15.7	0.0115	180.4
		Thicker	0.6	0.048	29.8
		Thickest	2.4	0.145	348.5
		Emulsion	0.15	0.2	30.2
				Total	**689.3**

Date	**Time**	**Class**	**Area (km^2)**	**Thickness assumed (mm)**	**Volume (m^3)**
5/10/2010	**21:51-22:22 UTC**	No Data	10.5	-	-
		Water	27.0	-	-
		Sheen	23.9	0.004	95.6
		Thin	15.7	0.0115	180.2
		Thicker	0.75	0.048	35.9
		Thickest	0.23	0.145	33.3
		Emulsion	0.12	0.2	24.9
				Total	**370.1**

Date	**Time**	**Class**	**Area (km^2)**	**Thickness assumed (mm)**	**Volume (m^3)**
5/11/2010	**14:05-14:49 UTC**	No Data	9.5	-	-
		Water	10.3	-	-
		Sheen	45.2	0.004	180.7
		Thin	0	0.0115	0
		Thicker	10.0	0.048	484.0
		Thickest	3.0	0.145	430.9
		Emulsion	0.08	0.2	16.5
				Total	**1112.3**

Date	**Time**	**Class**	**Area (km^2)**	**Thickness assumed (mm)**	**Volume (m^3)**
5/12/2010	**13:28-14:06 UTC**	No Data	17.7	-	-
		Water	2.3	-	-
		Sheen	34.8	0.004	139.1
		Thin	13.6	0.0115	156.3

Thicker	5.7	0.048	275.9
Thickest	4.0	0.145	585.8
Emulsion	0.03	0.2	5.9
		Total	**1163.3**

Table 2: Ocean Imaging LLC assumed thickness ranges by oil class

Class	Thickness Range	Assumed Thickness
Sheen	< 0.008 mm	0.004 mm
Thin	0.008 - 0.015 mm	0.0115 mm
Thick	0.016 - 0.08 mm	0.048 mm
Thickest	> 0.09 mm	0.145 mm
Emulsion	Thickness not defined	0.2 mm (estimate)

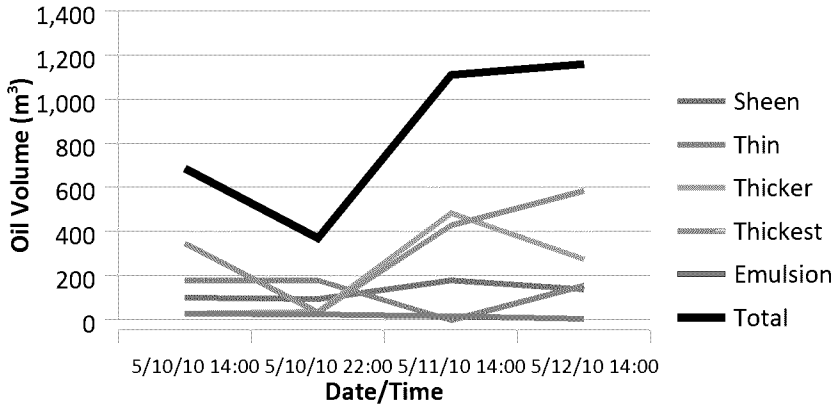

Figure 3. Estimated oil volume for each oil class and total oil for each analysis date shown in Figure 1, within a 5 km radius of the spill site. Note there was no thin oil observed on May 11, 2010.

2. Evaluation of Alternate Explanations

2.1 Entrainment of Oil Due to Breaking Waves

A review of the historic wind information from the offshore buoy (NOAA NBDC 42040) (Figure 2) in the vicinity of the spill site shows wind speeds varying from a low of 2.1 m/sec to a high of 9.5 m/sec (based on a 10 minute sampling interval) with a mean of 6 m/sec during the period of interest. Wind speeds were generally in range of 5 to 6 m/sec. These speeds are typical of the average during the spill period and just above the threshold for initiation of entrainment (typical threshold of 4 to 5 m/sec). If breaking wave induced entrainment were active during the times of the aerial imagery, the oil should have been mixed into the surface layer. It would therefore have been impossible to observe oil at the sea surface and to make oil thickness measurements from the imagery.

2.2 Surface Application of Dispersants

Dispersants were applied aerially during the time period of interest. The flight paths for dispersant application from May 9 to 11, 2010 are shown in Figure 4. The amount of dispersant applied was 55,932 gallons (211,702 liters) (May 9); 56,220 gallons (212,792 liters) (May 10); 7,940 gallons (30,052 liters) (May 11); and 39,710 gallons (150,302 liters) (May 12) (NOAA ERMA Response Web site). All dispersant applications were well to the east or southeast of the spill site during this period, and hence do not explain the variations in observed oil spill patterns and associated thicknesses in the vicinity of the spill site (Figure 1) with time.

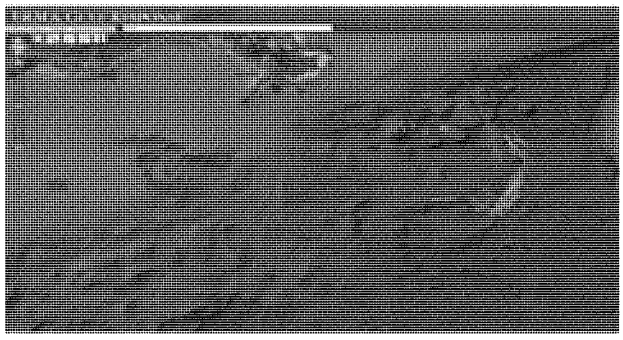

Figure 4. Aerial dispersant application flight paths on May 9, 2010 (purple), May 10, 2010 (yellow), and May 11, 2010 (blue) from NOAA Emergency Management Response Application (EMRA) Gulf Response.

2.3 Subsurface Application of Dispersants

Subsurface dispersants were also applied during this time period. The application rates, provided by BP (Olson, 2013), are shown in Figure 5 for the entire duration of the spill. The dispersant application rate was approximately constant during the May 10 test period at 10 gpm (342 barrels per day, 37.8 liters per minute). Figure 6 shows details for the May 10 and 11 time period, obtained from the pumping record for the dispersant application system. This figure shows that while dispersant application was initiated at 4:30 AM on May 10, the application was intermittent and at low rates until about 9:30 AM. From this time until about 2:00 AM on May 11, 2010 the application rate was constant at about 10 gpm (37.8 liters per minute). The pumping rate declined to half this value over the next several hours and then ceased by 3:00 AM. The principal dispersant application period was therefore about 16 to 17 hr in duration.

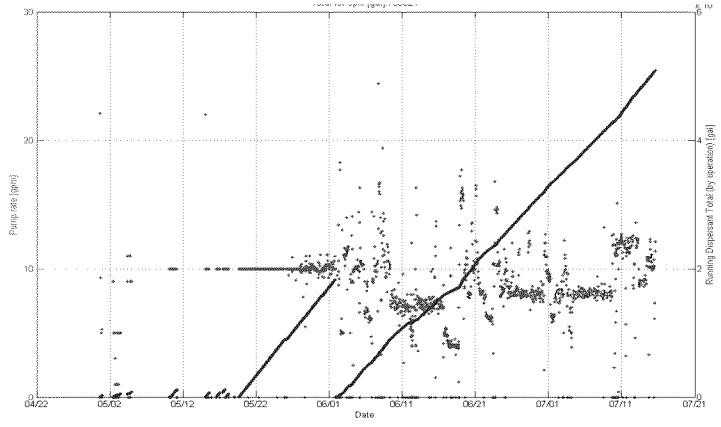

Figure 5. **Daily dispersant application pumping rate (gpm)(blue dots) vs time during the spill. The green line shows the cumulative application amounts (gallons) for each continuous application time period.**

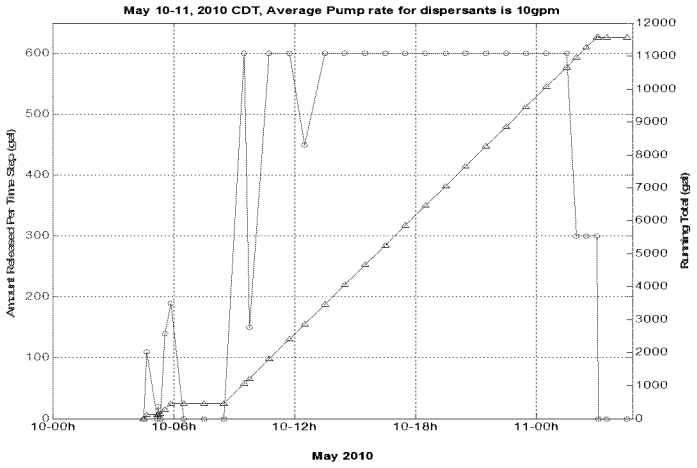

Figure 6. **Dispersant application rate (gallons per time increment, nominally 60 minutes, left axis, blue line) and cumulative amount of dispersant applied (gallons, 4.78 liters, right axis, green line) from 10 AM on May 10 to 6 AM on May 11, 2010, CDT times.**

The total dispersant release over the period from the dispersant pumping records (approximately 16 hr or 0.667 days) was 11,560 gal (275 barrels) or a rate of 412 barrels per day. The oil release rate during this period was approximately 47,234 barrels (1.98 million gallons) per day from the riser and 12,766 barrels (0.536 million gallons) per day from the kink, for a total release rate of 60,000 barrels (2.52 million gallons) per day (Lehr et al, 2010). Dispersants were applied to the riser release during this period using a wand (Figure 7). The type of wand and the location of the application (in the pipe, in the plume, or outside the plume) varied with time (Figure 8). This data was obtained by reviewing Remotely Operated Vehicle (ROV) video collected during this period. The application strategy typically used during most of the high release rate period was inside the broken riser. Figure 7 shows an ROV image of the application inside the riser pipe. The Dispersant to Oil Ratio (DOR) during this period, assuming complete mixing of oil and dispersant at the riser, would be 1:114. If the dispersant was not fully mixed with the oil, the likely case given the application method (Spaulding et al, 2015), a portion of the oil would remain untreated and the remaining portion treated at a higher DOR. In this scenario the untreated oil would continue to be transported to the sea surface without interruption while the droplet size distribution of the treated portion would be reduced, oil would be trapped subsurface, and therefore less oil transported to the surface.

A review of the timing of the dispersant application and the surface oiling images shows thick fresh oil near the spill source on May 10, 8:30 AM (CDT), occurring approximately 4 hrs after the initial dispersant was applied but almost coincidental with the highest application rates. The thick fresh oil was no longer observed at the surface near the spill site on May 10, 5:05 PM (CDT), approximately 12 hrs after dispersant treatment was initiated, or 8 hrs after the application rate first reached its peak value. Dispersant application ceased on May 11, 2:00 AM (CDT) and thick fresh oil was observed at the sea surface on May 11, 9:15 AM (CDT), approximately 7 hrs 15 min after the dispersant operation ceased. The dispersant application rate

was very close to its highest value for the period from 9:30 AM on May 10 to 2:00 AM on May 11, lasting approximately 16 hrs.

Figure 7. ROV image of dispersant being applied by a wand at the end of the riser pipe on May 10, 2010 at 09:00 GMT (GMT – 5 hrs= CDT).

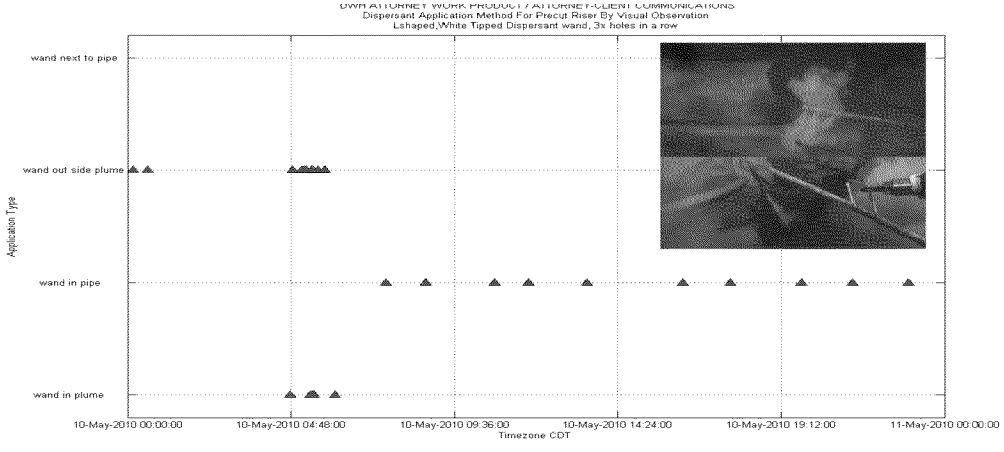

Figure 8. ROV image of dispersant being applied by a wand at the end of the riser pipe on May 10, 2010 at 09:00 GMT (GMT – 5 hrs = CDT)(Spaulding et al, 2015).

The timing at the beginning of the dispersant treatment operation suggests that dispersants, via the effect on oil droplet sizes and associated rise times, took at least 4 hours, but

not more than 12 hours to be effective in reducing the amount of oil at the sea surface. At the end of the dispersant application period, the time for the surface oiling pattern to resume to its pre-application characteristics was 7 hours or less.

2.4 OILMAP DEEP Simulations

OILMAP DEEP (ASA, 2013; Spaulding et al, 2015; Li et al, 2017b) was used to simulate the release during this on-off-on dispersant application period. The oil release rate was assumed to be 60,000 barrels per day. As a base case, no dispersant treatment was assumed. To simplify understanding of the results, the simulations explored the impact of the use of dispersants, but do not model the details of this off-on-off cycle of application for this event. The oil droplet sizes were estimated based on the riser exit Weber (We) number and Ohnesorge (Oh) number and assumed to have a log normal distribution following the methodology in OILMAP DEEP (Li et al, 2017a). Oil was assumed to be released at the plume trapping depth, 400 m above the sea floor (depth to sea bed - 1500 m) or water depth of 1100 m. Figure 9 shows the model predicted percent (%) of oil released that arrives at the sea surface vs time after its release with varying levels of treatment. For the untreated case, the figure shows that no oil reaches the surface until just over two hours after the time of release. This is the time that it takes for the largest oil droplets (a few millimeters in diameter) to reach the sea surface. The amount of oil reaching the sea surface then grows very quickly with time, with over 60% reaching the sea surface within three hours. This rapid growth is the result of increasing volumes of oil with decreasing droplet size. Twenty four hours after the release, 90 % of the oil is at the sea surface for the untreated case. The larger oil droplets and their volumes dominate the short term behavior, while the smaller droplets and their volumes determine the longer term behavior. A 1.5 mm droplet takes 6.3 hours to rise to the sea surface, while a 250 μm droplet requires 82 hours (3.4 days).

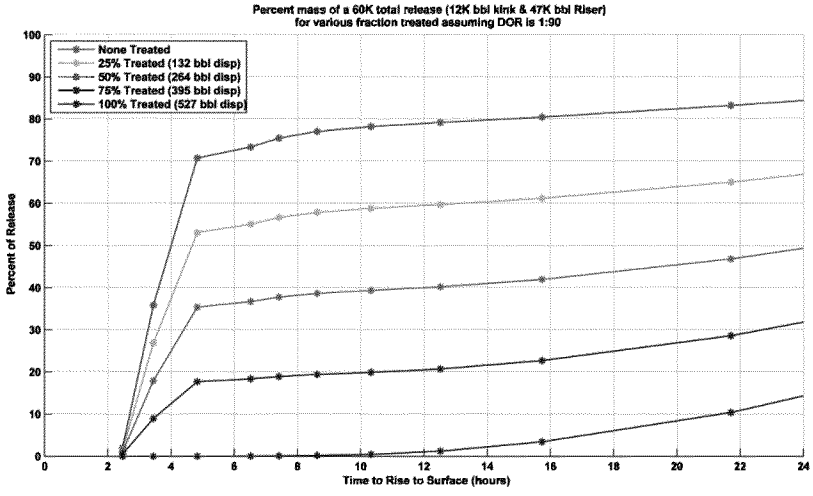

Figure 9. OILMAP DEEP predicted amount of oil reaching the sea surface vs time for varying levels of treatment. Simulations assume a 60,000 barrel/day release and a DOR of 1:90.

Simulations were performed by varying the percent of oil treated, all with an assumed dispersant to oil ratio (DOR) of 1:90. This assumption was made to make interpretation of the results easier to follow. The results of these cases are shown in Figure 9 for 25%, 50%, 75%, and

100% treatment. The corresponding amount of dispersant required to achieve the desired DOR are provided in the legend of the figure in barrels per day. Based on the amount of dispersant applied during the event (275 bbls) the treatment level could not have exceeded approximately 50%. Increasing the percent of oil treated by dispersants moves the percent of oil at the surface vs time curve to the right; extending the time required for oil to reach the sea surface. This is a direct result of the fact that treating oil with dispersants effectively lowers the oil-water interfacial tension and hence shifts the oil droplet sizes to lower values. The impact of this shift results in less oil reaching the surface immediately after the dispersant is applied, with the higher level of treatment resulting in greater reduction in the amount of oil reaching the surface. The amount reaching the surface clearly declines with level of treatment. Sixteen hours after the application of dispersant (the application period for the treatment event) the amount of oil on the sea surface is 61%, 42%, and 23% for the 25%, 50%, and 75% treatment cases, respectively. This analysis clearly shows that application of dispersant has an immediate impact on the mass of oil reaching the sea surface. For comparison, the volumes on the surface pre, during, and post the treatment event were estimated at 689, 370, and 1100 m^3, respectively. If the average of the pre and post values is used for a reference (894 m^3), the change from untreated to treated gives a reduction of about 40 %. This is consistent with the analysis shown in Figure 9 for the 50% treated case.

Before discussing the timing between the dispersant application and reduction in surface oiling, it is helpful to revisit the timeline shown in Figure 1. The timeline shown in the original figure accurately reproduces the time when dispersant treatment for this event started (May 10, 4:30 AM) and ended (May 11, 4 AM). It does not however address the issue of the application rate. Figure 6 clearly shows that in the initial stages of dispersant application, the rates were small and highly variable. They also decreased in a step fashion at the end of the period. Using the application rate data as a guide, dispersants were applied at full rate from approximately 9:30 AM on May 10 to 2:00 AM on May 11. With this revised timing, the image on the morning of May 10 was taken before dispersant application began in earnest, the image at the end of the day was well after the application began and images on May 11 and 12 were after the application ceased. The remotely sensed images are fully consistent with OILMAP DEEP predictions (Spaulding et al, 2015) and the impacts of dispersant treatment on oil reaching the sea surface.

2.5 SIMAP Simulations

The far-field oil transport and fate, SIMAP, (French McCay, 2004; French McCay et al., 2015, 2016) was used to simulate the rise of the oil droplets released from May 9 to May 14 of 2010, including consideration of the effects of subsea dispersant application. SIMAP quantifies transport, fate and concentrations of subsurface and floating oil. Processes simulated and applicable to this analysis include transport in the water column and on the surface, buoyancy-driven oil droplet rise, randomized dispersion from small-scale motions (mixing), spreading (gravitational and by shearing), evaporation of volatiles from surface oil, emulsification, entrainment of oil as droplets into the water (natural and facilitated by dispersant application), dissolution of soluble components, and biodegradation. The weathering processes affect the rise rate of the oil via change in oil density and droplet size as components dissolve and degrade (degradation only being important for small droplets over a longer time scale than in this analysis). The amount of floating oil observed at any given time is a function of the oil mass surfacing, advection, evaporation, and re-entrainment of surface oil into the water column. SIMAP was used to simulate the entire Deepwater Horizon spill; see French McCay et al. (2015,

2016, 2017) for details.

The oil droplet size and mass distributions calculated using OILMAP DEEP for May 9 1030 CDT to May 14 2330 CDT were input to SIMAP, and the amount of surfaced oil evaluated over time. The droplet size distributions were calculated on a daily increment, using the day's total dispersant application distributed evenly from 1030 CDT to 1030 CDT the next day (1030 CDT was the start time of oil release on April 22, 2010). The simulation assumed that for the oil released into the environment (total amount released minus the amount collected) the dispersant treatment effectiveness was 50% (Spaulding et al., 2015). SIMAP simulations were run using currents measured by Acoustic Doppler Current Profilers (ADCPs) at a number of locations near the wellhead (French McCay et al., 2015, 2017). Current speeds, based on ADCP measurements averaged over the water column, were ~2 cm/s (0.08 km/hr) to the ESE on May 10, as compared to ~8 cm/s (0.3 km/hr) based on estimates using the imagery. Thus, the apparently high eastward currents at the surface on May 10 as shown in Figure 1 were not simulated by the model. ADCP currents were not available at the surface and hence values from deeper depth with lower speeds were used.

Figure 10 shows the mass balance of oil (metric tons) in a 10 km by 10 km box (a circle within this has a 5 km radius) centered on the wellhead from May 9 to the 16th. The amount of floating oil (red line) increases rapidly from May 9 1030 CDT to May 10 0830 CDT, the period before and within a few hours after the oil was treated with the high application rate of dispersants at the wellhead (Figure 6). At the time when untreated oil released during the morning and mid-day of May 10 would reach the surface, the high rate of dispersant treatment results in a drop in the amount of oil surfaced, coincident with an increase in subsurface oil mass. After the dispersant treatment ceases (beginning May 12 1030 CDT in the simulation), the amount of floating oil increases again, although somewhat abated by evaporation, entrainment and wind-driven advection out of the 10 km x 10 km box when the winds reached 7-10 m/s on May 13 and 14. The peak amount on the surface was approximately 2,500 metric tons early on May 10, reduced to 1,000 metric tons on May 12 and 13 and then increased again to 1,500 to 2,000 metric tons on May 13 and 14. Dispersant treatment is therefore predicted to lead to a substantial reduction in surface oiling consistent with the imagery (Figure 1). The change in oil mass is approximately 50% between before/after and during dispersant treatment. This is consistent with the 40% change noted based on the observations.

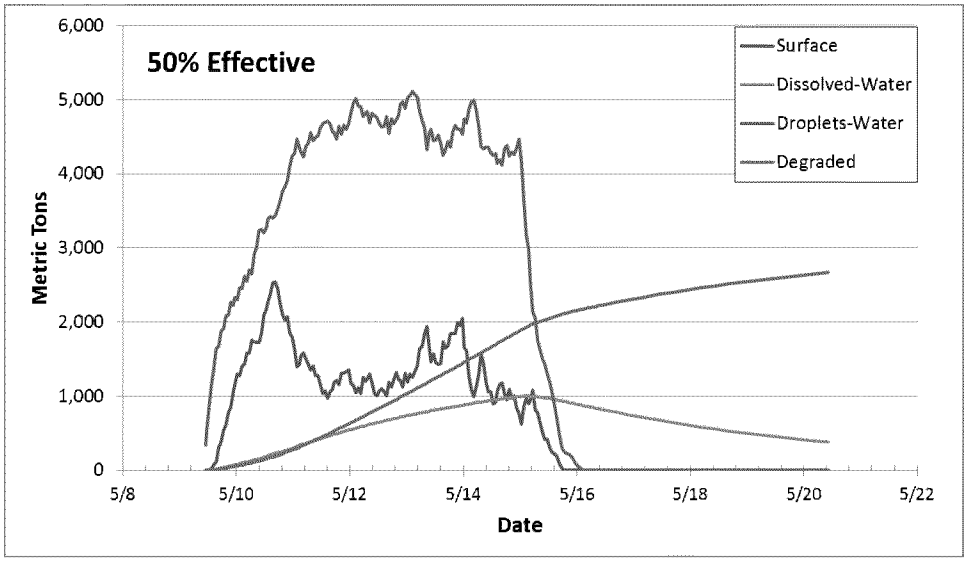

Figure 10. Oil released from May 9 10:30 to May 15 00:00, dispersant treatment assumed 50% effective, with wind. Oil on the surface (red), in the water column (dissolved(light blue) and in the form of droplets (dark blue)) and degraded (green) are shown.

To further evaluate the amount of oil surfacing in this period, Figure 11 shows the mass balance of oil in the 10 km x 10 km box for a simulation run without wind. This simulation eliminated evaporation and the re-entrainment and transport of floating oil (which increased on May 13-14 due to higher winds), such that the mass of floating oil accumulates until advected by currents (alone) out of the domain considered. The patterns of floating oil (red line) accumulation with no dispersant treatment, as compared to the drop in floating oil when dispersant treatment is included (May 10 1030 CDT to May 12 1030 CDT), are clearly seen in the model results. The floating oil increases May 9 to 10 1030 CDT, decreases to a lower level May 10 1030 CDT to May 12 1030 CDT while dispersant was used, and then increases dramatically over the next few days when the dispersant treatment was halted.

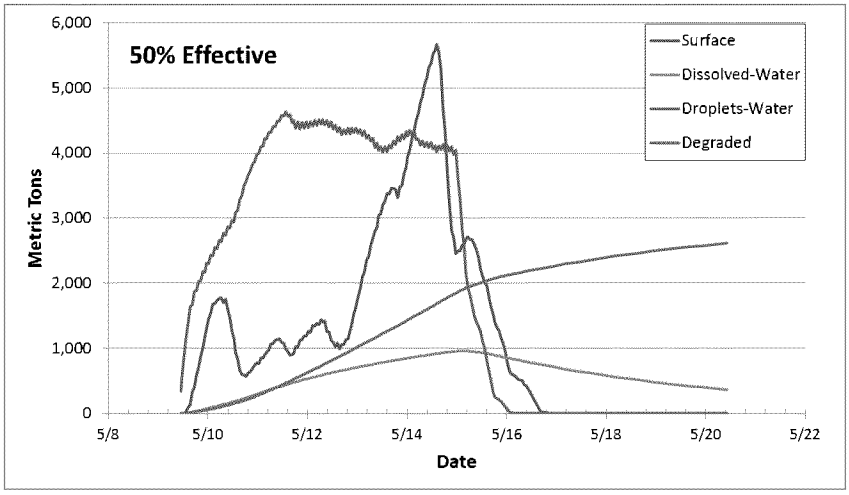

Figure 11. Oil released from May 9 10:30 to May 15 00:00, dispersant treatment

effectiveness of 50% assumed, no wind.

Figures 12 a ,b, c, and d show the floating oil distribution in the 10 km x 10 km box resulting from the oil released May 9 1030 CDT to May 14 2330 CDT. In Figure 12a, the distribution of untreated oil from May 9 1030 CDT to May 10 0830 CDT shows a similar spatial pattern to the interpreted imagery at that same time (Figure 1) with considerable thick oil on the surface. In Figure 12b, the surfaced oil from the dispersant-treated release between May 10 1030 CDT and May 10 1700 CDT is seen to have a much smaller footprint and has been transported eastward, although not at the speed seen in the field (as measured from Figure 1). In the model snapshots in Figures 12c and 12d, at times matching the May 11 and May 12 panels of Figure 1, the untreated oil has accumulated on the surface once again. The transport of the floating oil also matches observations.

Recently Testa et al (2017) used a particle tracking model to evaluate the effects of the changes in oil droplet sizes due to dispersant applications on the short term transport, fate, and surfacing of oil from the DWH spill. The simulations explored the impact of no dispersant application vs treatments with 50 and 100 % effectiveness, using oil release rates and dispersant application amounts consistent with post riser cut conditions for the spill. For the no treatment case, all of the oil released reached the sea surface within 7 hrs. This was reduced to 61% and 28% after 12 hrs when dispersant effectiveness was 50 % and 100 %, respectively. They predicted that 6 hr after the release the surface slick length was about 2 km for the no dispersant treatment case and disappeared for the 100% treatment case, reflecting the generation of many small droplets for the treated case. These results are consistent with the present analysis and show significant impacts of dispersant treatment on the surface oil signature with response times in the range of 7 to 12 hr period.

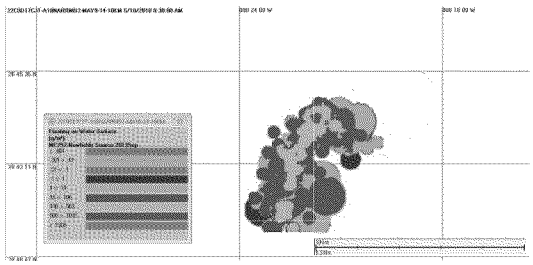

(a)

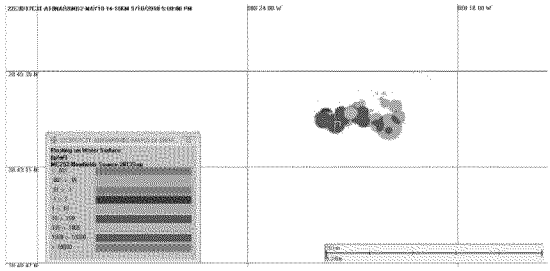

(b)

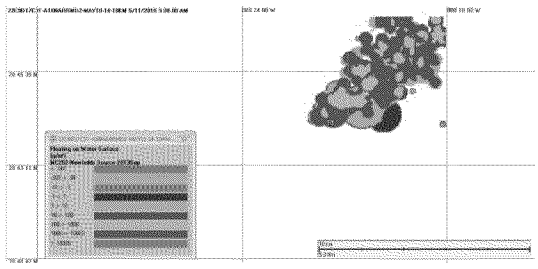

(c)

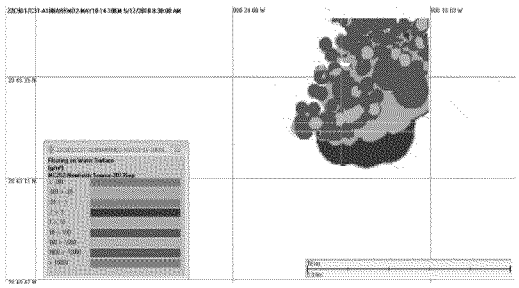

(d)

Figure 12. Floating oil (g/m^2) resulting from oil released from (a) May 9, 10:30 to May 10, 08:30, (b) May 10, 10:30 to May 10, 17:00, (c) May 10, 10:30 to May 11, 09:00, and (d) May 11, 10:30 to May 12, 08:30, dispersant treatment assumed 50% effective, with wind.

3. Conclusions

The question is what caused the dramatic decrease in surface oiling in the immediate vicinity of the spill site during this period. Can it be attributed to entrainment of oil due to breaking waves or to dispersant application, either at the surface or applied subsurface at the blowout release; all which would remove oil from the sea surface for a short period of time? Each possibility was explored in depth.

Given that the wind speeds were moderate (5 to 6 m/sec) during this period, it is unlikely that entrainment from the sea surface caused the disappearance and reappearance of oil. This is further supported by the availability of the imagery that shows oil thickness, which would not have been possible in the presence of significant breaking wave induced entrainment.

A review shows that surface applications of dispersants were well to the east or southeast of the spill site during this period and hence do not explain the variations in the observed surface oiling patterns and associated thicknesses in the vicinity of the spill site with time.

However, when OILMAP DEEP was applied to the release during this period, the observations could be explained. The dispersant pumping record was available at hourly intervals. Application of OILMAP DEEP showed that the subsurface application of dispersants qualitatively accounts for the change in amount of oil at the sea surface during the May 10 to 12, 2010 treatment event and gives results that are fully consistent with the observations.

Far-field modeling using SIMAP confirmed the findings using OILMAP DEEP. The amount of oil surfacing was dramatically reduced on May 10 and 11 when dispersants were applied at the wellhead. The modeled floating oil observations were in agreement with observations and highlight that the amount and locations of floating oil are the result of a balance of transport and physical-chemical processes that are highly sensitive to wind and currents.

4. References

ASA, *OILMAP DEEP Blowout Plume Model Technical Manual*, RPS ASA, Wakefield, RI, 2013.

French McCay, D.P., "Oil Spill Impact Modeling: Development and Validation", *Environmental Toxicology and Chemistry,* 23(10):2441-2456, 2004.

French McCay, D., Jayko, K., Li, Z., M. Horn, Y. Kim, T. Isaji, D. Crowley, M. Spaulding, L. Decker, C. Turner, S. Zamorski, J. Fontenault, R. Shmookler, Rowe, J.J., *Technical Reports for Deepwater Horizon Water Column Injury Assessment – WC_TR.14: Modeling Oil Fate and Exposure Concentrations in the Deepwater Plume and Rising Oil Resulting from the Deepwater Horizon Oil Spill.* DWH NRDA Water Column Technical Working Group Report. Prepared for National Oceanic and Atmospheric Administration (NOAA) by RPS ASA, South Kingstown, RI, USA. September 29, 2015. Administrative Record no. DWH-AR0285776 [https://www.doi.gov/deepwaterhorizon/adminrecord], 2015.

French McCay, D.P, Z. Li, M. Horn, D. Crowley, M. Spaulding, D. Mendelsohn, and C. Turner. "Modeling Oil Fate and Subsurface Exposure Concentrations from the Deepwater Horizon Oil Spill". In: *Proceedings of the 39th AMOP Technical Seminar on Environmental Contamination and Response*, Emergencies Science Division, Environment Canada, Ottawa, ON, Canada, 115-150, 2016.

French McCay, D., M. Horn, Z. Li, D. Crowley, M. Spaulding, D. Mendelsohn, K. Jayko, Y. Kim, T. Isaji, J. Fontenault, R. Shmookler, and J. Rowe, *Simulation Modeling of Ocean Circulation and Oil Spills in the Gulf of Mexico: Appendix VI Data Collection, Analysis and Model Validation.* Prepared by RPS ASA for the US Department of the Interior, Bureau of Ocean Energy Management, Gulf of Mexico OCS Region, New Orleans, LA. OCS Study BOEM 20xx-xxx. xxx p, 2017.

Lehr, B., S. Bristol and A. Possolo, *Deepwater horizon oil budget calculator: A report to the national incident command.* The Federal Interagency Solutions Group, Oil Budget Calculator Science and Engineering Team. http://www.restorethegulf.gov/sites/default/files/documents/pdf/OilBudgetCalc_Full_HQ-Print_111110.pdf (Accessed on April 1, 2012), 2010.

Li, Z., M. L. Spaulding, D. French McCay, and Jim Payne, "Development of a unified oil droplet size distribution model with application to surface breaking waves and subsea blowout releases considering dispersant effects", *Journal of Marine Pollution Bulletin*, http://dx.doi.org/10.1016/j.marpolbul.2016.09.008, 2017a.

Li Z, Spaulding M, Crowley D, Mendelsohn D, Galagan C., *Simulation Modeling of Ocean Circulation and Oil Spills in the Gulf of Mexico – Appendix III Blowout Model Technical Manual.* Prepared by RPS ASA for the US Department of the Interior, Bureau of Ocean Energy Management, Gulf of Mexico OCS Region, New Orleans, LA. OCS Study BOEM 20xx-xxx. xxx p, 2017b.

Olson, C. "Fulfillment NOAA Information Request 332 - Daily logs for subsurface dispersant application". Email communication from Chris J Olson (JMM Mgt; chris.olson@bp.com) to Jay Coady and George Graettinger (NOAA; jay.coady@noaa.gov, George.Graettinger@noaa.gov); Feb 18, 2013.
Attachments:
Dispensed Running Totals BP Log 1800 08172010.xls
Dispensed Running Totals BP Log 0300 06072010 (for NOAA iReq 332).xls

Spaulding, M.S., D. Mendelsohn, D. Crowley, Z. Li, and A. Bird, *Technical Reports for Deepwater Horizon Water Column Injury Assessment – WC_TR.13: Application of OILMAP DEEP to the Deepwater Horizon Blowout*. RPS ASA, 55 Village Square Drive, South Kingstown, RI 02879. Administrative Record no. DWH-AR0285366.pdf, 2015. [https://www.doi.gov/deepwaterhorizon/adminrecord]

Svejkovsky J, J. Muskat J, G, Graettinger, J. Mullin, "Operational Utilization of Aerial Multispectral Remote Sensing during Oil Spill Response: Lessons Learned During the Deepwater Horizon (MC-252) Spill", *Photogrammetric Engineering and Remote Sensing*, *78*(10), 1089-1102, 2012.

Svejkovsky, J., and M. Hess, "Expanding the Utility of Remote Sensing Data for Oil Spill Response" *Photogrammetric Engineering & Remote Sensing* 78 (10): 1011-014, 2012.

Testa, J. M., E. Eric Adams, E. W. North, and R. He, "Modeling the influence of deep water application of dispersants on the surface expression of oil: A sensitivity study", *J. Geophys. Res. Oceans*, 121, 5995–6008, doi:10.1002/2015JC011571, 2016.

Acknowledgements:

Funding of this research was provided in part by the US Department of the Interior, Bureau of Ocean Energy Management, Environmental Studies Program, Washington, DC (BOEM Contract Number M11PC00028). The opinions expressed by the authors are their own and do not necessarily reflect the opinion or policy of the U.S. Government. Any use of trade, firm, or product names is for descriptive purposes only and does not imply endorsement by the U.S. Government.

2017 International Oil Spill Conference

Comparative Study to Determine the Biodegradability of Dispersants at Environmentally Relevant Concentration

Yu Zhang[1], Mobing Zhuang[1], Pablo Campo[2], Ruta Suresh Deshpande[3], Devi Sundaravadivelu[3], Robyn N. Conmy[4] and Jorge W. Santo Domingo[4]

1. Department of Biomedical, Chemical and Environmental Engineering, University of Cincinnati, 2901 Woodside Drive, Cincinnati, OH 45221, USA
2. Cranfield Water Science Institute, Cranfield University, Cranfield MK43 0AL, UK
3. Pegasus Technical Services Inc., 46 E Hollister Street, Cincinnati, OH 45219, USA
4. U.S. Environmental Protection Agency, National Risk Management Risk Laboratory, 26 W. MLK Drive Cincinnati, OH 45268, USA

ABSTRACT

Chemical dispersant agents reduce the interfacial tension between oil and water, and increase the surface area to volume ratio of oil droplets thus facilitating the biodegradation of spilled oil. Dispersants are composed of surface active molecules known as surfactants and various commercial products contain Dioctyl Sulfosuccinate (DOSS) as the active ingredient. Since previous laboratory studies including the BFT were conducted at oil and dispersant concentrations significantly higher (~0.7 g/L oil with DOR of 1:25) than those typically found in field conditions, experiments were conducted at low levels of oil and dispersant (28 μg/L oil with DOR of 1:25) in order to determine the degradation trends at environmentally relevant concentrations. Experiments were conducted using two crude oils (Alaskan North Slope and Endicott) and two dispersant products (Corexit 9500 and Finalsol OSR 52) to study the biodegradation of dispersants and dispersed oil and oil alone samples were used as controls. Two

oil degrading cultures, isolated from the surface (meso) and deep sea (cryo) of the Gulf of Mexico, were enriched on crude oil at 25 and 5 °C and were used as the inocula. The biodegradation experiments were performed at 5 °C for 56 days and at 25 °C for 48 days using sterile GP2 artificial seawater as the media. The time series concentration of DOSS, the primary surfactant in the dispersants was monitored using LC-MS/MS in addition to the oil concentration which was measured using GC-MS/MS. Although the initial concentration of DOSS in Finasol OSR 52 was 20% higher than in Corexit 9500, over 95% of the anionic surfactant fraction was metabolized for both types of dispersant products by the end of the experiment at 25 °C while it persisted at 5 °C. The effect of dispersant and oil type on microbial community structure was also analyzed using PCR analysis. Results indicated that the abundance of *Thalassospira* correlated well with hydrocarbon degradation trends. The results from this study significantly expands on our understanding of biodegradation of DOSS, dispersed, and non-dispersed oil and also provides information regarding bacterial community composition.

Keywords: biodegradation, oil spills, dispersant, crude oil, RNA

INTRODUCTION

First generation chemical dispersants (industrial detergents) were primarily used in marine oil spills after the first major tanker catastrophe, the *Torrey Canyon* oil spill, in which large amount of alkylphenol surfactants were delivered to the contaminated area (Clayton, 1993; Committee on Effectiveness of Oil Spill Dispersants, 1989). The addition of dispersant lowered the interfacial tension between spilled oil and water, accelerate the breakdown of oil slicks, and prevent the resurfacing of small droplets (European Maritime Safety Agency, 2010). Moreover, discussions regarding dispersant utilization in deep-sea condition has come to the forefront after the GOM oil spill in 2010.

Corexit 9500, a well-known formula capable of dispersing heavy and weathered oils, is listed on the U.S. EPA National Contingency Plan Product Schedule and stockpiled around the world (Lessard and Demarco, 2010). Finasol OSR 52, another product that is widely stockpiled in Europe and European Free Trade Association countries, has not been completely evaluated for its toxicity and biodegradability. However, the pressing demand for deep-sea drilling requires continuing assessment of biodegradability of dispersants and dispersed oil (Zhuang et al. 2016).

In the aquatic environment, biodegradation is one of the predominant oil removal mechanisms in which bacteria utilize the spilled oil as a carbon source and thus degrade the oil components. While chemical dispersants increase the bioavailability of the oil, the degradation of the dispersants themselves can be a challenge for the microbial community. Several studies assessed the biodegradation of C9500, while only Bergueiro-Lopez et al. (1997) examined the metabolism of Finasol OSR 52 by employing a mixture of bacteria called BIOLEN IG 30. To

date, the biodegradability of various crude oils dispersed with C9500 have been assessed in laboratory experiments, such as Prude Bay crude oil (Venosa and Holder, 2007), Macondo crude oil (Wang et al. 2016), and South Louisiana crude oil (Campo et al. 2013). Results varied due to the differences in oil properties and microbial community structure. Only a limited number of studies have been conducted where the biodegradability of dispersed Endicott crude oil was evaluated, and with only one publication evaluating the biodegradation by monitoring total petroleum hydrocarbon concentration under anaerobic conditions (Personna et al., 2014).

In order to characterize the biodegradation of DOSS and hydrocarbons, experiments were set up to study the degradation of two crude oils (ANS and Endicott), two dispersants (C9500 and Finasol) and three dispersed oils (ANS dispersed by C9500, ANS dispersed by Finasol and Endicott dispersed by C9500) under two temperature conditions which represented the surface (25 °C) and deepwater (5 °C) environments, respectively.

METHODS

Cultures and Medium

Two mixed cultures of oil degrading bacteria were provided by EPA's Gulf Ecology Division at Gulf Breeze, FL. The mixed cultures were collected at a depth of 1240 m (cryo) and 5 m (meso) near the Macondo well at the GOM, enriched using crude oil and preserved in 10% glycerol till use. Sterilized GP2 artificial seawater was used as the media in this experiment and was prepared by dissolving several mineral salts in deionized water (Bidwell and Spotte, 1985).

Treatments

Dispersed oil treatment: The dispersed oil treatment was prepared in a 2 L baffled flask by adding the crude oil and the dispersant to 1.5 L of GP2 at a volumetric dispersant-to-oil ratio of 1:24 (10 µL dispersant: 240 µL oil). The baffled flask was shaken at 200rpm for 10-minutes, followed by a 10-minute settling period to allow the undispersed oil to rise to the top. After settling, 1 L of the dispersion was drained without disturbing the undispersed oil slick on the water surface. This procedure was repeated two more times which yielded 3 L of total dispersed oil and it was diluted into 12 L of GP2 (Panels A, B and C of Figure). Subsequently, a series of 250 mL silanized shaker flasks were filled with 100 mL aliquots of the dispersed oil.

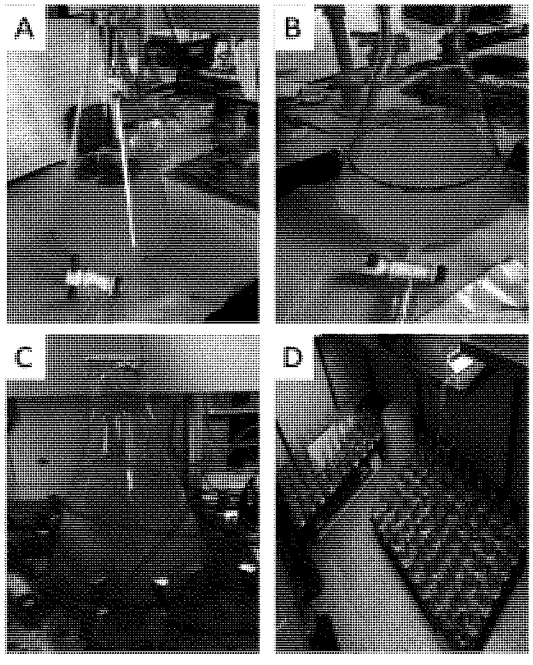

Figure Dispersed Oil Preparation (A, B and C) and Experiment Unit loading (D)

Non-dispersed oil treatment: To evaluate the biodegradation of crude oil alone, approximately 4 µL crude oil was directly pipetted into each shake flask containing 100 mL sterile GP2. The final concentration of oil in the samples was approximately 28 µg/L, which was

almost the same as the dispersed oil treatment.

Dispersant alone treatment: The dispersant alone treatments were prepared by spiking 20 µL of dispersant into 14 L of GP2 under continuous mixing, to yield a concentration similar to the dispersed oil treatment. After 30 minutes of continuously mixing, 100 mL of the solution was added into 250 mL silanized shaker flasks.

The dispersed oil, non-dispersed oil and dispersant alone treatments were then spiked with 0.5 mL of inoculum per flask with the cryo and meso cultures for the 5 and 25 °C experiments, respectively. After preparation, all the shaker flasks were placed on the orbital shakers in corresponding constant temperature rooms (5 or 25 °C) for the duration of the experiment (Panel D of Figure).

Oil component and DOSS analysis

DOSS and oil samples were prepared as described in Campo (2013). According to the ASTM D7730 Standard Method (ASTM D7730, 2011), DOSS was measured by using a 1200 series liquid chromatograph coupled with a 6410 tandem mass spectrometer (LC-MS/MS) from Agilent (Palo Alto, CA). Analysis of oil components was performed on an Agilent (Palo Alto, CA) 7890A GC coupled with an Agilent 7000 mass selective detector triple quadrupole and an Agilent 7693 series auto sampler. It was equipped with a DB-5 capillary column by J&W Scientific (30 m X 0.25 mm, and 0.25 µm film thickness) to achieved chromatographic separation of the alkanes and aromatics. A modified method based on EPA Method 8270D (2007) was followed.

RESULTS AND DISCUSSION

Biodegradation of DOSS

Table 1 summarizes the initial concentration, biodegradation rates and removal extents of DOSS, the active anionic surfactant in C9500 and Finasol, with and without crude oils at 25 °C. Although the initial concentration of primary surfactant (DOSS) in Finasol was around 20% higher than in C9500, over 95% of the anionic surfactant fraction was metabolized for both types of dispersant products by the end of the experiment at 25 °C while it persisted at 5 °C. Thus, the low temperature condition greatly inhibited the microbial uptake of DOSS.

At 25 °C, biodegradation was fast in the replicates with or without ANS. 96% and 98% of DOSS were degraded for dispersant alone and dispersed oil treatment for two dispersants by the end of experiment, respectively. The presence of ANS remarkably favored the biodegradation first order rate of C9500 by approximately 2.4-fold, but no such effect was observed for the experiment with Finasol and ANS. Besides, DOSS uptake occurred after an acclimation period of 2 days, and removal extents surpassed 98% by day 48 in the presence of Endicott.

Table 1 Summary of Biodegradability of two Dispersants at 25 °C

Treatments	Initial DOSS Concentration (μg/L)	Degradation rate (d^{-1})	Removal extent (%)
C9500 alone	203.97 ± 6.98	- 0.07 ± 0.009	96
C9500 + ANS	228.16 ± 11.94	- 0.16 ± 0.015	98
Finasol Alone	280.87 ± 21.19	- 0.060 ± 0.008	96
Finasol + ANS	234.11 ± 5.38	- 0.068 ± 0.006	98
C9500 + Endicott	206.96 ± 4.28	- 0.077 ± 0.007	98

Biodegradation of total alkanes

Table 2 presents the hopane-normalized concentration of total alkanes in dispersed oils. All the targets compounds were normalized by hopane concentration since it was unchanged through the whole experiments in all the treatments. The initial hopane-normalized concentration for 5 °C was almost twice as that of 25 °C because of the oil present in the enrichments. This was confirmed by analyzing the cryo and meso biomass alone, without the addition of any oil. The biodegradation of total alkanes occurred without any lag phase at 25 °C, regardless of the type of dispersed oil, while a 4-day acclimation period was observed at 5 °C. Over 90% of the total alkanes was metabolized by the meso culture by the end of experiment in all the cases.

Table 2 Biodegradability of Hopane-Normalized Total Alkanes in Dispersed Oils at 5 and 25 °C

Temperature	Treatments	Initial Concentration (mg total Alkanes / mg Hopane)	Lag Phase Period (d)	Removal extent (%)
25 °C	ANS + C9500	106.61 ± 3.64	0	92
	ANS + Finasol	113.17 ± 3.69	0	90
	Endicott + C9500	142.91 ± 3.33	0	94
5 °C	ANS + C9500	209.79 ± 7.72	4	85
	ANS + Finasol	220.56 ± 4.30	4	93
	Endicott + C9500	178.42 ± 1.77	4	94

At 5 °C, the presence of Finasol considerably favored the removal of alkanes than C9500 (93% vs. 85%). Although, ANS and Endicott crude oil are both medium oil (Table 3), the percentage of total alkanes in Endicott is much higher than ANS crude oil, especially for light alkanes. The remove extent of dispersed Endicott is higher than that of dispersed ANS due to the easier metabolism of short chain alkanes.

Table 3 Physical Properties of ANS and Endicott *

Property	ANS	Endicott
Density, ρ (g/mL)	0.8733	0.8838
Dynamic Viscosity, μ (cP, at 15 °C)	35	120
Kinematic Viscosity, ν (cSt, at 15 °C)	40	134
API gravity	28.24	23.00
Total Alkanes Concentration (mg total Alkanes / mg Crude Oil)	35.52	110.38
of Total PAHs Concentration (mg total PAHs / mg Crude Oil)	20.63	37.46

* General crude oil categories: Heavy (API < 22.3°), Medium (22.3° ≤ API < 31.1°), and Light (API ≥ 31.1°).
* Source: SL Ross Environmental Research, 2010.

Biodegradation of total PAHs

Table 4 presents total PAH degradation for all the dispersed oil treatments at two temperatures. Similar to alkanes, the hopane-normalized total PAH concentration at 5 °C was higher than at 25 °C because of the higher hopane content from the meso cultures. At 25 °C, a notable decline in total PAHs was observed after an acclimation period of 2 days, and, subsequently degraded up to 82% by day 48 in ANS + C9500 treatment. For the other two dispersed oils, PAHs persisted until the end of experiment. Such contrary and unexpected findings is explained in more detail under the microbial community structure section.

At 5 °C, a 12-day lag phase occurred before observable degradation ensued in dispersed ANS treatments, while the cryo culture began degrading PAHs after 32 days for dispersed Endicott. Similar to the alkanes, higher temperature considerably favored the biodegradation of ANS dispersed by C9500 by shortening the lag phase period. At the last sampling event, 21%,

28% and 15% of the initial loaded concentration persisted for ANS + C9500, ANS + Finasol and Endicott + C9500 treatment, respectively. Although Endicott contains more PAHs than ANS (as shown in Table 3), dispersed Endicott was easier to remove owing to the higher percentage of 2-ring compounds which biodegraded faster than 3- and 4- ring PAHs.

Table 4 Biodegradability of Hopane-Normalized Total PAHs in Dispersed Oils at 5 and 25 °C

Temperature	Treatments	Initial Concentration (mg total PAHs / mg Hopane)	Lag Phase Period (d)	Removal extent (%)
25 °C	ANS + C9500	44.38 ± 1.54	2	82
	ANS + Finasol	61.08 ± 2.33	48	3
	Endicott + C9500	53.81 ± 0.14	48	19
5 °C	ANS + C9500	51.17 ± 0	12	79
	ANS + Finasol	63.57 ± 2.25	12	71
	Endicott + C9500	58.55 ± 0.38	32	85

Microbial community structure

As mentioned previously, meso cultures showed significant differences in PAHs uptake between ANS + C9500 and ANS + Finasol experiments which were performed under the same conditions, except for the dispersant product. PCR analysis of these bacterial consortia provided a clearer understanding of the microbial makeup and an in-depth explanation for the inconsistent result.

Table 5 displays the significant species in the active community including *Alcanivorax, Pseudoidiomarina* and *Thallassospira* which were abundant in the C9500 experiment but not in the Finasol experiment. In the active community, *Alcanivorax,* one of the predominant

hydrocarbon-degrading bacteria in the contaminated seawater, (Cappello et al, 2007; Harayama et al, 2004; Wang et al, 2014) increased from 0.74% to a maximum of 69.3% of total abundance in the C9500 experiment. *Alcanivorax* is a ubiquitous bacteria that was found in the GOM during the DWH oil spill (Kostka et al., 2016). However, the same species in the Finasol experiment was consistently lower at around 20%. Moreover, similar trend were observed by comparing *Pseudoidiomarina* and *Thallassospira* (Moghadam et al., 2014). Hence, it is reasonable to infer this loss of active community resulted in the unusual persistence of aromatics at 25 °C

Table 5 Significant active genes of meso cultures in ANS alone treatment of ANS + C9500 (A) and ANS + Finasol (B) experiments

Species	Experiment	Initial Percentage (%)	Maximum Percentage (%)
Alcanivorax	A	33.13 ± 15.19	69.34 ± 2.10
	B	10.74 ± 3.39	20.58 ± 6.51
Pseudoidiomarina	A	0.15 ± 0.15	21.88 ± 3.88
	B	12.75 ± 1.49	14.93 ± 1.22
Thallassospira	A	0.02 ± 0.03	26.28 ± 2.99
	B	3.92 ± 0.83	0.82 ± 0.69

CONCLUSION

The goal of this work was to evaluate the effect of temperature on the biodegradability of dispersants and dispersed oils by using two oils (ANS crude oil and Endicott) and two dispersants (C9500 and Finasol OSR 52). This research not only evaluated the effect of dispersant type (Finasol and C9500) on ANS biodegradation, but also analyzed the biodegradation potential of two types of crude oil (ANS and Endicott) when dispersed with C9500.

DOSS disappeared promptly at 25 °C, while it persisted throughout the experiments at 5 °C. Additionally, the length of the acclimation period and removal extent were highly impacted by the addition of the dispersant. Similar to DOSS degradation, temperature affected the biodegradation of total alkanes significantly in both acclamation period and removal extent. Around 80% of the PAHs degraded at 5 °C whereas most PAHs persisted at 25 °C in ANS+Finasol and Endicott+C9500 treatment, which possibly resulted from the loss of several oil degrading microbial species such as *Alcanivorax, Pseudoidiomarina* and *Thallassospira.* Although the composition of Endicott considerably differs from ANS, especially the short chain paraffin and 2-ring PAHs, the degradation trends were similar to dispersed ANS, which indicated that the effect of C9500 on the two oils were similar. Since the PAHs persisted at 25 °C, and low activity of critical degrading species in meso cultures was observed, it is recommended that different cultures should be evaluated under the same test conditions in future experiments.

ACKNOWLEDGEMENTS

We acknowledge Jan Kurtz and Diane Yates from EPA's Gulf Ecology Division (GED) at Gulf Breeze, FL, who collected the water samples in the GOM and performed the enrichments and provided them for the experiments. The research was a product of the U.S. Environmental Protection Agency's National Risk Management Research Laboratory (NRMRL) and was partially funded by EPA, NRMRL, Cincinnati, OH, under Pegasus Technical Services, Inc. Contract EP-C-11-006.

REFERENCES

1. ASTM D7731-11e1, 2011. Standard test method for determination of

dipropyleneglycol monobutyl ether and ethylene glycol monobutyl ether in sea water by liquid chromatography/tandem mass spectrometry (LC/MS/MS). *ASTM International*, West Conshohocken, PA. *www.astm.org*

2. Bergueiro-Lopez J.R., Moreno-Garcia-Luengo S., Serra-Socias F., Fuertes- Perez A., Perez-Navarro-Gomez A., Morales-Correas N., Domingez-Laseca, F., 1997. FINASOL OSR 52 Active Components Biodegradation by Using the Biological Activator BIOLEN IG 30. *Spill Science & Technology Bulletin* 3(4), 269-272. doi: 10.1016/S1353-2561(97)00026-1
3. Bidwell J.P., and Spotte S., 1985. Artificial Seawaters: Formulas and Methods. Jones and Bartlett Publishers, Inc., Boston, Ma.
4. Campo P., Venosa A.D., Suidan M.T., 2013. Biodegradability of Corexit 9500 and Dispersed South Louisiana Crude Oil at 5 and 25 °C. *Environmental Science & Technolology* 47(4), 1960-1967. doi: 10.1021/es303881h
5. Cappello S., Denaro R, Genovese M., Giuliano P., Yakimov M.M., 2007. Predominant growth of Alcanivorax during experiments on "oil spill bioremediation" in mesocosms. *Microbiological Research* 162(2), 185-190. doi: http://dx.doi.org/10.1016/j.micres.2006.05.010
6. Clayton, John R., 1992. Oil Spill Dispersants: Mechanisms of Action and Laboratory Tests. 9-23.
7. Committee on Effectiveness of Oil Spill Dispersants, 1989. Using Oil Spill Dispersants on the Sea. 6-7.
8. European Maritime Safety Agency, 2010. Manual on the Applicability of Oil Spill Dispersants - Version 2. *www.emsa.europa.eu*
9. HarayamA S., Kasai Y., Hara A., 2004. Microbial communities in oil-contaminated seawater. *Current Opinion in Biotechnology* 15(3), 205-214. doi: http://dx.doi.org/10.1016/j.copbio.2004.04.002
10. Kostka, J. E., Prakash, O., et al., 2011. Hydrocarbon-degrading bacteria and the bacterial community response in Gulf of Mexico beach sands impacted by the Deepwater Horizon oil spill. *Applied and Environmental Microbiology* 77(22), 7962-7974.

doi: 10.1128/AEM.05402-11

11. Lessard P.R., Demarco G., 2000. The Significance of Oil Spill Dispersants. *Spill Science & Technolology Bulletin* 6(1), 59-68.
doi: http://dx.doi.org/10.1016/S1353-2561(99)00061-4

12. Moghadam M.S., Ebrahimipour G., Abtahi B., Ghassempour A., Hashtroudi M.S., 2014. Biodegradation of polycyclic aromatic hydrocarbons by a bacterial consortium enriched from mangrove sediments. *Journal of Environmental Health Science and Engineering* 12(1).
doi: 10.1186/s40201-014-0114-6

13. Personna Y.R., Boufadel M.C., Zhang S., 2014. Assessing weathered Endicott oil biodegradation in brackish water. *Marine Pollution Bulletin* 86, 102-110.
doi: http://dx.doi.org/10.1016/j.marpolbul.2014.07.037

14. SL Ross Environmental Research, 2010. Comparison of large scale (Ohmsett) and small scale dispersant effectiveness test results. *Report for U.S. Department of the Interior*, Minerals Management Service, Herndon, Va.

15. United State Environemtnal Protect Agency, 2007. Method 8270D Semivolatile Organic Compounds by Gas Chromatography/Mass Spectrometry (GC-MS). *https://www3.epa.gov/*

16. Venosa, A.D., Holder, E.L., 2007. Biodegradability of dispersed crude oil at two different temperatures. *Marine Pollution Bulletin* 54, 545-553.
doi: http://dx.doi.org/10.1016/j.marpolbul.2006.12.013

17. Wang J., Sandoval K., Ding Y., Stoeckel D.,1, Minard-Smithc A., Andersen G., Dubinsky E., Atlas R., Gardinali P., 2016. Biodegradation of dispersed Macondo crude oil by indigenous Gulf of Mexico microbial communities. *Science of the Total Environment* 557-558, 453-468.
doi: http://dx.doi.org/10.1016/j.scitotenv.2016.03.015

18. Wang W., Zhong R., Shan D., Shao Z., 2014. Indigenous oil-degrading bacteria in crude oil-contaminated seawater of the Yellow Sea, China. *Applied Microbiology and Biotechnology* 98(16), 7253-7269.
doi: 10.1007/s00253-014-5817-1

19. Zhuang M., Abulikemub G., Campo P., Platten W.E., Suidan M.T., Venosa A.D.,

Conmy R.N., 2016. Effect of dispersants on the biodegradation of South Louisiana crude oil at 5 and 25 °C. *Chemosphere* 144, 767-774.
doi: http://dx.doi.org/10.1016/j.chemosphere.2015.08.040

To: Willis-McFarlin, Jeannetta[Willis-McFarlin.Jeannetta@epa.gov]; Acheson, Carolyn[Acheson.Carolyn@epa.gov]; Adkins, Renata[Adkins.Renata@epa.gov]; Al-Abed, Souhail[al-abed.souhail@epa.gov]; Allen, Derrick[allen.derrick@epa.gov]; Barth, Edwin[Barth.Ed@epa.gov]; Bessler, Scott[Bessler.Scott@epa.gov]; Betts, Aaron[Betts.Aaron@epa.gov]; Brenner, Richard[brenner.richard@epa.gov]; Butler, Barbara[Butler.Barbara@epa.gov]; Carson, David[Carson.David@epa.gov]; Conmy, Robyn[Conmy.Robyn@epa.gov]; Dasu, Kavitha[Dasu.Kavitha@epa.gov]; Dyson, Brian[Dyson.Brian@epa.gov]; Evans, Gordon[evans.gordon@epa.gov]; Fetters, Kyle[Fetters.Kyle@epa.gov]; Ford, Robert[Ford.Robert@epa.gov]; Gilliland, Alice[Gilliland.Alice@epa.gov]; Goetz, Jennifer[Goetz.Jennifer@epa.gov]; Ha, HakSoo[Ha.Haksoo@epa.gov]; Hansen, Verle[hansen.verle@epa.gov]; Hantush, Mohamed[Hantush.Mohamed@epa.gov]; Herrmann, Ronald[Herrmann.Ronald@epa.gov]; Hicks, Henrietta[hicks.henrietta@epa.gov]; Jackson, Nicole[Jackson.Nicole@epa.gov]; Jacobs, Scott[Jacobs.Scott@epa.gov]; Kemper, Mark[Kemper.Mark@epa.gov]; Kremer, Fran[Kremer.Fran@epa.gov]; Lien, Bob[Lien.Bob@epa.gov]; Luxton, Todd[Luxton.Todd@epa.gov]; Lyons, Terry[Lyons.Terry@epa.gov]; McCauley, Paul[mccauley.paul@epa.gov]; McClellan, Kim[Mcclellan.Kim@epa.gov]; McKernan, John[McKernan.John@epa.gov]; Mills, Marc[mills.marc@epa.gov]; Newman, Tina[newman.tina@epa.gov]; Niazi, Mehran[Niazi.Mehran@epa.gov]; Parker, Randy[Parker.Randy@epa.gov]; Randall, Paul[Randall.Paul@epa.gov]; Richardson, Teri[Richardson.Teri@epa.gov]; Ricketts, Jonathan[Ricketts.Jonathan@epa.gov]; Rock, Steve[Rock.Steven@epa.gov]; Scheckel, Kirk[Scheckel.Kirk@epa.gov]; Schubauer-Berigan, Joseph[Schubauer-Berigan.Joseph@epa.gov]; Stoll, Sally[stoll.sally@epa.gov]; Timberlake, Dennis[Timberlake.Dennis@epa.gov]; Tolaymat, Thabet[Tolaymat.Thabet@epa.gov]; Voit, Jim[Voit.Jim@epa.gov]; Wetzel, Larry[wetzel.larry@epa.gov]; Wright, Stephen[Wright.Stephen@epa.gov]; Clark, Patrick[Clark.Patrick@epa.gov]; Yeardley, Roger[Yeardley.Roger@epa.gov]; Kozlowski, David[Kozlowski.David@epa.gov]
From: Kozlowski, David
Sent: Thur 3/19/2015 3:57:25 PM
Subject: RE: LRPCD Annual Accomplishment Report
2014 LRPCD Accomplishments_FINAL_Signed.docx

All,

It was brought to my attention that the previous version of our report included several comments from our review process. The attached version has all of those comments removed. I apologize for the earlier error. However, that error does not diminish the significant LRPCD accomplishments for FY 2014. Thanks!

David R. Kozlowski, PE, CSP

Associate Director

Land Remediation and Pollution Control Division

National Risk Management Research Laboratory

Office of Research and Development

(O) 513-569-7664

(C) 513-748-7178

From: Willis-McFarlin, Jeannetta
Sent: Thursday, March 19, 2015 11:27 AM
To: Willis-McFarlin, Jeannetta; Acheson, Carolyn; Adkins, Renata; Al-Abed, Souhail; Allen, Derrick; Barth, Edwin; Bessler, Scott; Betts, Aaron; Brenner, Richard; Butler, Barbara; Carson, David; Conmy, Robyn; Dasu, Kavitha; Dyson, Brian; Evans, Gordon; Fetters, Kyle; Ford, Robert; Gilliland, Alice; Goetz, Jennifer; Ha, HakSoo; Hansen, Verle; Hantush, Mohamed; Herrmann, Ronald; Hicks, Henrietta; Jackson, Nicole; Jacobs, Scott; Kemper, Mark; Kozlowski, David; Kremer, Fran; Lien, Bob; Luxton, Todd; Lyons, Terry; McCauley, Paul; McClellan, Kim; McKernan, John; Mills, Marc; Newman, Tina; Niazi, Mehran; Parker, Randy; Randall, Paul; Richardson, Teri; Ricketts, Jonathan; Rock, Steve; Scheckel, Kirk; Schubauer-Berigan, Joseph; Stoll, Sally; Timberlake, Dennis; Tolaymat, Thabet; Voit, Jim; Wetzel, Larry; Wright, Stephen; Clark, Patrick; Yeardley, Roger
Subject: FW: LRPCD Annual Accomplishment Report
Importance: High

FYI.....

From: Kozlowski, David
Sent: Thursday, March 19, 2015 10:55 AM
To: Willis-McFarlin, Jeannetta; Kozlowski, David
Cc: Gilliland, Alice; Newman, Tina
Subject: LRPCD Annual Accomplishment Report
Importance: High

Jeannetta,

Please distribute the attached report to all members of the Division. Thanks!

David R. Kozlowski, PE, CSP

Associate Director

Land Remediation and Pollution Control Division

National Risk Management Research Laboratory

Office of Research and Development

(O) 513-569-7664

(C) 513-748-7178

EPA
United States
Environmental Protection
Agency

FY 2014

Accomplishments

National Risk Management Research Laboratory

Land Remediation and Pollution Control Division

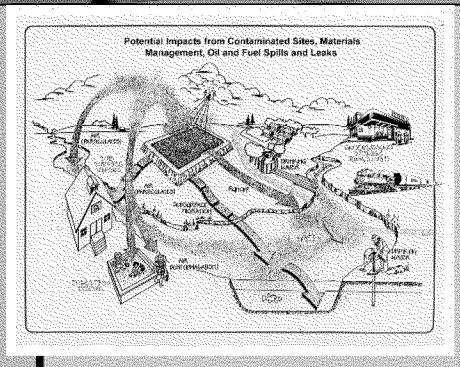

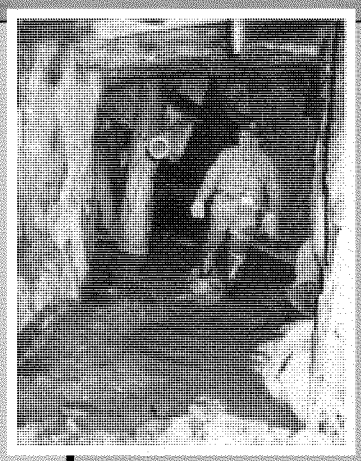

FY 2014 Annual Accomplishments Report

Concurrence

03-19-15

Joseph P. Schubauer-Berigan

Environmental Stressors* Management *Branch Chief

MAR 18, 2015

Randy A. Parker

Remediation and Redevelopment Branch Chief

3/19/15

Dennis L. Timberlake

Soils and Sediments Management Branch Chief

18 MARCH 2015

David Carson

Waste Management Branch Chief

3/19/15

David R. Kozlowski

Land Remediation and Pollution Control Division Associate Director

Approved

3/19/15

Alice Gilliland **Date**

Acting Land Remediation and Pollution Control Division Director

Foreword

The Land Remediation and Pollution Control Division (LRPCD) of the Office of Research and Development's (ORD's) National Risk Management Research Laboratory (NRMRL) based in Cincinnati, Ohio, conducts research that provides linkages between the natural and the built environment and supports place-based research programs. It integrates land use and waste and materials management to sustain ecosystem services. Land research improves land protection and vitalization and covers a broad range of issues associated with the management of contaminated sites and land-based sources of pollution. These issues include sustainable communities, materials and waste management, contaminated soil and sediment remediation, watershed protection, green infrastructure, and oil spills. LRPCD strives to be a top performing organization within EPA/ORD/NRMRL and has adopted the following mission and vision principles:

Vision: ***LRPCD is recognized as the nation's leader in providing solutions to the protection, restoration, and preservation of Earth's land resources for sustainability of the services these resources provide to society.***

Mission: ***To develop innovative and cost-effective solutions for sustainable land and materials management using cutting-edge techniques to advance the scientific foundation of risk-based decision analysis.***

LRPCD carries out research to improve response actions to **oil spills** including research on the use of remediation techniques such as dispersants and bioremediation. LRPCD funds received from the Oil Spill Liability Trust Fund over the last 21 years have resulted in numerous outputs that have had an important impact on the oil spill response community.

LRPCD has used budget allocations over the last dozen years from the **Leaking Underground Storage Tank** (LUST) Trust Fund for research efforts that helped develop a good understanding of the biodegradability of Methyl tertiary-Butyl Ether (MTBE) and other oxygenates in gasoline contaminating groundwater resources, as well as knowledge on the extent to which ethanol affects the fate of gasoline plumes in groundwater.

Research is further accomplished through the **LRPCD's four branches**: the *Soils and Sediments Management Branch*, the *Environmental Stressors Management Branch*, the *Waste Management Branch,* and the *Remediation and Redevelopment Branch*. Experts assigned to the branches work on research projects within the branch's scope, as well as on integrated multidisciplinary research teams across EPA.

Soils and Sediments Management Branch

EPA land researchers are working with regions and communities on soil and sediment contamination issues, using innovative sediment remediation techniques such as dredging, capping, and monitored natural recovery to make these waterways usable again. Sediments and soils may contain multiple chemical and biological contaminants (from mercury and arsenic to PCBs to EDCs to microbial pathogens). Emerging contaminants of concern such as endocrine disrupting chemicals (EDCs) come from municipal wastewater, concentrated animal feeding operations (CAFOs), and other sources. The land risk management research program is designed to investigate traditional and alternative sustainable remediation options for contaminated soils and sediments.

Environmental Stressors Management Branch

One of the most important services that ecosystems provide to communities and their inhabitants is usable water. Studying the interaction between land use and water quality at the watershed scale is a useful way to preserve these essential ecosystem services. Green infrastructure applications and technological approaches, managed properly, can reduce, capture, and treat stormwater runoff at its source before it can reach the sewer system. Researchers provide information and tools to environmental managers that enable them to assess the condition of aquatic resources, diagnose the causes of impairment, forecast effects of stressors, and develop and implement sustainable remediation and restoration strategies.

Waste Management Branch

Materials use challenges the capacity of the land, as well as air and water, to withstand the many resulting environmental problems, and it affects many other aspects of our future, such as the economy, energy, and climate. Materials management research advances the scientific foundation and provides innovative solutions for managing municipal, industrial, biological, and emerging wastes and materials. Our pioneering research in this area includes both traditional wastes and emerging materials such as nanomaterials. Land research provides technology and solutions for minimizing environmental risks from materials as they are used, reused, recycled, and ultimately disposed of on land.

Remediation and Redevelopment Branch

Imprudent land uses can easily compromise ecosystems and the services they provide. Many of the land use decisions that affect ecosystem services are made at the individual and community levels. Communities have to deal with the consequences of past and ongoing land use decisions. Researchers help communities revitalize land contaminated due to past land use decisions. Innovative techniques are developed to help communities deal in sustainable ways with brownfield, RCRA, and Superfund issues and historical contamination by hazardous waste left from such previous land uses as industry and mining. Land researchers currently help communities draft development plans that include sustainable land use decisions that will protect ecosystem services and thus keep the residents healthy and the communities economically viable far into the future, while valuing each community's unique social and historical attributes.

- LRPCD provides support to EPA regions and states through its branches and the **Engineering Technical Support Center (ETSC).** The ETSC ensures that ORD scientists and engineers are accessible to the Agency's Regional decision-makers and provides scientific and engineering knowledge and expertise in soil, sediment, and mine remediation and technology to Regional staff for risk management decisions. The ETSC has long been valued as a key support and technology transfer asset within the EPA. Since 2006, ETSC has worked on more than 300 sites in all ten Regions; 66% of these sites were on the National Priorities List. In FY13, ETSC scientists prepared reports on topics including Soil Vapor Extraction and Vapor Intrusion EIPs, and Chloronaphthalene. Highlights of technical support include 1) Eastern Michaud Flats, FMC Corporation/ J.R. Simplot (Pocatello, ID) - support to R10 on issues of groundwater contamination and implementing site-specific pump and treat options, 2) Omaha Lead (ASARCO) (Omaha, NE) - support to R7 to resolve problems of soil lead contamination, 3) San German Groundwater Contamination (San German, PR) - ETSC provided

expertise on vapor intrusion issues to R2 where VOC's and SVOC's were the contaminant of concern, and 4) Westlake Landfill (St. Louis, MO) - support and guidance on landfill issues. ETSC's Rare Earth Elements Report, which was downloaded 6477 times in FY13, was in the top 10 downloads from the EPA web site all year, in FY14 has been in the Top 4 EPA downloads, with 11,314 downloads through 3 quarters.

LRPCD's **three core competencies** *Waste and Materials Management*, *Land Management*, and *Land Systems Decision Analysis* allow the division to support the administrator's priorities and needs of the regions.

- ***Waste and Materials Management*** -- research is a necessary component to sustainable decision-making and materials management tools to be used by communities and involves waste minimization, Life Cycle Assessment (LCA), and materials management. This knowledge is applicable to homeland security and disaster recovery by advancing the scientific foundation and providing innovative solutions for managing municipal, industrial, biological, and emerging wastes and materials.

- ***Land Management*** -- we develop and apply new technologies and strategies that are essential to understanding and managing the risks associated with climate change and minimizing transport and cross/media contamination of air and water by reducing and controlling risks associated with prior and future land use decisions at the local site, ecosystem and landscape scales. These decisions affect both terrestrial and aquatic ecosystems, which are interconnected.

- ***Land Systems Decision Analysis*** -- we are making a strong commitment to conduct core research in the area of Decision Analysis (DA) related to land systems. We will enable land managers to collect, organize, and analyze the complex, multi-attribute datasets needed to make informed, sustainable land use and materials management decisions.

Highlights of the LRPC Division technical outputs and honors in FY 2014 included:

- **61 Journal Articles (32 published, 29 in review)**
- **54 presentations**
- **31 EPA Reports published or in review, 6 book chapters**
- **LRPCD had representatives (as officers, chairs, editors) on 52 committees or editorial boards**
- **11 LRPCD researchers are project leads or task leads, some for multiple projects/ tasks**
- **LRPCD researchers were involved in 52 RAP tasks**
- **56 RAP products and outputs**
- **200 + citations of articles authored by LRPCD researchers (for articles published 2011-2014)**

Table of Contents

FOREWARD iii

NATIONAL RESEARCH PROGRAMS1

1 SUSTAINABLE AND HEALTHY COMMUNITIES (SHC)1
2 SAFE AND SUSTAINABLE WATER RESOURCES (SSWR)2
3 CHEMICAL SAFETY FOR SUSTAINABILITY (CSS)3
4 OTHER PROGRAMS (ACE, HHRA, HSRP) 4

OUTPUTS & ACTIVITIES5

1 PUBLICATIONS**5**
- 1.1 Journal Articles 5
- 1.2 Book Chapters 7
- 1.3 EPA Reports8
- 1.4 Papers in Non EPA Proceedings 9
- 1.5 Other Reports9
- 1.6 Publications Under Review/Submitted 9
  - 1.6.1 Journal Articles9
  - 1.6.2 Book Chapters12
  - 1.6.3 EPA Reports12

2 Pathfinder Innovative Projects13
- 2.1 Biological Desalination of Seawater Using Algae 13
- 2.2 Cyanobacteria Assessment Network (CyAN) 13
- 2.3 Satellite Remote Sensing For Assessing Water Quality 13

3 COMMUNICATIONS & OUTREACH MATERIAL14
- 3.1 Fact Sheets 14
- 3.2 Videos 14
- 3.3 Websites15
- 3.4 Internal Communications 15
- 3.5 External Communications 16

4 PRESENTATIONS17

5 WORKSHOPS21

6 SEMINARS/WEBINARS21

7 DEMONSTRATION SITES22
- 7.1 Community-Scale 22

8 AGREEMENTS22
- 8.1 Cooperative Agreements 22
- 8.2 Interagency Agreements23
- 8.3 Cooperative Research and Development Agreements (CRADAs)26

9 REGIONAL AND PROGRAM SUPPORT 26
- 9.1 Regional & Applied Research Effort (RARE) 26
- 9.2 Regional Field Projects28
- 9.3 Regional Methods Projects 28
- 9.4 Program Support 29

10 WORKGROUPS29

11 COMMITTEES/ EDITORIAL BOARDS31

12 COLLABORATIONS34

13 HONORS AND AWARDS35
13.1 Scientific & Technological Achievement Awards (STAA) 35
13.2 EPA National Honor Awards.....36
13.3 ORD Honor Awards36
13.4 NRMRL Honor Awards36
13.5 Other Awards 36

14 OUTPUTS/ACTIVITIES TOTALS36

National Research Programs

LRPCD has participated in the development and implementation of many Research Action Plans (RAPs) over the last 2 years, as research was reorganized into six National Research Programs. This new structure resulted from the Path Forward initiative towards a focus on sustainability in all of the ORD research. The division's scientists and engineers broadly participated on the Research Action Plan development teams for realignment and integration of ORD's work into the new program areas identified for the Path Forward. LRPCD has scientists supporting all four of the major programs (SHC, SSWR, CSS, and ACE) including a number of project and task leaders. The division is working to support the Path Forward and to incorporate sustainability into all of its research efforts.

LRPCD has primary responsibility for large portions of the SHC program, and with a few exceptions, has achieved all of the RAP outputs that were scheduled for FY2013 for tasks in which it took the lead.

1 Sustainable and Healthy Communities (SHC)

How can we meet today's needs without compromising the ability of future generations to meet their needs? More specifically, how can we protect our shared environment - air, water, land, and ecosystems - in ways that sustain human health and well-being and are economically viable and socially just? Providing the scientific foundation to answer these questions is the goal of EPA's SHC research. Specific SHC RAP tasks that LRPCD scientists are involved in include:

- SHC 1.1.1.2 - DASEES (Decision Analysis for a Sustainable Environment, Economy, and Society)
- SHC 1.1.1.3 - Perspectives analysis and systems framing
- SHC 2.1.3.1 - An integrated study of sustainability in Puerto Rico at multiple spatial scales
- SHC 2.2.1.2 - Environmental factors related to key health outcomes
- SHC 2.2.1.5 - Development and application of community-based decision support tools
- SHC 2.2.2.1 - Identifying factors affecting children's exposures in their communities
- SHC 3.1.1.1 - Innovative physical, chemical and biological tools to assess the performance of sediment remediation
- SHC 3.1.1.2 - Passive sampling techniques for assessing the bioavailability, fluxes, and biotic uptake of contaminants & sediments as related to remediation activities
- SHC 3.1.3 - Science and engineering to restore contaminated sites
- SHC 3.1.3.2 - Technical support for policy, guidance, and targeted research for contaminated site management
- SHC 3.1.4.1 - Protocol development for oil spill countermeasure products listed on the National Contingency Plan Product Schedule (NCPPS)
- SHC 3.1.4.4 - Biodegradability of dispersants and dispersed oil at two temperatures

- SHC 3.1.4.5 - Research supporting LUST sites
- SHC 3.2.1.1 - State-of-the-practice for beneficial use of materials
- SHC 3.2.1 - Tools to assist states in developing beneficial use determinations for wastes
- SHC 3.2.2.1 - Technical report: design and operation of bioreactor landfills
- SHC 3.2.2.2 - Technical report: assessment of available infrastructure for energy recovery
- SHC 3.2.2.3 - Technical report: turning waste streams into community assets
- SHC 3.2.2.4 - Technical report: enhanced energy recovery technologies from waste Organics
- SHC 3.2.3.2 - Technical report: environmental and economic challenges for the enhancement of recyclability and alternative options for reuse of C&D materials
- SHC 3.3.1.7 - Effects of land use change associated with biofuel production scenarios on water quality and aquatic ecosystems
- SHC 3.2.4.1 - Support for OSWER in developing options for managing CCR
- SHC 4.1.1.1 - Synthesizing research and resources for a white paper on buildings and infrastructure solutions for communities and regional areas
- SHC 4.1.2.1 - Fostering sustainable solutions for land use planning and zoning for communities and regional areas
- SHC 4.1.4.1 - Tools for improving materials management
- SHC 4.2.1.1 - Methods to support sustainable design and comprehensive evaluation
- SHC legacy

2 Safe and Sustainable Water Resources (SSWR)

Increasing demands for sources of clean water - combined with changing land use practices, population growth, aging infrastructure and climate change and variability - pose significant threats to our water resources. The SSWR program is undertaking the development of sustainable solutions to 21st century water resource problems by integrating research on social, environmental, and economic outcomes to provide long-lasting solutions. Specific SSWR RAP tasks that LRPCD scientists are involved in include:

- SSWR 1.1C - Watershed integrity and sustainability
- SSWR 1.2C - Linking watershed processes to multiscale ecological tipping points
- SSWR 2.2A - Chemical and microbial contaminant grouping for evaluating ecological and human health
- SSWR 2.3A - Nutrient management for sustainability of upland and coastal ecosystems: building a locally applicable management tool box for application across the U.S.
- SSWR 2.3C - Cyanobacteria, nutrients, and land use - a nexus for sustainable water resources and human health protection
- SSWR 2.3E - Decision support tools to guide ecosystem management and restoration to reduce watershed N and P pollution

- SSWR 2.4 - Mitigating Environmental impacts of subsurface land use practices
- SSWR 2.4D - State of the science for application to mining: literature and laboratory assessments of predictive tests and review of ion removal technologies
- SSWR 3.1A - Watershed modeling
- SSWR 4.1A - CSO mitigation through multi-scale implementation of green infrastructure in communities
- SSWR 4.1C - Adaptive management green infrastructure and sustainable stormwater management w/in environmental justice urban communities
- SSWR 4.3D - Green infrastructure modeling tools and data inventories – stormwater calculator
- SSWR 5.3A - Water Technology Innovation Cluster (WTIC): Develop sustainable processes for contaminant (including nutrient) removal below the limits of current technologies that minimizes costs, energy consumption, environmental burden, chemical consumption, and associated greenhouse gases production
- SSWR 5.5B - Impact of water quality on lead and copper releases due to corrosion
- SSWR 5.5D - Assessing and controlling distribution system contamination
- SSWR 5.2G - Safe and Sustainable management of residuals from municipal wastewater
- SSWR 7.1B - Highly targeted programmatic support, RARE Projects, and Path Forward Innovation Projects
- SSWR legacy

3 Chemical Safety for Sustainability (CSS)

Chemical Safety for Sustainability is a major priority of EPA research. The result is an improved integration of the Office of Research and Development's chemical-related research. Moving toward a safer and more sustainable environment requires producing new and existing chemicals in safer ways. This research requires new information and methods to make better informed, more timely decisions about chemicals. Specific CSS RAP tasks that LRPCD scientists are involved in include:

- CSS 1.2.1 - Detecting, quantifying and characterizing nanomaterials
- CSS 1.2.2 - Environmental transport and transformation of nanomaterials
- CSS 2.1.2 - AOP-based effects monitoring and exposure reconstruction
- CSS 2.62 - Systems-based approach for assessing hazard and risk of manufactured nanomaterials and non-human species and ecosystems
- CSS 4.1.3 - Prediction tools, models and approaches to inform risk management actions and to incorporate sustainable development
- CSS 4.2.2 - Science, approaches, tools, and data for informing cumulative risk assessment and risk management for high priority classes/groups of chemicals
- CSS 5.1.2 – Assessment and mitigation case studies of targeted chemicals and products to identify areas to incorporate sustainability

4 Other Programs - Air, Climate and Energy (ACE), Human Health Risk Assessment (HHRA) and Homeland Security Research Program (HSRP)

As EPA moves forward, it is necessary to more fully understand the interplay between air, climate change, and the changing energy landscape to develop innovative and sustainable solutions to improve air quality and address climate change. LRPCD research in the **ACE** program area includes projects on the release of biofuels from underground storage tanks, and evaluating biogas management Technologies. LRPCD scientists assist the other two programs, **Human Health Risk Assessment (HHRA)** and **Homeland Security Research Program (HSRP)**, as needed.

- HSRP C.4.1.1 - Behavior of chemical, biological, or radiological (CBR) agents in waste treatment processes
- HSRP C.4.1.2 - behavior of chemical, biological, or radiological (CBR) agents in landfills

Outputs and Activities

In Fiscal Year 2014, in support of ORD RAPs in the SHC, SSWR, and CSS programs, LRPCD produced 30 outputs and 26 products (56 total). SHC: 19 outputs, 18 products. SSWR: 8 outputs, 4 products. CSS: 3 outputs, 4 products.

1 Publications

1.1 Journal Articles

1. Baker, L., G. Pierzynski, G. Hettiarachchi, **K. Scheckel**, and M. Newville. uXRF, uXAS and uXRD *Micro-X-Ray Fluorescence, Micro-X-Ray Absorption Spectroscopy, and Micro-X-Ray Diffraction Investigation of Lead Speciation after the Addition of Different Phosphorus Amendments to a Smelter-Contaminated Soil* Journal of Environmental Quality. 43(2): 488-497, (2014) DOI: 10.2134/jeq2013.07.0281 SHC 2.2.1.5
2. Beaulieu, J., R. Smolenski, C. Nietch, A. Townsend-Small, M. Elovitz, and **J. Schubauer-Berigan**. *Denitrification Alternates between a Source and Sink of Nitrous Oxide in the Hypolimnion of a Thermally Stratified Reservoir*. Limnology and Oceanography. 59(2): 495-506, (2014) DOI: 10.4319/lo.2014.59.2.0495 SSWR 1.2C
3. Blaine, A.C., C.D. Rich, L.S. Hundal, C. Lau, **M.A. Mills**, K.M. Harris, and C.P. Higgins. *Uptake of Perfluoroalkyl Acids into Edible Crops via Land Applied Biosolids: Field and Greenhouse Studies*. Environmental Toxicology and Chemistry. 47(24): 14062-14069, (2014) DOI: 10.1021/es403094q CSS 4.2.2
4. Bolan, N., A. Kunhikrishnan, R. Thangarajan, J. Kumpiene, J. Park, T. Makino, M. Kirkham, and **K. Scheckel.** *Remediation of Heavy Metal(loid)s Contaminated Soils – to Mobilize or to Immobilize?* Journal of Hazardous Materials. 266: 141-166, (2014) DOI: 10.1016/j.jhazmat.2013.12.018 SHC 2.2.2.1
5. Chang, H, S. Buettner, J. Seaman, P. Jaffe, P. Koster van Groos, D. Li, A. Peacock, **K. Scheckel** and D. Kaplan. Uranium Immobilization in an Iron-rich Rhizosphere of a Native Wetland Plant from the Savannah River Site under Reducing Conditions. Environmental Science and Technology. 48(16): 9270-9278, (2014) DOI: 10.1021/es5015136 SHC 3.1.3.2
6. Cho, J., M. Suidan and **A. Venosa**. *Biodegradation of Alkylates in Aquifer Material.* Journal of Environmental Sciences-China. 25(8): 1529-1538 (2013), DOI: 10.1016/S1001-0742(12)60180-6 SHC 3.1.4.5
7. **Conmy, R.N.,** P.G. Coble, J. Farr, A.M. Wood, K. Lee, S. Pegau, I. Walsh, C. Koch, M. I. Abercrombie, M.S. Miles, M.R. Lewis, S. Ryan, B. Robinson, T. King, and J. Lacoste. *Submersible Optical Sensors Exposed to Chemically-Dispersed Crude Oil: Wave Tank Simulations for Improved Oil Spill Monitoring.* Environmental Toxicology and Chemistry. 48(3):1803–1810, (2014) DOI: 10.1021/es404206y SHC 3.1.4.1
8. Etschmann, B.E., E. Donner, J. Brugger, D.L. Howard, M.D. de Jonge, D. Paterson, R. Naidu, **K. G. Scheckel**, C.G. Ryan and E. Lombi. *Laterally-resolved Cu Speciation in Biosolids by XANES Imaging.* Environmental Chemistry. 11(3): 341-350, (2014). DOI: 10.1071/EN13189 SHC 3.2.1

9. Gitipour, A., A. El Badawy, M. Arambewela, **B. Miller, K. Scheckel**, M. Elk, H. Ryu, V. Gomez-Alvarez, J. Santo Domingo, S. Thiel, and **T. Tolaymat**. *The Impact of Silver Nanoparticles on the Composting of Municipal Solid Waste*. Environmental Science & Technology. 47(24): 14385-14393, (2013) DOI: 10.1021/es402510a CSS 1.2.2
10. **Hantush, M.**, and A. Chaudhary. *Bayesian Framework for Water Quality Model Uncertainty Estimation and Risk Management.* Journal of Hydrologic Engineering, American Society of Civil Engineers (ASCE). 19(9), 04014015, (2014) DOI: 10.1061/(ASCE)HE.1943-5584.0000900 SSWR Legacy
11. Hoque, Y., **M. Hantush**, and R. Govindaraju. *On the Scaling Behavior of Reliability-Resilience-Vulnerability Indices in Agricultural Watersheds.* Ecological Indicators. 40: 136-146, (2014) DOI: 10.1016/j.ecolind.2014.01.017 SSWR 1.1C
12. Hoque, Y., C. Raj, **M. Hantush**, I. Chaubey, and R. Govindaraju. *How Do Land-Use and Climate Change Affect Watershed Health? A Scenario-Based Analysis.* Water Quality, Exposure and Health. 6: 19-33, (2014). SHC 3.3.1.7
13. Huang, X.L., A. El Badawy, M. Arambewela, **R. Ford**, M. Barlaz, and **T. Tolaymat**. *Characterization of Salt Cake from Secondary Aluminum Production.* Journal of Hazardous Materials. 273: 192-1999, (2014) DOI: 10.1016/j.jhazmat.2014.02.035 SHC 3.1.3.2
14. Juhasz, A., D. Gancarz, C. Herde, S. McClure, **K. Scheckel,** and E. Smith. Is *In Situ Pyromorphite Formation Required in Order To Reduce In Vivo Pb Relative Bioavailability in Contaminated Soils?* Environmental Science and Technology. 48(12): 7002-7009, (2014) DOI: 10.1021/es500994u SHC 2.2.1.5
15. Li, L.P., **K.G. Scheckel**, L.R. Zheng, G.T. Liu, W.Q. Xing, and G.Q. Xiang. *GQ Immobilization of Lead in Soil Influenced by Soluble Phosphate and Calcium: Lead Speciation Evidence*. Journal of Environmental Quality. 43(2): 468-474, (2014) DOI: 10.2134/jeq2013.07.0272 SHC 3.1.3.2
16. Li, L.P., W.Q. Xing, **K.G. Scheckel**, G.Q. Xiang, H.H. Ji, and H. Li. *Lead Retention in a Calcareous Soil Influenced by Calcium and Phosphate Amendments.* Journal of Hazardous Materials. 262: 250-255, (2013) DOI: 10.1016/j.jhazmat.2013.08.058 SHC 3.1.3.2
17. Lombi, E, E. Donner, **K. Scheckel**, R. Sekine, C. Lorenz, N. Von Goetz and B. Nowack. *Silver speciation and release in commercial antimicrobial textiles as influenced by washing.* Chemosphere. 111: 352-358, (2014) DOI: 10.1016/j.chemosphere.2014.03.116 CSS 1.2.2
18. Lunetta, R., B. Schaeffer, R. Stumpf, D. Keith, **S. Jacobs**, and M. Murphy. *Evaluation of cyanobacteria cell counts derived from MERIS imagery across the eastern USA.* Remote Sensing of Environment. (2014) DOI: 10.1016/j.rse.2014.06.008 SSWR 2.3C
19. Mackenbach, E.M., A. D. Harwood, **M. A. Mills**, P. F. Landrum, and M. J. Lydy. *Application of a Tenax Model to Assess Bioavailability of Polychlorinated Biphenyls in Field Sediments.* Environmental Toxicology and Chemistry. 33(2):286-92, (2014) DOI: 10.1002/etc.2423 SHC 3.1.1.1
20. Pinto, P., **S. Al-Abed**, C. Holder, and D. Reisman. *Evaluation of Metal Partitioning and Mobility in a Mine Tailing Pile under Oxic and Anoxic Conditions.* Journal of Environmental Management. 140: 135-144, (2014) DOI: 10.1016/j.jenvman.2014.03.004 SHC 3.1.3.2
21. **Randall, P.,** R. Fimmen, V. Lal, and R. Darlington. *In-Situ Subaqueous Capping of Mercury-Contaminated Sediments in a Fresh-Water Aquatic System, Part I - Bench-Scale Microcosm Study*

to Assess Methylmercury Production. Environmental Research. 125:30-40, (2013) DOI: 10.1016/j.envres.2013.03.012

22. **Randall, P.,** R. Fimmen, V. Lal, and R. Darlington. *In-Situ Subaqueous Capping of Mercury-Contaminated Sediments in a Fresh-Water Aquatic System, Part II - Evaluation of Sorption Materials.* Environmental Research. 125:41-51, (2013) DOI: 10.1016/j.envres.2013.03.010
23. Schaeffer, B.A., K.G. Schaeffer, D. Keith, R.S. Lunetta, **R. Conmy**, and R.W. Gould. *Barriers to Adopting Satellite Remote Sensing for Water Quality Management.* International Journal of Remote Sensing. 34(21): 7534-7544, (2013) DOI: 10.1080/01431161.2013.823524 SSWR Legacy
24. Settimio, L., M. McLaughlin, J. Kirby, K. Langdon, E. Lombi, E. Donner, and **K. Scheckel**. *Fate and Lability of Silver in Soils: Effect of Aging.* Environmental Pollution. 191: 151-157, (2014) DOI:10.1016/j.envpol.2014.04.030 CSS 1.2.2
25. Sharifi, A., L. Kalin, **M. Hantush**, S. Isik, and T. Jordan. *Carbon Dynamics and Export from Flooded Wetlands: A Modeling Approach.* Ecological Modeling. 263:196-210, (2013) DOI: 10.1016/j.ecolmodel.2013.04.023 SSWR 1.1C
26. Sharifi, A., L. Kalin, **M. Hantush**, and S. Isik. *Wetlands: Natural Purifiers of Our Water Bodies*. J. Lamar and B.G. Lockaby. Auburn Speaks. Auburn University, Auburn, AL, USA. 140-143, (2013). SSWR 3.1A
27. Schock, M.R., A.F. Cantor, S. Triantafyllidou, M.K. DeSantis, and **K. Scheckel**. *Importance of Pipe Deposits to Lead and Copper Rule Compliance.* Journal of The American Water Works Association. 106(7): E336-E349, (2014) DOI: 10.5942/jawwa.2014.106.0064 SSWR 5.5B
28. Silva, R.G., M. Nadagouda, C. Patterson, S. Panguluri, **T. Luxton**, E. Sahle-Demessie, and C. Impellitteri. *Polymorph-dependent titanium dioxide nanoparticle dissolution in acidic and alkali digestions.* Environmental Science: Nano. 1(3): 284-292, (2014). DOI: 10.1039/C3EN00103B CSS 1.2.1
29. Smith, E., **K. Scheckel, B. Miller**, J. Weber, and A. Juhasz. *Influence of In Vitro Assay pH and Chyme Composition on As Bioaccessibility in Contaminated Soils*. Science of the Total Environment. 473: 171-177, (2014) DOI: 10.1016/j.scitotenv.2013.12.030 SHC 2.2.1.5
30. Virkutyte, J., S. **Al-Abed, E. Barth**, D. Reible, P. Dunlap, and S. Chattopadhyay. *Catalytic Sorption of (Chloro)Benzene and Napthalene in Aqueous Solutions by Granular Activated Carbon Supported Bimetallic Iron and Palladium Nanoparticles*. ISRN Nanotechnology. 2013:1-8, (2013) CSS 5.1.2
31. Virkutyte, J., **S.R. Al-Abed,** H. Choi, and C. Bennett-Stamper. *Transport of TiO2 Nanoparticles and Nanostructured Particles through a Porous Medium.* Water Research. 443:188-194, (2014) CSS 5.1.2
32. Virkutyte, J., **S. R. Al-Abed**, H. Choi, and C. Bennett-Stamper. *Distinct Structural Behavior and Transport of TiO_2 Nano- and Nanostructured Particles in Sand.* Colloids and Surfaces A: Physicochemical and Engineering Aspects. 443:188–194, (2014) CSS 1.2.1

1.2 BOOK CHAPTERS

1. **Butler, B.** "Sampling and Modeling to Determine Aqueous Geochemical Controls on Metal Transport – North Fork Clear Creek in the Clear Creek Watershed, Colorado" in V.T. McLemore, K.S. Smith, and C.C. Russell (Eds.), Environmental Sampling and Monitoring for the Mine Life

Cycle, Appendix 5: Englewood, CO, Society for Mining, Metallurgy, and Exploration, Inc. 2014 (in press).

2. **Butler, B.** "Hardness", in V.T. McLemore, K.S. Smith, and C.C. Russell (Eds.), Environmental Sampling and Monitoring for the Mine Life Cycle, Appendix 3: Englewood, CO, Society for Mining, Metallurgy, and Exploration, Inc. 2014 (in press).
3. **Butler, B.**, and L. Guenzel. "Whole Effluent Toxicity (WET)", in V.T. McLemore, K.S. Smith, and C.C. Russell (Eds.), Environmental Sampling and Monitoring for the Mine Life Cycle, Appendix 3: Englewood, CO, Society for Mining, Metallurgy, and Exploration, Inc. 2014 (in press).
4. **Rock, S.** "A History of Phytotechnology", in K. Kennen and N. Kirkwood, Phyto: A Resource for Site Remediation and Landscape Design. Harvard University Press. 2014 (in press)
5. Smith, K.S., and **B. Butler.** "Conductivity and Specific Conductance", in V.T. McLemore, K.S. Smith, and C.C. Russell (eds.), Environmental Sampling and Monitoring for the Mine Life Cycle, Appendix 3: Englewood, CO, Society for Mining, Metallurgy, and Exploration, Inc. 2014 (in press).

1.3 EPA Reports

1. **Bessler, S., J. McKernan, S. Stoll**, and **R. Yeardley**. *Engineering Technical Support Center Annual Report Fiscal Year 2013; Technical Support and Innovative Research for Contaminated Sites.* U.S. Environmental Protection Agency, Washington, DC, USA. 2014. (EPA/600/R-14/195) SHC 3.13
2. **Butler, B.** *Pilot-Scale Treatment of Virginia Canyon Mine Drainage in Idaho Springs, Colorado, USA Using Octolig®.* U.S. Environmental Protection Agency, Washington, DC, USA. 2014. (EPA/600/R-14/249) SSWR 7.1B
3. Cox, L., **V. Hansen**, J. Andrews, J. Thomas, I. Heilke, N. Flanders, C. Walters, **S. Jacobs**, Y. Yuan, **A. Zimmer**, J. Weaver, R. Daniels, T. Moore, Y. Tina, D. Payne-Sturges, M. Mccullough, B. Rashleigh, M. Tenbrink, and B. Walton. *Land Use: A powerful Determinant of Sustainable and Health Communities.* U.S. Environmental Protection Agency, Washington, DC, USA. 2014. SHC 4.1.2.1 (Internal Report)
4. **Dyson, B.** *SHC Task 1.1.1.2 DASEES Progress Update.* U.S. Environmental Protection Agency, Washington, DC, USA. 2014. SHC 1.1.1.2 (Internal Report)
5. Foote, E., R. Fimmen, R. Darlington, J. Neff, G. Durell, **R. Brenner**, and **M. Mills**. *Technical Resource Document on Monitored Natural Recovery.* U.S. Environmental Protection Agency, Washington, DC, USA. 2014. (EPA/600/R-14/083) SHC 3.1.1.1
6. **Ford, R.**, M. Brooks, Enfield, and M. Kravitz. *Evaluating Potential Exposures to Ecological Receptors due to Transport of Hydrophobic Organic Contaminants in Subsurface Systems.* U.S. Environmental Protection Agency, Washington, DC, USA. 2014. (EPA/600/R-10/015), ERASC-009 F SHC 3.1.3.2
7. **Luxton, T., D. Carson, G. Evans, M. Kemper, K. Scheckel, S. Wright**, and H. Thurston. *Methods, Metrics and Indicators Available for Identifying and Quantifying Economic and Social Impacts Associated with Beneficial Reuse Decisions: A Review of the Literature.* U.S. Environmental Protection Agency, Washington, DC, USA. 2014. (EPA/600/R-14/247) SHC 3.2.1

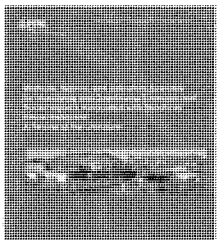

8. **Luxton, T.**, S. Harmon, T. Gerke, W. Platten, N. Sylvest, K. Rogers, and

K. Bradham. *Release of Micronized Copper Particles from Pressure Treated Wood Products.* U. S. Environmental Protection Agency, Washington, DC, USA. 2014. (EPA/600/R-14/365) CSS 1.2.2

9. **McKernan, J.**, R. Darlington, A. Dindal, and **D. Grosse**. *Sediment Ecotoxicity Assessment Ring (SEA Ring).* Environmental Technology Verification Report. U.S. Environmental Protection Agency, Washington, DC, USA. 2014.
10. **McKernan, J.**, and B. Yates. *ANDalyze Lead 100 Test Kit and AND1000 Fluorimeter Environmental Technology Verification Report and Statement.* U.S. Environmental Protection Agency, Washington, DC, USA. 2014. (EPA/600/R-14/052)
11. Townsend, T., **T. Tolaymat**, and H. Kim. *Assessment of Potential End-of-Life Management of Imported Drywall Products.* LRPCD, NRMRL, U.S. Environmental Protection Agency, Cincinnati, OH, USA. 2014 SHC 3.2.3.1 (Internal Report)
12. **Zimmer, A.**, and H. Ha. *Buildings and Infrastructure from a Sustainability Perspective, SHC 4.1.1.* (Internal Report). SHC 4.1.1.1

1.4 Papers in Non EPA Proceedings

1.5 Other Reports

1.6 Publications Under Review/Submitted

1.6.1 Journal Articles

1. Blaine, A.C., C.D. Rich, E.M. Sedlacko, L.S. Hundal, K. Kumar, C. Lau, **M.A. Mills**, K.M. Harris, and C.P. Higgins. *Perfluoroalkyl Acid Distribution in Various Plant Compartments of Edible Crops Grown in Biosolids-Amended Soils.* Submitted to Environmental Science & Technology. CSS 4.2.2
2. Burgess, R., R. Lohmann, **J. Schubauer-Berigan**, M. Perron, L. Lefkovitz, P. Reitsma, and M. Cantwell. *Application of Passive Sampling for Measuring Dissolved Concentrations (Cfree) of Organic Contaminants in the Water Column at Three Marine Superfund Sites.* Submitted to Environmental Toxicology and Chemistry. SHC 3.1.1.2
3. Chekli, L., B. Bayatsrmadi, R. Sekine, B. Sarkar, A. Maoz Shen, **K. Scheckel**, W. Skinner, R. Naidu, H. Shon, E. Donner, and E. Lombi. *Characterisation of Nanoscale Zero-Valent Iron for Soil and Groundwater Remediation: A Methodological Review.* Submitted to Critical Reviews Environmental Science and Technology. CSS 1.2.2
4. **Conmy, R.**, P. Coble, J. Farr, A.M. Wood, K. Lee, W.S. Pegau, I. Walsh, C. Koch, M. Abercrombie, M.S. Miles, M. Lewis, S. Ryan, B. Robinson, T. King, and J. Lacoste. *Performance of Submersible Optical Sensors Exposed to Chemically-Dispersed Crude Oil: Wave Tank Simulations for Improved Oil Spill Monitoring.* Submitted to Environmental Science & Technology. SHC 3.1.4.1
5. Cutler, W., A. El-Kadi, N. Hue, J. Peard, **K. Scheckel** and C. Ray. *Iron Amendments to Reduce Bioaccessible Arsenic.* Submitted to Journal of Hazardous Materials. SHC 3.1.3.2
6. Gerke, T., B. Little, **T. Luxton**, **K. Scheckel**, and B. Maynard. *Strontium Concentrations in Corrosion Products from Residential Drinking Water Distribution Systems.* Submitted to Environmental Science & Technology. SSWR 5.5D
7. Green, T., D. Thomas, A. El-Badawy, and **T. Tolaymat**. *Comparative Cytotoxicity of Silver*

Nanomaterials in a Murine Macrophage Cell Line. Submitted to Toxicology. CSS 1.2.1

8. Grosser, R. J., B. Morris, **D.A. Carson** and **W. J. Davis-Hoover.** *Enumeration of Bacteria from Landfill Bioreactor Leachates Using Culture-Independent Molecular and Classical Culture-Dependent Microbiological Methods*. Accepted for J. Solid Waste Tech. Management. SSWR 5.2G
9. **Herrmann, R.,** R. Grosser, D. Farrar, and B. Brobst. *Field Studies Measuring the Aerosolization of Endotoxin during the Land Application of Class B Biosolids.* Submitted to Journal of Environmental Quality. SSWR 5.2G
10. Hoque, Y., **M. Hantush**, and R. Govindaraju. *Development of Aggregate Measures of Watershed Reliability, Resilience and Vulnerability using Variational Bayesian Noise Principal Component Analysis*. Submitted to Ecological Modeling. SSWR 1.1C
11. Hoque, Y., S. Tripathi, **M. Hantush**, and R. Govindaraju. *Development of Aggregate Measures of Watershed Reliability, Resilience and Vulnerability using Relevance Vector Machine and Variational Bayesian Noisy Principal Component Analysis.* Submitted to Ecological Modeling. SSWR 1.1C
12. Kirichenko, O., J. Virkutyte, E. Shuvalova, E. Finashina, T. Brueva, L. Kustov, and **S. Al-Abed**. *Degradation of Tetrachloroethylene (PCE) in Aqueous Solutions by Supported Fe-Pd Nanoparticles.* Submitted to Environmental Technology. CSS 5.1.2
13. Kustov, L.M., **S.R. Al-Abed**, J. Virkutyte, O.A. Kirichenko, E.V. Shuvalova, G.I. Kapustin, I.V. Mishin, V.D. Nissenbaum, O.P. Tkachenko, and E.D. Finashina. *Novel Fe-Pd/SiO2 Catalytic Materials for Degradation of Chlorinated Organic Compounds in Water.* Submitted to Applied Catalysis B: Environmental. CSS 5.1.2
14. Lazorchak, J., M. Griffith, **M. Mills**, **J. Schubauer-Berigan**, F. McCormick, **R. Brenner**, and C. Zeller. *Proof of Concept for the Use of Macroinvertebrates as Indicators of PCB Contamination in Lake Hartwell.* Submitted to Environmental Toxicology and Chemistry. SHC 3.1.1.1
15. Meier, J., J. Lazorchak, **M. Mills**, P. Wernsing, and P. Baumann. *Monitoring Exposure of Brown Bullheads and Benthic Macroinvertebrates to Sediment Contaminants in the Ashtabula River Before, During, and After Remediation.* In review by Environmental Toxicology and Chemistry. SHC 3.1.1.1
16. **Niazi, M.**, C. Obropta, and R. Miskewitz. *Pathogen Transport and Fate Modeling In the Upper Salem River Watershed Using SWAT Model.* Submitted to Journal of Water Resources Planning and Management. SSWR 3.1A
17. Platten, W., P. Campo, M. Suidan and **A. Venosa**. *Evaluation of a Gravity Flow Membrane Bioreactor for Treating Municipal Wastewater.* Submitted to Water Research. SSWR 5.3A
18. Schaeffer, B., **R. Conmy**, A. Duffy, J. Aukamp, D. Yates, and G. Craven. *Northern Gulf of Mexico Estuarine Coloured Dissolved Organic Matter Derived from the MODIS Satellite.* Submitted to International Journal of Remote Sensing. SSWR 2.3A
19. **Scheckel, K.**, G. Diamond, M. Burgess, J. Klotzbach, M. Maddaloni, **B. Miller**, C. Partridge, and S. Serda. *Amending Soils with Phosphate as Means to Mitigate Soil Lead Hazard: A Critical Review of the State of the Science.* Submitted to Journal Of Toxicology And Environmental Health - Part B: Critical Reviews. SHC 2.2.1.2
20. Sekine, R., G. Brunetti, E. Donner, M. Khaksar, K. Vasilev, A. Jamting, **K. Scheckel**, P. Kappen,

H. Zhang, and E. Lombi. *Speciation and lability of Ag-, AgCl- and Ag2S-Nanoparticles in Soil Determined by X-Ray Absorption Spectroscopy and Diffusive Gradients in Thin Films.* Submitted to Environmental Science & Technology. CSS 1.2.2

21. Sharifi, A., L. Kalin, **M. Hantush**, J. Maynard, A. O'Geen, and R. Dahlgren. *Capturing Spatial Variability of Concentrations and Reaction Rates in Wetland Water and Soil through Model Compartmentalization.* Submitted to Journal of Hydrologic Engineering. SSWR 2.3E.
22. Stuckman, M., **K. Scheckel** and J. Lenhart. *Influence of Leaching Conditions on Arsenic Coordination and Release from Spent Water Treatment Adsorbents.* In review by Environmental Science and Technology. SHC 3.2.1
23. Sundaravadivelu, D., M. Suidan, **A. Venosa** and P. Rosales. *Effect of Operational Variables on the Performance of Oil Solidifiers under a Newly Developed Testing Protocol using a Light, Medium and Heavy Oil.* Submitted to Chemosphere. SHC 3.1.4.1
24. Vasileiadis, S., E. Puglisi, M. Trevisan, **K. Scheckel**, K. Langdon, M. McLaughlin, E. Lombi, and E. Donner. *Silver-induced Disturbance Increases Diversity in Soil Microbial Communities and Selects for Persistent/Resistant Phenotypes.* Submitted to PNAS (Proceedings of The National Academy of Sciences). CSS 1.2.1
25. Wang, H., K. Ho, **K. Scheckel**, F. Wu, M. Cantwell, D. Katz, D. Borsay, W. Boothman, and R. Burgess. *Toxicity, Bioaccumulation and Biotransformation of Silver and Titanium Dioxide Nanoparticles in Marine Organisms.* Submitted to ?? CSS 2.62
26. Xing, W., Y. Wang, **K. G. Scheckel**, L. Li, G. Xiang, D. Gong, and L. Shi. *Effects of Anions on the Immobilization of Heavy Metals in a Polluted Soil with Soluble Phosphate.* Accepted by Acta Scientiae Circumstantiae. SHC 2.2.1.5
27. Zhang, M., G. Abulikemu, P. Campo, W. Platten II, M. Suidan, and **R. Conmy.** *A Comparative Study on the Biodegradability of Crude Oil Dispersed with JD-2000 at 5 and 25 degrees C.* Submitted to Environmental Science and Technology. SHC 3.1.4.4
28. Zia, M.H., E. E. Codling, **K. G. Scheckel**, A. K. Rai, and R. L. Chaney. *Urban Soil Bioaccessible Lead Test: A Tool for Lead (Pb) Risk Assessment for Contaminated Urban Garden Soils.* In review by Environmental Toxicology and Chemistry. SHC 2.2.1.5
29. Zhao, L., B. Wang, P. Armenante, **R. Conmy**, and M. Boufadel. *Evaluation of Turbulence Structures in Laboratory Baffled Flasks under Different Mixing Energy: Implications for Dispersant Effectiveness Testing.* Submitted to Environmental Fluid Mechanics. SHC 3.1.4.1

1.6.2 Book Chapters

1. **Hantush, M.M.**, and L. Kalin. Modeling Nitrogen Fate and Transport at the Sediment-Water Interface. Book Chapter. Springer. In review.

1.6.3 EPA Reports

1. **Al-Abed, S.** *Critical Review of Treatment Technologies for Removal of Salts [Ca, HCO3, K, Mg,*

Na, SO4] from Water: Potential for Application to Coal Mining Impacted Water. U.S. Environmental Protection Agency, Washington, DC, USA. SSWR 2.4D

2. Bradley, P., W. Fisher, S. Yee, J. Carriger, **B. Dyson**, J. Bousquin, E. Huertas, and G. Gambirazzio. *Application of Formal Decision Process for Informing Watershed Management Options in Guanica Bay, Puerto Rico.* U.S. Environmental Protection Agency, Washington, DC, USA. SHC 1.1.1.2
3. Bradley, P., W. Fisher, **B. Dyson**, and A. Rehr. *Coral Reef and Coastal Ecosystems Decision Support Workshop.* U.S. Environmental Protection Agency, Washington, DC, USA. SHC 1.1.1.2
4. Cox, L., **V. Hansen**, J. Andrews , J. Thomas, I. Heilke, N. Flanders, C. Walters , **S. Jacobs**, Y. Yuan , I. Heilke, **A. Zimmer**, J. Weaver, R. Daniels, T. Moore, T. Yuen, D. Payne-Sturges , M. Mccullough, B. Rashleigh, M. TenBrink, and B. Walton. *Land Use: A Powerful Determinant of Sustainable and Healthy Communities.* U.S. Environmental Protection Agency, Washington, DC, USA, 2012. SHC 4.1.2.1
5. Dindal, A., and **T. Richardson**. *Generic Protocol for Verification of In Situ Chemical Oxidation.* LRPCD, NRMRL, U.S. Environmental Protection Agency, Cincinnati, OH, USA. In review.
6. Ely, C., **S. Rock.** *Food Waste to Energy: How Six Water Resource Recovery Facilities are Boosting Biogas Production and the Bottom Line.* U. S. Environmental Protection Agency, Washington, DC, USA. SHC 3.2.2.2
7. Fisher, W., J. Carriger, P. Bradley, and **B. Dyson**. *Values and Objectives of Stakeholders in Guernica Bay, Puerto Rico.* U.S. Environmental Protection Agency, Washington, DC, USA. (Internal Report) SHC 2.1.3.1
8. **Jacobs, S.**, and **J. Schubauer-Berigan**. *St. Francis Rain Garden Water Quality Sampling Interim Data Report; Total Nitrogen, Total Phosphorus, Sediments or Solids, and E. Coli for the period April to June, 2014.* U.S. Environmental Protection Agency, Washington, DC, USA. SSWR 4.1C
9. Jain, P., **D. Carson**, and **T. Tolaymat**. *Closed Waste Sites as Community Assets: A Guide for Municipalities, Landfill Owners, and Regulators.* U. S. Environmental Protection Agency, Washington, DC, USA. SHC 3.2.2.3
10. **Kremer, F.** *Materials Management: State of the Practice 2012.* LRPCD, NRMRL, U.S. Environmental Protection Agency, Cincinnati, OH, USA. SHC 1.1.1.2
11. **McKernan, J.** *Vapor Intrusion Pathway Screening for Soil Excavation Remedies.* U.S. Environmental Protection Agency, Washington, DC, USA. SHC 3.1.3.2
12. **McKernan, J.** *Engineering Issue Paper: Biotransformation Pathways of Dimethylarsinic (Cacodylic) Acid in the Environment.* U.S. Environmental Protection Agency, Washington, DC, USA. SSWR 7.1B
13. **Tolaymat, T.**, and A. El Badawy. *Evaluation of P-Listed Pharmaceutical Residues in Empty Pharmaceutical Containers.* U.S. Environmental Protection Agency, Washington, DC, USA.
14. **Tolaymat, T.**, and **B. Dyson.** *Materials Management: State of the Practice 2012.* U.S. Environmental Protection Agency, Washington, DC, USA. SHC 4.1.4.1
15. **Tolaymat, T., D. Carson,** and J. Powell. *Data Gap Analysis and Damage Case Studies: Risk Analyses from Construction and Demolition Debris Landfills and Recycling Facilities.* LRPCD, NRMRL, U.S. Environmental Protection Agency, Cincinnati, OH, USA. SHC 3.2.3.1
16. **Tolaymat, T.**, P. Jain, D. Meyer, W. Ingwersen, and **B. Dyson**. *Multimedia Environmental Assessment of Existing Materials Management Approaches for Communities.* U.S. Environmental

Protection Agency, Washington, DC, USA. SHC 4.1.4.1

17. **Tolaymat, T.**, and J. Morris. *Permitting of Landfill Bioreactor Operations: Ten Years after the RD&D Rule.* U. S. Environmental Protection Agency, USA, DC, Washington SHC 3.2.2.1

2 Pathfinder Innovative Projects (PIP) (PIP II - Ongoing)

2.1 **INNOVATIVE BIOTECHNOLOGY** - *Innovative Approach for Biological Desalination of Seawater Using Algae.* Endalkachew Sahle-Demessie (NRMRL/STD), **T. Tolaymat** (NRMRL/LRPCD) Ashraf Aly Hassan (NRMRL/STD), A. El Badawy (NRMRL/LRPCD). This study will investigate, evaluate and develop the principal components of a cost effective, engineered bioreactor to treat saline waters. This is an innovative biological desalination system for the removal of salinity from seawater using halophyte algae and to use the algae for bio-fuel production. This project addresses several fundamental challenges in different areas of modem biology and engineering. Advances made over recent years in biology and bioreactor technology have created an exciting research environment for tackling these challenges now with a realistic chance of success. If successful, this technology could alleviate freshwater shortage for millions of people by operating solely or combined with other available desalination technologies. It ensures that drinking water would be available, less polluted and cheaper while producing valuable biofuel as a byproduct.

2.2 **INNOVATIVE BIOTECHNOLOGY** - *Cyanobacteria Assessment Network (CyAN) for Freshwater Systems: an Early Warning Indicator for Toxic Blooms Using the MERIS Satellite.* Blake Schaeffer (NHEERL/GED), Ross Lunetta (NERL/ESD), **Scott Jacobs** (NRMRL/LPRCD), Richard Stumpf (NOAA), Lesley Vazquez-Coriano (OST/OW/HECD), **Robyn Conmy** (NRMRL/LRPCD), Darryl Keith (NHEERL/AED), Bryan Milstead (NHEERL/AED), James Hagy (NHEERL/GED), Keith Loftin (USGS) Cyanobacterial blooms occur worldwide and are associated with human respiratory irritation, taste and odor of potable water, and human illness as a result of ingestion or skin exposure during recreational activities. This project will develop an approach to detect and predict the development and dissipation of cyanobacteria blooms in our nation's freshwater systems using satellite technology.

2.3 **SATELLITE REMOTE SENSING FOR ASSESSING WATER QUALITY** - *Prototype Smart Phone Application to Report Water Quality Conditions.* The EPA Pathfinder Innovation Project has identified that environmental managers are typically limited in their time and ability to use and handle satellite remote sensing data due to the file size and complexity in the data structures. Therefore this project developed the Mobile Access to Remote Sensing (MARS) prototype mobile application. This application has the potential to disseminate satellite images as geo-referenced data images to mobile devices. Satellite images to be made available to stakeholders, federal and state policy makers, environmental managers and the general public. The same people will have the ability to send data back to the system. People will have the opportunity to be at a location, pull up the satellite imagery on their mobile device and view a map of their surroundings in terms of water quality parameters such as phytoplankton biomass, suspended material, light attenuation, and colored dissolved organic matter. They will also have the ability to provide their qualitative or quantitative assessment of the water quality

to the website for others to see and view. This will allow scientists to make connections between quantitative data and qualitative responses based on stakeholder perceptions. The application will also allow users to pull the historical archive of all available water quality parameters at that particular location for viewing of the historical record. Scientists and managers will be able to identify other projects focused within a particular water body. They can upload the parameters that they are focusing on and contact information. This is a way to connect policy makers, environmental managers, scientists, and lay people together who may not otherwise realize that they all have interests in the same system. http://gisstg2.rtpnc.epa.gov/hico/. Blake Schaeffer (NHEERL/GED), Darryl Keith (NERL/ESD), Ross Lunetta (NERL/ESD), **Robyn Conmy** (NRMRL/LPRCD), Richard Gould (Naval Research Laboratory). (SSWR)

3 Communications & Outreach Material

3.1 Fact Sheets

Added to the NSCEP pages of the EPA web site, as well at other appropriate web site project and topical pages.

1. *Comprehensive Technical Support Document on Rare Earth Elements is a Valuable Resource to Public and Private Sector Stakeholders.* Science in Action. U.S. Environmental Protection Agency, Washington, D.C., **Yeardley, R.B., D. Reisman,** and R. Weber. EPA/600/F-13/296 SHC 3.13
2. *Researchers Study Properties of Nanomaterials to Understand How They Are Transported and Transformed in the Environment.* Science in Action. U.S. Environmental Protection Agency, Washington, D.C., **Yeardley, R.B., et al.** (in review) CSS 1.2.2

3.2 Videos

1. ***Managers Videos: Interviews with scientists - Lek Kadeli and Mitch Kostich (NERL).*** LRPCD TTS Filmed and edited this video. Still in review with ORD communications.

2. ***Niagara River: Partnering to protect a valuable and limited water resource*** - Concept approved in Protrac. Script in production. SHC 3.1.1.1

For decades the U.S. EPA has worked to protect the nation's valuable and limited water resources. This continues to be a priority for the current administrator. The EPA also has a long history of collaborating with a large range of stakeholders, including communities, and other federal and state agencies. One project that highlights this type of collaboration is the Niagara River project. Here the EPA works with multiple partners to identify the sources and levels of contaminants that various tributaries are adding to the Niagara River, just upstream from Niagara Falls.

3. *Drinking Water Pilot Plant* - Video taken of pilot plant apparatus, and motion speeded up for use in a Powerpoint presentation. Done at the request of WSWRD DD, Thomas Speth.

3.3 WEBSITE

1. *LRPCD Internet* - Processed numerous JIRA requests to upload new pages (Hard Rock Mining Conference event page) and reports, and to fix issues found with internet and intranet pages.
2. *508 compliance/ Accessibility* - Produced and presented an internal presentation. Reviewed and gave input on a NRMRL SOP for 508 compliance.

3.4 INTERNAL COMMUNICATIONS

1. *NRMRL Communications Action Team (CAT)* - LRPCD staff took the lead this group, which started by addressing internal communications and producing an *Internal Communications Management Assessment*, with a list of recommended short- and long-term actions to improve internal communications. LRPCD staff also participating on the Scientific Interactions and Meeting Effectiveness teams to address these areas that were identified by the management assessment as areas for needed actions.
2. *Web Site Activity* - A complete inventory of LRPCD web pages was made and with input from the branch chiefs and ADD, disposition of each page (migrate, archive, or delete) under the new topical OneEPA web structure was determined. Working with TCOS staff, transformation of those pages that were identified for migration has begun. Once migration of existing pages is completed, analysis of what new pages are needed, and then production of new pages will start.
3. *Annual Division Report* - Produced for communication within LRPCD and to NRMRL and ORD management about the division's accomplishments for each year.

4. *Research Compass* - Articles about LRPCD scientists were posted in this ORD-wide email newsletter.
5. *NRMRL News* - Noteworthy weekly activities of LRPCD staff are sent to NRMRL and ORD IO, and published on the NRMRL main intranet page.

3.5 EXTERNAL COMMUNICATIONS

1. *Division External Communications* - In addition to fact sheets posted on the EPA web site, an article was published in Science Matters, information about projects was communicated via social media (Twitter), and a video project for EPA YouTube is in production.
2. 508 compliance - See *Web Site* section above.
3. Answering external inquiries - LRPCD gets 1- 2 inquiries per month by phone or email asking for environmentally-related information. Some relate to our research here, some not so much. Most inquiries are responded to. At least to acknowledge the request and inform them of the status, within a day or less. If they are related to what we do, inquiries are routed to the appropriate expert(s). Scientists may respond directly to the person inquiring or through the TTS. LRPCD have been generous with their time in providing useful information to citizens. Many inquiries don't relate to our research. In these cases, we try to supply them with contact information for their state environmental protection agencies - EPA, DEC, DNR, etc.

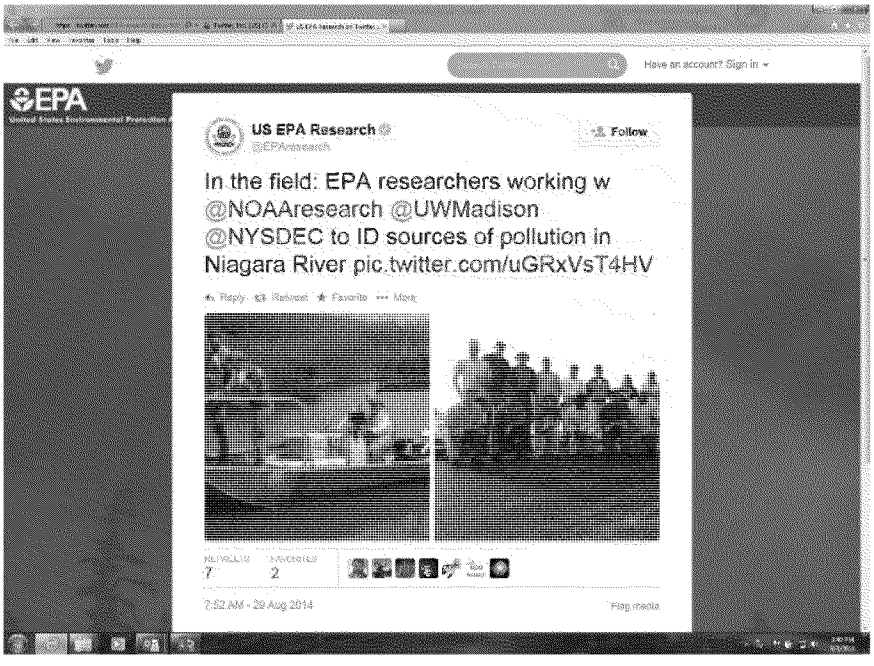

4 Presentations

1. **Al-Abed, S.**, *Nanotechnology and the Environment: Implications and Applications.* 2014 Central & Eastern European Conference on Health and the Environment. Cluj-Napoca, Romania. June 25-30, 2014. CSS 5.1.2
2. **Al-Abed, S.**, *Current and Innovative Remediation Technologies used in Contaminated Sites.* 2014 Central & Eastern European Conference on Health and the Environment. Cluj-Napoca, Romania. June 25-30, 2014. SHC 3.1.3.2
3. **Al-Abed, S.**, *Environmental Chemistry Principles in Site Remediation.* 2014 Central & Eastern European Conference on Health and the Environment. Cluj-Napoca, Romania. June 25-30, 2014. SHC 3.1.3.2
4. Arini, A., J. Cavallin, J. Berninger, R. Marfil-Vega, **M. Mills**, D. Villeneuve, and N. Basu. *Coupling in Vitro And In Vivo Neurochemical-Based Assessments of Wastewater Effluents from the Maumee River Area of Concern (AOC).* SETAC, Nashville, TN, USA. November 17 – 21, 2013. CSS 2.1.2
5. Benotti, M., L. Lefkovitz, and **M. Mills**. *Application of Polyethylene Devices (PEDs) for Monitoring PCBs at a Freshwater Sediment Remediation Site.* SETAC North America 34th Annual Meeting, Nashville, TN, USA. November 17 – 21, 2013. SHC 3.1.1.1
6. Benotti, M., **M. Mills**, and L. Lefkovitz. *Application of Polyethylene Devices (PEDs) for Monitoring PCBs at a Freshwater Sediment Remediation Site (Cincinnati, Ohio).* Working Together For Clean Water: 9th National Monitoring Conference, Cincinnati, OH, USA. April 28 - May 2, 2014. SHC 3.1.1.2
7. Buchholtz, R., M. tenBrink, J. Fiksel, **B. Dyson**, G. Foley, I. Heilke, M. Hoagland, A. Bassi, P. Bradley, E. Ruder, S. Yee, W. Berry, H. Walker, and J. Hunter. *Bringing Systems Thinking into Community-based Environmental Management.* 2014 Conference on Earth System Governance, Norwich, NA, UK. July 1 – 3, 2014. SHC 1.1.1.3
8. Chaudhary, A., and **M. Hantush**. *Application of Bayesian Monte Carlo Methods to a Lake Oxygen Recovery Model.* World Environment and Water Resources Congress. Austin, TX, USA. May 17-21, 2015. SSWR 2.3E
9. **Conmy, R**., R. Parsons, J. Farr and B. Schaeffer. *Estimating oil concentrations in the Deepwater Horizon subsea oil plume using in situ fluorescence.* Ocean Sciences Conference. Honolulu, HI, USA. February 24-28, 2014. SHC 3.1.4.1
10. **Conmy, R.B**., T. Robinson, M. King, P. Abercrombie, K. Coble, K. Lee and **A. Venosa**. *Optical tools in oil spill response: an historical and current perspective in decision-making.* Ocean Optics

Conference. Portland, Maine, USA. October 27-31, 2014. SHC 3.1.4.1

11. **Conmy, R.**, **A. Venosa**, S. Courtenay, T. King, B. Robinson, and S. Ryan. *Oil Droplet Size Distribution and Optical Properties during Wave Tank Simulated Oil Spills.* American Geophysical Union's 46th Annual Fall Meeting, San Francisco, CA, USA. December 9 – 12, 2013. SHC 3.1.4.4
12. **Conmy, R.**, P. Coble, J. Farr, A.M. Wood, R. Parsons, K. Lee, W.S. Pegeau, I. Walsh, C. Koch, M. Abercrombie, M.S. Miles, M. Lewis, S. Ryan, B. Robinson, T. King, and J. Lacoste. *Performance of Submersible Optical Sensors Exposed to Chemically-Dispersed Crude Oil: Wave Tank Simulations for Improved Oil Spill Monitoring.* International Oil Spill Conference, Savannah, GA, USA. May 5 – 8, 2014. SHC 3.1.4.1
13. **Davis-Hoover, W.**, M.M. Wade, and H. Salem. *Persistence of Chemical and Biological Agents in Landfill Leachates.* 2014 Conference on Remediation of Chlorinated and Recalcitrant Compounds, Monterey, CA, USA. May 19 - 22, 2014. HSRP C.4.1.2
14. **Ford, R.**, and J. Briskin. *Overview of EPA's Approach to Developing Prospective Case Studies Technical Workshop: Case Studies to Assess Potential Impacts of Hydraulic Fracturing on Drinking Water Resources.* Hydraulic Fracturing Case Studies. Research Triangle Park, NC, USA. July 30, 2014. NA
15. **Ford, R.**, G. Lombardo, and **J. McKernan**. *Fort Devens Superfund Site: Technical Support - A Vehicle for Research.* LRPCD Science Meeting, Cincinnati, OH, USA. October 24, 2013. SHC 3.13
16. Gatchett, A., **E. Barth**, and **J. McKernan**. *Overview of EPA Office of Research and Development's Technical Support Centers.* Ohio EPA Visit to AWBERC EPA, Cincinnati, OH, USA. August 6, 2014. SHC 3.13
17. **Gilliland, A.**, and C. Kloss. *Greening CSO Plans: Planning and Modeling Green Infrastructure (GI) for Combined Sewer Overflow (CSO) Control.* SSWR Webinar, Cincinnati, OH, USA. March 26, 2014. SSWR 4.3D
18. Green, T., A. El-Badawy, **T. Tolaymat**, and D. Thomas. *In Vitro Cytotoxicity and Phagocytosis of Silver Nanomaterials in Murine Macrophages.* Society of Toxicology. Phoenix, AZ, USA. March 23-27, 2014. CSS 1.2.2
19. Griggs, J., L. Santiago, **T. Luxton**, K. Rogers, C. Nelson, and K. Bradham. *Bioaccessibility and Solubility of Copper in Copper-Treated Lumber.* Conference on the Environmental Effects of Nanoparticles and Nanomaterials, Columbia, SC, USA. September 7 – 11, 2014. CSS 1.2.2
20. **Grosse, D.** *Overview of USEPA's ORD Technical Outreach and Support Activities.* National Conference on Mining-Influenced Waters. Albuquerque, NM, USA. August 12-14, 2014. SHC 3.13
21. **Grosse, D.**, and B. Schumacher. *Workshop: Vapor Intrusion (VI) Exposures - The Challenges of, Need for, and Benefits of Long Term Stewardship.* The 24th Annual AEHS International West Coast Conference on Soils, Water, Energy and Air, San Diego, CA, USA. March 18, 2014. SHC 3.13
22. **Hantush, M.**, and A. Chaudhary. *Risk-Based Estimation of TMDLs and Related Margin of Safety.* World Environmental & Water Resources Congress 2014, Portland, OR, USA. June 1 - 5, 2014. SSWR 3.1A
23. Hall, A., **M. Mills**, and **K. Fetters**. *Characterizing Polychlorinated Biphenyl (PCB) Sediment Contamination Using GIS.* 2014 ESRI User Conference. San Diego, CA, USA. July 14-18, 2014. SHC 3.1.1.1

24. **Hansen, V**. *A Framework for Applying Tools to Achieve Sustainable Land Use: Presentation of Phase 5 Concept Paper*. Research for More Sustainable Urban Land Management-Enhancing Transatlantic Transfer of Knowledge. Leipzig, NA, GERMANY. March 6-8, 2014. SHC 1.1.1.2
25. **Jacobs, S.** *Weaving Natural Processes into the Built Environment with Green Infrastructure - Cincinnati, OH*. Integrated Society of Exposure Sciences (ISES). Cincinnati, OH, USA. October 12-16, 2014. SSWR 4.1A
26. **Jacobs, S.** *Green Infrastructure and Storm Water Management*. Southwest Ohio Water Environment Association, Industrial Waste Committee's Annual Industrial Waste Seminar. Cincinnati, OH, USA. January 23, 2014. SSWR 4.1A
27. Keith, D., B. Schaeffer, R. Lunetta, **R. Conmy**, M.S. Murphy, and T. Hultgren. *Smart Phone Application Development and Demonstration in Support of EPA HICO Imagery for Coastal and Ocean Protection.* International Space Station Research and Development Conference. (3rd Annual), Chicago, IL, USA. June 17 - 19, 2014. SSWR 2.3A
28. Lazorchak, J., **R. Ford**, **B. Lien**, **M. Mills**, and H. Williams. *Evaluation of Cap Effectiveness for Reducing Aquatic Biota Exposure to PAHs using PEDs and HDs on the West Branch of the Grand Calumet River, IN.* SETAC Annual Meeting, Nashville, TN, USA. November17-21, 2013. SHC 3.1.1.1
29. Lazorchak, J., **M. Mills**, **R. Ford**, **B. Lien**, **P. Clark**, K. Fritz, J. Meier, A. Mucha S. Cieniawski, H. Williams, and D. Walters. *Great Lakes Areas of Concern (AOC): U.S. EPA Research on Assessing Remedy and Restoration Success.* Great Lakes Conference, East Lansing, MI, USA. March 4, 2014. SHC 3.1.1.1
30. **Lien, B**., and **R. Ford**. *Quantifying Seepage Flux Using Sediment Temperatures*. Eighth International Conference on Remediation and Management of Contaminated Sediments. New Orleans, LA, USA. January 12-15, 2015. SHC 3.1.1.1
31. **McKernan, J**. *Overview of Alternative Remediation and Treatment Technologies for Polychlorinated Biphenyls (PCBs).* Teleconference Meeting with Region 5 and the Mayor of Kalamazoo, MI to Discuss Alternative Remediation and Treatment Technologies for Polychlorinated Biphenyls (PCBs). Chicago, IL, USA. September 18, 2014. SHC 3.13
32. **McKernan, J**., M. Ellenbecker, C. Holcroft, and M. Petersen. *Development and Evaluation of Proposed Equations for Improved Exothermic Process Control.* 2014 ASHRAE Winter Training Conference. New York, NY, USA. January 18-22, 2014. SHC 3.13
33. **McKernan, J.**, V. Fong, **C. Acheson, R. Parker, T. Lyons, S. Bessler**, H. Rectanus, A. Dindal, and B. Yates. *Bioremediation Potential for Dioxin – Vietnam*. Vietnam Environmental Delegation, Research Triangle Park, NC, USA. November 7, 2013. SHC 3.13
34. **McKernan, J.**, V. Fong, **C. Acheson, R. Parker, T. Lyons, S. Bessler**, H. Rectanus, A. Dindal, and B. Yates. *Bioremediation Potential for Dioxin – Vietnam*. POPs/Dioxin Pollution Assessment and Remediation. Da Nang, NA, Vietnam. December 1-5, 2013. SHC 3.13
35. **McKernan, J.**, V. Fong, **C. Acheson, R. Parker, T. Lyons, S. Bessler**, H. Rectanus, A. Dindal, and B. Yates. *Bioremediation Potential for Dioxin – Romania*. 2014 Central & Eastern European Conference on Health and the Environment. Cluj-Napoca, Romania. June 25-30, 2014. SHC 3.13
36. **McKernan, J., B. Butler**, A. Levine and **D. Grosse**. *Stewardship Concepts for Management of Hard Rock Mining Wastewaters.* Hard-Rock Mining Conference—A National Conference on

Mining-Influenced Waters. Albuquerque, NM, USA. August 12-14, 2014. SHC 3.13

37. **McKernan, J., B. Butler**, A. Levine and **D. Grosse**. *Stewardship Concepts for Management of Hard Rock Mining Wastewaters - Romania.* 2014 Central & Eastern European Conference on Health and the Environment. Cluj-Napoca, Romania. June 25-30, 2014. SHC 3.13
38. **McKernan, J.**, H. Rectanus, **C. Acheson, S. Bessler**, and A. Dindal. *Bioremediation Potential for Dioxin.* 2014 Central & Eastern European Conference on Health and the Environment. Cluj-Napoca, Romania. June 25-30, 2014. SHC 3.13
39. **Niazi, M.,** and **J. Schubauer-Berigan.** *Contaminated Sediment Fate and Transport Model in the Tri-State Mining District.* National Conference on Mining-Influenced Waters. Albuquerque, NM, USA. August 12-14, 2014. SHC SHC 3.13
40. **Niazi, M.,** and **J. Schubauer-Berigan.** *Geospatial Analysis of Contaminated-Sediments and Water Quality in the Spring River Watershed.* SETAC North America 35th Annual Meeting. Vancouver, Canada. November 9-13, 2014. SHC 3.13
41. **Niazi, M., J. Schubauer-Berigan** and **M. Hantush**. *Contaminated Sediment Fate and Transport Model in the Tri-State Mining District.* National Conference on Mining-Influenced Waters. Albuquerque, NM, USA. August 12-14, 2014. SHC 3.1.3.2
42. Ramesh, R., **M. Hantush**, L. Kalin and A. Sharifi. *Application of a Risk-Based Approach to a Hypothetical TMDL Using a Wetland Nutrient Model.* EWRI World Environmental & Water Resources Conference. Portland, Oregon, USA. June 1-5, 2014. SSWR 2.3E
43. Ramesh, R., L. Kalin, **M. Hantush** and A. Sharifi. *Development of Risk-Based Nitrate TMDL for Restored Agricultural Wetland near Chesapeake Bay: A Case Study.* Alabama Water Resources Conference. Orange Beach, Alabama, USA. September 3-5, 2014. SSWR 2.3E
44. Ramesh, R., L. Kalin, **M. Hantush** and A. Sharifi. *Assessing Climate Change Impacts on the Functioning of a Restored Wetland.* World Environment and Water Resources Congress. Austin, TX, USA. May 17-21, 2015. SSWR 2.3E
45. Schaeffer, B.A. **R. Conmy**, R.S. Lunetta, R.P. Stumpf, and D. Keith. *Breaking the barriers to adopting satellite remote sensing for water quality management: monitoring cyanobacteria blooms.* World Lake Conference. Perugia, Italy. September 1-5, 2014. SSWR 2.3C
46. **Scheckel, K.**, *Fundamentals of Soil Chemistry: Soil Chemistry of Hazardous Materials.* 19th Annual Contaminated and Hazardous Waste Site Management Theory, Practice & Outdoor Field Demonstrations Course. Toronto, Ontario, Canada. June 2-14, 2014. SHC 3.1.3.2
47. **Scheckel, K.**, *MOST Project 4 – Remediation of Soil Polluted by Heavy Metals and/or PAHs.* China, August 25-29, 2014. SHC 2.2.1.5
48. **Schubauer-Berigan, J.**, *Long-Term Nitrogen and Phosphorus Fertilization after the Ecological and Biogeochemical Functions of a Tidal Freshwater Marsh.* Joint Aquatic Sciences Meeting. Portland, Oregon, USA. May 19-23, 2014. SSWR 2.3A
49. Sharifi, A., L. Kalin, **M. Hantush**, J. Maynard, A. O' Geen and R. Dahlgren. *Identifying Dominant Processes in Active and Passive Zones of a Restored Wetland through WetQual-Comp Model.* EWRI World Environmental & Water Resources Conference. Portland, Oregon, USA. June 1-5, 2014. SSWR 2.3E
50. Sharifi, A., **M. Hantush** and L. Kalin. *Modeling Nitrogen Dynamics in Wetland Soils and Water under Saturated and Unsaturated Wetland Conditions.* World Environment and Water Resources

Congress. Austin, TX, USA. May 17-21, 2015. SSWR 2.3E

51. Stockton, T., **B. Dyson**, J. Carriger, W. Fisher, and S. Yee. *DASEES: A Decision Analysis Tool with Bayesian Networks from the Environmental Protection Agency's Sustainable and Healthy Communities Research Program.* Presented at BayesiaLab Users Conference, Orlando, FL, USA. October 24, 2013. SHC 1.1.1.2
52. Sundaravadivelu, D, M. Suidan, **A.Venosa** and P. Rosales. *Effect of Salinity on the Effectiveness of Solidifiers for Crude Oil Spill Remediation.* International Oil Spill Conference. Savannah, GA, USA. May 5-8, 2014. SHC 3.1.4.1
53. TenBrink, M.B., J. Fiksel, **B. Dyson**, G. Foley, I. Heilke, M. Hoagland, A. Bassi, E. Ruder, S. Yee, P. Bradley, H. Walker, W. Berry, and J. Hunter. *Bringing Systems Thinking into Community-based Environmental Management.* 2014 Conference on Earth System Governance. Norwich, U.K. July 1-3, 2014. SHC 1.1.1.3
54. **Voit, J.** *Quality Assurance for Laboratory Research.* 2014 Central and Eastern European Conference on Health and the Environment. Cluj-Napoca, Romania. May 25-30, 2014. N/A

5 Workshops

5.1 Vapor Intrusion (VI) Exposures - The Challenges of, Need for, and Benefits of Long Term Stewardship

Workshop: The 24th Annual AEHS International West Coast Conference on Soils, Water, Energy and Air. March 18, 2014. Coordinators: D. Grosse and B. Schumacher.

This one-day technical workshop is focused on featuring scientific observations and evidence regarding the accessibility and predictability of vapor intrusion (VI) exposures. Many practitioners currently use a limited number of short duration samples for a limited-duration/one-time characterization and decision approach. The workshop will present the evidence for the optimal condition and frequency of ongoing monitoring and protection from VI exposure under both natural (varying) and engineered (controlled) attenuation scenarios. Presentations will also focus on evidence for temporal changes in VI primarily associated with natural factors affecting such parameters as: 1) VI sources; 2) subsurface contaminant migration; 3) building/structure behavior; and 4) atmospheric effects. Recent and future developments are anticipated to improve knowledge of toxicity and exposure durations of concern, as well as assessment and monitoring methodologies.

6 Seminars/Webinars

6.1 Greening CSO Plans: Planning and Modeling Green Infrastructure (GI) for Combined Sewer Overflow (CSO) Control. March 26, 2014. A. Gilliland, and C. Kloss

SSWR 4.3D

This webinar summarizes the recently released EPA document titled "Greening CSO Plans: Planning and Modeling Green Infrastructure for Combined Sewer Overflow (CSO) Control." This document is a technical resource intended to assist communities in developing and evaluating Combined Sewer Overflow (CSO) control alternatives that include green infrastructure. It is designed to provide municipal officials as well as sewer authorities with tools to help quantify green infrastructure contributions to an overall CSO control plan. This document is the result of a joint effort between EPA's Office of Water (OW) and Office of Research and Development (ORD), and it is intended for use by both policy-oriented as well as technical professionals working to incorporate green infrastructure into CSO Long Term Control Plans (LTCPs). This resource contains three main parts: (1) General overview of the regulatory and policy context for incorporating green infrastructure into CSO control programs; (2) Description of how municipalities may develop and assess control alternatives that include green infrastructure; and (3) Brief demonstration of a modeling tool, the Storm Water Management Model V. 5.0 (SWMM5), that can help quantify green infrastructure contributions to an overall CSO control plan.

7 Demonstration Sites

7.1 COMMUNITY-SCALE

1. **The Lick Run Watershed Project.** Cincinnati, OH. Ongoing project.

The Lick Run project is part of the *Linking Green Infrastructure (GI) with Sustainable Urban Community Research* project. LRPCD and other NRMRL scientists are currently collaborating with several municipalities, Cincinnati Municipal Sewer District (MSD), EPA Regions, the Office of Water, other National Labs/Centers, other Federal Agencies, nongovernmental organizations, and universities to plan and implement comprehensive green infrastructure and sustainability strategies.

The Lick Run Watershed project (Cincinnati, OH) outlines an innovative and comprehensive green infrastructure solution to stormwater management and community revitalization in a combined sewer overflow watershed. The Lick Run Watershed drains 2,700 acres on the west side of Cincinnati, OH entering the Mill Creek just above its confluence with the Ohio River near the downtown center. Several of the Lick Run field projects involve Cincinnati MSD green infrastructure efforts at the Quebec Heights/Glenwood Elementary location and the St. Francis Apartments rain gardens within the Lick Run sewershed. Efforts include consideration of the hydrology, water quality, and soils at these sites. To consider benefits of stream restoration on nutrient management, the ability for streams of varying integrity to process nitrogen will be assessed in streams that range from unaltered, channelized, and within pipe. Economic and social valuation will also be studied for the Lick Run effort to incorporate green infrastructure into the solution for sewershed management and decreased CSOs. Additional research will focus on hydrology and water quality parameters at Cincinnati MSD permeable parking lots being implemented in the area, as well as data management and meta-analysis research.

8 Agreements

8.1 COOPERATIVE AGREEMENTS

1. **ETV Materials Management and Remediation Center.** Battelle is the verification partner organization for the ETV Program's Materials Management and Remediation Center. LRPCD Remediation and Redevelopment Branch staff worked with Battelle to conduct performance verification tests and prepare reports of innovative environmental remediation and risk management technologies.
2. **Zelinsky Institute of Organic Chemistry in Moscow (Russia).** The agreement was established to jointly develop nano materials for remediating persistence organic pollutants such as PCBs. Additionally, the effects of using nano materials on the aquatic life such as planaria warms and mussels (University of Puschino) and Daphnia (Institute of Toxicology in St. Petersburg) are being investigated.
3. **Region 7 (via the LRPCD Engineering Tech Support Center).** Support for the Omaha Lead Superfund Site. Investigate the distribution and redistribution of lead in residential soils after typical homeowner earth disturbing activities (e.g., gardening). Soil samples (summer 2011) were collected from residential yards before and after excavation to elucidate the extent of soil mixing as a function of depth and excavation technique. These results will be analyzed and provided to Region 7 along with producing a peer reviewed journal article.
4. **Evaluation of Dispersant Effectiveness, Droplet Size Distribution and Fluorescence Forensic Tools during Simulated Deepwater Blowout Oil Spills (DFO Canada)**.

8.2 INTERAGENCY AGREEMENTS

1. **Regional Ecosystems Services Research Program (REServ) [Region 8] – *Balancing Ecosystems Services and Resource Extraction.*** The overall goal of the project is to develop a tool/framework for use by decision-makers to balance human need for extraction at currently un-mined sites with potential loss of ecosystem services if the location were to be mined. This will be based on evaluation of ecosystems services that have been lost at similar types of mining sites. LRPCD and EPA Region 8 collaborate with stakeholders through an Interagency Agreement between ORD, USGS and the Colorado School of Mines.
2. **Engineering Technical Support Center /Omaha Lead Site - *Addressing Community Health and Risk Management issues at the Omaha Lead Site.*** The Omaha Lead Site (OLS) includes surface soils present at residential properties and child-care centers in the city of Omaha, Nebraska. Over 125 years of historic lead smelting and refining operations resulted in the deposition of lead-containing particulates on surrounding residential properties. Blood lead screening of children living in zip codes nearest to the former lead-processing facilities have consistently exceeded the 10 micrograms per deciliter (µg/dl) health-based threshold more frequently than children living elsewhere in the county. ETSC's primary objective is to provide technical support to EPA Region VII and EPA NRMRL by coordinating and/or conducting the identification, compilation, and analysis of educational, social, and analytical data for the Omaha Lead Site area. The team is working with numerous agencies and stakeholders and applying statistical analysis and epidemiological methodology to gain insight and understanding pertaining to the corrective action measures.
3. **Strategic Environmental Research and Development Program (SERDP) - *Assessing the***

Potential Consequences of Subsurface Bioremediation. Provide fundamental data and numerical simulation on the impact of bioreductive remedial processes on the rates and mechanisms of undesirable colloid generation. Produce two products that will be directly beneficial to site managers and risk assessors in establishing environmentally acceptable endpoints (EAEs) associated with bioremediation impacted water quality issues.

4. **Strategic Environmental Research and Development Program (SERDP) - *Mechanisms and Permanence of Sequestered Pb and As in Soils and its Impact on Human Bioavailability.*** Provide basic research on the propensity of soils and soil amendments to decrease toxic metal bioavailability and increase long-term metal sequestration. This research will result in technically defensible cleanup goals, while ensuring protection of human health and the environment.
5. **Environmental Security Technology Certification Program - *Fate of Uranium during Transport across the Groundwater-Surface Water Interface.*** Gain fundamental scientific understanding of the coupled physical, chemical and biological processes affecting uranium in wetland sediments, along the discharge path from ground- to surface waters. This is required for decision making for environmental remediation and long-term stewardship at many DOE sites where uranium contaminated groundwater discharges to surface waters.
6. **Environmental Security Technology Certification Program (ESTCP): Sustainable Infrastructure - *Evaluation of Contaminated Sediment Resuspension from Dredging, Extreme Storm Events, and Propeller Wash in DOD Harbor*** – LRPCD scientists will evaluate and quantify resuspension of contaminated sediments and resulting effects on remedial efforts from dredging, extreme storm events and propeller wash by producing site-specific transport models. The effect of propeller wash on sediment caps will also be evaluated.
7. **Bureau of Safety and Environmental Enforcement (BSEE)** – ***Evaluation of Oil Fluorescence Characteristics to Improve Forensic Response Tools Project***. LRPCD scientists responded to an RFP and were awarded a one-year Interagency Agreement amounting to $670 K to study subsea oil spill dispersant application and effectiveness and optical proxies for oil chemistry such as advanced fluorescence techniques, This is a funds-in IA, and we are now in the process of awarding an intergovernmental agreement with the Department of Fisheries and Oceans (DFO) Canada to implement the study at DFO's wave tank in Halifax, NS.
8. **United States Geological Survey (USGS) - *Identifying Sediment Sources in the Sediment Total Maximum Daily Load Process.*** Collaborators: Region 3, Region 5, GWERD, and USGS. Sediment is one of the most common causes for the loss of stream-biologic integrity. Identifying sediment sources is an important step in the U.S. Environmental Protection Agency's sediment TMDL process, yet the States, Tribes, and local governments charged with this assessment are lacking standard guidance on appropriate tools available to quantify sediment sources and develop sediment budgets. The objective of this study is to develop a guidance document for sediment source analysis in 303D listed watersheds. Development of the guidance document will synthesize past or ongoing studies that incorporate sediment fingerprinting and sediment budget approaches in four to six 303D listed agricultural and urban watersheds. Development of these sediment-source approaches into a guidance document is being investigated.
9. **United States Geological Survey (USGS)** – ***Effects of Agricultural Tile Drain Systems on***

Hydrology and Water Quality. Collaborators: Region 7 and USGS. Midwest in the formation of the hypoxic zone in the Gulf of Mexico (Scavia et al. 2000, Integrated Assessment of Hypoxia in the Northern Gulf of Mexico, National Science and Technology Report). Effective management and reduction of excess nonpoint sources of nitrogen inputs is recognized as a major goal for reducing hypoxia and improving local water quality. The EPA Science Advisory Board (SAB) has also emphasized the importance of the reducing phosphorus as well as nitrogen to achieve these goals. As part of the Mississippi River Basin Initiative (MRBI), Boone River watershed was selected for 2010-2011 for targeted nutrient removal. In addition, the Boone River has been identified by the Nature Conservancy as a 'top priority for aquatic conservation'. The Nature Conservancy is currently working with partners such as the Iowa Soybean Association and the Iowa DNR on restoring oxbows in four tributary watersheds to the Boone River, including Lyons Creek which contains the native oxbow. Oxbows are being targeted for stacked benefits of nutrient reduction as well as habitat restoration. The purpose of this project is to collaborate with EPA ORD NRMRLs, EPA Region 7, the Nature Conservancy, Iowa Soybeans Association, and the Iowa DNR to develop and implement hydraulic monitoring in restored and native oxbows for the purpose of providing nutrient load reduction to surface waters that drain to the Mississippi River basin. Hydraulic variables will be monitored in the restored and native oxbows in Iowa to assess their effectiveness at reducing nutrients.

10. **Synchrotron Research (DOE/ Argonne Lab).** Founding member of the Materials Research Collaborative Access Team (MR-CAT) at Advanced Photon source operated by US Department of Energy at Argonne National Laboratory. This resource is funded by multiple divisions in NRMRL for access to the photon source for atomic level characterization (e.g. speciation) of environmental samples applicable to materials management and bioavailability research.
11. **Environmentally Benign Oil Simulants to Mimic the Behavior of Oil Droplets in the Ocean (DOI/ BSEE).** LRPCD has a one year interagency agreement (IA) with the Department of the Interior, Bureau of Safety and Environmental Enforcement to create an environmentally benign oil simulant. To advance the understanding by spill responders and the scientific community of how submerged oil plumes and floating slicks are transported in aquatic environments, without the risk of harming the ecosystem, a means to conduct experiments with oil simulants is needed to mimic the behavior of dispersed oil. Such experiments using materials that behave like oil but are environmentally benign would enable field testing without requiring rigorous permitting by the government. Previous studies have tried to simulate an oil spill, using floating objects such as peat moss or oranges. However, this only informs slick transport (with gross limitations) and is inadequate for providing any useful information on dispersed oil. This IA will address current critical knowledge gaps by: (1) Fabricating environmentally benign, optically active particles that simulate oil droplets in the water column using synthesis techniques that are readily scalable from bench to industrial production, (2) "Tuning" the oil simulant using innovative synthesis technique to allow flexibility in creating behaviors ranging from floating to sinking in the water column, (3) Detecting the oil simulant under dilute concentrations due to the high fluorescent signature of the oil simulant, and (4) Verifying the oil simulant behavior using commercial off-the-shelf (COTS) response tools, such as fluorometers and particle size analyzers.
12. **Flow Measurement and Water Quality Collection for Contaminated-Sediment Fate and**

Transport Modeling (DOI/ USGS). At the Spring River in the Tri-State Mining District (TSMD), flow measurement and water quality collection and analysis are first step of a three-phase framework of integrated modeling effort for the fate and transport of metals in overland flow and waterbody in the TSMD. This model will be used as a tool to guide remediation decision making, to evaluate the natural attenuation of contaminants, and to examine the effects of Best Management Practices (BMPs) on the long term exposure of the ecosystem to the heavy metals.

8.3 COOPERATIVE RESEARCH AND DEVELOPMENT AGREEMENTS (CRADAs)

1. **University of New South Wales (UNSW) (and other Australian agencies).** The agreement was established to conduct collaborative research using technologies developed by us at EPA in cleaning contaminated areas in Sydney Harbor. As part of the collaboration, UNSW will be sending research associates to be trained on how to make the materials (nano metallic materials supported on adsorptive surfaces) and their applications on contaminated sediments and water. Both countries environmental agencies will benefit from our collaborative research through publications, patents, and industrial use of the technology. The project is fully funded by the Australian Research Council (ARC) with no funding commitments from EPA.
2. **Aluminum Association Inc.** Secondary aluminum processing (SAP) wastes result from the smelting of primary aluminum waste and recycled aluminum productions. In 1999, it was reported that approximately 2 billion pounds of SAP waste was land filled in the U.S. The management of SAP has many potential problems including its potential to initiate the combustion or pyrolysis of other waste materials. The CRADA will provide $360K over two years to assist ORD in the evaluation of best management practices for the disposal of SAP wastes.
3. **Waters Corporation. Quantitative analytical methods development for the analysis of selected indicator contaminants of emerging concern in wastewater, biosolids, and receiving waters.** The overall goal of this project is to develop quantitative analytical methods for the sample extraction, cleanup, chromatographic separation and analysis for trace levels of selected indicator compounds to evaluate the occurrence and fate of contaminants of emerging concern (CECs) associated with wastewater (WW) treatment activities. These matrices include wastewater influent, wastewater effluent, and receiving waters.
4. **Evaluation of Dispersant Effectiveness, Droplet Size Distribution and Fluorescence Forensic Tools during Simulated Deepwater Blowout Oil Spills (DFO-Canada)**. This project will address the operational performance of the subsurface injection of dispersants into deepwater blowouts by developing methods focused on oil transport after dispersant injection.

9 Regional and Program Support

9.1 REGIONAL & APPLIED RESEARCH EFFORTS (RARE)

1. **Region 1 RARE Project – An investigation into the Extent and Biological Impact of Endocrine Disrupting Chemicals (EDCs) in a Highly-Effluent Dominated River in New England.** This project consists of LRPCD/SSMB and Region 1 examining the Assabet River for selected

pharmaceuticals and personal care products, including EDCs, perfluorinated chemicals, pharmaceuticals, and alkylphenols and evaluating potential in-stream exposure of river biota. This is a collaborative project that includes Region 2, EPA New England Regional Laboratory, EPA ORD NERL, USGS, USFW, US National Park Service, and UMass Amherst. The project is in its second year.

2. **Region 2 RARE Project – Evaluation of Solid Waste Containment Systems in Puerto Rico**. The performance of the majority of waste containment systems in Puerto Rico is thought to be questionable by US EPA Region 2 officials and they seek assistance from ORD waste and materials management researchers to determine causes for landfill performance issues in the challenging environment of Puerto Rico. The RARE support involved evaluations of selected solid waste containment systems to determine factors affecting performance with recommendations for improvement, including a subset that will be studies in detail. A final report has been written and is undergoing internal review/clearance.
3. **Region 4 RARE Project - Assessing Methods for Surface Coal-Mining Water Quality Prediction of Factors Affecting Total Dissolved Solids Production**. Overall goal is to understand the state of the science for evaluating acidity and release of ions from coal mining waste materials used as fill in order to assist in informing decisions for best management practices (BMPs).
4. **Region 7 RARE Project - Effects of Agricultural Tile Drain Systems on Hydrology and Water Quality.** The purpose of this project is to collaborate with EPA ORD NRMRLs, EPA Region 7, the Nature Conservancy, Iowa Soybeans Association, and the Iowa DNR to develop and implement hydraulic monitoring in restored and native oxbows for the purpose of providing nutrient load reduction to surface waters that drain to the Mississippi River basin. Hydraulic variables will be monitored in the restored and native oxbows in Iowa to assess their effectiveness at reducing nutrients.
5. **Region 7 RARE Project – Support for the Omaha Lead Superfund Site**. (via the LRPCD Engineering Tech Support Center) to Investigate the distribution and redistribution of lead in residential soils after typical homeowner earth disturbing activities (e.g., gardening). Soil samples (summer 2011) were collected from residential yards before and after excavation to elucidate the extent of soil mixing as a function of depth and excavation technique. These results will be analyzed and provided to Region 7 along with producing a peer reviewed journal article.
6. **Region 8 RARE Project - Beneficial Reuse of Solid Mine Waste for Use in Concrete Construction Materials**. The hope is that this research could lead to a fundamental change in how abandoned mine lands are restored, reclaimed, and mining influenced water problems mitigated. The current state of the art is to excavate the waste and isolate it in specially constructed repositories. Converting this waste into durable construction materials such as concrete and mortar could greatly reduce the costs of cleanup and provide economic opportunity in hundreds of economically depressed communities. This project could therefore also enhance the Administrator's environmental justice priority.
7. **Region 8 RARE Project - Recovery and Reuse of Metals from Mining Influenced Water**. The purpose of this effort is to assess the efficacy of the Octolig® technology for use at remote mining-influenced Superfund sites in Region 8. The goal is to evaluate the use of this product to remove

metals to below Water Quality Criteria, while producing a residual sludge having a volume at least 30% less than traditional methods; and to evaluate the potential for metals recovery from the concentrated end product.

8. **Region 9 RARE Project - Evaluating a Water Treatment Method to Prevent the Formation and Export of MeHg in Restored Wetlands and Rice lands of the Sacramento-San Joaquin Delta**. The RARE proposal builds upon USGS' Carbon Capture Farming Program (CCFP) at Twitchell Island, and presents scientists with an opportunity to study methyl mercury (MeHg) cycling in a unique environmental setting by comparing treated and untreated wetlands. The implementation of LICD in situ could potentially reduce the formation of MeHg in the restored wetlands, and the export of aqueous MeHg from the Delta islands. Restoring wetlands on deeply subsided islands within the Central and Western Delta could help reverse subsidence and increase habitat for fish and wildlife, capture and store huge quantities of atmospheric carbon, advance climate protection, and help stabilize the fragile network of levees (a linchpin of California's water supply system). Also, if innovations can be made to restoration techniques, restoring wetlands can help the public and private sectors with achieving pollutant load reductions consistent with the Total Maximum Daily Load (TMDL) allocation for methylmercury.

9.2 Regional Field Projects

1. **Region 1 Field Project - Fort Devens Superfund Site.** LRPCD, in collaboration with personnel from GWERD, is providing technical support to the Federal Facilities Superfund Section in Region 1 to address groundwater and sediment contamination from a closed landfill at the Former Fort Devens. Previous site research conducted by LRPCD and GWERD to characterize arsenic contamination within Plow Shop Pond, due east of the landfill, resulted in the design and installation of a subsurface barrier wall during Summer 2012 by the Army to prevent further contaminant discharge to the pond. Current technical support and field research efforts are focused on evaluation of contingency remedy performance to address contaminated groundwater migration into the public watershed, north of the landfill boundary. This work will support design of the final remedy to achieve site closure.
2. **Region 7 Field Project – Tri-state Mining District**. The Tri-State Mining District (TSMD) encompasses the Spring and Neosho River watersheds in Missouri, Kansas, Oklahoma, and tribal lands where mined ores containing lead, cadmium, and zinc, were processed for a over a century. After processing, the remaining waste material or chat was left on the land surface, often in large un-covered piles. Decades of exposure to wind and water erosive processes has led to widespread contamination of sediments in streams, rivers, reservoirs, and lakes throughout the TSMD. Several of these areas with chat piles are on the National Priorities List (NPL) as known sources of hazardous waste contamination. Ecological risk assessment studies determined that exposure to these metals in the surface water, pore water, and sediment pose elevated risk to the survival, growth, and biomass of benthic invertebrates in these aquatic environments. Analytically derived site specific toxicity thresholds (SSTT) for cadmium, lead, and zinc serve as preliminary remediation goals (PRG) for environmental risk managers tasked with developing remediation and restoration plans for the Spring and Neosho River watersheds.

9.3 Regional Methods Projects

1. **Regional Methods Project (EPA Region 8) - Development of a Method to Determine Steroids and Hormones in Water by Dansyl Chloride Chemical Derivitization and LC/MS/MS Detection.** Human and animal hormones and steroids (for example, estrogen in human oral contraceptives) enter waterways after incomplete removal during waste water treatment. Concern over this incomplete removal prompts current research and herein we propose to develop a method to evaluate ecosystem characteristics associated with the distribution of hormones and steroids in the water column. The method is based on a current method used at the Region 8 Laboratory to analyze for 17α-ethinylestradiol (EE2), the synthetic steroid in human oral contraceptives. The method is based on the derivitization of the EE2 with dansyl chloride and the determination of the resulting compound by LC/MS/MS. This project will expand this method to include other steroids and hormones in water samples.
2. **Region 5 RMI Project - Validation of Methods for Alkylphenols and their Ethoxylates in Biosolids, Sludge, Sewage Treatment Plant Effluent, and Sea Water by GC/MS and LC/MS/MS.** The project involves LRPCD/SSMB staff working with Region 5 to develop and validate LC/MS and GC/MS multi-lab methods for analyzing soils, sewage solids, and water for Alkylphenols ethoxylates and alkylphenols. These methods will be used to characterize concentrations found in biosolid land application, surface water and sewage effluent, and biosolids samples from sites within Region 5.
3. **Regional Methods Project (EPA Regions 3 and 5) - Identifying Sediment Sources in the Sediment TMDL Process**. Identifying sediment sources is an important step in the sediment TMDL process. An important but difficult management question is whether sediment is originating from upland soil erosion or channel bank erosion. Understanding the proportions and locations of sediment sources helps to focus stream restoration and soil conservation efforts in the strategic locations in a watershed. This project addresses the need to develop a guidance document for sediment source analysis in 303D listed watersheds.

9.4 PROGRAM SUPPORT

1. **Great Lakes National Program Office.** The Great Lakes National Program Office (GLNPO) oversees and helps all Great Lakes stakeholders work together in an integrated, ecosystem approach to protect, maintain, and restore the chemical, biological, and physical integrity of the Great Lakes. LRPCD collaborates with personnel within NERL to provide technical support to GLNPO in its effort to clean up contaminated waterways that discharge into the Great Lakes. The focus of these efforts are to support: 1) identification of contaminant sources to impacted rivers and harbors, 2) site characterization to assist design of appropriate remedies and monitor remedy performance, and 3) evaluation of ecosystem recovery in remediated waterways. In addition to providing technical assistance to GLNPO during the development and implementation of remediation projects, LRPCD has four active field projects that are venues for the development of alternative monitoring technologies and innovative analysis approaches to evaluate remedy effectiveness. The field research sites are located within the Ashtabula River (Ohio), the Ottawa River (Ohio), the Grand Calumet River (Indiana), and the Manistique River (Michigan).

10 Workgroups

1. **Nitrogen Coordination Team.** Scientists from LRPCD participated in a workgroup formed to communicate nitrogen research across the ORD programs.
2. **Strategic Environmental Research and Development Program (SERDP) and Environmental Security Technology Certification Program (ESTCP).** Scientists from LRPCD represented the agency on the SERDP and ESTCP Environmental Restoration committees. SERDP is DOD's environmental science and technology program, executed in partnership with DOE and EPA. SERDP invests in basic and applied research and advanced development. ESTCP is DOD's environmental technology demonstration and validation program. The program's goal is to identify and demonstrate cost-effective technologies that address DOD's highest priority environmental requirements.
3. **GLNPO Capping and In-Situ Treatment Work Group.** LRPCD actively participates and co-leads sub groups focused on the capping and in-situ treatment of contaminated sediments in the Great Lakes. The workgroup involves project managers, program managers, and researchers.
4. **GLNPO Contaminated Sediments Remedy Effectiveness Work Group.** LRPCD actively participates and co-leads sub groups focused on approaches for characterizing the efficacy of contaminated sediment remediation projects in the Great Lakes. The workgroup involves project managers, program managers, and researchers.
5. **OSWER Pharmaceutical Rule Making Work Group.** LRPCD actively participates and provides technical support and guidance to OSWER related to the pharmaceuticals in the environment. Recent studies focused on disposal of packaging containing prescription medicines and preprocessing measures.
6. **EPA National Remedy Review Board.** LRPCD is an active member of the EPA National Remedy Review Board (NRRB). The NRRB provides technical review of Superfund remedial investigations and feasibility studies (RI/FS) in order to help control response costs and promote consistent and cost-effective remedy decisions. The NRRB considers the nature of the site; risks posed by the site; regional, state, tribal and potentially responsible party (PRP) opinions on proposed actions; the quality and reasonableness of the cost estimates; and any other relevant factors or program guidance in making advisory recommendations. The overall goal of the review is to ensure sound decision making consistent with current law, regulations, and guidance.
7. **Chemicals of Emerging Concern Work Group for the International Joint Commission Canada and United States.** LRPCD supported the International Joint Commission Canada and United States to develop a Priority Cycle Report on Chemical of Emerging Concern. The Workgroup report was released at the IJC 2011 Biennial Meeting. http://meeting.ijc.org/sites/default/files/report/CECFactSheet.pdf
8. **OSWER Vapor Intrusion Workgroup.** The vapor intrusion pathway has become widely recognized as a potentially significant cause of exposure to toxic substances in indoor spaces. Numerous studies have indicated that the air in buildings overlying soil or groundwater contaminated with toxic vapor-forming substances may contain potentially harmful concentrations of these contaminants due to vapor intrusion (see, for example, U.S. Environmental Protection Agency [EPA], 2006, and McDonald and Wertz, 2007). To help assess and manage human exposures arising from vapor intrusion, a multi-stakeholder technical workgroup was established in

the early 2000's to expand the ongoing database, field studies and design of remedial approaches.

9. **National Mine Team Workgroup and Abandoned Mine Lands Workgroup.** The EPA AML Program is coordinated through the Agency's National Mining Team (NMT) and Abandoned Mine Lands Team (AMLT). These teams provide EPA headquarters a Regional core of expertise on issues at abandoned mine sites. The teams together serve as a focal point for coordinating and facilitating national technical, policy and process issues with stakeholders on abandoned/inactive mine research, characterization, clean-up and redevelopment activities.
10. **National Indian Working Group, AIEO.** In a manner consistent with the U.S. Environmental Protection Agency (EPA) Indian Policy, the mission of the Tribal Operations Committee (TOC) is to improve the conditions of Tribal health and the environment in Indian Country. The relationship between TOC and EPA will not substitute for the government-to-government relationship between EPA and tribal governments.
11. **EPA's Green Building Workgroup.** This workgroup was formed in July 2003 to bring together the many programs across the Agency that work with the building and development sectors to improve their environmental performance. The Workgroup seeks to build effective EPA leadership in the green building movement by jointly informing, coordinating, and guiding the development of Agency policies, programs, partnerships, communications, and operations that influence building and development. (http://www.epa.gov/greenbuilding/pubs/about.htm)
12. **U.S. - German Bilateral Workgroup.** Scientists from LRPCD's Remediation and Redevelopment Branch have shared research findings with the German Ministry of Education and Research (BMBF) since 1990. The first four phases of research were in Brownfield redevelopment and sustainable land re-use. The Workgroup is now in the process of writing a proposal for phase 5 that will address area-wide sustainable land management issues.
13. **EPA Technical Review Workgroup Bioavailability Committee.** LRPCD actively participates and provides technical support and guidance to OSWER related to site specific bioavailability issues pertaining to contaminated soils.
14. **EPA Technical Review Workgroup Lead Committee.** LRPCD actively participates and provides technical support and guidance to OSWER related to lead contaminated soils and sediments.
15. **External Advisory Board, USDA Project.** Bioenergy Feedstock Production Systems on Marginal Lands that Provide Ecosystem Services and Promote Regional Economic Activity.
16. **Coastal Response Research Center, American Petroleum Institute Shoreline Cleanup Technical Working Group.** Joint Analysis Group for DWH Spill, Enbridge Spill Chemistry Subgroup.
17. **Citizen Science Workgroup/ Community of Practice.** Citizen science means engaging the public in scientific investigations – asking questions, collecting data or interpreting results. Citizen science has the potential to provide environmental information that EPA would not otherwise be able to access or make it available at dramatically reduced cost. This group will learn how to match the strengths of citizen science with Agency needs.

11 Committees/ Editorial Boards – LRPCD staff have participated in the

following committees and editorial boards.

1. **ACWI National Subcommittee on Sedimentation,** http://acwi.gov/sos/index.html - Joseph Schubauer-Berigan.
2. **Advanced Photon Source,** Proposal Review Panel for Spectroscopy - Todd Luxton and Kirk Scheckel.
3. **Advisory Council for Advanced Spectroscopy and LERIX (ALS),** X-ray Science Division, Sector 20 Upgrade, Advanced Photon Source - Kirk Scheckel.
4. **AEHS West Coast Conference Vapor Intrusion Workshop,** Organizing Committee - Douglas Grosse.
5. **American Chemical Society,** Program Chair, Division of Environmental Chemistry- Souhail Al-Abed.
6. **American Chemical Society**, Award Committee, Division of Environmental Chemistry- Souhail Al-Abed.
7. **Australian Research Council (ARC)**, Proposal Review Member - Souhail Al-Abed.
8. **American Conference of Governmental Industrial Hygienists (ACGIH),** Industrial Ventilation Committee – John McKernan.
9. **American Industrial Hygiene Association (AIHA),** Engineering Committee - John McKernan.
10. **American Society of Heating, Refrigeration, and Air-Conditioning Engineers (ASHRAE),** Industrial Ventilation Committee – John McKernan.
11. **American Society of Civil Engineers (ASCE) Journal of Hydrologic Engineering,** Section Editor (Subsurface Hydrology) - Mohamed Hantush.
12. **ASCE Environmental Water Resources Institute (EWRI),** Chair of Technical Committee on Wetland Hydrology Technical Committee - Mohamed Hantush.
13. **ASCE Environmental Water Resources Institute (EWRI),** Chair of Task Committee on Wetland Processes Modeling Task Committee - Mohamed Hantush.
14. **ASCE Environmental Water Resources Institute (EWRI),** Technical Committee on Surface Water Hydrology- Mohamed Hantush.
15. **ASCE Environmental Water Resources Institute (EWRI)**, Task Committee on TMDL Analysis and Modeling – Mohamed Hantush.
16. **Auburn University Ph.D. Committee,** Affiliate Faculty Position at the School of Forestry and Wildlife Sciences - Mohamed Hantush.
17. **Australian Remediation Industry Cluster (ARIC),** A network of Australian and international expertise for environmental remediation efforts in Australia - Kirk Scheckel.
18. **Coastal Response Research Center,** American Petroleum Institute Shoreline Cleanup Technical Working Group, Joint Analysis Group for DWH Spill (Enbridge Spill Chemistry Subgroup, ICCOPR, NRT) - Committee / Board Member – Robyn Conmy.
19. **Consortium of Ocean Leadership,** Review panelist GOMRI Oil Spill RFP – Robyn Conmy.

20. **EPA National Tribal Science Council**, ORD representative - John McKernan.
21. **Environmental Health Officer Professional Advisory Committee,** Professional Image and Standards Subcommittee - John McKernan.
22. **Federal Interagency Sedimentation Project Committee,** http://water.usgs.gov/fisp/. Joseph Schubauer-Berigan.
23. **Florida Center for Solid and Hazardous Waste Management,** Executive Board - Thabet Tolaymat.
24. **Interagency Coordinating Committee for Oil Pollution Research,** EPA research representative – Robyn Conmy.
25. **International Conference on Remediation of Contaminated Sediments,** Technical Steering Committee - Marc Mills.
26. **International Conference on Modeling and Simulation of Diffusive Processes and Applications**, Varanasi, India (October 9-12, 2012), International Advisory Committee and Session Chair – Mohamed Hantush.
27. **International Journal of Phytoremediation,** Associate Editor - Steve Rock.
28. **International Perspectives on Water Resources & the Environment conference (2013),** Ezmir, Turkey. Advisory Board Committee & Organizer of a session on Uncertainty Methods for Water Quality Management – Mohamed Hantush.
29. **International Phytotechnology Society,** Officer on the Board - Steve Rock.
30. **International Society of Trace Element Biogeochemistry,** Chair of the International Committee - Kirk Scheckel.
31. **International Society of Trace Element Biogeochemistry,** Secretary - Kirk Scheckel.
32. **Journal of Hazardous Materials,** Editorial Board – Paul Randall.
33. **Journal of Hydrologic Engineering Committee,** Chair of award committee for the nomination of Journal of Hydrologic Engineering best Technical, Case Study, Technical Note, and Discussion papers published (2012-2013) - Mohamed Hantush.
34. **Journal of Water Quality, Exposure and Health,** Associate Editor - Mohamed Hantush.
35. **Marion L. and Chrystie M. Jackson Soil Science Award**, Chair of the Committee of the Soil Science Society of America – Kirk Scheckel.
36. **National Synchrotron Light Source, Brookhaven National Lab,** Imaging and Microprobes: Chemical and Materials Proposal Review Panel - Kirk Scheckel.
37. **Ocean Optics Conference Planning Committee (2012)** – Robyn Conmy.
38. **Office of Superfund Remediation and Technology Innovation (OSRTI) and the Office of Federal Facilities Restoration and Reuse Office (FFRRO)**, National Remedy Review Board – Ed Barth.
39. **Ohio River Basin Alliance,** EPA representative on Steering Committee – Verle Hansen.
40. **Ohio River Basin Alliance,** member of the Working Group for Sustainable Growth & Competiveness – Verle Hansen.

41. **Ohio Valley Chapter, Society of Environmental Toxicology and Chemistry,** Board of Directors - Joseph Schubauer-Berigan.
42. **Port of Greater Cincinnati Development Authority,** Brownfield Assessment Advisory Group - Douglas Grosse, Verle Hansen.
43. **Remediation Journal,** Editorial Board - Ed Barth.
44. **Sigma Xi Scientific Professional Society: Sigma Xi Federal Environmental Chapter,** Senior Emeritus Consultant, former Sec. Treasurer, Vice-Pres. and President – Douglas Grosse.
45. **Soil Science Society of America Journal,** Associate Editor - Robert Ford.
46. **Southwest Ohio Water Environment Association (WEF),** Industrial Waste Committee – Douglas Grosse.
47. **Steering committee for Defining Safer Chemicals for Brominated Flame Retardants and Phthalates** – Paul Randall.
48. **Thomas More College,** Adjunct Professor of Environmental Geosciences – Edwin Barth.
49. **University of Cincinnati Alumni Association, College of Engineering and Applied Sciences,** Board of Directors – Douglas Grosse.
50. **University of Cincinnati, U.C. College of Medicine,** Adjunct Professor in Industrial Ventilation - Edwin Barth.
51. **USEPA Global Change Research Program (GCRP),** Technical Steering Committee - Verle Hansen.
52. **World Environment and Water Resources Congress (2014),** Organizer of Special Session on Risk and Reliability in TMDL development and implementation – Mohamed Hantush.

12 Collaboration – LRPCD staff have a long history of collaboration that fits in well with the Path Forward's commitment to integrated transdisciplinary research (ITR). LRPCD staff work in partnership with many groups from different disciplines, perspectives, and experiences to define problems, conduct research, and deliver products and outcomes. Among LRPCD's collaborators are:

1. **U.S. EPA** - Office of Policy, Economics, and Innovation (OPEI), Office of Superfund Remediation and Technology Innovation (OSRTI), Office of Brownfields Cleanup and Redevelopment (OBCR), OEI, Ecosystem Services Research Program, ORD Sustainable Technology Division, Office of Water (OW), NERL, NCEA, NHEERL, NHSRC, Great Lakes National Program Office (GLNPO), EPA Environmental Response Team, Office of Solid Waste and Emergency Response (OSWER), EPA Landfill Methane Outreach Program (LMOP), Office of Prevention, Pesticides and Toxic Substances (OPPTS), Office of Emergency Management (OEM).
2. **EPA Regions** - All EPA Regions.
3. **State Agencies** – State Departments of Health and Environmental Protection, Interstate Technology and Regulatory Council (ITRC), Oregon DEQ, Colorado, Pennsylvania Fish and Boat Commission, Ohio EPA, Iowa, Tennessee Department of Environment and Conservation (TDEC), Texas, Louisiana, Alabama, Mississippi, Florida, Alaska, California, Delaware, New York, Association of

State and Territorial Solid Waste Management Officials (ASTSWMO), The Northeast Waste Management Officials Association (NEWMOA).

4. **Other Federal Agencies** – U.S. Department of Defense (DOD), National Aeronautics and Space Administration (NASA), U.S. Dept. of Energy (DOE) including Advanced Photon Source of Argonne National Laboratory, U.S. Army Corps of Engineers (USACE), U.S. Forest Service (USFS), U.S. Geological Survey (USGS), Bureau of Land Management (BLM), U.S. Geological Survey (USGS), U.S. Dept. of Agriculture (USDA), U.S Fish and Wildlife Service (USFWS), U.S. Navy, U.S. Marine Corps, National Oceanic and Atmospheric Administration (NOAA), U.S Fish and Wildlife Service (USFWS), U.S. Forest Service (USFS), Argonne National Labs (DOE), U.S. Geological Survey (USGS), U.S. Dept. of Defense (DOD), U.S. Coast Guard, U.S. Dept. of Interior's Bureau of Ocean Management, Regulation and Enforcement (BOMRE), Small Business Administration (SBA), Occupational Safety and Health Administration (OSHA), Center for Disease Control (CDC) including National Institute of Occupational Safety and Health (NIOSH), Consumer Products Safety Commission (CPSC), Federal Trade Commission (FTC).
5. **Academia** - Carnegie Mellon University, Colorado School of Mines, Purdue University, University of Cincinnati, Clemson University, Colorado State, University of Texas, University of Arizona, University of Illinois-Chicago, North Carolina State University, Clemson University, University of Toledo, Bowling Green State University, Iowa State University, University of South Korea, National Academy of Science, University of Wisconsin, University of Florida, University of Arizona, University of Kentucky, University of Washington, Dartmouth, Temple University, Woods Hole Oceanographic Institute, University of New Hampshire, University of Georgia, Indiana University, University of California - Los Angeles (UCLA) Center for Environmental Implications of Nanotechnology.
6. **Business/ Industry** – EnviMSI, Prima, Neptune and Company, URS Corp., Battelle, Tetra Tech, The National Lime Association, N-Viro, Pegasus Technical Services, EnviroScience, PhycoTech, Alcoa, Olin Chemical, Aquablok, Trojan Technologies, Waste Management, Inc. (WM), U.S. Gypsum, Georgia-Pacific, Severn Trent, Graver Tech, Alcan Ind., JNM Environmental, Applied Minerals, Inc., American Petroleum Institute, Osmose, Inc. Environmental Research and Education Foundation (EREF), The Aluminum Association.
7. **Other** – Stella, MO, German Ministry for Education and Research (BMBF), Abandoned Mine Lands Team, National Mining Team, Engineering Forum, The Water Environment Federation (WEF), The Water Environment Research Foundation (WERF), Fairfield OH WWTP, D.C. Water and Sewer Authority, Ohio River Sanitation Commission, East Bay Municipal Utilities Division, Water Reclamation District of Greater Chicago, Cincinnati Metropolitan Sanitation District, Hamilton County Soil and Water Conservation District, Cincinnati Parks, South/ Southwest Hazardous Substance Research Center, Washington DC Mayor's Initiative Team, Piedmont Research Station, Polk County Solid Waste Division (FL), Florida Center for Solid and Hazardous Waste Management, Pima-Maricopa Indian Community (AZ), Fats and Proteins Research Foundation, Edgewood Chemical Biological Center, Commonwealth Scientific and Industrial Research Organisation (CSIRO)-Australia, Desert Research Institute, Fisheries and Oceans (DFO)-Canada, Gulf Coast Ecosystem Restoration Task Force, DFO Bedford Institute of Oceanography (BIO), Environment Canada, Coastal Response Research Center (CRRC), ITRC Biofuels Team.

13 Honors and Awards

13.1 Scientific & Technological Achievement Awards (STAA)

- **Level III**
  - Karen Bradham, **Kirk Scheckel,** David Thomas, Clay Nelson, Michael Hughes, Aaron Yeow, Sophia Serda, Sharon Harper. Assessing and Predicting the Risk of Soil Arsenic on Human Health.
- **Honorable Mention**
  - **Barbara Butler.** Effect of Imposed Anaerobic Conditions on Metals Release From Acid-Mine Drainage Contaminated Streambed Sediments
  - William Shuster, **Patrick Clark,** and Brooke Furio. Understanding the Role of Urban Soils in the Development of Effective Green Infrastructure.

13.2 ORD Honor Awards

- **Bronze Medal**
  - **Robyn Conmy** (with NHEERL, NERL, and Regional staff) Hyperspectral Imager for the Coastal Ocean Team - *For advancing innovative space-based sensor technology to monitor water quality in coastal and in-land waters.*
  - **Brian Dyson** (with NHEERL NERL, and Regional staff) - Guanica Bay Community Support Team - *For addressing the sustainability of local environmental decisions made in Guanica Bay, Puerto Rico as a transdisciplinary team.*
  - **Edwin Barth** (with NHEERL NERL, and Regional staff) Microbial Dose-Response (MDR) Team - *For outstanding accomplishments in the assessment of public health risks from exposure to Bacillus anthracis to inform clean up decisions.*
  - **Douglas Grosse** and **John McKernan** (with OSP and NCEA staff) - Exceptional/ Outstanding ORD Technical Assistance to the Regions or Program Offices. ORD Technical Support Center Directors - *In recognition for outstanding technical support and assistance provided by the Technical Support Center Directors at the request of U.S. EPA Program and Regional Offices.*
  - **Mohamed Hantush** - Exceptional/ Outstanding ORD Technical Assistance to the Regions or Program Offices - *Dr. Hantush played a key role in helping the Region 10's Office of Water and Watersheds Sole Source Aquifer program make a timely, science driven, determination on Leque Island project.*

13.4 NRMRL Honor Awards

- **Albert Venosa**

13.5 Other Awards

- **ORD Safety, Health, and Environmental Management 2014 Safety Award – Carolyn Acheson.**

14 Output /Activity Totals

Journal Articles published	32	RAP Tasks	52
Journal Articles in review	29	RAP Project and Task Leads	11
Presentations	54	RAP Outputs and Products	56
EPA Reports	31		
Awards	11	Workgroups	17
Citations (2011-2014)	200+	Agreements/ CRADAs	20
Committees/ Editorial Boards	52	Regional Projects	14

To: Conmy, Robyn[Conmy.Robyn@epa.gov]
From: Barron, Mace
Sent: Fri 3/17/2017 12:40:18 PM
Subject: RE: any luck in tracking down more oil spill mitigating agents?

What is the new oil to test?

From: Conmy, Robyn
Sent: Thursday, March 16, 2017 10:43 AM
To: Barron, Mace <Barron.Mace@epa.gov>; Wilson, Gregory <Wilson.Gregory@epa.gov>; Principe, Vanessa <Principe.Vanessa@epa.gov>
Subject: RE: any luck in tracking down more oil spill mitigating agents?

Hey Mace,

Here is what we are thinking ….

Phase 3 – We originally budgeted for testing 1 each of a SWA, solidifier and bioremediation agents. But instead, I would propose to conduct tests only with 1 SWA (Cytosol) and 1 solidifier (CI Agent or Gelco 200) and not running the bioremediation agent at this time. Instead we can reserve those funds for conducting a tox test with the new 3rd potential oil with and without oil that arrived this week. Thoughts?

Phase 2 – We originally budgeted for 4 dispersants and we have completed 3 (corexit, finasol, accel) with Dorado and Endicott. But instead of adding a 4th dispersant, I think it is best to test the new potential reference oil with and without corexit. Thoughts?

Swapping out the tests should be budgetary neutral considering that one-Phase 1 and one-Phase 2 test would be equal to the proposed Phase 2 tests of new oil with and without corexit.

Mace, can you provide volume budgets of product and oil? We can then ship to hydrosphere.

Robyn

<>/<>/<>/<>/<>/<>/<>/<>/<>/<>/<>/<>/<>/<>/<>/<>/<>/<>

Robyn N. Conmy, Ph.D.

Research Ecologist

USEPA/NRMRL/LRPCD

26 West MLK Drive

Cincinnati, Ohio 45268

513-569-7090 (office)

513-431-1970 (EPA mobile)

727-692-5333 (Personal mobile)

conmy.robyn@epa.gov

From: Barron, Mace
Sent: Wednesday, March 15, 2017 4:45 PM
To: Conmy, Robyn <Conmy.Robyn@epa.gov>; Wilson, Gregory <Wilson.Gregory@epa.gov>; Principe, Vanessa <Principe.Vanessa@epa.gov>
Subject: any luck in tracking down more oil spill mitigating agents?

The tox lab asked if we would be shipping anything to them? As a reminder:

phase 2) 2 oils+4 dispersants

*testing completed on dorado and Endicott, plus finasol, accel and corexit

**still need one more dispersant

Phase 3) other oil agents (e.g., oil eater II, etc)

*need to track some down!

To: Conmy, Robyn[Conmy.Robyn@epa.gov]
From: Andrew Remsen
Sent: Thur 3/16/2017 2:15:23 PM
Subject: Fwd: update
DE manuscript Ohmsett baffle march 6th 2017.docx
TF ohmsett baffle march 10 2017.docx

Just talked with Michel. He decided during our conversation to split this into two papers, one of just the baffle flask DE vs. Ohmsett DE and experiment scaling and the other one discussing in-situ validation of the Ohmsett DE by fluorometers and LISST data. The first version he sent I started reading yesterday did not have the LISST data. I said we'd take a look and comment.

On Wed, Mar 15, 2017 at 11:51 PM, Michel Boufadel <boufadel@gmail.com> wrote:

> Hi Drew,
> Please find attached the updated files. For the phone conversation, tomorrow Thursday at 11:00 am is good for me. But the afternoon is also good.
>
> Thank you,
>
> Michel

--
Michel C. Boufadel, PhD, PE, BCEE
Director, Center for Natural Resources Development and Protection (NRDP)
Professor, John A. Reif, Jr. Dept. Civil and Environmental Engineering
The New Jersey Institute of Technology
Room 435 Colton Hall
323 MLK Blvd, Newark, NJ 07102-1824
Ph: 973-596-6079
email: boufadel@gmail.com
http://nrdp.njit.edu

Dispersion Effectiveness of Dispersants in wavetank and the EPA Baffled Flask

Michel Boufadel[1], Zhong Pan[1], Timothy Steffek [2], Alan Guarino (3), Brian Robinson[4], Thomas King[4],Andrew Remsen[5], and Robyn Conmy[6]

[1]Center for Natural Resources Development and Protection, New Jersey Institute of Technology, Newark, NJ 07102, USA, boufadel@gmail.com; http://nrdp.njit.edu. [2] Bureau of Safety & Environmental Enforcement, Oil Spill Preparedness Division, 45600 Woodland Road, VAE-OSPD, Sterling, VA 20166, USA. [3] Ohmsett, Leonardo, New Jersey, [4] Department of Fisheries and Oceans, Canada, Bedford Institute of Oceanography, 1 Challenger Drive, Dartmouth, Nova Scotia B2Y 4A2, Canada. [5] Pegasus Environmental Services, Cincinnati, Ohio; [6] National Risk Management Laboratory, US Environmental Protection Agency, Cincinnati Ohio, 45269.

Abstract

The study evaluated the dispersion effectiveness (DE) in the Ohmsett tank with Hoover Offshore Oil Pipeline System (HOOPS) oil and five dispersants: Accel Clean DWD, Corexit 9500, Finasol OSR 52, Marine D-Blue Clean, and ZI-400. The DE of the control was 62% and that of the dispersants varied from 75% to 95%. The Sauter mean diameter was around 120 microns for the control, and around 20 microns for all dispersant except Marine D Blue. Fluorescence measurements correlated well with the DE and the droplet sizes.

The background water for each DE test in the Ohmsett tank was used as the same temperature to replicate the tank experiments in the EPA's Baffled Flask Test. Additional BFTs were conducted using synthetic seawater and also using Alaskan North Slope (ANS) oil. A linear correlation between the DE (in percentage) of the oil HOOPS in the BFT and the DE of HOOPS in the Ohmsett tank revealed the relation:
DE (BFT, Ohmsett water)=0.63 * DE(Ohmsett tank) +6. The slope being less than 1.0 reflects the impact of high dilution in the Ohmsett wavetank.

In the BFT, the DE of HOOPS with Ohmsett water was larger than the DE of HOOPS in synthetic seawater for the corresponding dispersant. This could have occurred because the surface tension in the Ohmsett water was around 72 mN/m, and thus smaller than that of the synthetic seawater at 75 mN/m. However, a more likely reason appears to be the lower hardness of the Ohmsett water in comparison to that of synthetic or ocean seawater, as the hardness tends to precipitate the dispersant. The Ohmsett water had a hardness of 4,700 mg/L as $CaCO_3$ and is thus equal to 70% of that of the synthetic seawater (6,500 mg/L as $CaCO_3$). The DE of the ANS in the BFT was larger than that of the HOOPS in the BFT for all dispersants. This is possibly because ANS has a higher asphaltene content (7%) in comparison to HOOPS (2%), and the asphaltene molecules are polar and could act as (slow) surfactants.

1.0 INTRODUCTION

The dispersion of oil in seawater depends on a variety of factors including oil and water properties, and the mixing energy and duration (Zhao et al. 2014). Testing a particular chemical dispersant is a challenge in and by itself due to the issue of scale: small scale experiments are well controlled but do not mimic the dilution observed at the large scale (NRC 2005, Lee et al. 2011). Researchers have relied on using intermediate scale systems, namely wavetanks (sometimes labeled mesocosms). Examples of these tanks include the 32 m long wavetank of Department of Fisheries and Oceans, Canada located in Halifax Nova Scotia (Wickley-Olsen et al. 2007, Wickley-Olsen et al. 2008, King et al. 2014). The largest wavetank for oil spill research in the world, and the topic of this paper, is the Ohmsett wavetank in Leonardo New Jersey managed by the Department of Interior's Bureau of Safety and Environmental Enforcement. The Ohmsett tank is 203 m long, 20 m wide, 3.4 m deep (water depth 2.4 m), giving a water volume of approximately 10,000 m^3. The tank is equipped on its south end with a flap-type wave generator hinged at the bottom, and it was used herein to produce waves of period T=2.0 s and wave height of 0.60 m.

In our attempt to address the issue of scaling, we conducted dispersion effectiveness (DE) tests in the Ohmsett tank and compared to those obtained from EPA's BFT. We used for this purpose the oil known as HOOPS (Hoover Offshore Oil Pipeline System) and five dispersants: Accel Clean DWD, Corexit 9500, Finasol OSR 52, Marine D-Blue Clean, and ZI-400 (Table 1). The DE results in the Ohmsett tank were strengthened with measurements of the oil droplet size distribution (DSD) (Li et al. 2009) and fluorometry (Conmy et al. 2014).

The BFT test was conducted using the same Ohmsett water used for each Ohmsett DE test and at the same temperature measured in the Ohmsett tank. Additional BF tests were conducted using Alaskan North Slope (ANS) oil, as ANS was used as benchmark in the past. BF tests were also conducted using synthetic seawater (Aquarium System of Mentor, Ohio, USA), as such is done in the standard BFT (Sorial et al. 2004). Correlations were then obtained between the DEs in various systems, and implications on scaling up were presented.

METHODS

The Ohmsett tank is equipped with two movable bridges (i.e., main towing bridge and auxiliary bridge) that span the width of the tank for mounting instruments (e.g., altimeter and high resolution camera). To inhibit biological growth, an electro-catalytic process is used to oxidize chloride ion to hypochlorite. In the standard operation, at 30 ‰ salinity, with a through reactor flow rate of approximately 80 liter per minute at 20°C, the optimal production of equivalent chlorine is approximately 0.75 kg per minute. More chlorine (and thus salt) can be added to the water if algal blooms are visually observed in the tank, which occurs usually in the summer.

In the Ohmsett tank, each the dispersion effectiveness (DE) test started by activating the wavemaker to provide regular waves whose period was 2.0 s and their height was approximately 0.60 m. Then, when the waves propagated and reached the opposite side of the tank, around 80 liters of the oil HOOP were applied onto the water surface at approximately 100 m from the wavemaker. Then, just seconds prior to the waves start breaking above the slick, 8 liters of

dispersants were sprayed from the bridge onto the slick. At the end of each DE experiment, the mass of oil on the surface $m_{oil,surface}$ was skimmed off of the surface and weighted. The DE is defined as:

$$DE = \frac{m_{oil} - m_{oil,surface}}{m_{oil}} \times 100 = \frac{m_{dispersed}}{m_{oil}} \times 100 \quad (1)$$

Where m_{oil} is the mass of spilled oil and $m_{dispersed}$ is the mass of oil dispersed into the water column.

Water samples were taken from the Ohmsett tank prior to each DE test in the tank (October 14th through October 22nd), and additional samples were taken through November 5nd. The water samples were analyzed for air-water surface tension, inorganic ions, BTEX (benzene, toluene, ethylbenze, and xylene), and total organic carbon (TOC).

A LIMNOS water sampler (Hydro-Bios, Germany) was used to collect the water samples from the Ohmsett tank. Two certified-clean PYREX screw cap glass 250 ml jugs (Corning, NY) were attached to the sampler, and then the sampler was lowered in the water to a specific location using a rope attached to the device. When the sampler reached 1.2 m below the water surface, release a weighted messenger down the rope which triggers the bottles to open and start filling. In general, it took around 30s to fill out the bottle. The jugs were preserved on ice in coolers and shipped to the laboratory at NJIT within 1 day of collection. At the laboratory, they were stored at 4 °C in the refrigerator prior to analysis and/or usage.

Water Analytes

The surface tension was measured using a Kruss Wilellmy Plate tensiometer, and it was viewed as an integrated measure for the presence of surfactants in the Ohmsett water. This is because the Ohmsett water was suspect of containing many surfactants whose interactions are no known. Thus, measuring the concentration of the surfactant directly would not promising. Also, some surfactants were proprietary.

Chloride and nitrate were analyzed using ion chromatography system (Dionex ICS-1500, Thermo Scientific, Somerset, NJ) consisting of a liquid eluent (10 mM KOH), a high-pressure pump, a sample injector, a guard and separator column, a chemical suppressor, a conductivity cell, and a data collection system. The ion chromatography system was coupled with a Dionex AS50 autosampler (Thermo Scientific, Somerset, NJ) for sample analysis. Before running samples, calibrations for chloride and nitrate were conducted using chloride and nitrate standard solution, respectively. The concentrations of chloride and nitrate were obtained from the calibration curves with the known standards.

Sulfate, SO_4^{2-}, was measured using the SulfaVer 4 method (EPA Method 8051). It relies on using a UV/Visible Spectrophotometer (Cole Parmer 4802 scanning double beam UV/Visible spectrophotometer, IL, USA) and test kits (HACH 2106769). All the water samples were diluted 1:10 with deionized water (DI) water, prior to analysis, as the instrument's range is from 2.0 mg/L to 70 mg/L.

Cations (sodium, calcium, magnesium, potassium, and zinc) were quantified using a flame atomic absorption spectrometer (Perkin Elmer Analyst 400, Waltham, MA). Appropriate hollow-cathode lamps for targeted metal elements were installed before analysis. Standard calibration curves for determining the targeted elements were conducted immediately before running samples.

BTEX (benzene, toluene, ethylbenzene, o-, m-, and p- xylenes) was measured using the Purge and Trap (P&T) Gas Chromatography with Photon Ionization Detector (PID). BTEX standard stock solution were prepared based on Restek 502.2 Calibration Mix #4 (Cat #: 30045) and Mix #5 (Cat #: 30046). A series of BTEX standard working solutions (10, 25, 50, 100, and 200 ppb) were prepared by diluting the stock standards with DI water.

The chromatographic system consisted of a gas chromatograph (GC) (Varian 3400 GC, Varian, Walnut Creek, CA, USA) equipped with a PID (Model 4420, O-I Corporation). A Restek GC column (Crossbond 6% Cyanopropylphenyl-94% dimethylpolysiloxane) 105 m × 0.53 mm I.D. × 3.0 μm was used with helium as carrier gas. Injector and detection port temperatures were 150 °C and 200 °C, respectively, with splitless mode. The column oven temperature program involved an initial temperature of 35 °C for 10 min. The oven is heated at a rate of 7 °C/min to a final temperature of 240 °C, which was held for 1.5 min. The helium flow was 1.5 mL/min. The column pressure is 20 psi at 22 °C. Under these conditions, the compounds eluted in less than 12 min and the total chromatographic run time was 35 min.

The purge and trap unit (Tekmar LSC 2000 and Tekmar ALS2016 Automatic Sample Heater) was used to extract BTEX from liquid matrix for introduction into a GC for separation and quantification. The purge and trap procedure was as follows. A 5-mL aliquot of each sample (BTEX standard solution or Ohmsett water samples) was poured into the purge vessel. BTEX was then extracted by purging helium through the aqueous solution and trapped. The BTEX is concentrated onto an adsorbent trap, and excess water is removed from trap. The adsorbent material was subsequently heated so that the desorbed analyst was directly transferred into the GC column and analyzed.

Total organic carbon content of the samples was measured using Shimadzu Total Organic Carbon Analyzer (TOC-L, Shimadzu, USA). The instrument utilizes a catalytic oxidation combustion technique at high temperature (680 °C), to convert organic carbon in the aqueous samples into CO_2. The CO_2 generated by oxidation is measured with a Non-dispersive Infra-Red (NDIR) sensor. Prior to TOC analysis, a volume of 30-40 mL water sample was filtered through a 0.45 μm syringe filter (Millipore) to remove suspended materials that might clog the sample flow line.

A LISST (Laser in Situ Scattering and Transmissiometry) was placed in the tank within the oil slick at an approximate depth of 0.8 m. It provided the range of oil droplets from 2.7 microns to 461 microns (inclusive). The LISST has been successful in providing the droplet size distribution following surface applications (as done herein) (Li et al. 2008), from underwater releases(Brandvik et al. 2013), and in laboratory flasks (Pan et al. 2017).

FLUOREMETER METHODS AND LOCATIONS DREW PLEASE PROVIDE THE

LOCATION OF THE FLUOROMETERS IF YOU KNOW. DO YOU KNOW WHERE THE LISST WAS LOCATED WITH RESPECT TO THE SLICK AND DISTANCE FROM THE WAVEMAKER?

Baffled Flask Test (BFT)

The EPA's official standard protocol baffled flask test (BFT), a modification of the swirling flask test (Venosa et al. 2002, Kaku et al. 2006, Venosa and Holder 2013, Zhao et al. 2015), was adopted to evaluate the oil dispersion effectiveness in the presence of different dispersants. The BFT relies on using a 200-mL screw-cap trypsinizing flask with four baffles equally distributed on the side to allow for better mixing. The baffled flask is equipped with a glass stopcock near its bottom so that a subsurface water sample could be collected without disturbing the surface oil layer. The BFT protocol is as follows: A volume of 120 mL Ohmsett water (or synthetic seawater) are added to the baffled flask, followed by the addition of 100 μL of oil using a 250-μL SGE™ gastight glass syringe with a steel luer lock tip. The oil should be dispensed onto the center of the water surface gently. The exact mass of oil added is derived from the weight difference between the glass syringe with oil and that after dispensing the oil. Subsequently, 5 μL of the dispersant is added to the center of the oil slick in the baffled flask using a 1-10 μL Brinkmann Eppendorf repeater plus micropipette (Fisher Scientific, Pittsburgh, PA), giving the dispersant-to-oil volumetric ratio (DOR) of 1:20. The dispersant should be released as close as possible to the surface of the oil slick without actually touching it.

Following the addition of oil and dispersants, the flask was placed on the orbital shaker (Lab-Line Instruments Inc., Melrose Park, IL), whose diameter is 2.0 cm. The rotation speed was 200 rpm, to provide the mixing energy to the solutions in the test flasks, estimated to be approximately 0.7 watt/kg by the Boufadel group (Kaku et al. 2006, Zhao et al. 2015). At NJIT, the experiments were performed in the Thermo Scientific Precision™ refrigerated incubator at the desired temperature. After 10 min of mixing time, the flask was removed from the shaker and kept stationary on the bench top for 10 min. Subsequently, the first 5 mL of sample was drained from the stopcock and discarded (Sorial et al. 2004, Sorial et al. 2004). Then, 40 mL of sample was collected into a 50 mL graduated cylinder. A subsample of 30 mL was used for liquid-liquid extraction (EPA 1996) prior to oil concentration measurement. For each dispersion effectiveness test, triplicate experiments (three BFTs) were performed simultaneously.

The dispersion effectiveness (DE) in the BFT is defined similarly to that in the Ohmsett tank, that is the mass of dispersed oil in the water column, m_{disp} (g), divided by the total mass of oil added, m_{oil}. The DE in percentage is given by Eq. 1, repeated herein for convenience:

$$DE = \frac{m_{disp}}{m_{oil}} \times 100 \qquad (1)$$

where, m_{oil} (g) is the mass of the specific oil added to test flask.

Synthetic seawater at the salinity of 34 ppt was used in the BFT, and it was prepared by dissolving 34 g of the commercially available Instant Ocean sea salt (Aquarium System of Mentor, Ohio, USA) in 1 L of ultrapure deionized water (Millipore, 18.2 MΩ*cm). The mixture

was vigorously agitated using a magnetic stirrer. The seawater was filtered through 0.2 μm membrane filters (Millipore) to remove any suspended materials, and the solution was kept in the refrigerator at 15 ± 1 °C.

Oil Properties

Oil Physical Properties

Measurements of the initial oil density and viscosity were obtained using an Anton Paar SVM 3000 Stabinger Viscometer equipped with a hot filling attachment (Anton Parr, Quebec, Canada). Approximately 10 mL of ANS and HOOP was aspirated into a syringe with a luer slip tip (Becton, Dickinson and Company, New Jersey, USA), taking care not to draw up any air bubbles into the sample. The syringe was then connected to the sample inlet port on the instrument and pressure was slowly applied to the plunger until oil was seen exiting the waste line. The sample measurement occurred at 15, 25, 40 and 50°C. The instrument would automatically take three readings of density and viscosity and report an average, and this process was repeated five times at each selected temperature. In between samples, the sample path was cleaned with toluene and acetone followed by air drying with a built-in blower.

Oil Chemical Properties

At NJIT, the mass of dispersed oil in the BFT was obtained using gas chromatography with a flame ionization detector (GC-FID). The initial oil composition in terms of the major groups: saturates, aromatics, resins, and asphaltenes (SARA) was also measured using thin layer chromatography (TLC).

Oil measurement using GC-FID

The extraction procedure included (1) decanting the 30 mL of water sample after BFTs to a 125-mL separatory funnel, (2) adding DCM and shaking vigorously for ~2 minutes, (3) allowing the DCM-oil and water phases to separate for ~5 minutes (the DCM is heavier than water and thus occupies the bottom of the separatory funnel), and (4) opening the stopcock and allowing the lower layer (DCM-oil phase) to drain into a clean glass beaker. Drain just to the point that the upper layer barely reaches the stopcock. The procedure should be repeated until complete separation (DCM layer turned colorless). Subsequently, the extract is then passed through medium of glass wool and anhydrous sodium sulfate to remove residual moisture, followed by adjusting the final extract to 16 mL using DCM. For this project, the samples were stored in 16-mL crimp style glass vials with aluminum/Teflon seals and mixed by inverting many times and then stored in a refrigerator at 4 °C until the time of analysis. The holding time was less than 2 weeks.

The solvent extract following the liquid-liquid extraction is then transferred into an auto-sampler vial and stored at -20°C for GC-FID analysis. Sample extracts (1 μL) are injected using an Agilent CTC Analytics and PAL Automatic Liquid Sampler into the Agilent GC (HP 6890 GC System) with duel FIDs. Sample introduction used splitless injection which is set to oven track mode (2°C higher than the oven temperature program). The column used for separations was a Supelco MDN-5s (Restek, Cat. No. 12723) 30 m × 250 μm × 0.25 μm (length × i.d. × film thickness). The column is Rtx-5Sil MS (Crossbond 5%, diphenyl 95%, dimethyl polysiloxane)

and its maximum temperature limits was 350 °C. Hydrogen was used as a carrier gas with a flow rate of 3.0 mL/min. The GC oven is programmed to an initial oven temperature of 35°C, held for 2 min, followed by an increase to 320°C at 20°C/min, and held at 320°C for 10 min, with a total run time of 26.25 min. The GC-FID is operated at 320°C with the hydrogen flow set at 30 mL/min and the air flow set at 400 mL/min. The EzChrom Elite Chromatography Data System for data acquisition and processing.

For the calibration of the GC-FID on the oils at NJIT, a 10,000 ppm of crude oil stock solution in DCM was prepared by adding 500 mg of HOOPS or ANS (measured using a 1-mL gas-tight syringe) to 50 mL of volumetric flask, immediately followed by filling DCM up to the mark. Subsequently, the stopper was inserted the flask was shaken thoroughly to ensure the uniform mixing of the solution. An eight point calibration was generated using standards (25, 50, 100, 250, 500, and 1000 ppm) prepared from the serial dilution of 10,000 ppm of crude oil stock that was used to generate the oil samples (e.g. HOOPS and ANS). Then, the oil standards were transferred into an auto-sampler vial and stored at -20°C for GC-FID analysis. The mass of dispersed oil in the water column was computed as:

$$\text{Total oil dispersed (g)} = \text{Oil}_{\text{GC-FID}} \times V_{\text{DCM}} \times \frac{V_{\text{tw}}}{V_{\text{ew}}} \qquad (2)$$

where, $^{\text{Oil}_{\text{GC-FID}}}$ is the oil mass measured by GC-FID; V_{DCM} is the volume of DCM extract; V_{tw} is the total volume of seawater in the baffled flask and V_{ew} is the total volume of seawater extracted.

Saturates, aromatics, resins, and asphaltene (SARA)

The measurement of the SARA was conducted using thin layer chromatography with flame ionization detection (TLC-FID) using an Istroscan MK-6 following the thin layer chromatography procedure of (Napolitano et al. 1998). The procedure includes four steps: (1) sample and standard preparation; (2) spotting; (3) solvent development; (4) scanning. A 5 mL subsample, initially extracted using dichloromethane (DCM, pesticide quality) and stored at 4 °C, was concentrated to 1 mL under nitrogen. A volume of 3 µL of samples was loaded into an auto-spotter, which served to deliver a consistent small amount of sample (2 µL) along a chromarod. Upon completion of spotting, the chromarods were developed to separate the four SARA oil fractions by placing successively the chromarods in a chamber of humidity (70 mL of pure water and 30 mL of concentrated sulfuric acid) for 10 min., hexane (100 mL) for 18 min., toluene (100 mL) for 8 min. and methanol-DCM (5–95 mL) for 2 min., respectively. The samples were then air-dried for 2 min., emplaced in the Iatroscan (Shell, USA) for blank scans (about 20 min) followed by a final scan. Sample peaks were integrated to determine the relative proportion of the alkane, aromatic, resin and asphaltene compounds of the samples.

RESULTS

The time and date of each dispersant was made random with the only proviso that no two consecutive tests are conducted with the same dispersant. Table 2 reports these times and dates.

The measurement of the surface tension gave values that were between 70 mN/M and 75 mN/m with the exception of two samples whose surface tension was 48 mN/m and 55 mN/m. These low values could be to localized high concentrations of surfactant, which would locally affect oil

dispersion but would probably have no impact on the test-average value. Discarding these two values gives a surface tension average of 72.5 mN/m ± 3.0 mN/m, which is close to the theoretical value based on clean seawater (around 75 mN/m). Nevertheless, the lower surface tension in the Ohmsett tank in comparison to that of the synthetic seawater is consistent, and thus could result in an enhanced dispersant effectiveness in the Ohmsett water. Also note that natural systems (oceans) have natural biosurfactants in them, and thus, the actual surface tension is always smaller than the theoretical value by a few percents. It is also of importance to note that the surface tension measurements were made to provide the background surfactant concentration in the Ohmsett water, and not the surfactant concentration during a dispersion effectiveness test.

Table 3 report the ion composition and resulting salinity in the Ohmsett water, synthetic seawater, and ocean water. The salinity values were comparable at around 35,000 mg/L, and thus are not expected to affect dispersion effectiveness. of water average of 35,000 mg/L. However, the composition of the water is different. Table 8 indicates that the proportion of major ions in synthetic water is very close to that in the oceans, and thus, the two waters (ocean and synthetic) would be considered identical in terms of major ions. The concentrations of chloride and sodium of the Ohmsett water were close to those of the synthetic water. But the proportion of sulfate in Ohmsett water was 4% while it was around 8% in synthetic seawater. Also, the concentration of magnesium was 2.5% in Ohmsett water, while it was around 4% in synthetic or ocean water. These ions could play an important role in altering the effectiveness of a dispersant, as addressed in the Discussion.

The BTEX content in the water never exceeded 2.7 mg/L and the TOC content remained below 7.5 mg/L (Boufadel et al. 2017). These small values are not expected to affect water quality for dispersion effectiveness, where the hydrocarbon concentration could reach up to a few thousand mg/L.

Table 4 reports the physical properties of the oils used in the study at four different temperatures selected to provide a broad characterization of the oils. One notes that the density of HOOPS is slightly smaller than that of ANS; by approximately 2% at the corresponding temperature. However, the viscosity of HOOPS is around two thirds of that of ANS at the corresponding temperature. Note that the Ohmsett water temperature was around 15°C.

Table 5 provides the oil chemical composition in terms of the four major groups known as SARA (Saturates, Aromatics, Resins, and Asphaltenes). The two oils have essentially the same fraction of aromatics (around 28%). The fractions of saturates and resins in the HOOPS are a few percent larger than those in the ANS. The asphaltenes fraction in the HOOPS was less than 2% while it is around 7% for the ANS. Thus, the major difference between the two oils seems to be the asphaltenes fraction.

Table 6 reports the DE of the oil HOOPS in the Ohmsett tank for the five dispersants along with the control (oil without dispersant). The DE for the control was around 62%. The DE in the baffled flask was not evaluated, but a recent work by Pan et al. (2017) found it to be less than 30% for ANS. The dispersants Corexit9500A and Finasol OSR 52 performed essentially the same (considering the statistical deviation) at a DE (Eq 1) of approximately 90%. The remaining dispersants, Accell Clean, Marine D-blue and ZI-400 performed the same at a DE (Eq. 1) of

approximately 75%. For each of the Accell Clean and the ZI-400, there was a test whose DE was less than 50%. These were taken as outliers as they were lower than the control. However, removing these outliers completely would have resulted in biasing the DE of these dispersants by keeping only the high values. Thus, as a compromise, the DE for those tests was assumed equal to that of the control when computing the averages.

The LISST provided data for the duration of each DE test, which varied from 30 minutes to one hour. For most tests, the droplet size distribution (DSD) did not vary much with time. However, there were some exceptions. But investigating the evolution of the DSD with time is beyond the scope of this work, and thus we obtained the time-average DSD from each test, and then we averaged between tests for each dispersant. This resulted in 6 graphs, one for the control and five for the dispersants.

Figure 1 reports the DSD results as obtained from the LISST, and Table 7 reports the Sauter Mean Diameter (D_{32}) and the D50 (volume mean diameter). For the control case (Figure 1a), one notes a unimodal (i.e., one peak) DSD with a peak at around 240 microns. The D32 was 120 micron. The dispersant Accell Clean (Figure 1b) gave a multimodal distribution with peaks (or mode) at 2.72 microns, 75 microns, and 461 microns, and a D_{32} of 15 microns. The dispersant Corexit 9500A (Figure 1c) gave an obvious bimodal distribution with peaks at 2.72 microns and 88 microns. Very little volume existed at 461 microns, when compared to Accell DWD (Figure 1b). The D32 of Corexit 9500A was equal to 20 microns, larger than that of the Accell Clean at 15 microns, a small difference, probably due to the high volume at small diameters for the Accell Clean. Figure 1d, for Finasol, is similar to Figure 1b for Accell Clean. However, the D32 for the Finasol test was 28 microns (Table 7), probably due to the larger volume fraction volume fraction at the largest bin size for Finasol (Figure 1e). The dispersant Marine D Blue (Figure 1e) gave DSD that increased gradually from around 20 microns until reaching a sharp maximum at 460 microns. The D32 was equal to 57 microns. Figure 1f shows a biomodal distribution for ZI400 with a peak at 2.72 microns and another at approximately 180 microns. The D32 of this case was around 22 microns.

It is possible that values outside of the 2.71-461 microns range got "folded into the extremities of the range, providing larger volume fractions there. But the control DSD provides valuable information. For example, there were no "particles" at the 2.71 micron for the control case (Figure 1a), thus, whatever was observed in the dispersant tests reflected oil droplets that are equal to or smaller than 2.71 microns. It is possible that there were oil droplets larger than 461 microns, and thus the reading there reflected a wide range of larger droplets (as large as a few millimeters). However, the D32 provides a holistic measure, and thus most likely tempered the impact of the extreme values. This could be noted by comparing the D32 of Finasol to Corexit 9500A; Finasol had a large volume fraction at the bin size 461 microns, but the D32 of the two is close, 28 microns for Finasol to 20 microns for Corexit 9500 A.

Also, with the exception of Marine D Blue, all the DSDs had peaks at 2.72 microns and a minimum at around 5.27 microns. This is most likely due to the mechanism of tip-streaming, whereby the dispersant on the oil droplet causes the oil to slough off as small streams (Gopalan and Katz 2010, Zhao et al. 2017).

From Figure 1 and Table 7, it is reasonable to state that from the point of view of droplet size (i.e., through the D32), all dispersant with the exception of Marine D. Blue behaved similarly with a D32 around 20 microns.

Hi Drew. It is here that we need your input. The fluorometer data show.

ccccccccccccccccccccccccccc
Figure 4 reports HOOPS dispersion effectiveness in the baffled flask with different dispersants using Ohmsett wavetank water and synthetic seawater. Each "trial" in the figure represents a time/day where a DE experiment was conducted in the Ohmsett tank, as reported in Table 2. The average DE values of all trials are reported in Table 6 along with their standard deviations.

One notes in Figure 4 and Table 6 for the BFT with HOOPS that Corexit 9500A had the highest overall DE (around 85%). The DE of Accel Clean in Ohmsett water was close to that of Corexit 9500 in Ohmsett, but its DE in synthetic seawater seems dropped below 60%. The remaining three dispersants behaved similarly to each other in Ohmsett water with a DE of approximately 50%. The DE of Marine D Blue and ZI-400 was only around 30% in synthetic seawater. The DE of all dispersants in synthetic seawater was lower than the DE in Ohmsett water.

Figure 5 reports the DE of the ANS in the baffled flask with different dispersants using Ohmsett wavetank water and synthetic seawater. The averages are reported in Table 6, where one notes that the dispersant Accel Clean performed the best in Ohmsett water with an average DE of 91% Corexit 9500 was second at around 70%. The DE of the remaining dispersants in Ohmsett water was markedly lower (50% to 40%), and the DE of ANS in synthetic seawater was comparable to its DE in Ohmsett water for all dispersants, except for Marine D Blue, which was 20 points lower in synthetic seawater. Thus, in general the impact of water source (Ohmsett water or synthetic seawater) seems to be less important for the ANS than for the HOOPS. Also, when comparing the BFT results, one notes a larger variability for the DE of ANS in comparison with the DE of HOOPS for both Ohmsett water and synthetic seawater.

Figure 6 shows the correlation between the dispersion effectiveness (DE) for HOOPS and all dispersants using the BFT with Ohmsett water and the DE in the Ohmsett tank with HOOPS (only HOOPS was used in the Ohmsett tank). A linear correlation was obtained between the DEs for the HOOPS as:

$$\mathrm{DE(BFT,\ Ohmsett\ water)} = 0.63 * \mathrm{DE(Ohmsett\ tank)} + 6.4; R^2 = 0.12 \qquad (3)$$

The positive intercept (6.4%) suggests that at low DE (e.g., due to an ineffective dispersant), the DE of the BFT would be larger than that in the Ohmsett tank, which could be viewed as reflecting the high mixing energy in the baffled flask test in comparison with the Ohmsett tank; the energy dissipation rate in the BFT is around 1.0 watt/kg (Zhao et al. 2015), while it can be estimated at less than at 0.1 watt/kg in the Ohmsett tank under the current breaking conditions. However, the R^2 is small, and such an argument might not strongly favored considering that the intercept is only around 6%.

The slope value of 0.63 (i.e., less than 1.0) is most likely due to the large dilution in the Ohmsett tank which allows the dispersed oil to spread into the water column. Thus, if a dispersant is effective (i.e, the DE in the Ohmsett tank is large), the DE in the BFT would be, in general, smaller than that in the Ohmsett tank.

Figure 7 shows the correlation between the DE in the BFT with synthetic seawater and HOOPS to that in the Ohmsett tank (where only HOOPS was used). A best fit straight line gave the equation:

$$\text{DE(BFT, synthetic seawater)} = 1.28 * \text{DE(Ohmsett tank)} - 62; R^2 = 0.27 \quad (4)$$

Although the slope is larger than 1.0 suggesting more effectiveness in the BFT (in contrast to Eq. 3), the magnitude of the negative intercept is large, and thus the left hand side of Eq. 4 remains negative up to a DE around 50%. Note that the control case had a DE (Ohmsett tank) of around 62% giving a DE (BFT, synthetic water)=16. Comparing Eqs 3 and 4, one notes that the DE of BFT in synthetic water is always smaller than that in Ohmsett water, and the difference decreases with an increase in the Ohmsett DE (i.e, the dispersant itself).

Using 20 oils and comparing the EPA's BFT to DE in the Ohmsett wave tank conducted by SL Ross (2010), Venosa and Holder (2011) found the relation:

$$\text{DE(BFT, synthetic seawater)} = 0.49 * \text{DE(Ohmsett tank)} + 62.3 \quad (5)$$

Which is very different from Eq. 4 that we obtained based on our results. However, Eq. 5 was developed using only Corexit 9500A, while we used five dispersants including Corexit 9500A. In addition, the estimation of the DE in the Ohmsett tank is always challenging, as it is subject to meteorological conditions, and for these reasons, we used surrogate measurements to get a better appreciation of the uncertainty. Furthermore, we used only 15 tests for five dispersants, which probably did not provide a sufficiently high number for samples for a strong statistics.

Figure 7 illustrates the correlation between the dispersion effectiveness (DE) using the BFT with synthetic seawater with HOOPS and the DE in the BFT using Ohmsett water with HOOPS. A linear correlation was obtained between the DE and is given by:

$$\text{DE(BFT, synthetic seawater)} = 1.08 * \text{DE(BFT, Ohmsett water)} - 21; R^2 = 0.92 \quad (6)$$

The almost 1.0 slope and the negative intercept suggest a close one-to-one relation between the DEs where that of the synthetic seawater is lower by 21 points. This indicates that the synthetic water with HOOPS in the BFT produced DE that are only offset by around 21% from the DE in the BFT with Ohmsett water and HOOPS.

SUMMARY

The study evaluated the dispersion effectiveness (DE) in the Ohmsett tank with Hoover Offshore Oil Pipeline System (HOOPS) oil and five dispersants (Table 1). Surrogate measurements of droplets size distribution and fluorescence were used to build confidence in the experimentally obtained DE values. The background water for each DE test in the Ohmsett tank was used as the same temperature to replicate the experiments in the Baffled Flask Test (Pan et al. 2017). Additional BFTs were conducted using Alaskan North Slope (ANS) oil and synthetic seawater.

The Ohmsett tank DE provided a two tier system for the performance of dispersants: Corexit9500A, and Finasol OSR 52 provided a DE of approximately 90% while Accell Clean, Marine D-blue, and ZI-400 provided a DE of approximately 75%.

The droplet size distribution from the LISST was multimodal (i.e., possessing multiple peaks) for all dispersants except Marine D blue. The Sauter mean diameter, D_{32}, was equal to 120 microns for the control case, and around 20 microns for all dispersants except Marine D. Blue whose D_{32} was around 58 microns.

The results from the baffled flask test (BFT) indicated that, in Ohmsett water, Corexit 9500 provided the highest dispersion effectiveness (DE) for (HOOPS) crude oil at around 89%, followed by Accell Clean DWD at about 78%. The remaining three dispersants (Finasol OSR 52, Marine D-Blue, and ZI-400) provided a DE between 45% and 53%. The DE of Alaska North Slope (ANS) oil in Ohmsett water was largest for Accell Clean at 91%, followed by Corexit 9500 at around 70%. Finasol and Marine D-Blue provided a DE around 50%, while ZI-400 had a DE around 40%.

The DE of HOOPS was lower when using synthetic seawater in comparison to DE of HOOPS in Ohmsett water; the decrease in DE was 6% (i.e., 6 points on the 100 point scale) for Finasol, 12% for Corexit, and around 20% for Accell, Marine D-Blue, and ZI-400. However, the DE with ANS of most dispersants in synthetic seawater was similar to the DE in Ohmsett water, with the exception of Marine D-Blue with ANS whose DE dropped from 50% in Ohmsett water to 30% in synthetic seawater.

A linear correlation between the DE (in percentage) of the oil HOOPS in the BFT and the DE of HOOPS in the Ohmsett tank revealed the relation:

$$\mathrm{DE(BFT,\ Ohmsett\ water)} = 0.63 * \mathrm{DE(Ohmsett\ tank)} + 6.4; R^2 = 0.12 \quad (3)$$

A slope smaller than 1.0 suggests that the large dilution in the Ohmsett tank played a major role in the dispersion of oil. The coefficient of determination, R^2, was small, suggesting that more data are needed.

DISCUSSION

Sulfate is a constituent of surfactant (specifically sulfate-based surfactant, e.g. Sodium lauryl sulfate and sodium dodecyl sulfate), acting as the hydrophilic head group to interact with water-soluble molecules. Thus, a large value of sulfate could enhance dispersion????

Numerous studies have noted that the anionic surfactants present in dispersants could be precipitated out of solution by hard water ions, namely calcium and magnesium(Park et al. 2016)(Fainerman et al. 2012, Park et al. 2016). In essence, water hardness salts ($CaCl_2$ and $MgCl_2$ in the concentration ratio of 2:1) interact with the anionic surfactant (e.g. sodium dodecyl sulfate, SDS), to form $Ca(DS)_2$ and $Mg(DS)_2$, reducing therefore, the interaction of the SDS with oil, and subsequently the DE. The hardness is defined as:

$$\mathrm{Hardness} = \mathrm{Hardness\ due\ to\ Ca} + \mathrm{Hardness\ due\ to\ Mg} \quad (7)$$

To compute the hardness as mg/L of CaCO3, one notes that the equivalent weights of $CaCO_3$, Ca, and Mg are 50, 20, and 12, respectively. Thus, the hardness as mg/L of $CaCO_3$, is expressed as:

$$\text{Hardness (as mg/L of } CaCO_3) = C_{Ca} * \frac{50}{20} + C_{Mg} * \frac{50}{12} \quad (8)$$

Where C_{Ca} and C_{Mg} are the concentrations of the calcium and magnesium ions in mg/L, respectively. Converting the percentages of Table 3 to mg/L by multiplying by the salinity (34,000 mg/L or 36,000 mg/L), one obtains the following values. For Ohmsett water, C_{Ca}=1%*36,000=360 mg/L and C_{Mg}=2.5%*36,000=900 mg/L. For ocean water, C_{Ca}=1%*34,000=340 mg/L and C_{Mg}=4%*34,000= 1,360 mg/L. Then inputting the values in Eq. 8, one obtains that the water hardness of Ohmsett water is approximately 4,650 mg/L while it is 6,500 mg/L in synthetic or ocean water. Thus, the hardness of the Ohmsett water is around 70% that of the synthetic seawater (or ocean water). Therefore, the larger DE of HOOPS in the BFT in Ohmsett water in comparison with BFT in synthetic water and for ANS with Marine D-Blue (Table 6) is likely due to the smaller hardness of the Ohmsett water. However, the small hardness does not explain why there was no difference in the DE of ANS between Ohmsett water and synthetic seawater with the remaining dispersants.

When using the Ohmsett water in the BFT, the performance of each dispersant with the two oils (HOOPS and ANS) was comparable; dispersants Accell and Corexit 9500 performed well (70% to 90%), while the remaining dispersant's DE was less than 50% with either oil. The DE was much smaller when using synthetic seawater, and the decrease was largest for HOOPS.

The DE of HOOPS was smaller than that of ANS in the BFT for both Ohmsett and synthetic water. To provide an interpretation of these results, we consider the physical and chemical properties of each oil, as reported in Tables 4 and 5. Table 4 shows that there was a decrease in the density of both oils with temperature, and that HOOPS is slightly lighter than ANS at the same temperature. However, the difference in density between the two oils is small (less than 2%), and is not expected to affect dispersion effectiveness, especially that the DE of the lighter oil (HOOPS) was smaller than the heavier oil (ANS). The viscosity of ANS at 15°C was 18 cp (Table 4) which is approximately 1.5 times that of HOOPS (12 cp) at that temperature. But a higher viscosity suggests a lower DE (Pan et al. 2017), while the opposite is noted herein, which indicates that such a viscosity change was not important to impact the DE. The impact of viscosity on dispersion was investigated in prior works using the model VDROP- the V stands for viscous (Zhao et al. 2014), and it was found that only when the viscosity reaches a few hundred centipoise (cp) that one could detect its presence. Therefore, the difference in the DE of the two oils could not be related directly to their physical properties.

Looking at the SARA of both oils in Table 5, one notes that the asphaltenes content in the ANS is around 7% per mass, while it is less than 2% per mass for the HOOPS. As the asphaltenes molecules are large polar molecules and behave as slow surfactants (Fingas and Fieldhouse 2006), it is possible that they worked with the added surfactants to increase the dispersion effectiveness (DE).

ACKNOWLEDGEMENT
This work was funded through Contract E14PC00018 from the Bureau of Safety and Environmental Enforcement to NJIT. However, no official endorsement should be implied.

Reference

Boufadel , M. C., Z. Pan and T. Steffek (2017). Chemical Characterization of the Ohmsett Tank Water: Filtration and Potential Impact on Dispersant Effectiveness Test Results. 40th Seminar of the Arctic Marine Oil Spill Program, Calgary, Alberta Canada, Environment Canada.

Brandvik, P. J., Ø. Johansen, f. Leirvik, U. Farooq and P. S. daling (2013). "Droplet breakup in subsurface oil releases - Part I: Experimental study of droplet breakup and effectiveness of dispersant injection." Mar Pollut Bull **73**: 319-326.

Conmy, R. N., P. G. Coble, J. Farr, A. M. Wood and e. al. (2014). "Submersible Optical Sensors Exposed to Chemically Dispersed Crude Oil: Wave Tank Simulations for Improved Oil Spill Monitoring." Environmental Science and Technology **48**: 1803–1810.

EPA (1996). "Method 3510C: separatory funnel liquid-liquid extraction. Revison 3. pp.1-8.".

Fainerman, V., S. Lylyk, E. Aksenenko, N. Kovalchuk, V. Kovalchuk, J. Petkov and R. Miller (2012). "Effect of water hardness on surface tension and dilational visco-elasticity of sodium dodecyl sulphate solutions." Journal of colloid and interface science **377**(1): 1-6.

Fingas, M. and B. Fieldhouse (2006). A review of knowledge on water-in-oil emulsions. Proceeding of: Environment Canada Arctic and Marine Oil Spill Program Technical Seminar (AMOP) Proceedings, British Columbia, Canada, Environmental Canada.

Gopalan, B. and J. Katz (2010). "Turbulent shearing of crude oil mixed with dispersants generates long microthreads and microdroplets." Physical review letters **104**(5): 054501.

Kaku, V. J., M. C. Boufadel and A. D. Venosa (2006). "Evaluation of mixing energy in laboratory flasks used for dispersant effectiveness testing." J. Environ. Eng. **132**(1): 93-101.

King, T. L., B. Robinson, M. Boufadel and K. Lee (2014). "Flume tank studies to elucidate the fate and behavior of diluted bitumen spilled at sea." Marine pollution bulletin **83**(1): 32-37.

Lee, K., T. Nedwed and R. C. Prince (2011). Lab tests on the biodegradation rates of chemically dispersedoil must consider natural dilution. International Oil Spill Conference.

Li, Z., K. Lee, T. King, M. C. Boufadel and A. D. Venosa (2008). Oil droplet size distribution as a

function of energy dissipation rate in an experimental wave tank. International Oil Spill Conference, American Petroleum Institute.

Li, Z., K. Lee, T. King, M. C. Boufadel and A. D. Venosa (2009). "Evaluating chemical dispersant efficacy in an experimental wave tank: 1- Dispersant effectiveness as function of the energy dissipation rate." Environmental Engineering Science **26**(6): 1139-1148.

Napolitano, G. E., J. E. Richmond and A. J. Stewart (1998). "Characterization of petroleum-contaminated soils by thin-layer chromatography with flame ionization detection." J. Soil Contam. **7**(6): 709-724.

NRC (2005). Oil Spill Dispersants: Efficacy and Effects. Washington, DC, National Academies Press.

Pan, Z., L. Zhao, M. C. Boufadel, T. King, B. Robinson, R. Conmy and K. Lee (2017). "Impact of mixing time and energy on the dispersion effectiveness and droplets size of oil." Chemosphere **166**: 246-254.

Park, C. M., J. Heo, N. Her, K. H. Chu, M. Jang and Y. Yoon (2016). "Modeling the effects of surfactant, hardness, and natural organic matter on deposition and mobility of silver nanoparticles in saturated porous media." Water Research **103**: 38-47.

SLRoss (2010). Comparison of large scale (Ohmsett) and small scale dispersant effectiveness test results. M. M. S. Report for U.S. Department of the Interior. Herndon, VA.

Sorial, G. A., A. D. Venosa, K. M. Koran, E. Holder and D. W. King (2004). "Oil Spill Dispersant Effectiveness Protocol. I: Impact of Operational Variables." J. Envir. Engrg **130**(10): 1073-1084.

Sorial, G. A., A. D. Venosa, K. M. Koran, E. Holder and D. W. King (2004). "Oil spill dispersant effectiveness protocol. II: Performance of revised protocol." J. Environ.Eng. **130**(10): 1085-1093.

Sorial, G. A., A. D. Venosa, K. M. Koran, E. Holder and D. W. King (2004). "Oil spill dispersant effectiveness protocol. I: Impact of operational variables." J. Environ.Eng. **130**(10): 1073-1084.

Venosa, A. D. and E. Holder (2011). Laboratory-Scale Testing of Dispersant Effectiveness of 20 Oils Using the Baffled Flask Test, a white paper as a result of funding from BOEMRE to the US EPA under Interagency Agreement No.RW95778401 N.

Venosa, A. D. and E. L. Holder (2013). "Determining the dispersibility of South Louisiana crude oil by eight oil dispersant products listed on the NCP Product Schedule." Mar. Pollut. Bull. **66**(1): 73-77.

Venosa, A. D., D. W. King and G. A. Sorial (2002). "The baffled flask test for dispersant effectiveness: a round robin evaluation of reproducibility and repeatability." Spill Sci. Technol. Bull. **7**(5): 299-308.

Wickley-Olsen, E., M. C. Boufadel, T. King, Z. Li, K. Lee and A. D. Venosa (2007). Regular and Breaking Waves in Wave Tank for Dispersion Effectiveness Testing. Proceedings of the Arctic and Marine Oil Spill, Edmonton Alberta, Canada.

Wickley-Olsen, E., M. C. Boufadel, T. King, Z. Li, K. Lee and A. D. Venosa (2008). Regular and breaking waves in wave tank for dispersion effectiveness testing. Proceedings of the 2008 International Oil Spill Program.

Zhao, L., B. Wang, P. M. Armenante, R. Conmy and M. C. Boufadel (2015). "Characterization of Turbulent Properties in the EPA Baffled Flask for Dispersion Effectiveness Testing." J. Environ.Eng.: 04015044.

Zhao, L., J. Torlapati, M. C. Boufadel, T. King, B. Robinson and K. Lee (2014). "VDROP: A comprehensive model for droplet formation of oils and gases in liquids-Incorporation of the

interfacial tension and droplet viscosity." Chem. Eng. J. **253**: 93-106.
Zhao, L., F. Gao, M. C. Boufadel , T. King, B. Robinson and K. Lee (2017). "Investigation of underwater horizontal oil jet with and without dispersants: modeling and experimental methods." AIChE Journal.

ENVIRONMENTAL Science & Technology

Article

pubs.acs.org/est

Submersible Optical Sensors Exposed to Chemically Dispersed Crude Oil: Wave Tank Simulations for Improved Oil Spill Monitoring

Robyn N. Conmy,[†,*] Paula G. Coble,[‡] James Farr,[□] A. Michelle Wood,[§,◆] Kenneth Lee,[//,¶] W. Scott Pegau,[⊥] Ian D. Walsh,[#] Corey R. Koch,[#] Mary I. Abercrombie,[‡] M. Scott Miles,[▽] Marlon R. Lewis,[○] Scott A. Ryan,[//] Brian J. Robinson,[//] Thomas L. King,[//] Christopher R. Kelble,[§] and Jordanna Lacoste[○]

[†]National Risk Management Research Laboratory, Office of Research and Development, U.S. Environmental Protection Agency, 26 West Martin Luther King BoulevardCincinnati, Ohio 45268, United States

[‡]College of Marine Science, University of South Florida, St. Petersburg, Florida 33701, United States

[□]Office of Response and Restoration, National Oceanic and Atmospheric Administration, 1305 East-West Highway, Silver Spring, Maryland 20910, United States

[§]Atlantic Oceanographic & Meteorological Laboratory, National Oceanic and Atmospheric Administration, 4301 Rickenbacker Causeway, Miami, Florida 33149, United States

[//]Department Fisheries and Oceans Canada, Bedford Institute of Oceanography, Dartmouth, Nova Scotia, Canada

[⊥]Oil Spill Recovery Institute, 300 Breakwater Avenue, Cordova, Alaska 99574, United States

[#]WET Labs, Inc., PO Box 518, Philomath, Oregon 97370, United States

[▽]School of Coast and Environment, Louisiana State University, Baton Rouge, Louisiana 70803, United States

[○]Department of Oceanography, Dalhousie University, Halifax, Nova Scotia, Canada

[*] Supporting Information

In situ fluorometers were deployed during the Deepwater Horizon (DWH) Gulf of Mexico oil spill to track the subsea oil plume. Uncertainties regarding instrument specifications and capabilities necessitated performance testing of sensors exposed to simulated, dispersed oil plumes. Dynamic ranges of the Chelsea Technologies Group AQUAtracka, Turner Designs Cyclops, Satlantic SUNA and WET Labs, Inc. ECO, exposed to fresh and artificially weathered crude oil, were determined. Sensors were standardized against known oil volumes and total petroleum hydrocarbons and benzene-toluene-ethylbenzene-xylene measurements - both collected during spills, providing oil estimates during wave tank dilution experiments. All sensors estimated oil concentrations down to 300 ppb oil, refuting previous reports. Sensor performance results assist interpretation of DWH oil spill data and formulating future protocols.

INTRODUCTION

SMART (special monitoring of applied response technologies) protocols use real-time fluorescence monitoring in decision-making during oil spill dispersant operations[1] to determine efficacy of chemically enhanced dispersion and dispersed oil transport.[2] Chemical dispersants applied to oil slicks (in the presence of mixing energy) reduce the oil−water interfacial tension, forming small oil droplets (<100 um) that are less likely to recoalesce,[3] removing oil from the water surface and suspending neutrally buoyant oil droplets as a subsurface plume. This reduces risk to shorelines and air−water interface biota and also increases microbial biodegradation rates of oil.[4−6] Under SMART, in situ monitoring of surface waters (<2 m) and below (2 - 10 m) evaluates efficacy. Monitoring requires rapid, reliable, easy-to-operate in situ fluorometers. Validation with oil/water samples yields oil mapping with finer temporo-spatial resolution not achieved through coarse discrete measurements alone.

Fluorescence has been an oil spill monitoring tool for more than 30 years.[7,8] Measurements are inherently sensitive, conducted without laborious extraction techniques, time

Received: September 20, 2013
Revised: December 17, 2013
Accepted: December 30, 2013
Published: December 30, 2013

dx.doi.org/10.1021/es404206y | Environ. Sci. Technol. 2014, 48, 1803−1810

efficient, chemistry dependent and indicators of hydrocarbon concentration.[9,10] Low viscosity physically dispersed crude oils typically have two broad UV peaks with excitation (Ex) between 240 and 300 nm and emission (Em) centered at ~350 nm (low molecular weight polycyclic aromatic hydrocarbons, LMW PAH, <3 benzene rings) and ~450 nm (higher MW PAH, >3 benzene rings).[11,12] Fluorescence signatures discriminate oils[11−14] but are complicated by varying concentration, degree of chemical and physical dispersion, oil age and state (fresh, weathered, mousses),[11,14,15] and interference of fluorophores with spectro-chemical similarities. Such is the case with colored dissolved organic matter (CDOM) and oil aromatic fractions, which exhibit broad fluorescence peaks and complex spectra. However, crude oils have peak maxima at slightly shorter wavelengths relative to aquatic CDOM (humics, fulvics), facilitating discrimination.

Optical oil detection is a function of matching Ex/Em wavelengths with oil (center wavelength (CWL) and filter bandwidth), power of the light source, and detector sensitivity. Numerous submersible fluorometers are commercially available, each with unique configurations for detecting compounds[16] (and references therein), thus expanding their use in spill response efforts and SMART protocols.[17] Reviews of commercial off-the-shelf (COTS) sensors[17−19] highlight the need for robust calibrations, operational procedures and scalability testing.[20] Reviews have targeted easy-to-conduct, low-cost bench-scale testing. Often tests are conducted in the absence of dispersant, in small flasks with insufficient mixing energy to physically disperse oil into water,[21] at elevated oil concentrations irrelevant to field observations, with limited oil type and weathering states, and without calibration to standards or hydrocarbon concentrations. Thus there are confidence challenges in establishing saturation cutoffs and detection limits relevant for field applications. Effectiveness in quantitative monitoring also remains unclear.[19] Hence, caution must be exercised when scaling up experimental designs to real-world conditions and decision-making. Rather, a combination of laboratory, wave tank, and field studies has been recommended to establish the best degree of confidence for detecting chemically dispersed oil during environmental spills.[22]

SMART provides guidance on surface, not deepwater spill response like the 2010 Deepwater Horizon spill (DWH) where ~800 million liters of light Louisiana sweet crude oil was released from 1500 m ocean depth. Seven million liters[23] of chemical dispersant (Corexit© 9527, 9500A) were applied to reduce environmental impacts of oil, and aid worker safety. The response effort proved challenging partly due to the inability to visually inspect the subsea oil plume. The horizontal, vertical and temporal extent of, and heterogeneity of the plume equated to a "needle-in-the-haystack" situation with grab sampling too coarse to capture its magnitude and extent. Sample number limitations and oil stratification within bottles during the 1−2 h profiler transit time also contributed to challenges in quantifying oil.[24] Thus, responders and scientists were evermore reliant on submersible sensors in lieu of visual observations to provide critical tracking measurements. Initial plume tracking between 1000 and 1400 m was conducted using WET Labs, Inc. ECO fluorometers. Their accessibility and wavelength configuration- wide filter bandwidth and ExEm370/460 nm CWL (Supporting Information (SI) Table S2) to capture broad nature of the peaks- is appropriate for crude oil fluorescence detection. Chelsea Technologies Group AQUAtracka fluorometers were deployed to monitor the transport and fate of oil at large distances from the wellhead and after well capping (latter response, low concentrations).[24] This unit employs filters (ExEm239/360 nm CWL) to capture peak fluorescence from petroleum aromatic fractions with elevated sensitivity (higher signal-to-noise) due to a xenon lamp light source and a photomultiplier tube (PMT) detector; possibly aiding MC252 oil tracking which has a small fraction of highly fluorescing molecules (~20%).[24]

In the wake of the spill many questions remain regarding oil quantification and fate of the subsea oil plume, as well as sensor applicability to detect oil (dynamic range, detection limits, and wavelength configuration).[25] Effects of concentration, dispersant to oil ratio (DOR), dispersant effectiveness,[26] and fluorescence signatures[12] contribute to uncertainties in selecting sensors. Moreover, concerns persist on sensor reliability and applicability of laboratory calibrations using flasks, high oil concentrations and insufficient mixing energies to real-world conditions[19,25] To address uncertainties the performance of select COTS in situ fluorometers deployed during DWH (Chelsea Technologies Group, Turner Designs, WET Labs, Inc.) and a UV spectrophotometer (Satlantic) was evaluated in the Bedford Institute of Oceanography (BIO) wave tank. This work is timely, as findings will assist in the calibration and interpretation of DWH fluorescence measurements. It also coincides with the National Oil and Hazardous Substances Pollution Contingency Plan (NCP) amendments pertaining to fluorometer protocols, reflecting the need for improved confidence in sensors for estimating spilled oil concentrations.

EXPERIMENTAL SECTION

Wave Tank Description. Experiments were conducted at the BIO, Center for Offshore Oil, Gas and Energy Research (COOGER; Dartmouth, Nova Scotia) wave tank, measuring 32 m long, 0.6 m wide, and 2 m high (1.5 m water depth; 28 800 L volume) (SI Figure S1). Water from the Bedford Basin of Halifax Harbor was pumped into the tank through a coarse (25 μm pore size) and fine (5 μm pore size) serial filtration system. Breaking and nonbreaking waves (computer-controlled flat-type wave maker) provided mixing energies to achieve dispersant effectiveness observed in the field. The tank was drained and cleaned with Big Orange detergent and seawater (tank walls, bottom, wave maker and absorbers) after each experiment to remove all oil and surfactants, and sensor optical windows were also cleaned.

Experimental Design. Experiments were conducted using MC252 crude oil (Discoverer Enterprise drillship recovered, May 31−June 7, 2011), and Corexit© 9500 chemical dispersant (1:25 DOR). Artificially weathered oil was generated by bubbling with nitrogen for 36 h (average time responders typically begin dispersant) resulting in mass reduction by 7%. Experimental duplicate and triplicate treatments were run with random design, reducing effects from confounding factors such as wind, rain, temperature, salinity, and seawater quality (SI Table S1). Prior to experiments, oil and dispersant mixtures were prepared in 1 L of seawater by orbital shaker agitation (20 min). Fluorometers (WET Labs, Inc. ECO, Chelsea Technologies Group AQUAtracka, Turner Designs Cyclops) and a UV spectrophotometer (Satlantic SUNA) were deployed at the same cross-sectional position within the tank 20 m from the wave generator (10 m downstream from oil release). Configuration specifications are shown in SI Table S2 and Figure S1. A laser in situ scattering and transmissometry particle size analyzer (Sequoia Scientific LISST-100X, C-Type,), 1 m

downstream from sensors, collected continuous particle size distribution measurements. Sensors were mounted so that optical windows were positioned 65 cm deep in the tank and warmed up for 15 min prior to oil addition and collection of baseline. A stepwise addition experiment (EXP_{ADD}) of chemically dispersed fresh oil (300 ppb to 12 ppm, tank operated in steady-state mode) was conducted to establish response linearity and dynamic range of sensors to MC252 oil. Each addition of oil/dispersant was allowed to homogenize, with wave mixing, for 1 h prior to subsequent oil additions. Water samples were collected during the final 5 min of each step and sensors were cleaned in between steps using lens wipes and solvent. There was no indication of sensor fouling from oil as sensor response was checked pre- and postcleaning. Continuous optical data were collected during the 9 h experiment and manufacturer calibrations applied.

Dilution experiments (EXP_{DIL}) were conducted with 100 mL of fresh or weathered oil added, with or without dispersant (only chemically dispersed results reported here). Maximum concentration in the tank was less than 3 ppm, when fully dispersed. To simulate field conditions, ocean waves were generated with tank in flow-through mode (flow rate of 3.8 ± 0.2 L s^{-1}) allowing transport of dispersed oil away from the slick and dilution to extinction.[27,28] EXP_{DIL} were conducted for 90 min, where discrete oil concentration samples were collected at 15 time points via tubing through an inlet located next to the sensor deployment frame. Three-dimensional excitation emission matrix fluorescence spectroscopy (EEMS) analyses confirmed the position of fluorescence peaks and degree of chemical dispersion.

Submersible Sensor Data Processing. Sensor specific blanks (2 min average) prior to oil addition were subtracted. Manufacturer calibrations yielded data in recommended units (carbazole and perylene for AQUAtrackas, quinine sulfate dihydrate for ECO, uM nitrate for SUNA weighted index of UV absorption 210−370 nm, and none was provided for the Cyclops). Final 5-min signal averages for each concentration during the EXP_{ADD} was regressed (model 1, linear least-squares) to ppm oil, benzene-toluene-ethylbenzene-xylene (BTEX) or total petroleum hydrocarbons (TPH) values. Regressions were applied to EXP_{DIL} fluorescence and absorption data. Sensor performance and vicarious calibration were validated with laboratory chemistry results. LISST-11X dispersed oil droplet size distribution recorded 32 particle size intervals logarithmically spaced from 2.5−500 μm in diameter, with the upper size in each bin 1.18 times the lower. Distribution is expressed as the average volumetric concentration of droplets within each size range interval. Total particle concentration (TPC) represents the sum of all particle concentrations between 2.5 and 500 μm.[27]

Discrete Samples Analyses. Oil/water samples were collected at time points and analyzed for TPH, BTEX and PAH. TPH values were acquired using a GC-FID (gas chromatograph-flame ionization detector, Agilent 6890 and Supelco column). Extraction methods[29] were used and samples were concentrated under nitrogen to a final volume of 1.0 mL prior to analysis. Peak quantification, using the total area under the curve, yielded hydrocarbon concentrations in seawater. A spike and recovery study with blanks and duplicates verified extraction method efficiency. BTEX (volatile hydrocarbons) were measured via GC-MS (GC-mass spectrometry, Agilent 5973) using a modified version[29] of the standard EPA Method 8240 (purge and trap) for oil applications. A 5 mL sample was transferred into the purge chamber and purged with helium for 11 min. The volatiles were trapped and then desorbed at 225 °C for 2 min. The MS was used in selected ion monitoring mode (SIM) for six ions: 77, 78, 91, 92, 105, and 106 amu. BTEX calibration standards were prepared by diluting a certified standard mix (Supelco). Both standard and samples (blanks and duplicates) were purged, trapped and analyzed in the same manner.

EEM and absorbance spectra were collected with a Horiba Scientific AquaLog spectrofluorometer with a CCD detector. Oil/water samples were analyzed for fluorescence peaks within 10 min of collection. Samples within a 1 cm cuvette were scanned over Ex 220−550 nm and Em 213−610 nm (1 s integration), blank subtracted, inner-filter effect corrected, quinine sulfate dihydrate normalized, and Rayleigh scatter masked.[30,11]

RESULTS AND DISCUSSION

An EEM contour plot of chemically dispersed MC252 oil (4 ppm) collected during an EXP_{DIL} illustrates the UV fluorescent peak maxima centered on ExEm270/325 and ExEm260/450 nm

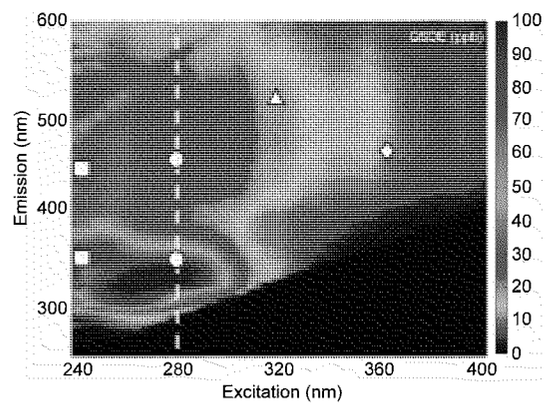

Figure 1. Fluorescence EEM of chemically dispersed fresh MC252 oil (4 ppm) concentration in a EXP_{DIL}. Center Wavelengths (CWL) of Chelsea Technologies Group AQUAtrackas $ExEm_{239/360}$ and $ExEm_{239/440}$ (□), Turner Designs Cyclops $ExEm_{320/510}$ (△), and WET Labs, Inc. ECO $ExEm_{370/460}$ (◊) along with the fluorescence intensity ratio (FIR = $ExEm_{280/340:280/445}$; ○) are overlaid for reference.

(Figure 1). Color map units are ppb QSDE (Quinine Sulfate Dihydrate Equivalents), scaled to peak maximum. CWL of the sensors tested are overlaid illustrating that all sensors were configured to detect some portion of the broad oil signal. Note that the symbols do not take into account wavelength bandwidths, which increases a sensor's ability to detect oil. For reference purposes, white circles on the dotted line represent the fluorescence intensity ratio (FIR) wavelengths used to indicate chemical dispersion of oil.[12]

Manufacturer calibrated sensor response at six cumulative oil concentrations during the EXP_{ADD} is shown in Figure 2 and SI Figure S2. The addition of oil and dispersant formed an oil plume with a sharp leading edge that passed in front of the sensors causing a rapid increase in signal followed by a decrease as the oil mixed/dispersed in the tank. Values at the end of each step (tank homogeneously mixed) are representative of sensor response for a specific oil concentration and established that all sensors detected chemically dispersed oil down to 300 ppb, a critical finding. This is below the laboratory detection limit for GC-FID TPH method, making sensor-estimated oil concentrations evermore valuable for tracking low concentration

dx.doi.org/10.1021/es404206y | Environ. Sci. Technol. 2014, 48, 1803−1810

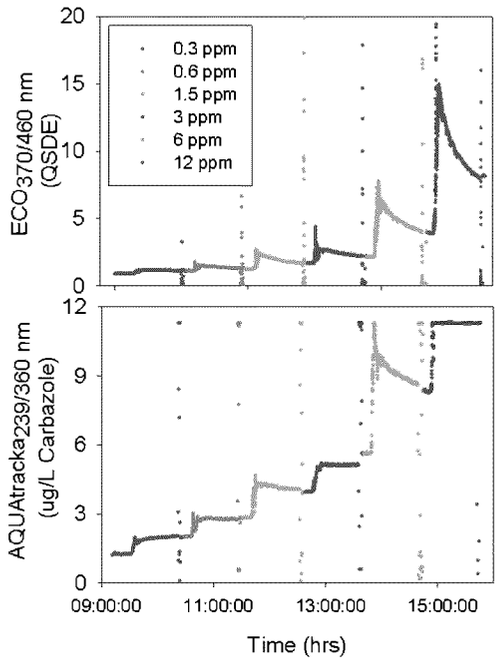

Figure 2. Fluorescence intensity of the ECO and $AQUA_{239/360\ nm}$ sensors exposed to chemically dispersed MC252 crude oil during EXP_{ADD} within the wave tank.

plumes. It also refutes previous notions during the DWH response that certain sensors may not detect oil <1 ppm. This was supported by earlier calibration tests using small flasks which may have been biased by underachieving proper mixing energies negatively impacting dispersant efficiency and solubility of fluorescence molecules into the water phase.[22] Strong linearity of sensor response at the lowest concentrations suggests possible lower detection limits less than 300 ppb (not tested with this experimental design). In any case, sensor response at 300 ppb improves confidence in the instruments deployed for DWH subsea plume monitoring, thereby demonstrating ability to detect low concentrations of oil.

Sensor dynamic range was established during the EXP_{ADD} by regressing fluorescence and absorption averages with oil concentration (Figure 3). Generally, submersible sensors were linearly correlated with TPH, BTEX and oil load, regardless of optical configuration. The ECO was operated in digital mode (no gain control) and the SUNA employed autoadjusting integration time, evidenced by lack of saturation over the entire concentration range. The Cyclops was operated with 100X gain for concentrations ≤6 ppm, but 10X for 12 ppm to avoid saturation. The AQUAtrackas employ BITE (Built in Test Circuitry) to extend calibration intervals. However saturation was exhibited by the $AQUAtracka_{239/360\ nm}$ sensor at 12 ppm oil. This is attributed to higher detector sensitivity, increased power of the light source (flash lamp opposed to LED) and/or wavelength filters closely aligned to the fluorescence maxima of crude oil. The longer wavelength emission $AQUA\ tracka_{239/440\ nm}$ sensor however did not saturate. Regression equations were employed to calibrate sensors during EXP_{DIL} (Figure 3). This aligns results with response effort measurements: sTPH (speciated TPH; water-insoluble heavy saturate fraction; aromatics > naphthalene; less laborious analytical screening) supplemented with BTEX (more laborious screening) values (Figure 3). All sensors exhibited squared correlation coefficients greater than 0.96. The 12 ppm value for the $AQUAtracka_{239/360\ nm}$ and SUNA (for BTEX) was excluded from the calculation due to saturation. The ECO and BTEX regression excluded values above 1.5 ppm, thereby increasing performance at low concentrations. TPH values for lowest concentration additions are absent because they were below the detection limit of the laboratory-based GC-FID TPH analysis. For all sensors, signal-to-noise ratios permitted detection at low concentrations. Findings demonstrate that all sensors would have been valuable tools during the DWH response given that sTPH and tVOA (total volatile organic analysis; water-soluble fraction; namely BTEX and naphthalene) in field samples were within the linear range of sensors tested in this study.[24] During the spill, sTPH from GC-MS ranged between <1 - 1000 ppb, with subsea plume (900−1300 m) maximum of 485 ppb, 1.2 km from the wellhead and detectable levels extending >10 km from source. In the plume, tVOA concentrations were higher than sTPH, with a maximum of 2112 ppb.

Sensor performance as a function of dispersant presence, oil state, and plume dilution was examined during EXP_{DIL}. TPH and BTEX-calibrated sensor responses for one-fresh and one-weathered, chemically dispersed oil EXP_{DIL} are shown in Figure 4 and SI Figure S3, respectively. Left panels show TPH-calibrated sensor and discrete TPH results (open circles), right panels show BTEX-calibrated sensor and discrete BTEX results (gray circles) over the course of the 90 min experiment. Due to a delayed shipping issue, the $AQUAtracka_{239/440\ nm}$ was operated only during one EXP_{DIL} and appears in the latter figure. EXP_{DIL} particle size distribution (PSD) and concentration of fresh oil droplets corresponding to Figure 4 are shown in Figure 5 (left). Histograms represent a composite of the entire duration of a flow-through experiment (90 min). Presence of particles observed in the <100 um size classes are indicative of chemical dispersion. All experiments using dispersant exhibited oil droplet size ranges consistent with adequate dispersant effectiveness (droplets <100 μm, Figure 5).[26]

For all experiments, MC252 oil state (fresh or weathered) did not appear to influence the sensor response. All sensors responded similarly to both (Figure 4 and SI Figure S3), verified with similar particle size distribution. Like sensor response as a function of oil state lends support for applying regression equations calculated with fresh oil to dilution experiments using weathered oil. Note that oil artificially weathered by 7% may represent oil exposed to physical processes (volatilization due to photo-oxidation, evaporation or dissolution) that occur during a spill of short duration, not necessarily of a prolonged spill with extensive weathering. However, the degradation of light crude oil and the addition of dispersant have been shown to increase the occurrence of longer wavelength fluorescence peaks.[11,15] Hence, sensors may be better capable of detecting extensively weathered oil where wavelength configuration better overlaps with longer fluorescence peaks (Figure 1). This is particularly true for lighter crudes such as MC252 oil that contain a higher proportion of simpler, lower molecular weight hydrocarbons that are more readily physically and biodegraded compared to heavy crudes.[31]

Tank hydrodynamics affected the movement and dispersion of oil within the tank, which varied during dilution experiments. Total particle concentration (TPC) as a function of time was influenced by tank mixing, where experiments exhibited either a gradual or rapid (Figure 5, left and right) decay of oil droplets. Three tests exhibited a gradual increase in signal as oil passed the sensors in the tank followed by gradual decay with dilution (Figure 4). For these cases, maximum values were 4−5 ppm

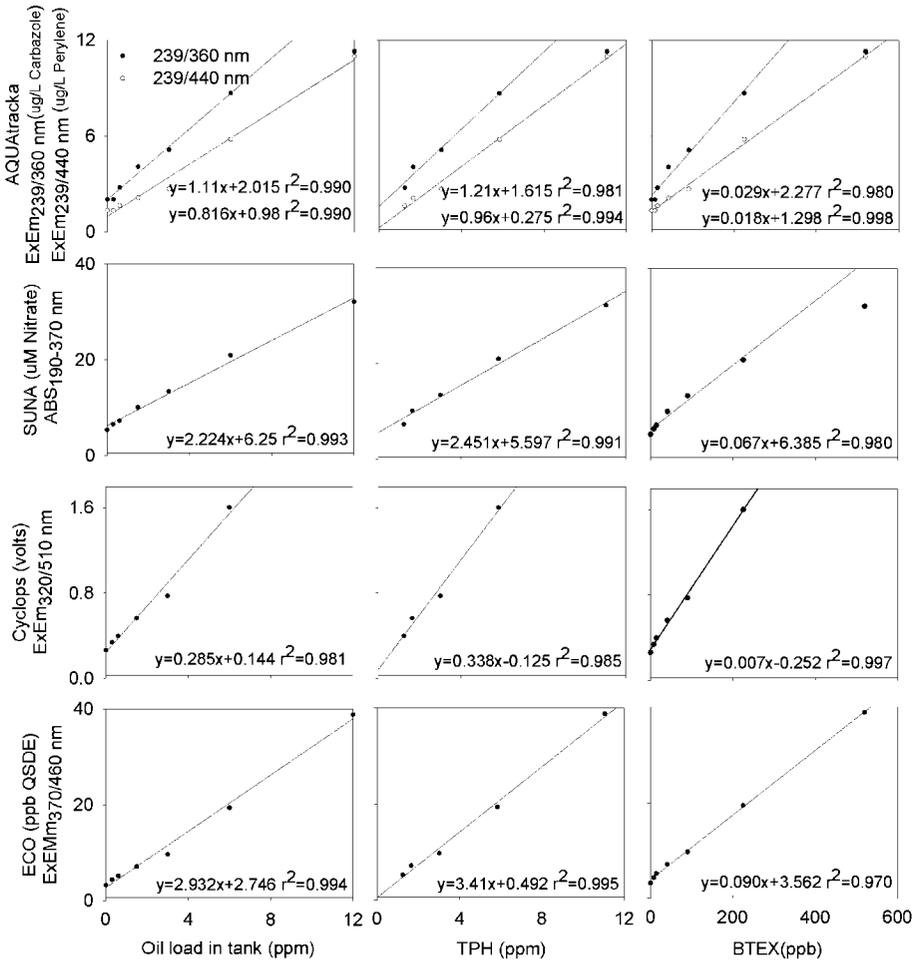

Figure 3. Fluorometric (submersible fluorometers) and spectrophotometric response (SUNA) as a function of oil concentration between 300 ppb and 12 ppm during EXP_{ADD}. Fewer TPH data points due to concentrations below the detection limit of TPH laboratory method.

TPH and 200−250 ppb BTEX, with subsequent plume dilution to 2−3 ppm TPH and 50 ppb BTEX. LISST-100X response (Figure 5, left) indicates like mixing and dispersing conditions in those experiments. Plume dynamics differed in two tests, where steep increases in oil concentration were followed by rapid decay (Figure 6), supported by TPC and droplet size distribution (Figure 5, right) and maximum TPH and BTEX values of 6 ppm and 250 ppb, followed by dilution to concentrations akin to all experiments. TPH and BTEX-calibrated sensor responses follow the chemistry and oil droplet results in all experiments. Agreement among these parameters is critical as they are used in concert during oil spills to track chemically dispersed oil plumes and confirm degree of dispersant effectiveness.

Sensor response during chemically dispersed EXP_{DIL} was validated with chemistry results to verify sensor performance. Percent differences ($\%_{dif}$) and mean absolute error (MAE) between estimated (from sensors) and actual (chemistry results) oil concentrations were calculated for each time point in experiments, providing performance metrics for estimates of TPH and BTEX for sensors exposed to oil. The MAE and mean, median and average $\%_{dif}$ for each sensor for all time points and for time points excluding 0−10 min are listed in Table 1. Time points <10 min were excluded from calculations due to heterogeneity and timing of the plume leading edge in the tank. The percentage of experiments where calibrated sensor responses were within ±25% and +30% of chemistry results are reported.

Based on $\%_{dif}$, the ECO and $AQUAtracka_{239/440\ nm}$ consistently better estimated BTEX, with 91% and 86% of time points within 30%$_{dif}$, respectively. The $AQUAtracka_{239/440\ nm}$ had the lowest median $\%_{dif}$ of <7.96. These values may be biased, however, as the $AQUAtracka_{239/440\ nm}$ was used in only one flow-through EXP_{DIL}. The ECO median $\%_{dif}$ was slightly higher (12%), but had the highest percentage of time points within ±30%$_{dif}$ (91%). Accuracy was also high with MAE of ±17.27 and 12.41 ppb for the ECO and $AQUAtracka_{239/440\ nm}$, respectively. The $AQUAtracka_{239/440\ nm}$, Cyclops and SUNA exhibited similar performance for BTEX where 71−79% values were within ±30%$_{dif}$. The $AQUAtracka_{239/360\ nm}$ also exhibited higher accuracy (MAE ± 12.43 ppb), but estimates were less consistent (71% of measurements within 30%$_{dif}$). BTEX consists of single ring aromatics, which are highly volatile and moderately soluble (relative to higher ring no. PAHs) in the shallow water of the wave tank, but any loss did not impact the $\%_{dif}$. Extrapolating this to real-world scenarios, surface spills typically have reduced BTEX or tVOA due to evaporation; however subsea oil plumes would likely retain higher dissolved concentrations.[6] Thus the ECO, $AQUAtracka_{239/360\ nm}$ and $AQUAtracka_{239/440\ nm}$ are each well suited for estimating BTEX in the deep sea, but they do vary with accuracy and precision. Results may differ for medium and

dx.doi.org/10.1021/es404206y | Environ. Sci. Technol. 2014, 48, 1803−1810

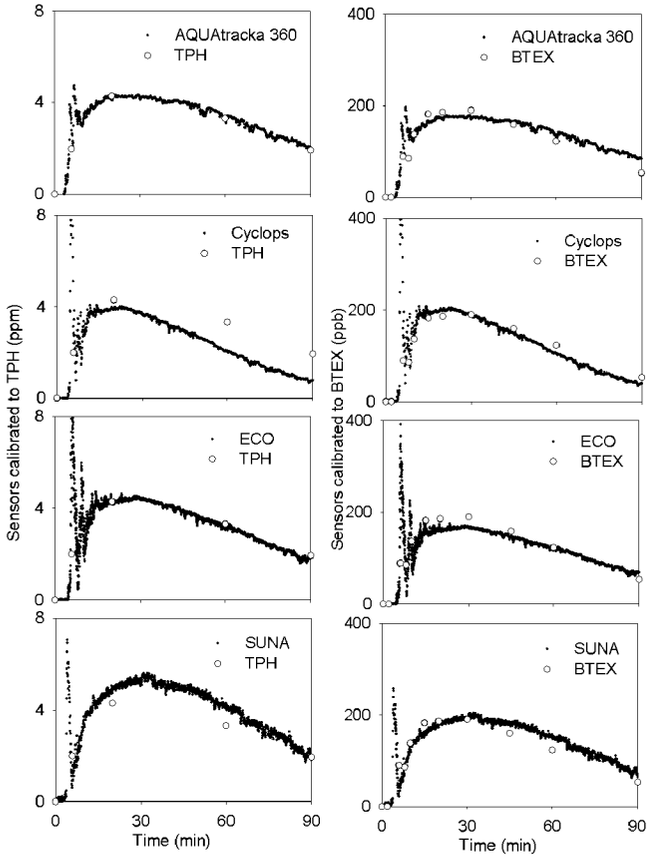

Figure 4. Response of TPH and BTEX-calibrated sensors exposed to chemically dispersed fresh crude oil. TPH and BTEX values from discrete samples are represented by open and gray circles, respectively. Wave tank was operated in flow-through mode (EXP_{DIL}) to observe fluorescence values during the dilution of an oil spill.

heavy oil, however, as BTEX concentrations would vary from the light crude oil tested here.

TPH was better estimated by the SUNA, with respect to both accuracy and precision, followed by the $AQUAtracka_{239/360\ nm}$, with 97% and 84% of time points within 30%$_{dif}$ of actual oil concentrations and MAE of +0.47 and 0.58 ppm, respectively.

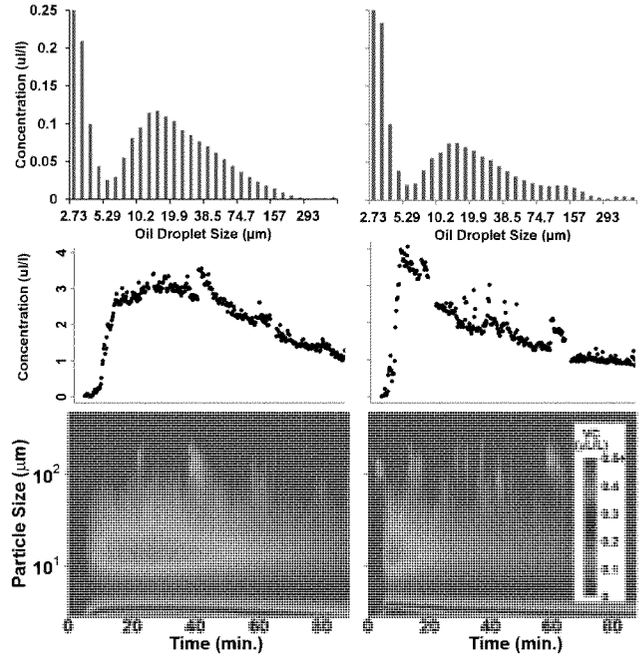

Figure 5. Particle size distribution and concentration within wave tank corresponding to experiments shown in Figures 4 and 6. Histogram plots are composites of entire flow-through experiment. Total particle concentration as a function of time (middle) is shown in scatter plot. Contour plots represent Particle size and volume concentration (VC) as a function of time for chemically dispersed fresh (left) and weathered (right) MC252 crude oil with gradual and rapid decay, respectively.

SUNA had the lowest median %$_{dif}$ of 11% for time points >10 min.

The remaining sensors exhibited median %$_{dif}$ of 18.72−23.87% with fewer values within 30%$_{dif}$ (60−71%) and higher MAE (0.77−0.81 ppm). Compared to BTEX, TPH laboratory analysis captures more compound types which are present at higher concentrations in oil. The SUNA's high performance in estimating TPH may result from absorption, not fluorescence, being measured over a wide wavelength range and oil being comprised of more chromophores than fluorophores. Tank

Table 1. Percent Differences (%$_{dif}$) between Sensors and Chemistry[s]

		TPH (ppm)					BTEX (ppb)				
		ECO	AQUA	AQUA	Cyclops	SUNA	ECO	AQUA	AQUA	Cyclops	SUNA
		370/460 nm	239/360 nm	239/440 nm*	320/510 nm	ABS	370/460 nm	239/360 nm	239/440 nm*	320/510 nm	ABS
all time points	mean %$_{dif}$	31.69	30.24	41.98	40.32	27.92	26.67	30.93	23.14	31.99	30.45
	median %$_{dif}$	23.54	21.15	26.21	25.54	15.68	13.66	20.95	12.34	24.41	23.74
	min %$_{dif}$	0.27	1.96	2.16	1.73	0.76	1.63	3.19	5.29	0.01	0.65
	max %$_{dif}$	183.78	186.85	194.19	199.92	214.04	122.22	128.82	85.95	114.40	140.97
	[MAE]	± 0.91	± 0.67	± 0.78	± 0.90	± 0.68	± 23.53	± 13.46	± 12.41	± 32.22	± 27.68
time points >10 min	mean %$_{dif}$	25.52	19.37	19.22	30.94	13.88	15.54	23.88	14.17	21.11	22.85
	median %$_{dif}$	23.85	18.72	23.87	21.29	11.20	12.00	15.14	7.96	16.67	19.95
	min %$_{dif}$	0.27	1.96	2.16	1.73	0.76	1.63	3.19	5.29	0.01	0.65
	max %$_{dif}$	74.55	53.83	35.22	127.31	46.00	85.57	83.18	31.26	87.71	81.00
	[MAE]	± 0.78	± 0.58	± 0.81	± 0.77	± 0.47	± 17.27	± 12.43	± 12.41	± 29.13	± 24.50
% of >10 min time points	<25%$_{dif}$	56%	72%	57%	56%	90%	86%	68%	86%	64%	63%
	<30%$_{dif}$	69%	84%	71%	60%	97%	91%	71%	86%	79%	74%

[s]Asterisk represents sensor with only one experiment. MAE is mean absolute error.

dx.doi.org/10.1021/es404206y | Environ. Sci. Technol. 2014, 48, 1803−1810

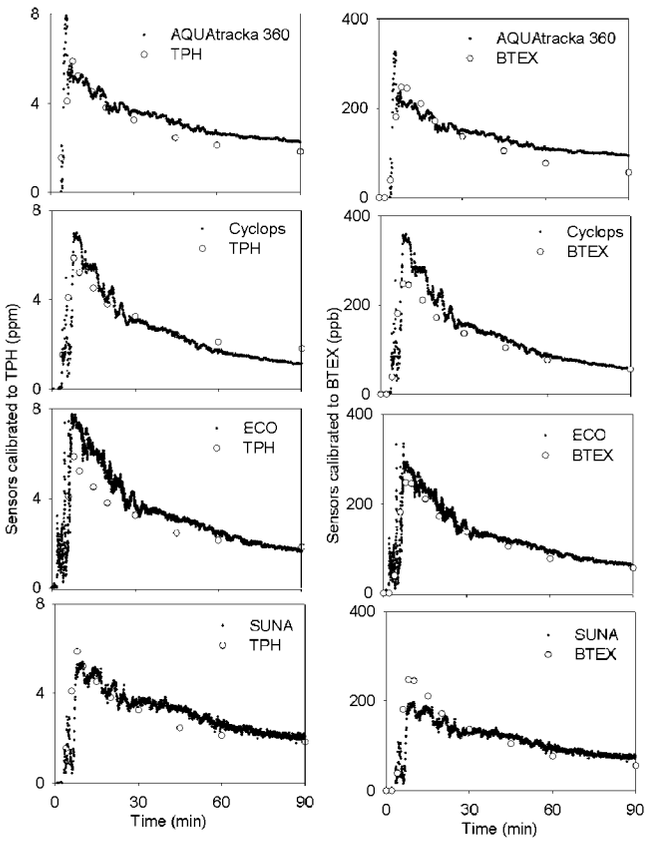

Figure 6. Response of TPH and BTEX-calibrated sensors exposed to chemically dispersed fresh crude oil for dilution experiment with steep increase in particles, followed by rapid decay. TPH and BTEX values from discrete samples are represented by open and gray circles, respectively. Wave tank was operated in flow-through mode (EXP_{DIL}) to observe fluorescence values during the dilution of an oil spill.

results indicate that of the sensors used in the DWH subsea plume, both the $AQUAtracka_{239/360\ nm}$ and ECO would have detected low TPH concentrations. The former may have exhibited better accuracy and precision. However, it could also be speculated that the $AQUAtracka_{239/360\ nm}$ with its narrower dynamic range would have saturated at high concentrations early in the spill and impeded plume tracking. Results are critical and provide evidence that ECO data from early in the spill (high concentrations) can be compared with AQUA data from later in the spill (low concentrations), and that sensors could provide oil concentrations with reasonable accuracy.

Wave tanks simulate natural variability observed in real spills. Thus, vicarious calibration is expected to be more accurate than a laboratory calibration, even though it may suffer from poorer precision. These findings demonstrate the sensitivity of COTS sensors exposed to chemically dispersed MC252 oil and increase confidence using in situ measurements during DWH to fill in the data gaps of coarse discrete samples. During an oil spill, sensor choice should be a function of oil concentration, calibration to TPH or BTEX and trade-offs between accuracy and precision. This work has large implications for plume tracking and understanding fate and transport of spilled oil in the environment.

ASSOCIATED CONTENT

* Supporting Information

Additional information as noted in the text. This material is available free of charge via the Internet at http://pubs.acs.org.

AUTHOR INFORMATION

Corresponding Author

*Phone: 513-569-7090; fax: 513-569-7620; e-mail: conmy.robyn@epa.gov.

Present Addresses

◆University of Oregon, Institute of Ecology and Evolution and Institute of Environmental Science, Oregon, USA.

¶Commonwealth Science and Industrial Research Organization, Wealth from Oceans Flagship, Perth, Australia.

Notes

The authors declare no competing financial interest.

ACKNOWLEDGMENTS

We thank all funding sources for the experiments at COOGER-BIO (Department of Fisheries and Oceans, Canada): IOOS support (Alliance for Coastal Technology), NOAA's supplemental DWH appropriation, salary support from home institutions, DFO Canada and internal travel support by Horiba JY, Oil Spill Recovery Institute, WET Labs, Inc. This document has been reviewed by the U.S. Environmental Protection Agency National Risk Management Research Laboratory and approved for publication. Approval does not signify that the contents reflect the views of the Agency, nor does mention of trade names or commercial products constitute endorsement or recommendation for use. This is a contribution from the Land Remediation and Pollution Control Division.

REFERENCES

(1) Report, S. P. Special Monitoring of Applied Response Technologies Protocol Report; National Oceanic and Atmospheric Administration, U.S. Coast Guard, U.S. Environmental Protection Agency, 2006; p 43.

(2) Henry, C. B., Roberts, P.O.; Overton, E.B. A primer on in situ fluorometry to monitor dispersed oil. In International Oil Spill Conference, 1999; pp 225-228.

(3) Li, M.; Garrett, C. The relationship between oil droplet size and upper ocean turbulence. Mar. Pollut. Bull. 1998, 36, 961−970.

(4) Lessard, R. R.; Demarco, G., The significance of oil spill dispersants. Spill Sci. Techno. Bull., 2000, 6, (59−68).

(5) Venosa, A. D.; Zhu, X. Biodegradation of crude oil contaminating marine shorelines and freshwater wetlands. Spill Sci. Technol. Bull. 2003, 8, 163−178.

(6) Camilli, R.; Reddy, C. M.; Yoerger, D. R.; Mooy, B. A. S. V.; Jakuba, M. V.; Kinsey, J. C.; McIntyre, C. P.; Sylva, S. P.; Maloney, J. V. Tracking hydrocarbon plume transport and biodegradation at deepwater horizon. Science 2010, 330 (6001), 201−204.

(7) Green, D.; Humphrey, B.; Fowler, B. The use of flow-through fluorometery for tracking dispersed oil. In Internationl Oil Spill Conference, 1983; pp 473−478.

(8) Page, D. S.; Foster, J. C.; Hotham, J. R.; Pendergasst, E.; Herbert, S.; Gonzalez, L.; Gilfillan, E. S.; Hanson, S. A.; Gerber, R. P.; Vallas, D. Long-term fate of dispersed and undispersed crude oil in two nearshore test spills. In International Oil Spill Conference, 1983; pp 479−482.

(9) Keizer, P. D.; D. C., G., Jr. Detection of trace amounts of oil in sea water by fluorescence spectroscopy. J. Fish. Res. Board Can. 1973, 30, 1039−1046.

(10) Østgaard, K.; Jensen, A. Evaluation of direct fluorescence spectroscopy for monitoring aqueous petroleum solutions. Int. J. Environ. Anal. Chem. 1983, 14, 55−72.

(11) Bugden, J. B. C.; Yeung, C. W.; Kepkay, P. E.; Lee, K. Application of ultraviolet fluorometry and excitation-emission matrix spectroscopy (EEMS) to fingerprint oil and chemically dispersed oil in seawater. Mar. Pollut. Bull. 2008, 56 (4), 677−685.
(12) Kepkay, P.; Young, W.; Bugden, J. B. C.; Li, Z.; Lee, K. Ultraviolet fluorescence spectroscopy (UVFS): A new means of determining the effectiveness of chemical dispersants on oil spills. In International Oil Spill Conference, Savannah, GA, 2008; pp 639−44.
(13) Li, J.; Fuller, S.; Cattle, J.; Way, C. P.; Hibbert, D. B. Matching fluorescence spectra of oil spills with spectra from suspect sources. Anal. Chim. Acta 2004, 514 (1), 51−56.
(14) Christensen, J. H.; Hansen, A. B.; Mortensen, J.; Andersen, O. Characterization and matching of oil samples using fluorescence spectroscopy and parallel factor analysis. Anal. Chem. 2005, 77, 2210−2217.
(15) Zhou, Z.; Liu, Z.; Guo, L. Chemical Evolution of Macondo crude oil during laboratory degradation as characterized by fluorescence EEMs and hydrocarbon composition. Mar. Pollut. Bull. 2012, 66, 164−175.
(16) Conmy, R. N.; Chen, R. F.; Castillo, C. E. D.; Downing, B. Calibrations and quality control of in situ sensors. In Fluorescence Applications in Aquatic Science; Cambridge University Press, 2013.
(17) Report, S. L. R. E. R. Updating the SMART dispersant monitoring protocol: Review of Commercial-Off-The-Shelf instruments; S.L. Ross Environmental Research, 2008; p 19.
(18) Lambert, P. A literature review of portable fluorescence-based oil-in-water monitors. J. Hazard. Mater. 2003, 102, 39−55.
(19) Fuller, C. B.; Bonner, J. S.; Page, C. A.; Arrambide, G.; M.C. Sterling, J.; Ojo, T. Field Instruments for Real Time In-Situ Crude Oil Concentration Measurements; Texas A&M University, 2003; p 10.
(20) Wilde, S. Procedures for monitoring dispersant operations. In 10th Environmental and Scientific Coordinators Workshop , Queenscliff, Australia, 2001, 2001; pp 163−177.
(21) Srinivasan, R.; Lu, Q.; Sorial, G. A.; Venosa, A. D.; Mullin, J. Dispersant effectiveness of heavy fuel oils using baffled flask test. Environ. Eng. Sci. 2007, 24 (9), 1307−1320.
(22) Report, N. R. C. Oil Spill Dispersants: Efficacy and Effects; Washington, DC, 2005; p 400.
(23) Report Oil Budget Calculator: Deepwater Horizon; Federal Interagency Solutions Group, 2010; p 217.
(24) Report, J. A. G. Deepwater Horizon Oil Spill: Review of Subsurface Dispersed Oil and Oxygen Levels Associated with the Deepwater Horizon MC252 Spill of National Significance; National Oceanic and Atmospheric Administration, 2012; p 93.
(25) Report, J. A. G. Review of Data to Examine Subsurface Oil in the Vicinity of DWH MC-252; National Oceanic and Atmospheric Administration, May 19−June 19, 2010; p f29.
(26) Lee, K.; Li, Z.; Boufadel, M. C.; Venosa, A. D.; Miles, M. S. Wave Tank Studies on Dispersant Effectiveness As a Function of Energy Dissipation Rate and Particle Size Distribution; Department of Fisheries and Oceans Canada, 2009; p 67.
(27) Li, Z.; Lee, K.; King, T.; Boufadel, M. C.; Vensosa, A. D. Evaluating crude oil chemical dispersion efficacy in a flow-through wave tank under regular non-breaking wave and breaking wave conditions. Mar. Pollut. Bull. 2009, 58, 735−744.
(28) Li, Z.; Lee, K.; King, T.; Boufadel, M. C.; Vensosa, A. D. Effects of temperature and wave conditions on chemical dispersion efficacy of heavy fuel oil in an experimental flow-through wave tank. Mar. Pollut. Bull. 2010, 60, 1550−59.
(29) Cole, M. G.; King, T. L.; Lee, K. Analytical technique for extracting hydrocarbons from water using sample container as extraction vessel in combination with a roller apparatus. Anal. Chem. 2007, 77, 2210−17.
(30) Coble, P. G. Characterization of marine and terrestrial DOM in seawater using excitation-emission matrix spectroscopy. Mar. Chem. 1996, 51, 325−346.
(31) Atlas, R. M.; Hazen, T. C. Oil biodegradation and bioremediation: A tale of the two worst spills in U.S. history. Environ. Sci. Technol. 2011, 45 (16), 67−09−15.

To: Craig Watts[craig@hydrosphere.net]; Holder, Edith[holder.edith@epa.gov]; Conmy, Robyn[Conmy.Robyn@epa.gov]
Cc: Peter Meyer[pmeyer@hydrosphere.net]; Cris Griffin[cgriffin@hydrosphere.net]
From: Barron, Mace
Sent: Wed 9/21/2016 3:21:07 PM
Subject: RE: Final report for recent round of toxicity tests

There should be 2 other dispersants coming, but we are having trouble procuring samples. Robyn may be able to provide an update.

Mace

From: Craig Watts [mailto:craig@hydrosphere.net]
Sent: Wednesday, September 21, 2016 10:08 AM
To: Barron, Mace <Barron.Mace@epa.gov>; Holder, Edith <holder.edith@epa.gov>; Conmy, Robyn <Conmy.Robyn@epa.gov>
Cc: Peter Meyer <pmeyer@hydrosphere.net>; Cris Griffin <cgriffin@hydrosphere.net>
Subject: RE: Final report for recent round of toxicity tests

To all:

Should we be expecting a third dispersant for toxicity testing?

Craig

From: Craig Watts
Sent: Wednesday, September 21, 2016 11:02 AM
To: 'Barron, Mace' <Barron.Mace@epa.gov>; 'Holder, Edith' <holder.edith@epa.gov>; 'Conmy, Robyn' <Conmy.Robyn@epa.gov>
Cc: Peter Meyer <pmeyer@hydrosphere.net>; Cris Griffin <cgriffin@hydrosphere.net>
Subject: RE: Final report for recent round of toxicity tests

Mace,

We are re-running one of the acute studies. The Finasol report will be delayed by a week.

Craig

From: Craig Watts
Sent: Friday, September 16, 2016 9:40 AM
To: 'Barron, Mace' <Barron.Mace@epa.gov>; Holder, Edith <holder.edith@epa.gov>; Conmy, Robyn <Conmy.Robyn@epa.gov>
Cc: Peter Meyer <pmeyer@hydrosphere.net>; Cris Griffin <cgriffin@hydrosphere.net>
Subject: RE: Final report for recent round of toxicity tests

Mace,

We have made the changes and corrections and renamed the report 16119 REV 091616. Here is the link to the revised report.

https://www.dropbox.com/s/conr0126ep4mepf/16119%20REV%20091616.pdf?dl=0

We have not received any Finquel. Finasol is the one we are wrapping up early next week.

Craig

From: Barron, Mace [mailto:Barron.Mace@epa.gov]
Sent: Thursday, September 15, 2016 4:20 PM
To: Craig Watts <craig@hydrosphere.net>; Holder, Edith <holder.edith@epa.gov>; Conmy, Robyn <Conmy.Robyn@epa.gov>
Cc: Peter Meyer <pmeyer@hydrosphere.net>; Cris Griffin <cgriffin@hydrosphere.net>
Subject: RE: Final report for recent round of toxicity tests

Hey guys:

Just very few minor revisions requested from my technical review:

Table 2: A. Punctulata

* Acute column: please either spell out not applicable in the cell or add a footnote defining "NA".

*chronic column: replace NA with a footnote or something specifying the organism age or life stage tested.

Table 12:

*report the NOEC and IC24 values in uL/L

Please do provide a revised copy, as well as a revised excel sheet with the toxicity summary tables.

Thanks again for your work with EPA and Pegasus.

PS: also, could you update us what is next on your schedule for this work (e.g., finquel? Anything else to be completed from testing samples we have provided?

From: Craig Watts [mailto:craig@hydrosphere.net]
Sent: Thursday, September 15, 2016 2:35 PM
To: Barron, Mace <Barron.Mace@epa.gov>; Holder, Edith <holder.edith@epa.gov>; Conmy, Robyn <Conmy.Robyn@epa.gov>
Cc: Peter Meyer <pmeyer@hydrosphere.net>; Cris Griffin <cgriffin@hydrosphere.net>

Subject: RE: Final report for recent round of toxicity tests

Mace,

Spreadsheets? You have a beautiful report in front of you!

Here is your spreadsheet.

Craig

From: Barron, Mace [mailto:Barron.Mace@epa.gov]
Sent: Thursday, September 15, 2016 2:56 PM
To: Craig Watts <craig@hydrosphere.net>; Holder, Edith <holder.edith@epa.gov>; Conmy, Robyn <Conmy.Robyn@epa.gov>
Cc: Peter Meyer <pmeyer@hydrosphere.net>; Cris Griffin <cgriffin@hydrosphere.net>
Subject: RE: Final report for recent round of toxicity tests

Thank you!

I was able to download a copy and will provide a technical review in next few days.

Could you also provide a copy of just the tox results in excel format similar to what you provided for the dilbits (attached).

Much appreciated,

Mace

From: Craig Watts [mailto:craig@hydrosphere.net]
Sent: Thursday, September 15, 2016 1:49 PM

To: Barron, Mace <Barron.Mace@epa.gov>; Holder, Edith <holder.edith@epa.gov>; Conmy, Robyn <Conmy.Robyn@epa.gov>
Cc: Peter Meyer <pmeyer@hydrosphere.net>; Cris Griffin <cgriffin@hydrosphere.net>
Subject: Final report for recent round of toxicity tests

To all,

So much for our effort to simply and streamline the reports. The Corexit report weighs in at over 15 MB and 111 pages. Instead of choking everyone's email server, I will share a link to the file on our DropBox account:

https://www.dropbox.com/s/aoi238renwts50v/16119.pdf?dl=0

Please look over the report and let us know if you have any questions or if you would like to see any changes.

We have all of the testing completed for the Finasol product with the exception of the two acute EC50 tests; they are going up today. The report for Finasol should go out this same time next week.

Regards,

Craig

Providing Environmental & Product Toxicity Testing since 1986

Craig Watts, Lab Director

Hydrosphere Research

11842 Research Circle

Alachua, FL 32615-6817

T (386) 462-7889

www.hydrosphere.net

To: Dapper, Marilyn[Dapper.Marilyn@epa.gov]
Cc: Conmy, Robyn[Conmy.Robyn@epa.gov]
From: Yeardley, Roger
Sent: Mon 1/9/2017 4:59:11 PM
Subject: Dispersants Rpt. compliance cont.
E12PG00037_Final Report_EPA_600_F_16_250.docx

Marilyn,

Attached is the updated Dispersants Effectiveness Report with the new cover graphic. It needs to have the EPA # or #s for the separate Appendices document entered on pages 9 and 157 however (and possibly other places if there are references to the Appendices in the report.. we might do a search for the words Appendix and Appendices within the report), before it can receive final certification of 508 compliance and be published on the web site. Given that, I don't know if you want to wait until the EPA #s issue gets sorted out or do some sort of check now, and then a final one when these additional edits are made. Your call. Thanks.

Roger

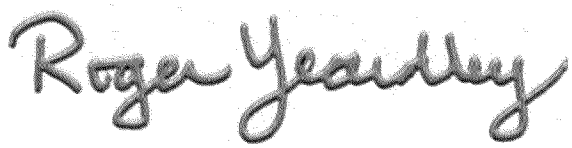

Roger Yeardley, Jr.

Physical Scientist

U.S. EPA/ ORD/ NRMRL/

Land Remediation and Pollution Control Division

26 West M.L. King Drive, MS 190

Cincinnati, OH 45268

Phone: 513-569-7548

FAX: 513-569-7620

United States
Environmental Protection
Agency

EPA/600/F-16/250 | September 2016 | www.epa.gov/research

Dispersant Effectiveness, In-Situ Droplet Size Distribution and Numerical Modeling to Assess Subsurface Dispersant Injection as a Deepwater Blowout Oil Spill Response Option

and

Evaluation of Oil Fluorescence Characteristics to Improve Forensic Response Tools

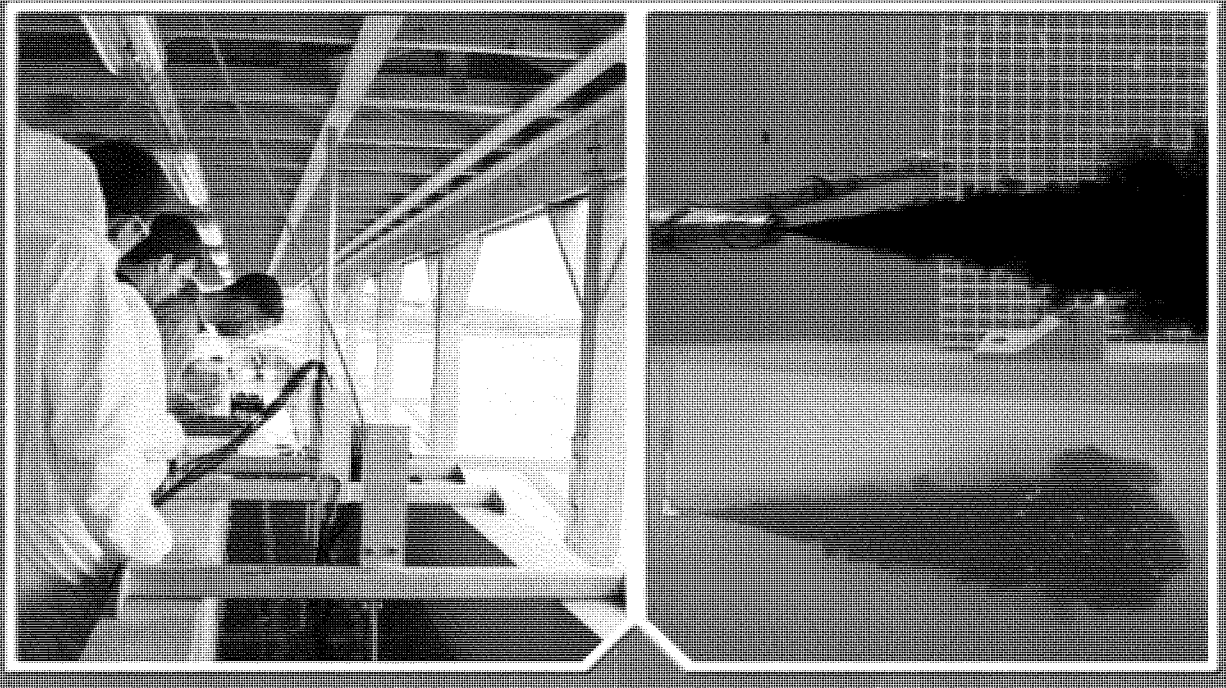

Office of Research and Development
National Risk Management Research Laboratory
Land Remediation and Pollution Control Division

EPA/600/F-16/250
September 2016

IAA No. E12PG00037

Final Report

Dispersant Effectiveness, In-Situ Droplet Size Distribution and Numerical Modeling to Assess Subsurface Dispersant Injection as a Deepwater Blowout Oil Spill Response Option

and

Evaluation of Oil Fluorescence Characteristics to Improve Forensic Response Tools

Submitted to:

Bureau of Safety and Environmental Enforcement

Submitted by:

Robyn N. Conmy, Ph.D.
U.S. Environmental Protection Agency, Office of Research and Development
26 W. Martin Luther King Drive, Cincinnati, OH 45268
*Tel: 513-569-7090, Fax: 513-569-7620, Email: conmy.robyn@epa.gov

Thomas King, M.Sc.; Brian Robinson, M.Sc; Scott Ryan, M.Sc; Youyu Lu, Ph.D.;
Department of Fisheries and Oceans Canada, Bedford Institute of Oceanography
1 Challenger Drive, Dartmouth, Nova Scotia, Canada B2Y 4A2
Tel: 902-426-4172, Tom.King@mar.dfo-mpo.gc.ca

Mary Abercrombie, M.Sc.
University of South Florida, College of Marine Science
140 7th Ave South, St. Petersburg, FL 33701
*Tel: 727-553-1140, Email: mabercrombie@marine.usf.edu

Michel Boufadel, Ph.D.
New Jersey Institute of Technology, Civil and Environmental Engineering
University Heights, Newark, NJ 07102
Tel: 973-596-5657, Email: michel.boufadel@njit.edu

Haibo Niu, Ph.D.
Dalhousie University, Department of Engineering
PO Box 550, Truro, N.S. Canada
Tel: 902-893-6714, Email: haibo.niu@dal.ca

September 30, 2016

Notice/Disclaimer

The U.S. Environmental Protection Agency, through its Office of Research and Development, funded and conducted the research described herein under an approved Quality Assurance Project Plan (Quality Assurance Identification Number XXXXXX-XX-X-X). It has been subjected to the Agency's peer and administrative review and has been approved for publication as an EPA document. Mention of trade names or commercial products does not constitute endorsement or recommendation for use.

This draft report contains scientific observations from a series of subsurface oil injection experiments and high resolution fluorescence analyses. Findings are subject to institutional review and are considered draft, thus the information provided here should not be parsed. Refrain from citing or posting until report is considered final. Upon review, approval does not signify that the contents reflect the views of the U.S. EPA, DFO Canada, or BSEE, nor does the mention of trade names or commercial products constitute endorsement or recommendation for use.

Forward

The U.S. Environmental Protection Agency (US EPA) is charged by Congress with protecting the Nation's land, air, and water resources. Under a mandate of national environmental laws, the Agency strives to formulate and implement actions leading to a compatible balance between human activities and the ability of natural systems to support and nurture life. To meet this mandate, US EPA's research program is providing data and technical support for solving environmental problems today and building a science knowledge base necessary to manage our ecological resources wisely, understand how pollutants affect our health, and prevent or reduce environmental risks in the future.

The National Risk Management Research Laboratory (NRMRL) within the Office of Research and Development (ORD) is the Agency's center for investigation of technological and management approaches for preventing and reducing risks from pollution that threaten human health and the environment. The focus of the Laboratory's research program is on methods and their cost-effectiveness for prevention and control of pollution to air, land, water, and subsurface resources; protection of water quality in public water systems; remediation of contaminated sites, sediments and ground water; prevention and control of indoor air pollution; and restoration of ecosystems. NRMRL collaborates with both public and private sector partners to foster technologies that reduce the cost of compliance and to anticipate emerging problems. NRMRL's research provides solutions to environmental problems by: developing and promoting technologies that protect and improve the environment; advancing scientific and engineering information to support regulatory and policy decisions; and providing the technical support and information transfer to ensure implementation of environmental regulations and strategies at the national, state, and community levels.

Cynthia Sonich-Mullin, Director
National Risk Management Research Laboratory

Abstract

The 2010 Deepwater Horizon oil spill highlighted the need for better understanding the interaction of dispersants and crude oil during high-pressure releases. This report summarizes a study to assess the operational performance of subsurface injection dispersant use on high-pressure releases within a flume tank. Dispersion experiments were conducted using South Louisiana Crude, Alaskan North Slope Crude and Intermediate Fuel Oil 120 oils, with Corexit 9500 and Finasol OSR 52 dispersants and four dispersant-to-oil ratios (DOR 0, 1:20, 1:100, 1:200) at warm and cold temperatures. *In situ* plume dispersion was monitored for particle concentration and Droplet Size Distribution (DSD; LISST-100X), and fluorescence intensity. Samples were collected for Total Petroleum Hydrocarbons and Benzene-Toluene-Ethylbenzene-Xylene concentrations. Empirical data was subsequently used as input variables to refine numerical models of droplet size formation (VDROP-J, JETLAG and Modified Weber Number). This project also generated a fluorescence library of 25 oil types to expand community knowledge base on optical signatures as a function of oil type. In general, the addition of dispersant decreased the oil Volume Mean Diameter (VMD), creating smaller droplets. Dispersions at DOR =1:20 yielded VMD <70 µm and exhibited bimodal DSD, suggesting that produced droplets would likely remain dispersed in the presence of mixing energy. Water temperature did not appear to influence the droplets for lighter crude oils. DSD results suggest a separation of particles within the plume. *In situ* fluorescence was found to be a reliable proxy for oil concentration. These findings have implications for the fate and transport of oil plumes-both for spill response monitoring and numerical modeling.

Acknowledgements

The research presented in this report was funded by the Bureau of Safety and Environmental Enforcement (BSEE) through Interagency Agreement E12PG00037. Efforts were partially supported by the U.S. Environmental Protection Agency - Office of Research and Development (EPA ORD) and the Department of Fisheries Oceans Canada – Bedford Institute of Oceanography (DFO-BIO). This work was a highly collaborative effort and the authors would like to thank all of the contributors. The numerical modeling components are contributions by collaborators Dr. Michel Boufadel and Feng Gao (New Jersey Institute of Technology) and Dr. Haibo Niu and Linlu Weng (Dalhousie University). The high-resolution fluorescence component is a contribution of Mary Abercrombie (University of South Florida). A special thanks to all of the DFO and BDR Contracting staff who made the tank experiments possible: Patrick Toole, Claire McIntyre, Cody Sherren, Jennifer Mason, Peter Thamer, Gary Wohlgeschaffen, Susan Cobanli, and Rod Doane.

Table of Contents

Notice/Disclaimer iii
Forward iv
Abstract v
Acknowledgements vi
List of Figures ix
List of Tables x
Acronyms and Abbreviations xi
Executive Summary xii
Task A.1 Introduction & Relevance 1
Task A.2 Experimental Methods 5
A.2.1 Flume Tank Description, Flow Calibration, and Operation 5
A.2.2 Waste Water Treatment 8
A.2.3 Subsurface Oil Injection System 8
A.2.4 Submersible Sensor Deployment 12
A.2.5 VOC Air Monitoring 14
A.2.6 Discrete Water Sample Collection 14
A.2.7 Oil and Dispersant Samples 14
A.2.8 Experimental Design – Core and Complimentary Experiments 16
A.2.9 Submersible Sensor Calibration Experiments 17
A.2.10 Submersible Fluorometer and LISST Data Processing 18
A.2.11 Analytical Chemistry Analysis 20
A.2.12 Numerical Modeling Methods 21
TASK A.3 RESULTS 22
A.3.1 ANS Dispersion Effectiveness 22
A.3.2 IFO 120 Dispersion Effectiveness 36
A.3.3 SLC Dispersion Effectiveness 46
A.3.4 Gas Condensate Dispersion Effectiveness 51
A.3.5 Tank Dilution Series Fluorescence Measurements 53
A.3.6 VOC Air Monitoring 58
A.3.7 VDROP-J and JETLAG Numerical Plume Modeling 68

A.3.8 Weber Number Scaling Numerical Plume Modeling..... 70
Task B.1 Introduction & Relevance..... 72
Task B.2 Experimental Methods..... 81
B.2.1 Sample Preparation..... 81
B.2.2 Artificial Seawater Protocol..... 81
B.2.3 Dispersed Oil in Seawater Protocol..... 81
B.2.4 Spectrophotometric Analysis..... 82
Task B.3 Results & Discussion..... 86
B.3.1 Oil Fluorescence Properties..... 86
B.3.2 Fluorescence as a Function of Chemistry..... 99
B.3.3 Flume Tank and Baffled Flask EEM Comparison..... 110
B.3.4 PARAFAC Modeling..... 112
DOR 0..... 114
DOR 1:100..... 119
DOR 1:20..... 123
PARAFAC Summary..... 126
References..... 128
Appendices (Separate Document)..... 132
APPENDIX A – Experiment Logs..... 132
APPENDIX B – Analytical Chemistry Results..... 132
APPENDIX C – Jet Release LISST Oil Droplet Size Distribution Histograms..... 132
APPENDIX D – Jet Release LISST Oil Droplet Size Distribution Time Series Contours..... 132
APPENDIX E – Submersible Fluorescence Time Series..... 132
APPENDIX F – Excitation Emission Matrix Contours..... 132
APPENDIX G – VDROP-J and JETLAG Numerical Plume Modeling Report..... 132
APPENDIX H – Weber Number Scaling Numerical Plume Modeling Report..... 132

List of Figures

Figure 1. Photos of subsurface oil injection at the BIO flume tank showing the formation of the subsurface oil plume. Note that the background grid size is 1.5 cm x 1.5 cm.

Figure 2. Photo of the DFO BIO flume tank (top) and cross-section of the tank showing the high-flow manifolds used to generate horizontal water currents (not to scale).

Figure 3. Schematic diagram showing the location of the subsurface injector and *in situ* instrumentation submerged within the tank.

Figure 4A. Photo of the pressurized oil vessel used to hold the oil for the subsurface release.

Figure 4B. Schematic diagram of the pressurized oil vessel for subsurface oil release system in the flume tank.

Figure 5. LISST DSD and VMD (left panels) and time series of concentration and particle size (right panels) for ANS and Corexit 9500 warm water treatments. From top to bottom, DOR = 0, 1:200, 1:100, 1:20.

Figure 6. LISST DSD and VMD (left panels) and time series of concentration and particle size (right panels) for ANS and Corexit 9500 cold water treatments. From top to bottom, DOR = 0, 1:200, 1:100, 1:20.

Figure 7. *In situ* submersible fluorescence time series of sub-injection plume of ANS and Corexit 9500 warm water (left panels) and cold water (right panels) treatments. From top to bottom, DOR = 0, 1:200, 1:100, 1:20.

Figure 8. Downstream LISST DSD and VMD (left panels) and time series of concentration and particle size (right panels) for ANS and Corexit 9500 warm water treatments. From top to bottom, DOR = 0, 1:200, 1:100, 1:20.

Figure 9. Downstream LISST DSD and VMD (left panels) and time series of concentration and particle size (right panels) for ANS and Corexit 9500 cold water treatments. From top to bottom, DOR = 0, 1:200, 1:100, 1:20.

Figure 10. LISST DSD and VMD (left panels) and time series of concentration and particle size (right panels) for ANS and Finasol OSR 52 warm water treatments. From top to bottom, DOR = 1:200, 1:100, 1:20. Refer back to Figure 5 for ANS DOR = 0.

Figure 11. *In situ* submersible fluorescence time series of sub-injection plume of ANS and Finasol OSR 52 warm water treatments. From top to bottom, DOR = 1:200, 1:100, 1:20.

Figure 12. Downstream LISST DSD and VMD (left panels) and time series of concentration and particle size (right panels) for ANS and Finasol OSR 52 warm water treatments. From top to bottom, DOR = 1:200, 1:100, 1:20. Refer back to Figure 6 for ANS DOR = 0.

Figure 13. LISST DSD with TPC for ANS with Corexit 9500 and Finasol OSR 52 warm water treatments. DOR = 0 (top panel); DOR = 1:20 experiments are middle and bottom panels.

Figure 14. LISST DSD with TPC (Total Particle Concentration) for DOR = 1:20 experiments of ANS and Corexit 9500 treatments. Water temperatures increase from top to bottom panels.

Figure 15. LISST TPC (Total Particle Concentration) for DOR = 1:20 experiments of ANS and Corexit 9500 treatments as a function of water temperature.

Figure 16. LISST DSD and VMD (left panels) and time series of concentration and particle size (right panels) for IFO 120 and Corexit 9500 warm water treatments. From top to bottom, DOR = 0, 1:200, 1:100, 1:20.

Figure 17. LISST DSD and VMD (left panels) and time series of concentration and particle size (right panels) for IFO 120 and Finasol OSR 52 warm water treatments. From top to bottom, DOR = 1:200, 1:100, 1:20. Refer to Figure 16 for IFO 120 DOR = 0.

Figure 18. Downstream LISST DSD and VMD (left panels) and time series of concentration and particle size (right panels) for IFO 120 and Corexit 9500 warm water treatments. From top to bottom, DOR = 0, 1:200, 1:100, 1:20.

Figure 19. Downstream LISST DSD and VMD (left panels) and time series of concentration and particle size (right panels) for IFO 120 and Finasol OSR 52 warm water treatments. From top to bottom, DOR = 0, 1:200, 1:100, 1:20. Refer to Figure 18 for ANS DOR = 0.

Figure 20. LISST DSD with TPC for IFO 120 with Corexit 9500 and Finasol OSR 52 treatments at warm temperatures. DOR = 0 (top panel); DOR = 1:20 experiments are middle and bottom panels.

Figure 21. LISST DSD and VMD (left panels) and time series of concentration and particle size (right panels) for IFO 120 and Corexit 9500 cold water treatments. From top to bottom, DOR = 0, 1:200, 1:100, 1:20.

Figure 22. Downstream LISST DSD and VMD (left panels) and time series of concentration and particle size (right panels) for IFO 120 and Corexit 9500 cold water treatments. From top to bottom, DOR = 0, 1:200, 1:100, 1:20.

Figure 23. LISST DSD and VMD for IFO 120 (top; DOR = 1:100) and ANS (bottom; DOR = 1:200) with Corexit 9500 during cold water treatments.

Figure 24. LISST DSD and VMD (left panels) and time series of concentration and particle size (right panels) for SLC and Corexit 9500 warm water treatments. From top to bottom, DOR = 0, 1:200, 1:100, 1:20.

Figure 25. Downstream LISST DSD and VMD (left panels) and time series of concentration and particle size (right panels) for SLC and Corexit 9500 warm water treatments. From top to bottom, DOR = 0, 1:200, 1:100, 1:20.

Figure 26. LISST DSD with TPC for SLC with Corexit 9500 treatments at warm temperatures. DOR = 0 (top panel); DOR = 1:20 experiments are bottom panels.

Figure 27. *In situ* submersible fluorescence time series of sub-injection plume of SLC and Corexit 9500 warm water treatments. From top to bottom, DOR = 0, 1:200, 1:100, 1:20.

Figure 28. LISST DSD and VMD (top panels),time series of concentration and particle size (middle panels), and fluorescence time series (bottom panels) for Gas Condensate and Corexit 9500 warm water treatments. Left panels are DOR = 0 and right panels are DOR = 1:20.

Figure 29. Calibration lines for fluorometer response vs TPH concentrations.

Figure 30. Calibration lines for fluorometer response vs BTEX concentrations.

Figure 31. Total Particle Concentration and fluorescence time series for ANS crude oil with Corexit 9500 dispersant.

Figure 32. VOC results for subsurface injection experiments (cold water season) using Alaska North Slope crude oil and four treatment conditions (no dispersant, DOR 1:200, DOR 1:100, DOR 1:20). Replicate treatments represented by light blue, dark blue and green colored lines.

Figure 33. VOC results for subsurface injection experiments (warm water season) using Alaska North Slope crude oil and four treatment conditions (no dispersant, DOR 1:200, DOR 1:100, DOR 1:20). Corexit 9500 was used as the treating agent. Replicate treatments represented by light blue, dark blue and green colored lines.

Figure 34. VOC results for subsurface injection experiments (warm water season) using Alaska North Slope crude oil and four treatment conditions (no dispersant, DOR 1:200, DOR 1:100, DOR 1:20). Finasol OSR 52 was used as the treating agent. Replicate treatments represented by light blue, dark blue and green colored lines.

Figure 35. VOC results for subsurface injection experiments (cold water season) using IFO 120 and four treatment conditions (no dispersant, DOR 1:200, DOR 1:100, DOR 1:20). Corexit 9500 was used as the treating agent. Replicate treatments represented by light blue, dark blue and green colored lines.

Figure 36. VOC results for subsurface injection experiments (warm water season) using IFO 120 and four treatment conditions (no dispersant, DOR 1:200, DOR 1:100, DOR 1:20). Corexit 9500 was used as the treating agent. Replicate treatments represented by light blue, dark blue and green colored lines.

Figure 37. VOC results for subsurface injection experiments (warm water season) using IFO 120 and three treatment conditions (DOR 1:200, DOR 1:100, DOR 1:20). Finasol OSR 52 was used as the treating agent (note – these treatments were not tested in triplicate).

Figure 38. VOC results for subsurface injection experiments using gas condensate and two treatment conditions (no dispersant, DOR 1:20). Corexit 9500 was used as the treating agent.

Figure 39. VOC results for subsurface injection experiments using Sweet Louisiana Crude oil and four

treatment conditions (no dispersant, DOR 1:200, DOR 1:100, DOR 1:20). Corexit 9500 was used as the treating agent.

Figure 40. Fluorescence peaks of S. Louisiana sweet crude dispersed in ppb QSE (Quinine Sulfate Equivalents). Symbols represent Fluorescence Intensity Ratio (FIR) locations and the Center Wavelength (CWL) reported by sensor manufacturers. Bandwidths (BW) are not shown.

Figure 41. Twenty-five oil samples stored in glass bottles.

Figure 42. Trypsinizing baffled flasks containing dispersed oil in artificial seawater (top) and corresponding samples removed from each flask, ready for spectrofluorometric analysis.

Figure 43. Alaska North Slope dispersed oil in artificial seawater at DOR 1:20 with locations of F_{max1}, F_{max2}, F_{max3} and F_{max4} indicated. Note that maximum fluorescence intensity at F_{max3} is mostly obscured by masking of second order Rayleigh scattering.

Figure 44. Photographs of pre-analysis samples and corresponding example EEMs of Type I (left) and II (right) oils; DOR = 1:20 for Arabian Light (light oil, API gravity > 31.1°), Mesa (medium oil, API gravity 22.3 – 31.1°) and heavy oils (IFO 40 and Santa Clara, API gravity < 22.3°).

Figure 45. F_{max1} fluorescence for Light Oils (API gravity > 31°), in order of increasing density: 1. Scotian Shelf Condensate, 2. Federated, 3. Brent, 4. MC252—Discoverer Enterprise, 5. Hibernia, 6. MC252—generic, 7. Terra Nova, 8. Gullfaks, 9. Arabian Light. Note discrepancy in Scotian Shelf Condensate fluorescence pattern (circled) from that of all other Light Oils. It's particularly unusual that fluorescence intensity at highest DOR is lower than that at DORs 1:200 and 1:100.

Figure 46. F_{max1} fluorescence for Heavy Oils (API gravity < 22.3°), in order of increasing density: 1. Santa Clara, 2. IFO 40, 3. Cold Lake Dilbit, 4. Access Western Blend Dilbit, 5. Hondo, 6. IFO 120, 7. IFO 180, 8. Belridge Heavy, 9. IFO 300. Note discrepancy in Intermediate Fuel Oils (circled) from that of all other Heavy Oils.

Figure 47. For all oil types at DOR 0, total concentration of 2-ring, 3-ring, and 4-ring PAHs (µg/L) against fluorescence intensity (RU) at F_{max1} (top), and against F_{max2} (bottom). Strong linear correlation exists between 2-ring PAHs and F_{max1} fluorescence, but little to no correlation between 3-ring or 4-ring PAHs and F_{max1} fluorescence intensity (top). Strong linear correlation also exists between 2-ring PAHs and F_{max2}, but no correlation between 3-ring PAHs or 4-ring PAHs and F_{max2} (bottom).

Figure 48. For all oil types at DOR 0, total concentration of 2-ring, 3-ring, and 4-ring PAHs (µg/L) against fluorescence intensity (RU) at F_{max3} (top), and against F_{max4} (bottom). Strong linear correlation exists between 3-ring and 4-ring PAHs and both F_{max3} and F_{max4} fluorescence; however, only moderate correlation exists between 2-ring PAHs and F_{max3} and F_{max4} fluorescence intensity.

Figure 49. For all oil types at DOR 1:20, total concentration of 2-ring, 3-ring, and 4-ring PAHs (µg/L) against fluorescence intensity (RU) at F_{max1} (top), and against F_{max2} (bottom). A moderate logarithmic correlation is exhibited between 2-ring PAHs and fluorescence intensity (RU) at F_{max1} and a weaker correlation between 2-ring PAHs and F_{max2}, but no correlation exists between 3-ring or 4-ring PAHs

and fluorescence intensity at either F_{max1} or F_{max2}.

Figure 50. For all oil types at DOR 1:20, total concentration of 2-ring, 3-ring, and 4-ring PAHs (µg/L) against fluorescence intensity (RU) at F_{max3} (top), and against F_{max4} (bottom). A strong logarithmic correlation is exhibited between 2-ring PAHs and fluorescence intensity at F_{max3}. Moderate correlations exist between 3-ring PAHs and F_{max3} as well as between 2-ring PAHs and F_{max4}. However, only a weak logarithmic correlation exists between 4-ring PAHs and fluorescence intensity at F_{max3}, and there is no correlation between 3-ring or 4-ring PAHs and F_{max4}.

Figure 51. Chemical Dispersibility Ratio (CDR) vs. decreasing oil density (top) and Fluorescence Dispersibility Ratio (FDR) vs. decreasing oil density (bottom) show only a weak correlation between chemistry and oil density, and a moderate correlation between fluorescence and oil density. With the removal of the data point for Scotian Shelf Condensation, correlation between fluorescence and oil density improves to $R^2 = 0.71$.

Figure 52. Fluorescence Dispersibility Ratio (FDR) vs. Chemical Dispersibility Ratio (CDR) shows weak correlation between these two ratios.

Figure 53. South Louisiana Crude MC252 EEMS from BFT (left panels) and tank experiments (right Panels) for DOR = 0, 1:100 and 1:20.

Figure 54. Example of split half validation for the 6-component model of 25 oil types at DOR 0 showing individual fit of data splits (Set 1, left; and Set 2, right) compared to overall model for Mode 2 (top) and Mode 3 (bottom) loadings.

Figure 55. Mode 3 Loadings (Excitation) and Mode 2 Loadings (Emission) for all 25 oil types—DOR0 using 6-component model. Note difference in x-axis scales. Although components are tightly spaced, all appear as separate and distinct peaks.

Figure 56. Variation per Component shows Component 1 accounted for >20% to 40% (unique fit and fit) of the data, while Component 2-contributed 5-10% (unique fit and fit) and Components 3-6 accounted for 5% or less of the data, respectively. While Component 6 accounted for a very low percentage of the data, the 6-component model was still a better fit to the data than the 5-component model.

Figure 57. EEM views of the six components of PARAFAC model for 25 oil types at DOR 0. Component #1: F_{max} = Ex 224nm/Em 335nm; Component #2: F_{max} = Ex 230nm/Em 340nm; Component #3: Fmax = Ex 239nm/Em 363nm; Component #4: Fmax = Ex 218nm/Em 290 nm; Component #5: Fmax = Ex 221nm/Em 322nm; Component #6: Fmax = Ex 260nm/Em 474-511nm.

Figure 58. Mode 3 Loadings (Excitation) and Mode 2 Loadings (Emission) for all 25 oil types—DOR 1:100 using 5-component model. Note difference in x-axis scales. Although components are tightly spaced, all appear as separate and distinct peaks.

Figure 59. Variation per Component shows Component 1 accounted for >35% to almost 50% (unique fit and fit) of the data, while Components 2-5 accounted for 5% or less of the data, respectively.

Figure 60. EEM views of the five components of PARAFAC model for 25 oil types at DOR 1:100. Component #1: F_{max} = Ex 224nm/Em 335nm; Component #2: F_{max} = Ex 254-266nm/Em 455-501nm; Component #3: F_{max} = Ex 230nm/Em 344nm; Component #4: F_{max} = Ex 242nm/Em 363 nm; Component #5: F_{max} = Ex 218nm/Em 290nm.

Figure 61. Mode 3 Loadings (Excitation) and Mode 2 Loadings (Emission) for all 25 oil types—DOR 1:20 using 5-component model. Note difference in x-axis scales. Effect of full dispersion appears to broaden and shift emission peaks to longer wavelengths.

Figure 62. Variation per Component shows Component 1 accounted for 25 to 30% of the data (unique fit and fit) while Component 2 has increased to >10% to 25% (unique fit and fit) of the data. Contribution from Component 3 and 4 have increased, as well.

Figure 63. EEM views of the five components of PARAFAC model for 25 oil types at DOR 1:20. Component #1: F_{max} = Ex 224nm/Em 335nm; Component #2: F_{max} = Ex 233-266nm/Em 432-450nm; Component #3: F_{max} = Ex 230-242nm/Em 501-520nm; Component #4: F_{max} = Ex 233nm/Em 349nm; Component #5: F_{max} = Ex 218nm/Em 290nm.

List of Tables

Table 1. List of hydrocarbon fluorometers used in this study. QSDE and PAH represent quinine sulfate dihydrate and petroleum aromatic hydrocarbons, respectively.

Table 2. Water sample collection strategy for the core and complimentary experiments. TPH and BTEX represent Total Petroleum Hydrocarbons and Benzene-Toluene-Ethylbenzene-Xylene, respectively.

Table 3. Physical and chemical property measurements of the oils used in this study.

Table 4. Step-wise sensor calibration experiment parameters.

Table 5. Calibration equations for the submersible fluorometers. Data in this report have fluorescence signal in the manufacturer recommended units.

Table 6. Summary of maximum VOC concentrations at the various treatment conditions tested in this study. Results are for only for warm water experiments.

Table 7. Sensor specifications as listed from manufacturers. Wavelengths listed as Center Wavelengths (CWL) with Full Width at Half Max (FWHM) and Bandpass (BP). Standards used are QS (Quinine Sulfate Dihydrate), NDD Salt (Napthalene Disulfonic Disodium) and PTSA Salt (Pyrenetetrasulfonic Acid Tetrasodium) (From Conmy et al., 2014b).

Table 8. List of oil samples used for EEM analyses. Oils separated by API (American Petroleum Institute) gravity.

Table 9. EEM fluorescence and chemical characteristics. Refer to Supplemental Table A for full table.

Table 10. Individual hydrocarbon compounds reported as Total Alkanes, Total 2-ring, 3-ring and 4-ring PAHs.

Acronyms and Abbreviations

ADV	Acoustic Doppler Velocimetry
ANS	Alaskan North Slope
BIO DFO	Bedford Institute of Oceanography Dept. of Fisheries and Oceans Canada
BSEE	Bureau of Safety and Environmental Enforcement
BTEX	Benzene-Toluene-Ethylbenzene-Xylene
CRRC	Coastal Response Research Center
DCM	Dichloromethane
DE	Dispersion Effectiveness
DOR	Dispersant to Oil Ratio
DSD	Droplet Size Distribution
DWH	Deepwater Horizon Horizon
EEMS	Excitation Emission Matrix Spectroscopy
EPA	U.S. Environmental Protection Agency
GC-FID	Gas Chromatography-Flame Ionization Detector
GC-MS	Gas Chromatography Mass Spectrometry
GoM	Gulf of Mexico
IFO 120	Intermediate Fuel Oil 120
LISST	Laser In Situ Scattering Transmissometry
NEBA	Net Environmental Benefit Analyses
NJIT	New Jersey Institute of Technology
NRDA	Natural Resource Damage Assessments
NRT	National Response Team
OMA	Oil-Mineral Aggregate
PARAFAC	Parallel Factor Analysis
PSC	Particle Size Concentration
SLC	South Louisiana Crude
STP	Standard Temperatures and Pressures
TPC	Total Particle Concentration
TPH	Total Petroleum Hydrocarbons
UAC	Unified Area Command
VMD	Volume Mean Diameter
VOC	Volatile Organic Compounds
WG-50	Wave Gauges

Executive Summary

This report summarizes two projects covered under an Interagency Agreement between the Bureau of Safety and Environmental Enforcement (BSEE) and the U.S. Environmental Protection Agency (EPA) in collaboration with the Bedford Institute of Oceanography, Department of Fisheries and Oceans Canada (BIO DFO), New Jersey Institute of Technology (NJIT) and Dalhousie University. Both projects dovetail together in addressing the ability to differentiate physical from chemical dispersion effectiveness using dispersed oil simulations within a flume tank for improving forensic response monitoring tools. This report is split into separate Tasks based upon the two projects funded by BSEE:

1) Dispersant Effectiveness, In-Situ Droplet Size Distribution and Numerical Modeling to Assess Subsurface Dispersant Injection as a Deepwater Blowout Oil Spill Response Option.
2) Evaluation of Oil Fluorescence Characteristics to Improve Forensic Response Tools.

TASK A: Dispersant Effectiveness, In-Situ Droplet Size Distribution and Numerical Modeling to Assess Subsurface Dispersant Injection as a Deepwater Blowout Oil Spill Response Option.

The main objectives of work under Task A were to evaluate high velocity subsurface releases of physically and chemically dispersed oil using a flow-through wave (flume) tank. This project addressed three issues: (1) performance evaluation of dispersants for subsurface injection into sub-sea blowouts, (2) tracking, modeling, and predicting the movement and spread of the deepwater plume and oil surfacing from deepwater blowouts, and (3) evaluating the influence of dispersant applications in reducing the concentration of volatile organic compounds emanating from the water surface. Oil dispersion experiments were conducted in the flume tank at the Department of Fisheries and Oceans Canada, Bedford Institute of Oceanography (DFO BIO), which is equipped with an underwater oil release system to simulate a high-pressure release of oil (akin to a deepwater blowout). Subsea

plume simulations were generated with a pressurized underwater oil release system adapted from existing technology developed by Masutani and Adams (2000). To mitigate wall effects and to generate oil droplets in the size range observed at depth during the Gulf of Mexico Deepwater Horizon (GoM DWH) oil spill, a high flow-rate of oil (3.8 L/min) was released through a small diameter nozzle (2.4 mm). Although it is impossible to simulate in the tank the extreme hydrostatic pressures that exist at 1500 m water depth, underwater high-pressure release of crude oil can be simulated with and without dispersant addition. The researchers also recognize that the shallow nature of the tank does not allow for investigating the rise velocity of the droplets that would be observed in a long (`1500m) water column. Rather, the tank allows for gathering data on the differences in droplet size and distribution during physical and chemical dispersion (akin to that observed during DWH) and for observing the vertical and horizontal movement of the droplets. Although results cannot be directly scaled or translated to a deepwater spill in the ocean, results are still useful for understanding the formation and movement of oil droplets under varying oil and dispersant type, dispersant amount and water temperature.

A total of 48 core and 24 complimentary flume tank experiments were conducted to evaluate the effectiveness of dispersant injection and attenuation of the plume as a function of oil type (US EPA reference oils: Alaskan North Slope (ANS) pipeline blend for a light-medium crude, IFO 120 for a heavy refined product and South Louisiana Crude (SLC) for a light crude, and also a gas condensate), chemical dispersant type (Corexit 9500 and Finasol OSR 52), dispersant-to-oil ratio (DOR of 0, 1:20, 1:100, and 1:200; corresponding to DOR concentrations of 0, 5, 1, and 0.5%) and water temperature (< 10 °C for low temperature and > 10 °C for higher temperature). Experiments were conducted at a fixed horizontal current flow rate of 1 cm/s (~ $1/8^{th}$ of deep water flow rates in the GoM). Faster current was not permissible as it would have resulted insufficient time for collection of *in situ* measurements and discrete samples. Experiments were conducted using oil at 80 °C, although this is lower than the reservoir temperatures for the DWH Macondo wellhead (estimated at 130°C), this is as high as the experimental design would allow for safety reasons given the limits of the pressurized canister.

Time series dispersion effectiveness was evaluated by measuring dispersed oil concentrations from samples collected in the flume tank, and via *in situ* droplet size distribution analysis and fluorescence measurements. Discrete samples were collected for oil chemical analysis of Total Petroleum Hydrocarbons (TPH) using gas chromatography coupled to a flame ionization detector (GC-FID) and the analysis of Benzene-Toluene-Ethylbenzene-Xylene (BTEX) via gas chromatography mass spectrometry (GC-MS), employed to quantify oil concentration and partitioning of hydrocarbon compounds in seawater.

The produced Droplet Size Distribution (DSD) was determined by using Laser *In-Situ* Scattering and Transmissometry instruments (LISST-100X, type C; Sequoia Scientific Inc. Seattle, WA) to track the full range diameters of chemically and physically dispersed oil droplets. Larger oil droplets, whether physically or chemically dispersed, may be capable of coalescing and rising to the surface under less energetic mixing conditions. The LISST measures particle size and outputs the concentration of particles in 32 logarithmically spaced size bins between 2.5 to 500 µm, thus facilitating a comparison between natural (physical) and chemical dispersion efficiency of crude oil. All submersible sensors were operated with real-time data acquisition throughout each experiment. *In situ* fluorescence was monitored real-time using two Chelsea Technologies Group AquaTrackas (crude and refined oil types), one Sea Bird – Wet Labs Inc. ECO (gelbstoff type), two Turner Designs Inc. Cyclops (crude and refined oil types) and one GmBH Trios (hydrocarbon type) fluorometers. Many of the fluorescence sensors used in this study are the same models employed to track the subsea plume during the DWH oil spill and confirm dispersion effectiveness. Sensors used in this work are also ones provided as examples in the National Response Team (NRT) *Subsea Dispersant Monitoring and Assessment Interim Guidance* Document, that states "the Risk Plan should use a properly calibrated oil-specific fluorometer (e.g., Chelsea UV AQUAtracka, Turner Designs Cyclops, Wet Labs ECO, or equivalent oil-specific instrument) to enable ongoing improvements in sampling".

Also monitored during experiments was the level of Volatile Organic Compounds (VOC) above the air-water interface of the tank using a handheld photo-ionization detector based

meter to evaluate concentrations from the perspective of worker safety. Cautioned are the implications of these shallow water tank results, however as the short vertical water column did not allow for any stripping or dissolving of volatile compounds into the water column as would be expected during a deepwater oil release. Correlations between *in situ* fluorescence data, droplet size distribution, total particle concentration, and oil chemistry serve as inputs to the modeling activities of this project.

Oil droplet size distribution (DSD) data from this study is essential for the improvement of oil spill trajectory and ocean circulation modeling processes to predict the fate and transport of subsurface plumes and surface oil slick movement. This has implications for improving the scientific and response community's understanding on the impacts of dispersant application at depth, ultimate fate of subsurface dispersed oil plumes and potential natural resource damages. Recent advancements in the use of numerical modelling have allowed oil droplet size predictions resulting from a subsurface release. Several different mathematical approaches have been used to determine how oil would behave flowing out of an orifice at high pressure. This includes the modified Weber Number technique (Johansen et al., 2013) and the VDROP-J model (Zhou et al., 2014) to predict oil droplet breakup taking into account oil viscosity and interfacial tension. However, there is a limited amount of large scale real world data to help validate the output of these models. This study provided the opportunity to further test these techniques through the use of several different oil types and treatment conditions. Additional results from the numerical modelling using data obtained from tank experiments are presented in Appendix G, with Part 1 using the modified Weber Number and Part 2 using VDROP.

The premise for this research is that the evaluation and efficacy of chemical dispersants at depth will differ dramatically from conventional use of chemical dispersants for treating surface oil slicks. This is due to difference in mixing energy, where for surface slicks is provided mainly through naturally occurring surface waves and currents, particularly breaking waves. Monitoring of DSD is essential in differentiating between chemically and physically dispersed oil. Tank observations using underwater injection experiments provide

evidence of stable dispersion that may be expected during subsea dispersant injection. Larger oil droplets, whether physically or chemically dispersed, may be capable of coalescing and rising to the surface under less energetic mixing conditions. The experimental results from this work demonstrate the chemical dispersion of oil into small droplets and help to predict the likelihood of coalescence and resurfacing of oil. Results of the project provide spill responders with critical information on the utility of subsurface dispersant application as an oil spill response option and the modeling capabilities that are available to predict oil trajectory during deep water blowouts. Both assist decision-making regarding countermeasures.

TASK B: Evaluation of Oil Fluorescence Characteristics to Improve Forensic Response Tools.

This project addresses the evaluation of oil fluorescence characteristics and sensor performance for improving response tools used to inform oil spill countermeasure decision-making. Fluorescence has long been used as 'one tool in the toolbox' for surface spills and used to supplement visual confirmation during response efforts. Recent oil and gas production in extremely remote locations brings an increased risk of spills in under-the-ice and/or deep-sea environments. For releases in these environs, responders will be evermore reliant on submersible sensors for plume tracking when the human eye cannot be employed. As such, the oil spill community has identified the need for better characterization of spilled oil by fluorometers.

Submersible fluorometers deployed during the 2010 DWH oil spill highlighted the challenges in ensuring selection of the optimum sensor configuration as fluorescence peaks occur over a wide nanometer range, vary in shape and wavelength position, are dependent on oil type due to chemical differences, and are affected by the addition of dispersants. This project addresses these concerns through the following objectives: (1) Characterization of oil optical properties as a function of oil type, DOR and concentration; (2) Generation of a comprehensive Excitation Emission Matrix Spectroscopy, or Matrices (EEMs) library that will

be subjected to advanced statistical analyses for identification of wavelength regions best suited for oil detection; and (3) Evaluation of sensor performance through a series of experiments in a flume tank capable of static and flow-through operations, where sensor data will be validated with chemical and optical analyses.

A series of bench-scale dispersed oil-in-seawater experiments were conducted on 25 oils at 4 dispersant-to-oil ratios (DORs) using Corexit 9500 chemical dispersant. Analysis of the resulting 3D fluorescence EEMs show oil-specific results as well as differing effects of dispersant and DORs. Results will inform the identification of optimum oil detection wavelengths in the marine environment as well as confirmation of the chemical effectiveness of dispersant application. Samples were prepared using baffled flasks to physically disperse the oil within seawater. The effect of dispersant on oil-specific fluorescence is shown, where shifts in intensity and peak wavelengths were observed. Results were compared to chemistry results of oil components.

Results of the laboratory EEMs analysis were compared to EEMs collected under Task A of this project to compare the applicability of baffled flask fluorescence to large scale mixing experiments in the flume tank.

Given recent advances with *in situ* fluorometers, enabling detection at lower UV-wavelengths, these findings help to discern wavelength regions influenced by dispersed oil within seawater, improve the interpretation of fluorescence data, and inform decision-making by responders. Findings from this project will serve to improve confidence in field data, filling operational gaps and formulating operational guidelines.

Findings: Tasks A and B

Overall findings from both tasks of this project include:

1. Addition of either Corexit 9500 or Finasol OSR 52 chemical dispersants to Alaskan North Slope (ANS), IFO 120 and South Louisiana Crude (SLC) oils decreased the Volume Mean Diameter (VMD) and shifted the DSD to smaller droplets. In general, Corexit 9500 produced smaller droplets compared to Finasol OSR 52.

2. Dispersions created without chemical dispersants or DOR = 1:200 yielded VMD larger than 70 µm and exhibited unimodal DSD. Dispersions created with DOR = 1:20 yielded VMD between 2.5 to 70 µm size range with a bimodal distribution. This suggests that produced droplets from a DOR = 1:20 dispersant injection with ANS would likely remain dispersed in the presence of mixing energy given the larger proportion of small droplet sizes observed.
3. Particle size analyses near the injection release (LISST Release) exhibited larger VMD compared to those generated further downstream from release in the tank (LISST Downstream) indicating a shift from larger to smaller droplets within the plume, with and without the presence of dispersant during the 12 minute experiments for ANS and SLC oils. This effect was not always observed with the heavier IFO 120 oil because small droplets were less predominant for this heavier oil.
4. For ANS, dispersion with < 70 um droplet VMD was observed for the DOR = 1:20 treatments at both cold and warm water temperatures. Water temperature did not appear to influence the DSD or VMD for this lighter crude oil. However, a temperature effect was observed on the Total Particle Concentration (TPC), where lower temperatures were coincident with fewer particles dispersed within the plume for a given volume of oil injected.
5. The addition of Corexit 9500 or Finasol OSR 52 to IFO 120 during warm temperature experiments resulted in a shift in DSD and a decrease in VMD; however bimodal distribution was not achieved and even DOR = 1:20 did not yield VMD less than 70 µm in most cases. At cold water temperatures, lower droplet sizes were not observed with the addition of dispersant, where DOR = 1:20 remained well above 200 µm. This suggests that dispersant addition to this oil at cold or warm temperatures would not yield droplet sizes that would likely remain in suspension.
6. For experiments conducted at water temperatures less than 5 °C, The LISST particle size analyzed yielded unexpected DSD where even a unimodal distribution was not measured. Chemistry and *in situ* fluorescence data indicate that the oil was in fact dispersed adequately. This suggests operational problems with the LISST below 5 °C,

even though it is within the operating temperature of the LISST (manufacturer manual). Additional testing of the cold water temperature limits of the sensor is recommended.

7. SLC oil was more dispersible compared to ANS for treatments with and without chemical dispersant. Bimodal distribution was observed during DOR = 1:20 and some DOR = 1:100 experiments indicating that the jet release of this particular oil into warm water produced smaller droplets than the ANS.
8. *In situ* fluorescence serves as a good proxy for oil concentration during the subsurface injection experiments. Given the experimental design, fluorescence is better suited for correlation with particle size analysis and concentration. Heterogeneity of the produced plumes and the short time scale of experiments (~12 min) led to difficulties in correlations between the plume particle size analyses and chemistry results. This is in part due to discrete samples representing 15 second averages as opposed to instantaneous measures given by fluorometers and particle size analyzers.
9. VOC air monitoring was conducted above the tank at two horizontal locations during experiments. The gas condensate exhibited the highest surface VOC concentrations, followed by ANS and SLC which exhibited similar values. Lowest concentrations were observed for IFO 120 experiments. High VOC concentrations in the air were usually accompanied by lower BTEX concentrations in the water. For all oils tested, the addition of chemical dispersants (DOR = 1:20) resulted in a reduction in VOC concentrations within air compared to experiments without dispersant near the jet release location above the tank.
10. Computer programs for jet hydrodynamics, droplet size distribution, and movement of oil droplets within the jet/plume were employed where developed models were calibrated to experimental data obtained from the oil jet experiments in the flume tank. The models VDROP-J and JETLAG were used to predict the streamwise velocity and the holdup along the centerline of the plume, where both models were in agreement, implying that VDROP-J is capable of predicting the average droplet size

distribution in the plume. In the absence of dispersant, the model VDROP-J predicted the oil DSD measured by the LISST. In the presence of dispersant, the VDROP-J model captured the overall trend of the DSD, but was challenged in capturing the peak in droplet concentration observed for 5 microns. The observed peak is could be due to tip-streaming (when high DORs oil droplets shed filaments from their edges resulting in smaller droplets), and VDROP-J does not yet have a module for this component.

11. The Modified Weber Number approach developed by SINTEF is a recent and promising approach for predicting DSD. Previously, the method has been validated solely by a light crude oil. For this project, median droplet diameters (d_{50}) and the relative droplet size (d_{50}/D) were calculated based on the measured droplet sizes obtained from the tank experiments, and the relations between d_{50}/D and modified Weber number, Reynolds number, and oil concentration were quantified. Results demonstrate that chemical dispersants tested here reduced the droplet size of ANS in both cold and warm temperatures and that dispersants tested here are more effective in reducing droplet size with ANS compared to IFO 120. A two-step Rosin-Rammler approach was found to better predict the droplet size distribution in the empirical data as indicated by higher regression coefficients.
12. Fluorescence EEMs were generated for 25 oil types under varying DOR. Oils could be separated into two categories based on dispersiblity; where light, medium and heavy oils were found in each category. Fluorescence peaks are chemistry dependent and were well correlated with Total Petroleum Hydrocarbon (TPH) and Benzene-Toluene-Ethylbenzene-Xylene (BTEX) concentrations. EEMs generated from tank and Baffled Flask Test (BFT) experiments were in agreement with respect to fluorescence peak position and Fluorescence Intensity Ratio (FIR) values as an indication of dispersion effectiveness.

Task A.1 Introduction & Relevance

The 2010 Deepwater Horizon (DWH) oil spill in the Gulf of Mexico has highlighted the pressing need for a better understanding of the interaction of chemical dispersants and crude oil at ocean depth. Early in the blowout release, partial emulsification of oil was observed as it rose to the surface from 1500-m depth, and surface slicks were not continuous (JAG report, 2010). A decision was made to inject dispersants directly at the release point as a possible means to increase efficiency of dispersion and to potentially reduce the amount of dispersant needed if applied at the air-sea interface (CRRC Report, 2010). Large quantities of chemical dispersant were applied via subsurface injection and traditional spraying from aircraft onto the surface oil slick (Oil Budget Calculator, 2010). At a Coastal Response Research Center (CRRC) workshop to discuss the use of subsurface chemical dispersants as an oil spill response option, recommendations to the RRT (Regional Response Teams) by spill response and research expert attendees were made on potential advantages of subsurface dispersant injection given the rate of continuous oil release and preliminary evidence of the dispersant efficacy from the DWH spill (CRRC, 2010). Potential advantages of this application included the fact that the fresh (unweathered) oil was considered well suited for dispersion, operators were able to inject the dispersant directly into the oil stream thereby maximizing dispersant/oil contact, sufficient control of DOR (Dispersant-to-Oil Ratio) could be maintained, injection may minimize the need for surface dispersant application because of reduced oil surfacing and optimized subsurface application would likely promote formation of smaller, more stable droplets of oil, enhancing biodegradation (Lee et al., 2009).

As recommended by the interagency Unified Area Command (UAC) and on-site emergency spill response coordinators, a large-scale environmental monitoring program was implemented to detect and characterize dispersed oil based on field data and plume modeling outputs. This allowed for tracking the subsurface oil plume emanating from the blowout wellhead. Droplet Size Distribution (DSD) analysis using the LISST-100X Laser *in-situ*

Scattering and Transmissometry System (Sequoia Scientific Inc. Seattle, WA) and fluorescence intensity from submersible fluorometers were used as an indication of Dispersion Effectiveness onboard the research vessels, where particle concentrations were monitored to evaluate oil dispersion (presence of small droplets ≤ 70 μm) based on previous studies for surface dispersant applications (Li et al., 2009b). Data analysis of the monitoring samples provided sound evidence of the presence of oil-bearing small particles both in surface waters and in the subsurface plume (JAG report, 2010). Furthermore, a negative correlation between subsurface dispersant injection and low molecular weight compounds in surface waters was observed. In contrast, a strong positive correlation was observed in the subsurface. These results suggest that subsurface dispersant use may have promoted the formation of small oil droplets in the deep sea. This would likely enhance the natural weathering and dissolution of oil in the water column, thus suppressing the presence of oil organic compounds in surface waters.

Although subsurface *in situ* dispersants were used to counter a deepwater spill blowout, much uncertainty still exists in terms of the DE (Dispersion Effectiveness) with this type of application. For example, assumptions of the optimal DOR are based on empirical data mostly obtained from bench-scale experimental protocols that have been designed for testing at standard temperatures and pressures (STP), whereas conditions at a wellhead on the ocean floor or anywhere along a riser beneath the ocean surface could be significantly different. Hence, DOR for direct injection needs to be better understood. Although theoretical analyses and experiments suggest that jet breakup of the oil is insensitive to the absolute value of system hydrostatic pressure for incompressible liquid-liquid systems (Masutani and Adams, 2000), the effects of several ambient environmental factors on subsurface dispersant effectiveness, including high release pressure, high oil temperature, low water temperature, and the presence of methane and suspended sediments in the oil plume and/or surrounding water column remain to be clarified. Improved understanding on the influence of these factors on DE and the interaction of crude oil and chemical dispersant under a range of turbulent regimes at depth is required for informed decision-making for future subsurface dispersant use.

For evaluating chemical dispersion effectiveness, standard laboratory tests are inherently limited in simulating real field operational performance due to space constraints that are critical for transport and dilution efficiency (NRC, 2005). To address the need to evaluate chemical dispersion effectiveness under more realistic oceanographic and environmental conditions, a meso-scale wave tank capable of generating breaking and regular non-breaking wave conditions is currently in operation at the Bedford Institute of Oceanography (BIO), Dartmouth, Nova Scotia. This tank facility has been used previously to characterize the tank hydrodynamics and the efficacy of several oil dispersant formulations on dispersion of different oil types, including fresh and weathered crude oils and heavy fuel oils under breaking wave conditions (Figure 1) (Lee et al., 2009; Li et al., 2008; Wickley-Olsen et al., 2007). Mathematical modeling and experimental measurements have been used in the characterization of the fluid dynamics of the flume tank. In modeling, computer fluid dynamics software packages have been used to conduct numerical simulation of the fluid field and transport phenomena of the flume tank under both non-breaking and breaking wave conditions. Experimentally, wave gauges (WG-50) have been used to monitor wave profiling throughout the flume tank under various hydrodynamic conditions. Acoustic Doppler Velocimetry (ADV) has been employed to evaluate the *in situ* instantaneous three-dimensional velocity distribution, which is used to compute the velocity gradients and energy dissipation rates (ε) in the tank. Using this facility, previous experiments have assessed chemical dispersant effectiveness as a function of energy dissipation rate and particle size distribution (Li et al., 2009a) and demonstrated that the effectiveness of a dispersant is strongly dependent on wave conditions, dispersant type, and oil type (Lee et al., 2009). A strong correlation has been established between dispersion effectiveness and *in-situ* droplet size distribution within the hydrodynamic regime, particularly energy dissipation rate, under a variety of non-breaking wave and breaking wave conditions (Li et al., 2008; Li et al., 2009a). The flume tank has also been operated in flow-through mode to accommodate the effects of underwater currents on dispersion and dilution of oil (Li et al., 2009b; Li et al., 2010). Experiments have also shown the reliability of fluorescence measurements as a proxy for oil concentration within physically and chemically dispersed oil (Conmy et al., 2014).

Experimental studies have also been conducted to better understand oil-mineral aggregate (OMA) formation and the influence of mineral fines on the physical and chemical dispersion of oil (Lee et al., 2009).

This report summarizes results from a project that addresses the operational performance of subsurface injection dispersant use on high pressure releases of oil within the flume tank. Developed methods were focused on monitoring subsurface oil transport by outfitting a new high-flow flume tank at the Department of Fisheries and Oceans Canada (DFO) Bedford Institute of Oceanography (BIO) facility with a new underwater high flow rate oil injection system. In this way, the efficiency of chemical dispersion during high pressure releases within the tank can be quantitatively evaluated and compared to experiments with physical dispersion (without dispersant addition). This work has implications for field response options. To this end, the **objectives** of this work were to:

1) Refine existing equipment, technologies, and methodologies for subsurface dispersant application evaluation and monitoring by measuring dispersed oil concentration, fluorescence, and *in situ* oil droplet size distribution,
2) Evaluate effects of water temperature and dispersant type on dispersion efficacy and dispersed oil droplet size distribution of oil at high temperatures,
3) Evaluate dispersion effectiveness (DE) as a function of oil type and dispersant-to-oil ratio (DOR) for subsurface dispersant injection,
4) Assess the effect of dispersant application on the VOC concentration in air above the air-sea interface of the flume tank,
5) Integrate droplet size distribution into deepwater blowout transport/behavior models to enable prediction of the dispersed oil droplets under high flow subsurface release velocities.

During the DWH spill, small droplet ($d \leq 70\mu m$) concentrations were monitored to aid in evaluating oil dispersion efficiency. The particle size and distribution data obtained from the field monitoring program during the DWH oil spill had a significant role in supporting

emergency oil spill response operations, fate and transport modeling, and impact assessment. Findings from this study will have significant implications in further supporting emergency response operations, spill transport models and assessments for future deepwater spills.

Task A.2 Experimental Methods

A.2.1 Flume Tank Description, Flow Calibration, and Operation

Oil dispersion experiments were conducted in the flow-through flume tank at BIO. The BIO flume tank is rectangular shaped with dimensions of 32 m in length x 2 m in height x 0.6 m in width, with an operational water height of 1.65 m. It was fabricated with carbon steel (3/16") and the interior and exterior surfaces are coated with a marine epoxy paint finish to reduce corrosion while operating under marine conditions. Two sets of manifolds consisting of five inflow and outflow pipes (each constructed of 4" PVC pipe and equipped with a ball valve so that the flow rate can be controlled) are fixed (1.1 m from the outer edges) at both ends of the tank (Figure 2). Two high flow centrifugal pumps (Magnatex 3575 Series, 3" suction, 4" discharge, 600 gpm, Houston, TX), one connected to the inflow manifold and the second connected to the outflow manifold provide a flow-through system used to generate horizontal water currents in the tank. A fiberglass holding tank is used to supply seawater for the system to ensure that a constant flow rate is maintained.

Seawater was obtained from the Bedford Basin, which is directly adjacent to the tank. Two smaller pumps (5 HP Pacer S Series Centrifugal Pump, 110 gpm, Lancaster, PA) were used to pull seawater (~50 cm below the surface) through a 3" suction hose from the Basin. A foot valve was installed at the end of the hose to maintain prime water in the line between fillings. Prior to entering the tank, the seawater was filtered through high-flow polypropylene bag filters (5 µm and 25 µm, Atlantic Purification, Dartmouth, NS).

During normal operations, the flume tank (31,500 L) and holding tanks (25, 000 L) were filled

with filtered seawater. A stainless steel baffle was mounted (~0.5 m) in front of the influent manifold to control current flow. Flow gauges on the influent and effluent lines were monitored and valve adjustments were made to obtain a balanced flow rate, and so that the operational volume was maintained throughout the experiment. Water current velocities were measured at various depths and locations in the tank using an ADV (Nortek Vectrino+, Boston, MA) and the flow rates adjusted until the horizontal water current velocities (3.5 cm/s) were consistent at all measured depths.

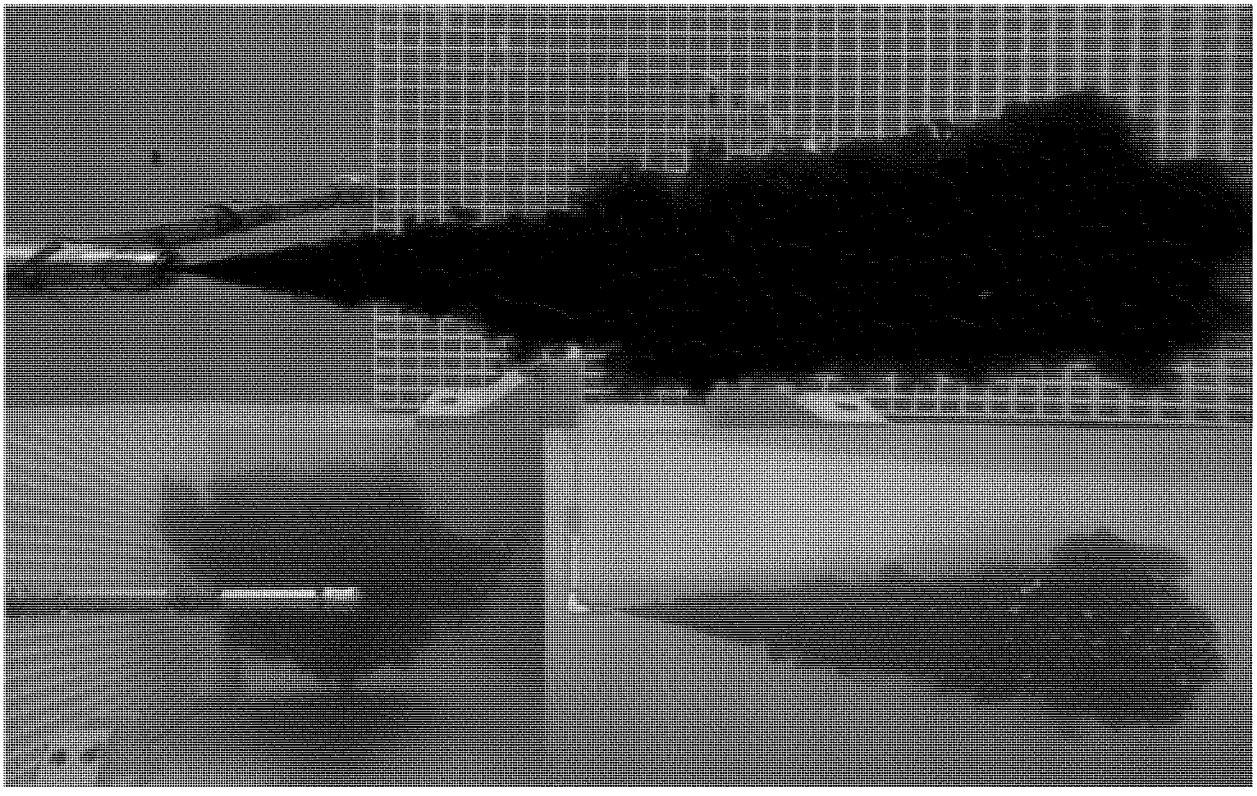

Figure 1. Photos of subsurface oil injection at the BIO flume tank showing the formation of the subsurface oil plume. Note that the background grid size is 1.5 cm x 1.5 cm.

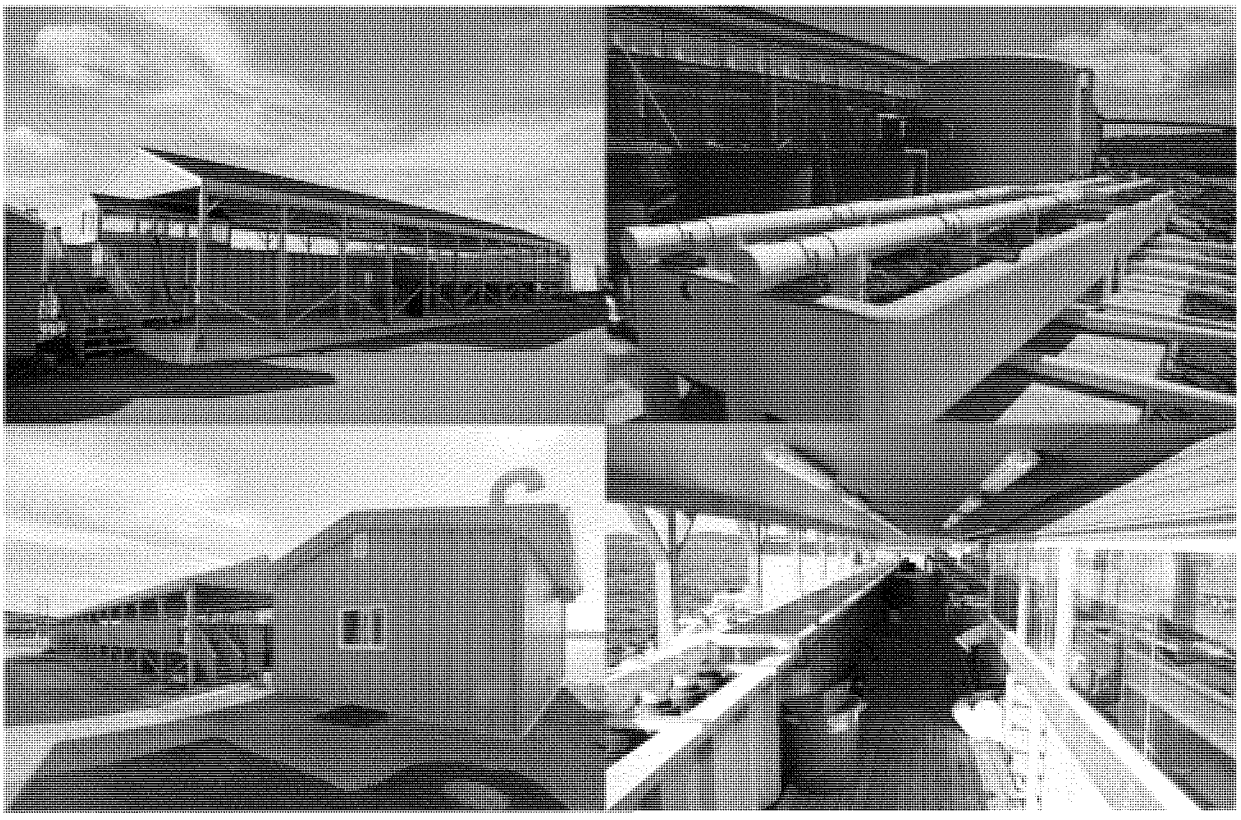

Figure 2. Photo of the DFO BIO flume tank (top) and cross-section of the tank showing the high-flow manifolds used to generate horizontal water currents (not to scale).

A.2.2 Waste Water Treatment

Oil absorbent pads (New Pig, Tipton, PA) are used to manually remove oil from the water surface. The remaining water in the tank is removed by pumping it through an effluent pipe that discharges the waste water over layers of polypropylene PomPom Oil-Mops (New Pig, Tipton, PA) that filter the waste water by removing any remaining insoluble oil prior to discharging it back into the Bedford Basin. Water samples are collected from the treated effluent and the PomPom's are changed if total petroleum hydrocarbon concentrations exceed the minimum guidelines (10 ppm) for wastewater discharge in Canada. Pads and Oil-Mops are discarded as oily waste disposal.

A.2.3 Subsurface Oil Injection System

A custom (engineered in-house) subsurface oil injection system was used to generate dispersed oil plumes in the tank (Figure 3). Briefly, the system consists of a 2 L stainless steel pressure vessel that rests in a support rack. A series of valves and pressure gauges are connected to the pressure vessel. The assembled system is fastened to the outer wall of the tank by way of a quick connect bulkhead fitting. From the same location inside the tank, the fitting connects the outer assembly to a nozzle (2.4 mm inner diameter), which extends mid-width perpendicular to the tank wall (20 cm off the bottom and 9 m downstream from the inflow manifold) and is angled at the tip, so as to direct the discharge plume downstream. Given the shallow nature of the tank, this release setup enabled using the horizontal length of the tank to capture the plume movement.

For each experiment, oil or oil/dispersant premix is added to the pressure vessel (Figure 4A) in order to reduce the influence of any additional confounding factor of mixing effectiveness. Inside the pressure vessel is a copper coil that is connected to a water bath to permit the oil to be heated to 80°C, which takes 30 minutes. Although lower than the estimated oil temperature during the DWH release (~130°C), this is the highest temperature permissible in the pressure vessel to avoid risk of explosion. The vessel is then pressurized (40 psi for ANS, SLC and Condensate; 60 psi for IFO 120) with compressed Nitrogen. A ball valve connected to

the pressure vessel is manually opened and oil is released through the subsurface nozzle into the flume tank (Figure 4B). The release time and total volume (determined by mass) of oil injected are recorded. After each experiment, the entire subsurface injector system was cleaned by flushing repeatedly with toluene, acetone and fresh water until no visible oil remained prior to next experiment.

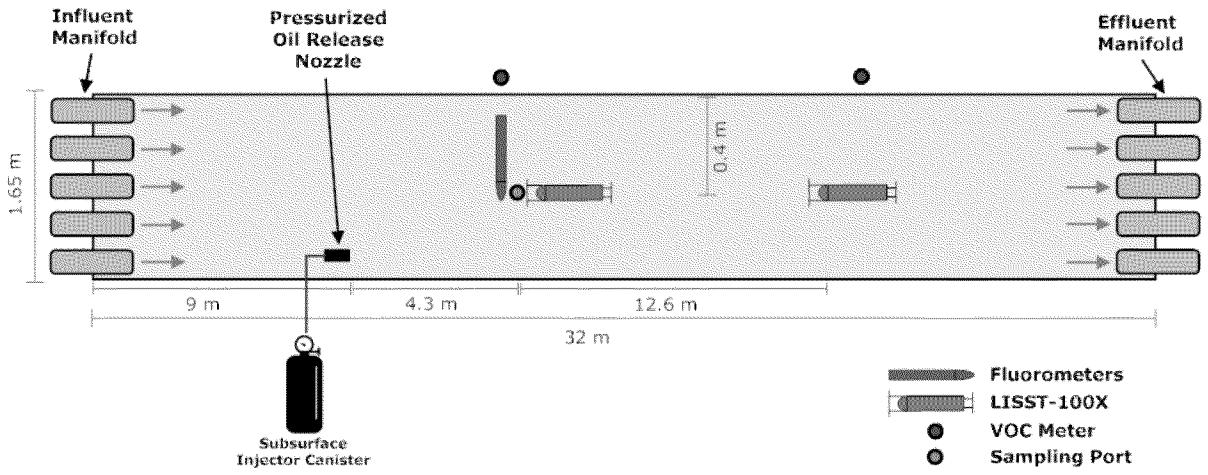

Figure 3. Schematic diagram showing the location of the subsurface injector and *in situ* instrumentation submerged within the tank.

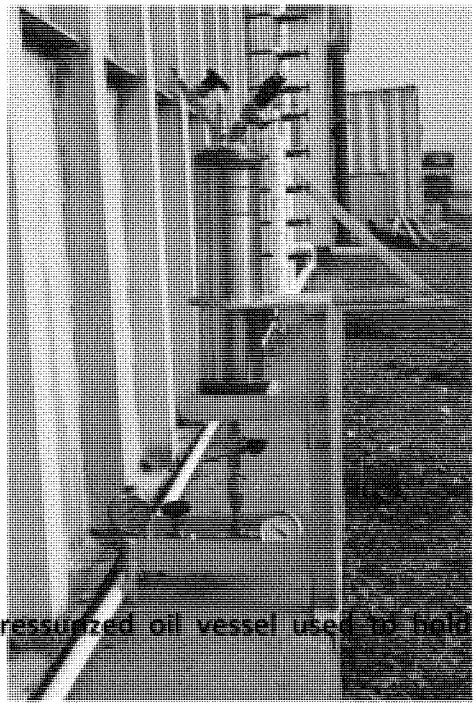

Figure 4A. Photo of the pressurized oil vessel used to hold the oil for the subsurface release.

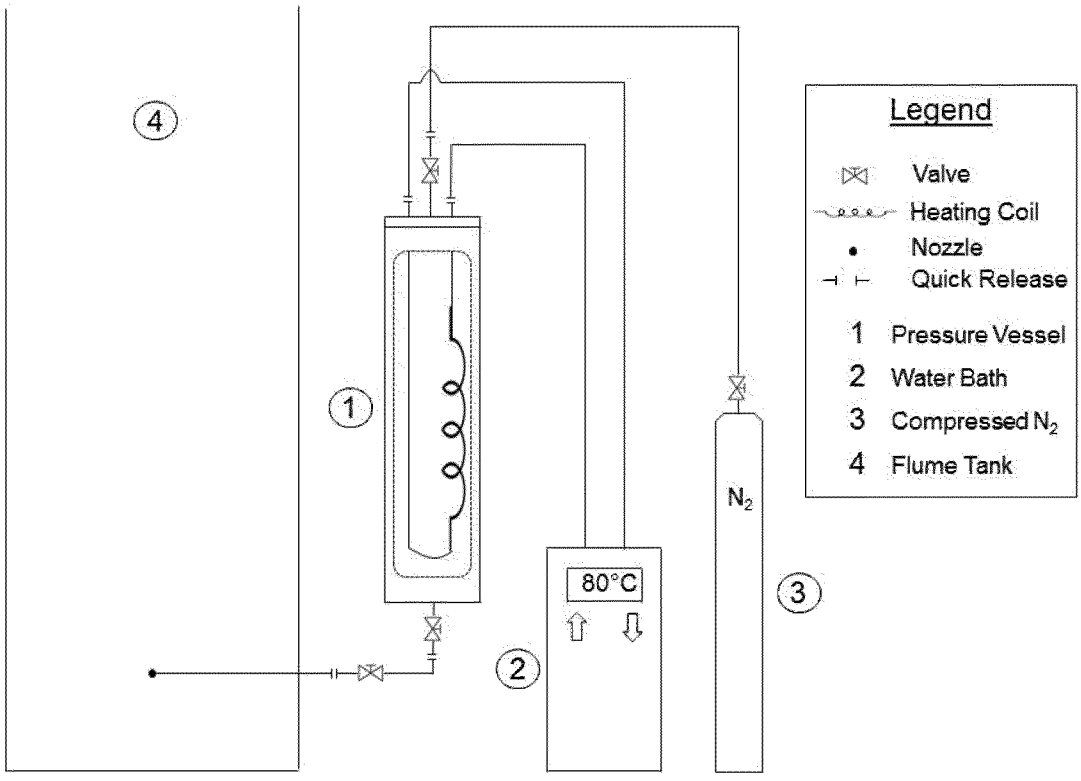

Figure 4B. Schematic diagram of the pressurized oil vessel for subsurface oil release system in the flume tank.

A.2.4 Submersible Sensor Deployment

Fluorescence- A total of six hydrocarbon fluorometers that are used worldwide during oil spill response were evaluated during this study (Table 1). The fluorometers were mounted on an aluminum frame located 4.3 m from the oil release point with their UV windows and at a depth of 0.4 m. The instruments were attached to a crosspiece support bar, so that they were all located the same distance downstream from the oil release point with the UV window pointed directly down at the bottom of the tank.

Table 1. List of hydrocarbon fluorometers used in this study. QSDE and PAH represent quinine sulfate dihydrate and petroleum aromatic hydrocarbons, respectively.

Instrument	Excitation/Emission wavelengths and Units
Chelsea UV AQUAtracka (Refined)	239/360nm, µg/L Perylene
Chelsea UV AQUAtracka (Crude)	239/440nm, µg/L Carbazole
Turner Designs Cyclops (Fine Oil)	254/350nm, Volts
Turner Designs Cyclops (Crude Oil)	365/510nm, Volts
Sea Bird – WET Labs ECO-FLU	370/460nm, µg/L QSDE
GmbH Trios	254/360nm, µg/L PAH

Several different data acquisition systems were used to control and collect data from the *in situ* fluorometers. The GmBH Trios was operated by the manufacturer's power supply and data acquisition system using the MSDA_DE software, which provided a real-time display of the signal intensity in calibrated units of µg/L PAH. The sampling rate was set at one reading every five seconds and raw data was saved as a comma delimited (.csv) file. The two Turner instruments were connected to a Databank Handheld Datalogger (Turner Designs, Sunnyvale, CA), which powered both instruments and recorded data at a sampling rate of 1 reading

every 3 seconds. The datalogger auto-gain feature cycles through settings of 1x, 10x, and 100x depending on the signal intensity. Raw data was recorded as signal intensity in mV and was offloaded from the datalogger via USB connection to a laptop and saved as a text (.txt) file. The Sea Bird - WET Labs and Chelsea instruments were connected to a custom-built power supply and data acquisition system (Pace Scientific XR5-SE datalogger; Mooresville, NC), which collected data from the instruments at a sampling rate of one reading per second. The signal was recorded internally on the datalogger and then sent via wireless connection to a laptop in real-time display. Raw data was recorded as signal intensity in mV and offloaded as a .txt file.

Particle Size Analysis - Oil droplet size was measured *in situ* using two LISST-100X particle size analyzers (Sequoia Scientific, Seattle, WA). The instrument measures particle sizes in the range of 2.5 – 500 µm in 32 logarithmically spaced bins. The first LISST was located immediately after the aluminum frame supporting the fluorometer package at a distance of 5.1 m from the oil release point and the second LISST was located at 16.9 m from the oil release point and both at a depth of 0.4 m (Figure 3). Placement was informed by the numerical modeling team of this project to maximize oil droplet detection without saturating the instrument. Both instruments were connected via a 20 m cable to laptops running the LISST-SOP data acquisition software (version 5). Prior to the start of each experiment, a background scatter file of the seawater quality in the tank was generated and used later to subtract from the final experimental data file. The instruments were operated in real-time mode with a sample acquisition rate of one measurement every three seconds.

Supplemental Measures - Weather conditions (air temperature, wind speed, wind direction, humidity, rainfall) for all experiments were recorded using a Vantage VUE Weather station (Davis Instruments, Hayward, CA). Water temperature and salinity were measured using a YSI handheld probe. Underwater video of oil droplets and the transport of the plume were captured using a GoPro Hero4 digital camera, as well as a Sony RX100 III digital camera with underwater housing.

A.2.5 VOC Air Monitoring

Surface volatile organic compound (VOC) concentrations were monitored using handheld ToxiRAE Pro PID portable gas detectors (RAE Systems, San Jose, CA). Two detectors were used for each experiment, and they were positioned 0.4 m above the water surface at distances of 5.1 and 16.9 m from the oil release point (Figure 3). The detectors were calibrated using a certified 25 ppm benzene calibration gas (AirLiquide, Dartmouth, NS) according to the manufacturer's recommended procedure. Instrument drift was checked periodically against the calibration gas and recalibrated if necessary. During the experiments, the handheld meters were set to datalogging mode, which recorded VOC concentrations as ppm of benzene every three seconds. This data was offloaded and saved as a .txt file for processing.

A.2.6 Discrete Water Sample Collection

Water samples for chemical analysis were collected at various time points throughout the experiments (Table 2). Three ¼" stainless steel tubes were attached to the aluminum fluorometer frame, so that the end of the tube was located at the same depth as the instrument UV windows (0.4 m). These were attached via peroxide cured silicon tubing (Cole Parmer, Vernon Hills, IL) to a Masterflex L/S multi-channel digital peristaltic pump (Cole Parmer, Vernon Hills, IL) which flowed to a three-way valve system. When the valve was set to bypass mode, the water in the lines was continuously primed and flowing, so it could instantaneously be switched to sample mode to allow for sample collection. The pump flow rate was set to approximately 120 mL/min, and all tubing was flushed with clean seawater for 5 minutes prior to the start of any experiment. Tubing was replaced on an as needed basis. Water samples from the effluent manifolds were also collected through a 1" sampling valve at the exit of effluent pipe prior to it entering the treatment system.

A.2.7 Oil and Dispersant Samples

Four different hydrocarbon products were tested in this study to cover a range of viscosity

and physico-chemical characteristics: Two crude oils, a fuel oil, and a gas condensate. Samples of Alaska North Slope crude oil (ANS) and Intermediate Fuel Oil 120 (IFO 120) were obtained from BSEE. Sweet Louisiana Crude was obtained from NOAA. Gas Condensate was obtained from Exxon Mobil and originated from the Sable Offshore Energy Project. Physical properties of the samples (Table 3) were measured using an Anton Paar SVM 3000 Stabinger Viscometer (Anton Paar, Saint Laurent, QC). Supplies of chemical dispersants (Corexit 9500 and Finasol OSR 52) were purchased from the manufacturers.

Table 2. Water sample collection strategy for the core and complimentary experiments. TPH and BTEX represent Total Petroleum Hydrocarbons and Benzene-Toluene-Ethylbenzene-Xylene, respectively.

Time (min)	TPH (Tank)	TPH (Effluent)	BTEX (Tank)	BTEX (Effluent)	Fluorometry (Tank)	Fluorometry (Effluent)
Background	X		X		X	
T = 0	X	X	X			
T = 0.5	X					
T = 1.0	X		X		X	
T = 1.5	X					
T = 2.0	X	X	X		X	
T = 2.5	X					
T = 3.0	X		X			
T = 3.5	X					
T = 4.0	X	X	X	X		
T = 4.5	X					
T = 5.0	X		X	X		
T = 6.0	X	X	X	X		
T = 8.0	X	X	X	X		X
T = 10.0	X	X	X	X		
T = 12.0	X	X	X	X		
Total # Samples/Expt	16	7	11	5	3	1
Total # of Samples	TPH – 1725					

Analyzed	BTEX – 1200 Fluorometry – 300

Table 3. Physical and chemical property measurements of the oils used in this study.

Oil Type	Measurement Temperature (°C)	Density (g/mL)	Kinematic Viscosity (centistokes)	BTEX Content (%)
Alaska North Slope (ANS)	50	0.8529	6.4	2.3
	40	0.8600	8.3	
	25	0.8704	13.1	
	15	0.8777	18.9	
Intermediate Fuel Oil (IFO 120)	50	0.9345	134.0	0.2
	40	0.9411	240.3	
	25	0.9515	781.4	
	15	0.9587	2481.5	
Gas Condensate (CND)	50	0.7247	0.4	13.4
	15	0.7466	0.5	
Sweet Louisiana Crude (SLC)	50	0.8219	3.2	2.4
	40	0.8291	4.0	
	25	0.8733	5.8	
	15	0.8473	8.2	

A.2.8 Experimental Design – Core and Complimentary Experiments

Both the flume tank and holding tanks were filled with filtered seawater as described above. Seawater temperature and salinity were recorded using a handheld probe (YSI Incorporated,

Yellow Springs, OH). After the flume tank was filled, the *in situ* instrumentations including the fluorometers, LISSTs, and VOC meters were positioned in desired locations as indicated previously. The subsurface oil release system was filled with oil or oil/dispersant premix, which was heated to operating temperature. The water supply lines leading to the high flow pumps were primed and the inflow and outflow pumps were started. The system was run in recirculation mode for 10 minutes to allow current flow to stabilize in the flume tank. At a set time point prior to oil injection (5 minutes), data-logging on all instruments was started and background seawater samples were collected. After the oil was injected into the tank, the real-time readout of the fluorometer signal was monitored. Once the first spike in signal intensity was observed (usually after 2 minutes based on the fluorometer signal readout), a stopwatch was started and the first chemistry samples were collected. At this point the high flow system was switched from recirculation mode to flow through, which diverted the water flow into the effluent treatment system instead of returning it to the holding tank. The experiment ran for 12 minutes, at which point the high flow pumps were turned off and the instrument data acquisition was stopped. The tank was cleaned and drained as described above. Tank and instruments were cleaned using Big Orange Degreaser (Zep Superior Solutions, Atlanta, GA), to prevent any potential contamination between experiments. Instrument windows were cleaned using disposable alcohol wipes (Bausch and Lomb, Vaughan, ON). Water samples were returned to the lab and stored at 4°C.

A.2.9 Submersible Sensor Calibration Experiments

The calibration experimental setup was similar to the core and complimentary experiments, except that the oil was added in a step-wise (tank dilution series measurements) fashion to the flume tank as shown in Table 4. Calibration experiments were conducted in such a way to create a series of known concentrations of dispersed oil in the flume tank. Predetermined amounts of oil and dispersant (Corexit 9500) premix were added to the tank (Alaska North Slope, ANS, crude was used at a DOR of 1:20) using the subsurface injector.

The flume tank was operated in recirculation mode and oil/dispersant premix injections

occurred every 45 minutes, which provided a sufficient time for the dispersed oil concentrations to stabilize in the tank (previous testing of this system showed that hydrocarbon concentrations in the tank are homogenous after 45 minutes of recirculation). The recirculation of water in the tank provided sufficient mixing energy to allow small droplets generated by the subsurface injector to remain dispersed in the water column. *In situ* instrumentation was located at the same locations as all other experiments. Water samples were collected at 45 minute time intervals after each oil addition.

Upon reaching homogeneity in the tank (i.e. 45 minutes after each oil addition), the average fluorometric intensity signal collected over a 4 minute time period was calculated. Fluorometers were calibrated to manufacturer suggested units using factors provided. Triplicate water sample analysis results for Total Petroleum Hydrocarbons (TPH) and Benzene-Toluene-Ethylbenzene-Xylene (BTEX) were averaged that correspond with the same time points. Fluorescence and chemistry averages were regressed to generate calibration curves of TPH and BTEX vs signal intensity for oil additions ranging from 1 to 18 ppm. Higher variability at low concentrations resulted in the exclusion of some data points in the regression calculation.

A.2.10 Submersible Fluorometer and LISST Data Processing

Raw LISST data files were processed using a statistically-based quality control script written using the R statistical package (www.r-project.org). In summary, this script identifies and removes "Over Range" samples (defined as 0 µL/L across all particle size bins) and outliers. Outliers are defined as any reading that is greater than the moving mean (5 data points before and after the targeted time point) of the dataset multiplied by four times the standard deviation (over the same interval as the moving mean). Due to the potential for one or more extreme outliers to skew both the moving mean and standard deviation calculations for points around them, this outlier detection routine is run iteratively, excluding previously flagged points, until no more outliers are detected. Once these QC steps have been performed, the script calculates a number of parameters from the data such as Total Particle Concentration (TPC), Volume Mean Diameter (VMD), and Particle Size Concentration (PSC). It

then goes on to detect the plume curve (if present) and time-normalizes the data based on that location. Data are presented as Droplet Size Distribution (DSD). Plots presented include data 2 minutes before and 8 minutes after the start of the plume curve. Data from the Downstream LISST were normalized so that the plume began at t = 5 min in order to visually convey that the plume was detected in the tank roughly 3 min after detection by the LISST further upstream near point of injection release.

Similar to the LISST data, a script was used to detect outliers in data collected from the *in situ* fluorometers. Curve detection was then performed and the data was time-normalized to include 2 minutes of data before, and 8 minutes of data after the start of the plume curve. The baseline of the plume curve was then calculated using data points observed in the first minute preceding the start of the curve and this baseline was subtracted from the data. Finally, factory calibration factors were applied to the data values for each instrument before plotting.

Table 4. Step-wise sensor calibration experiment parameters.

Oil Addition #	Mass of Oil Added for each Addition (g)	Cumulative Oil Concentration in Tank (mg/L)
1	9.45	0.3
2	9.45	0.6
3	12.6	1
4	63	3
5	94.5	6
6	189	12
7	189	18

A.2.11 Analytical Chemistry Analysis

Total Petroleum Hydrocarbon (TPH) Analysis - The method used for extraction and processing of TPH samples was developed by DFO in-house (Cole et al., 2007; King et al., 2015). Water samples were collected in pre-weighed 125 mL amber glass bottles and filled to approximately 90 mL. Sample bottles were weighed and a mass difference was used to determine the total volume of the collected water sample. The samples were immediately stored at 4°C until ready for further processing. Within 24 hrs of collection, 10.0 mL of dichloromethane (DCM) was added to each sample. The samples were shaken by hand for 30 seconds, and then placed on a Wheaton R2P roller (Wheaton, Millville, NJ) set at 9 rpm. After 18 hours on the roller, a Pasteur pipette was used to transfer the DCM solvent layer into a pre-weighed 15 mL graduated centrifuge tube. The solvent was then evaporated under a gentle stream of nitrogen using an N-Evap (Organomation, Berlin, MA) and topped up with DCM to a final volume of 1.00 mL. The solvent extract was transferred into an auto-sampler vial and stored at -20°C for GC-FID analysis.

Sample extracts (1 µL) were injected using an Agilent 7683 auto-sampler into an Agilent 7890B GC, using splitless injection set to oven track mode (2°C higher than the oven temperature program). The column used for separations was a Supelco MDN-5s 30 m × 250 µm × 0.25 µm (length × i.d. × film thickness). Hydrogen was used as a carrier gas with a flow rate of 3.0 mL/min. The GC oven is programmed to an initial oven temperature of 35°C, held for 2 min, followed by an increase to 320°C at 20°C/min, and held at 320°C for 10 min, with a total run time of 26.25 min. The GC flame ionization detector (FID) was operated at 320°C with the hydrogen flow set at 30 mL/min and the air flow set at 400 mL/min. An eight point calibration was generated using standards prepared from the appropriate crude oil stock that

was used to generate the TPH samples (e.g. ANS, IFO 120, SLC or Gas Condensate). Peak quantification was performed using relative response factors. Routinely the method of extraction was tested for efficiency by a spike and recovery study. Typically, a mean percent recovery of >90% was calculated from filtered seawater spiked with crude oil. Lab and field blanks were incorporated in the method.

BTEX Analysis - EPA Method 8240 (purge and trap) was modified by running a gas chromatograph/mass spectrometer in selected ion monitoring mode to include ethylbenzene (Cole et al., 2007). To summarize, water samples for BTEX (benzene, toluene, ethylbenzene and [m,p & o] xylene) analysis were collected in 40 mL purge and trap vials. The vials were spiked with 40 µL of 6N HCl to serve as a preservative, so that they can be stored at 4°C for up to 14 days.

The purge and trap system was a Teledyne Tekmar Stratum PTC purge and trap concentrator equipped with a Tenax/silica gel/charcoal trap. The auto-sampler was a Teledyne Tekmar Aquatek 70-vial unit. The auto-sampler transferred a 5 mL aliquot of sample into the purge and trap chamber, where it was purged with helium for 11 minutes. During this process, the volatiles were trapped on the Tenax trap and then desorbed at 225°C for 2 min. The desorbed gases enter a heated transfer line connected to the Agilent 6890 GC injector and subsequently proceed to the GC column (Supelco MDN-5s 30 m × 250 µm × 0.25 µm length × i.d. × film thickness).

The GC oven was programmed at an initial oven temperature of 50°C, held for 8 min, followed by an increase to 280°C at 40ºC/min, and held at 280°C for 2 min, for a total run time of 18 min. The gases exiting the GC column were detected by an Agilent 5973 mass selective detector (MS) used in selective ion mode (SIM) monitoring for six ions: 77, 78, 91, 92, 105 and 106 amu. BTEX standards were prepared in 40 mL purge and trap vials. Samples and standards were analyzed using this method, along with sample blanks and duplicate samples.

A.2.12 Numerical Modeling Methods

Refer to Appendices G and H for numerical modeling components.

TASK A.3 RESULTS

The overarching objective for this project was to evaluate the operational performance of the subsurface injection of dispersants during deepwater blowouts. Presented here are the results from a series of flume tank subsurface injection experiments where dispersion effectiveness was evaluated via response monitoring tools (fluorescence and particle size analyzers), discrete water sample chemistry analysis and VOC air monitors. The logs for all experiments conducted can be found in Appendix A. Corresponding chemistry results for each experiment are tabulated in Appendix B.

A.3.1 ANS Dispersion Effectiveness

Injection experiments were conducted using ANS crude oil, chemically dispersed with Corexit and Finasol. Regardless of warm ($\geq$ 11°C) or cold (5.4 – 10.7°C) water temperatures, the addition of the two tested dispersant lowers the VMD of ANS and shifts the DSD to smaller droplets within the plume. An example of this trend is shown in Figures 5 and 6. Note that LISST histogram plots have constrained Y-axes; thus lines that extend slightly above the top of the plot area represent values that were truncated. Histograms in these figures correspond to time points at the leading edge of the plume (~2-3 min from oil release). Contour plot X-axis represents experiment elapsed time. Plots for triplicate experiments for each treatment are shown in Appendices C and D. All plots represent data from the LISST positioned closest to the jet release (denoted as Jet Release LISST throughout the document) and in close proximity to the submersible fluorometers. Histograms represent the particle concentration for a given size class (Y axes). Contour plots represent the 10 minute time series of the plume, where colored contours represent

the particle concentration (normalized to max value for comparison purposes), Y axes represent the droplet sizes in µm and X axes are time in minutes. Time is elapsed time since oil injection into the tank. These contours allow for ascertaining how the DSD shifts over the duration of the release. A second LISST positioned further downstream of release (denoted as Downstream LISST throughout the document) allows for comparing the evolution of the plume in space and time since release of the plume. For warm temperature experiments, there is a slight decrease in VMD for DOR = 1:200 and 1:100 (Corexit) compared to the no-dispersant treatment (DOR = 0), in this case ~130 µm down to ~80 µm (exact numbers are within text of the figures). A large shift in DSD is observed for the DOR 1:20 treatment, where VMD is ~ 10 µm. The cold water treatments exhibit this same trend, where VMD is ~ 10 µm for the DOR = 1:20 treatment (Figure 6). *In situ* submersible fluorescence from multiple fluorometers was recorded during experiments. Example time series for each dispersant and temperature treatment are shown in Figure 7 and illustrate the impact of dispersant at DOR = 1:20 in the plume. With DORs of 0, 1:200 and 1:100, the plumes tend to exhibit a spike in fluorescence shortly after release (within 2 min), and then a sharp decline in signal that is brought to extinction by 4 minutes. For DOR = 1:20, however, the signal remains elevated and with variability for up to 6 minutes. This indicates that more oil is remaining submerged in the plume for a longer time period. Time series fluorescence plots for triplicate experiments for each treatment are shown in Appendix E.

The Downstream LISST positioned further from the jet release and the fluorometers serves as an indication of plume evolution through the tank. Plots of the Downstream LISST DSD and VMD for all dispersant treatments for warm and cold water experiments are shown in Figures 8 and 9, respectively. Comparing these to the LISST results near the jet release illustrates the decrease in Total Particle Concentration (TPC; represents the maximum concentration for the entire plume) as the plume disperses through the tank (note the change of Y axis scale). Also evident is a shift to smaller particles for all DOR treatments as the plume moves through the tank. Where the decrease in TPC suggests plume dilution in

the tank, the DSD shift to smaller particles suggests that within each experiment larger droplets were removed from the plume within 6 minutes of the oil release, most likely rising to the surface of the tank.

Warm water experiments conducted with ANS and Finasol OSR 52 dispersant also yield a shift in DSD towards smaller VMD for DOR = 1:20 (Figure 10). However the shift is smaller than that observed with Corexit 9500 (Figure 5), with lowest VMD on the order of ~50-60 µm. DOR = 1:200 and 1:100 treatments exhibited spikes in fluorescence signal that taper off within 3 minutes of oil release (Figure 11). Fluorescence for DOR = 1:20 Finasol OSR 52 treatments exhibited a decrease in intensity at ~4 minutes which is faster than that for treatments with Corexit 9500. The Downstream LISST exhibited a similar shift in DSD and TPC that was observed with Corexit 9500 treatments (Figures 12 and 13).

Water temperatures for experiments ranged between 5.4 – 20.8 °C. In general there was no clear trend on the influence of temperature on DSD, VMD fluorescence intensity, or oil concentrations for the time series for DOR = 0, 1:200 or 1:100 treatments. This suggests that water temperature has little effect on the dispersibility of ANS (80 °C oil temperature) when released as a jet with little or no exposure to chemical dispersant (in this case the pre-mixing process prior to release). In contrast, DOR = 1:20 experiments showed a decrease in total particle concentration (TPC) with decreasing temperature even though no effect was observed on DSD for the two temperatures. Figure 14 shows three examples of this effect, where TPC values for each DOR = 1:20 experiment increase as a function of temperature (Figure 15). It is important to note that for all treatments using ANS, the experiment at the lowest temperature (SubANS-10R; 5.4 °C) exhibited anomalous dispersion compared to the other DOR = 1:200 treatments (Appendices C and D). Because this occurred in only one experiment out of 33 experiments with ANS, it is difficult to ascribe a cause for this other than an improper jet release of oil.

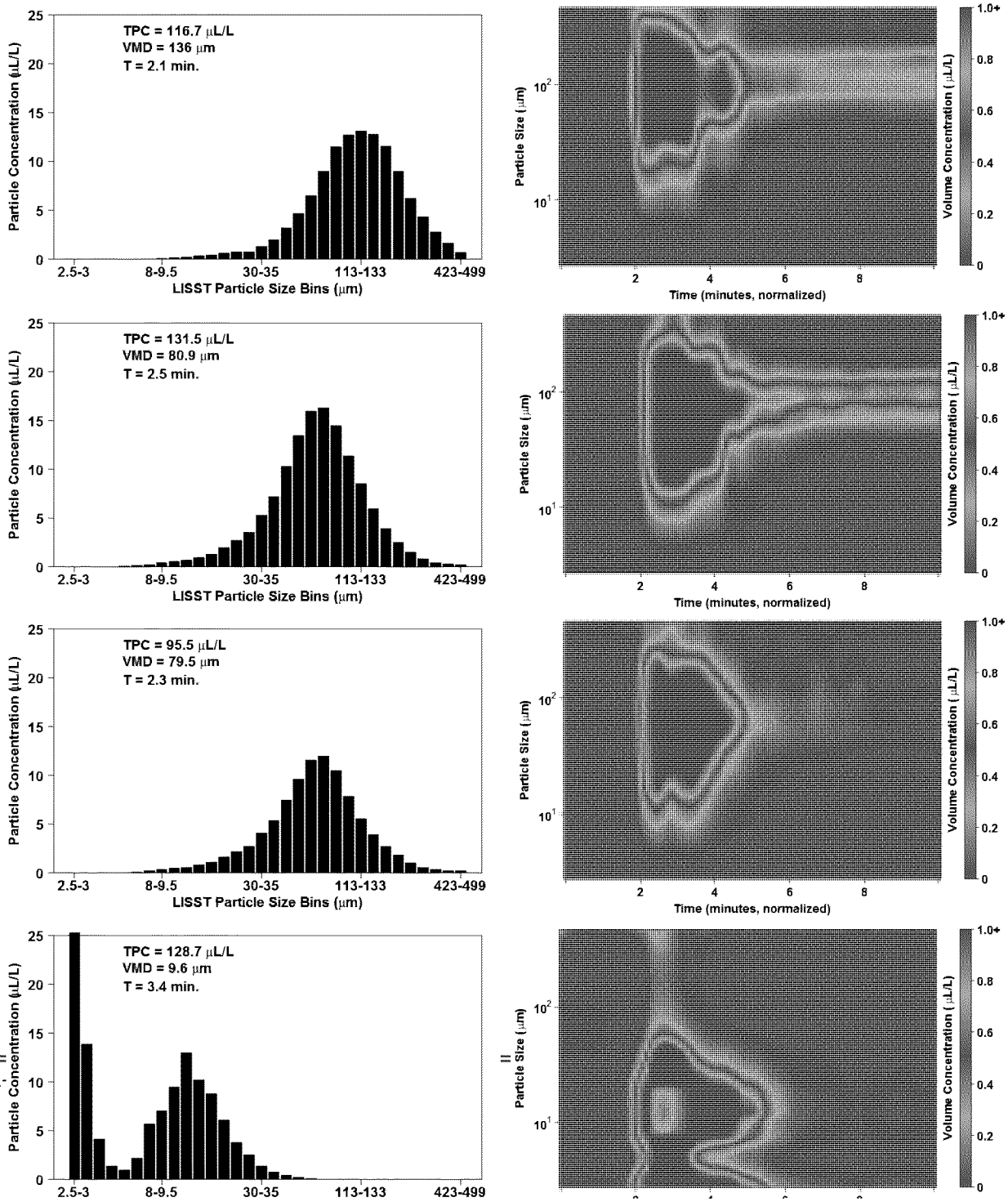
TPC = 116.7 µL/L
VMD = 136 µm
T = 2.1 min.
Particle Concentration (µL/L)
LISST Particle Size Bins (µm)
2.5-3
8-9.5
30-35
113-133
423-499
Particle Size (µm)
Time (minutes, normalized)
Volume Concentration (µL/L)
TPC = 131.5 µL/L
VMD = 80.9 µm
T = 2.5 min.
TPC = 95.5 µL/L
VMD = 79.5 µm
T = 2.3 min.
TPC = 128.7 µL/L
VMD = 9.6 µm
T = 3.4 min.

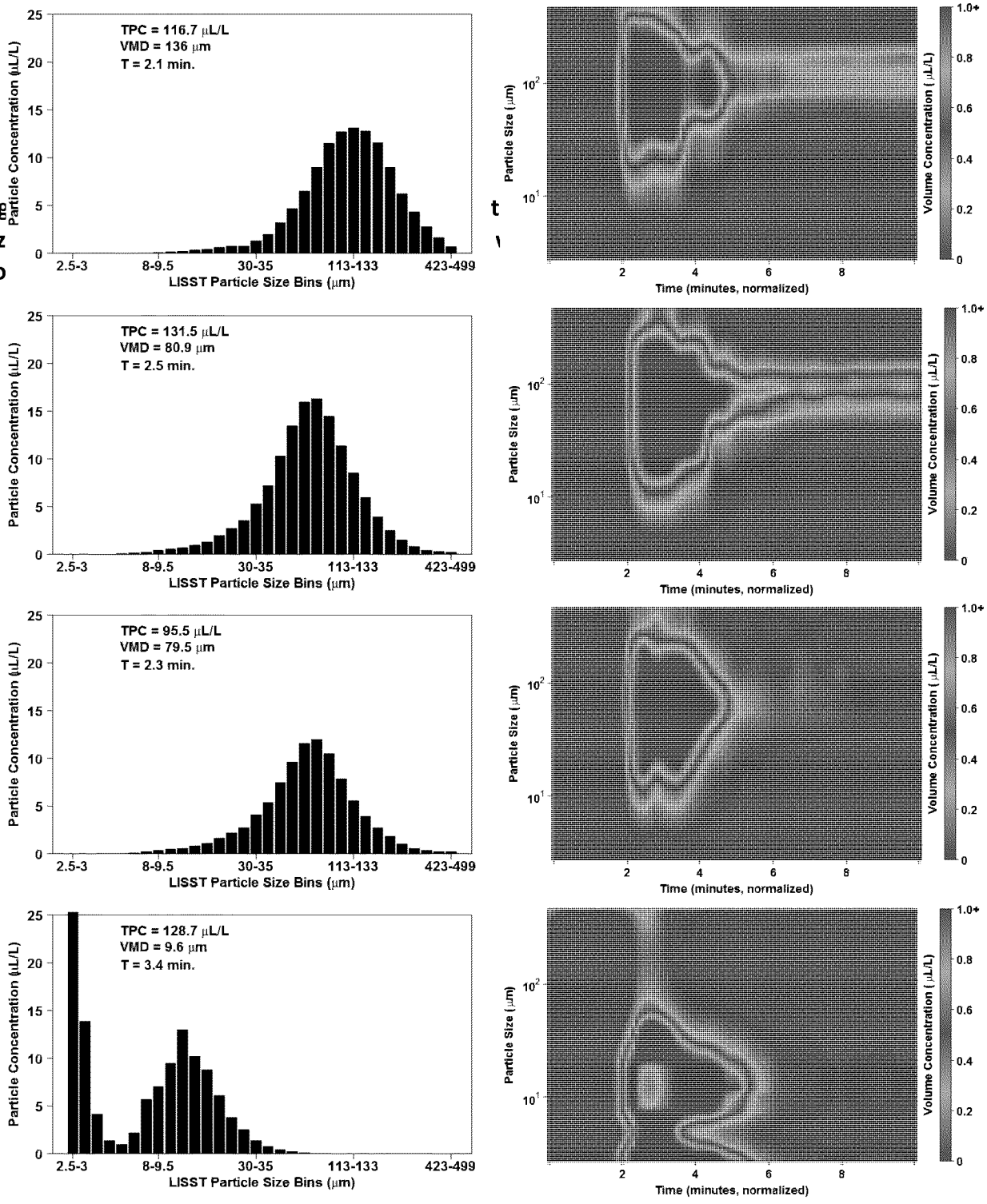
TPC = 116.7 µL/L
VMD = 136 µm
T = 2.1 min.
TPC = 131.5 µL/L
VMD = 80.9 µm
T = 2.5 min.
TPC = 95.5 µL/L
VMD = 79.5 µm
T = 2.3 min.
TPC = 128.7 µL/L
VMD = 9.6 µm
T = 3.4 min.
Particle Concentration (µL/L)
LISST Particle Size Bins (µm)
2.5-3
8-9.5
30-35
113-133
423-499
Particle Size (µm)
Volume Concentration (µL/L)
Time (minutes, normalized)

Fig
siz
bo
t

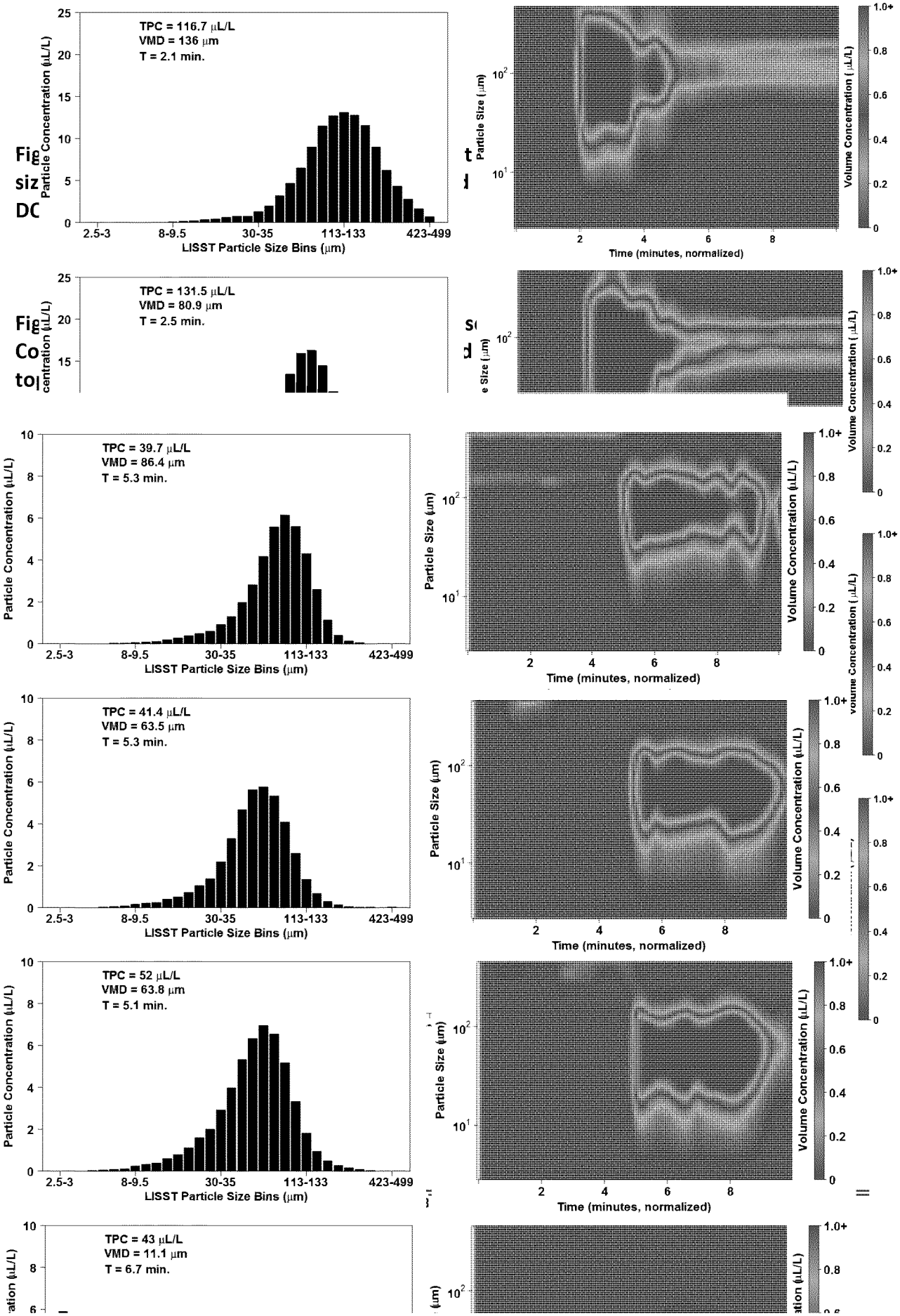
TPC = 116.7 µL/L
VMD = 136 µm
T = 2.1 min.
Particle Concentration (µL/L)
LISST Particle Size Bins (µm)
2.5-3
8-9.5
30-35
113-133
423-499
Particle Size (µm)
Time (minutes, normalized)
Volume Concentration (µL/L)
TPC = 131.5 µL/L
VMD = 80.9 µm
T = 2.5 min.
TPC = 39.7 µL/L
VMD = 86.4 µm
T = 5.3 min.
TPC = 41.4 µL/L
VMD = 63.5 µm
T = 5.3 min.
TPC = 52 µL/L
VMD = 63.8 µm
T = 5.1 min.
TPC = 43 µL/L
VMD = 11.1 µm
T = 6.7 min.

Figure 8. Downstream LISST DSD and VMD (left panels) and time series of concentration and particle size (right panels) for ANS and Corexit 9500 warm water treatments. From top to bottom, DOR = 0, 1:200, 1:100, 1:20.

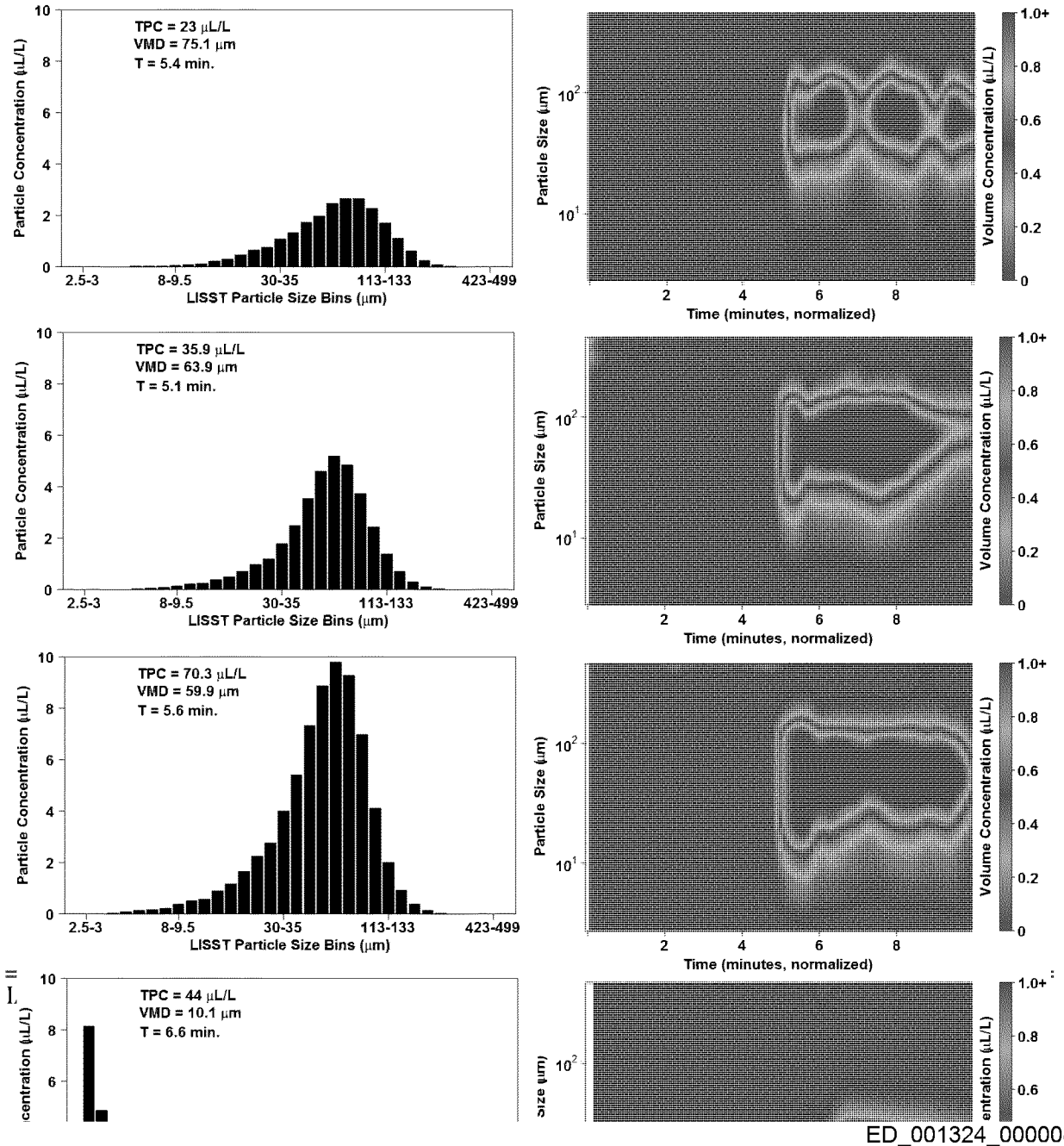

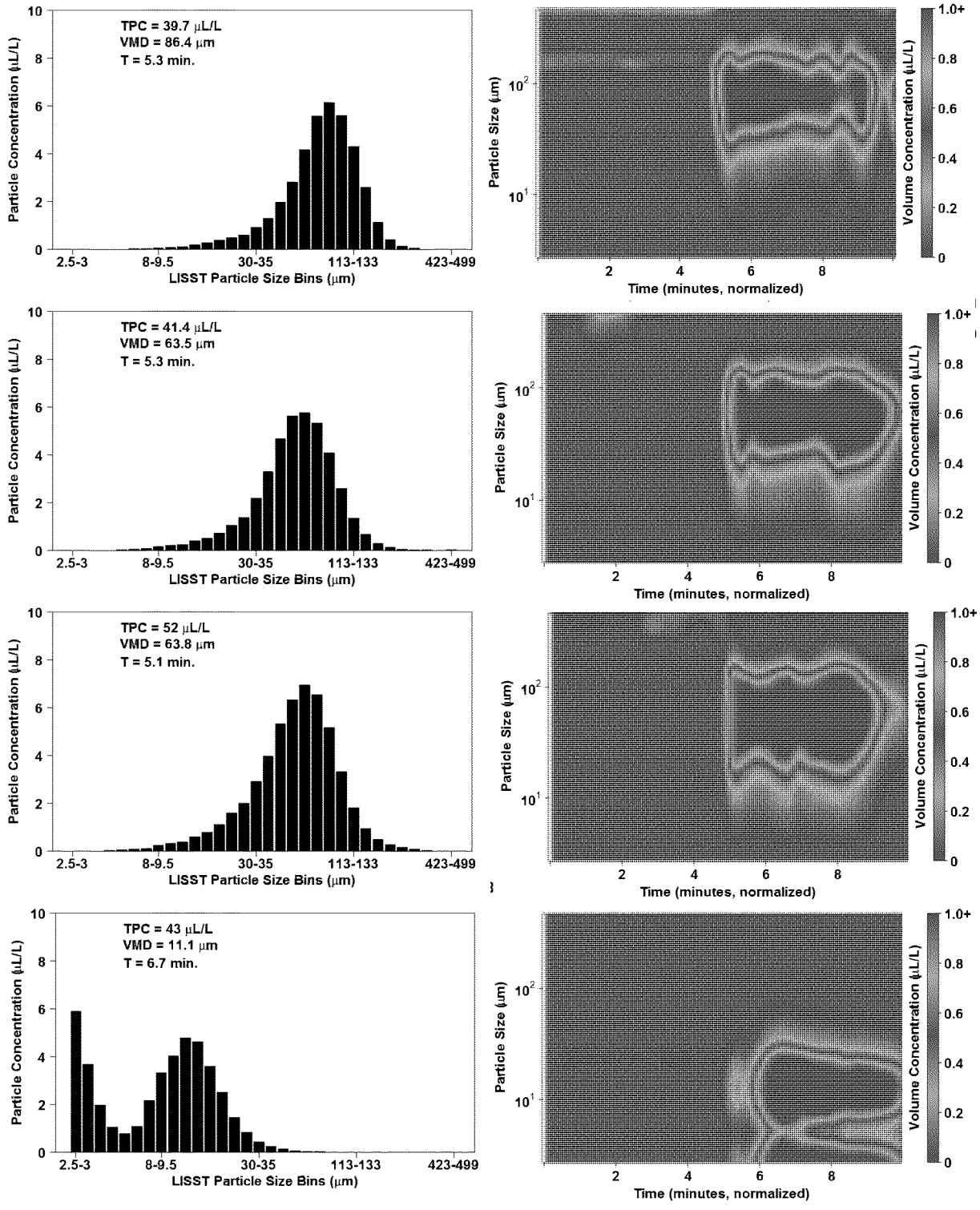

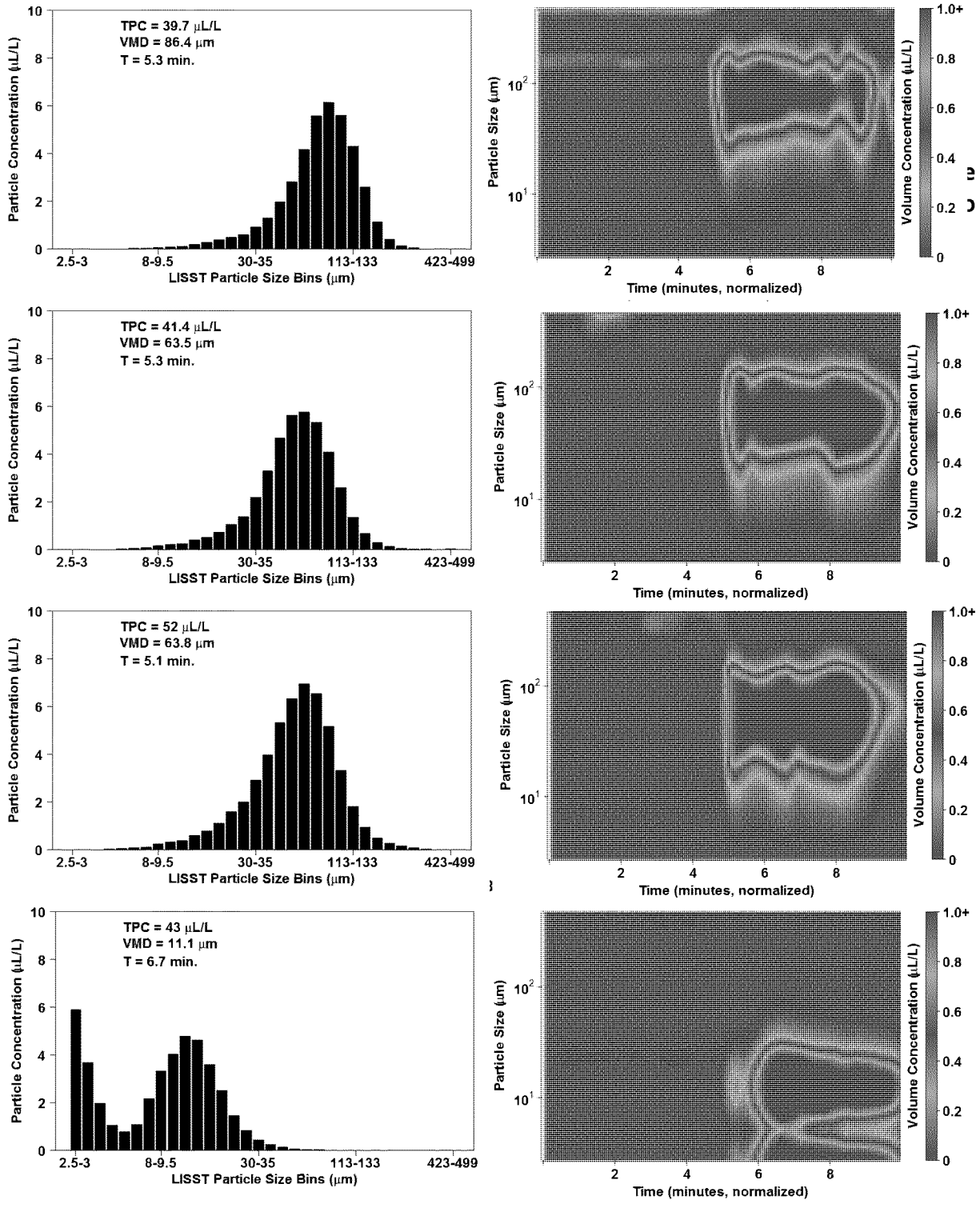
TPC = 39.7 µL/L
VMD = 86.4 µm
T = 5.3 min.
TPC = 41.4 µL/L
VMD = 63.5 µm
T = 5.3 min.
TPC = 52 µL/L
VMD = 63.8 µm
T = 5.1 min.
TPC = 43 µL/L
VMD = 11.1 µm
T = 6.7 min.
Particle Concentration (µL/L)
LISST Particle Size Bins (µm)
2.5-3
8-9.5
30-35
113-133
423-499
Particle Size (µm)
Time (minutes, normalized)
Volume Concentration (µL/L)

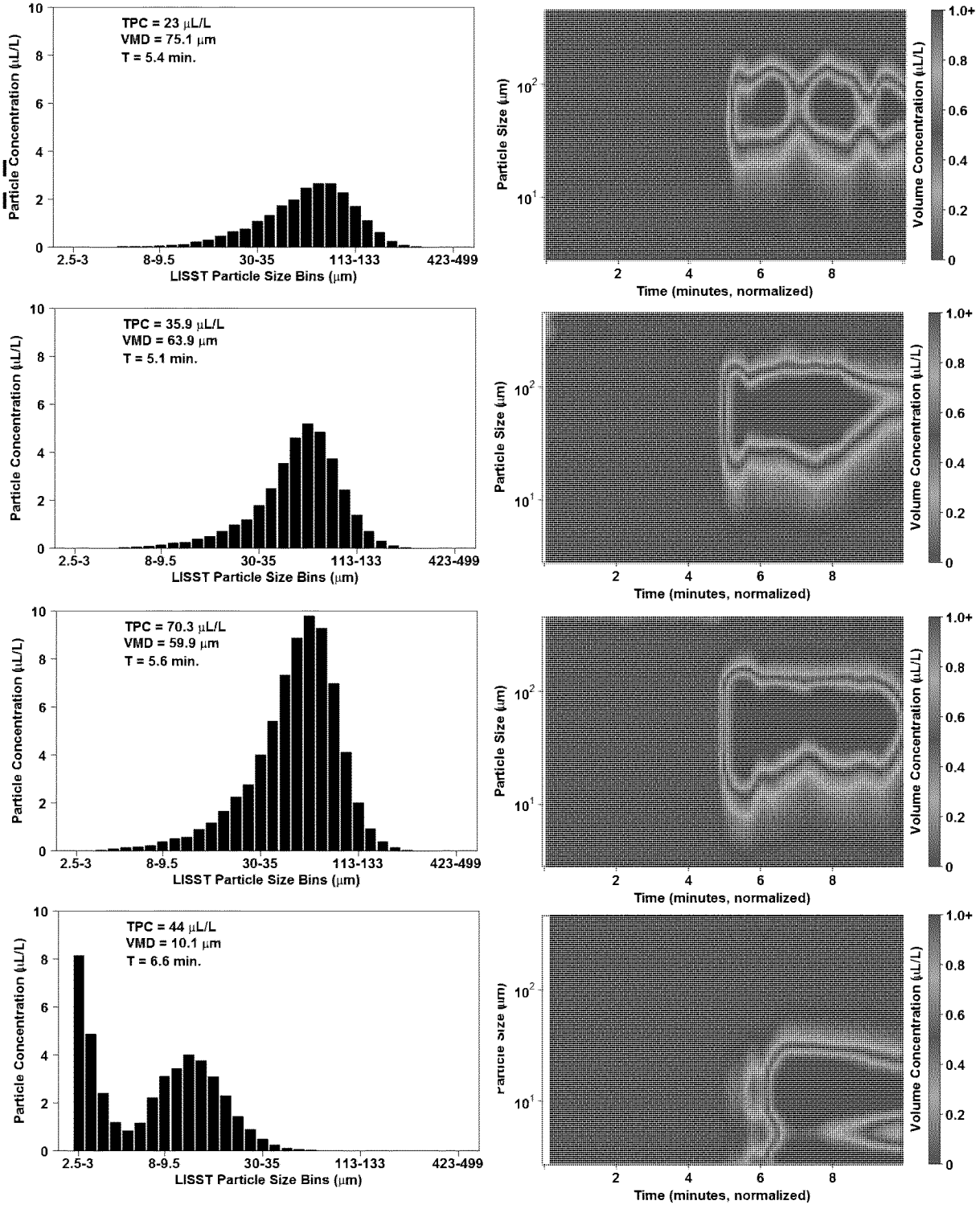
TPC = 23 µL/L
VMD = 75.1 µm
T = 5.4 min.
TPC = 35.9 µL/L
VMD = 63.9 µm
T = 5.1 min.
TPC = 70.3 µL/L
VMD = 59.9 µm
T = 5.6 min.
TPC = 44 µL/L
VMD = 10.1 µm
T = 6.6 min.
Particle Concentration (µL/L)
LISST Particle Size Bins (µm)
2.5-3
8-9.5
30-35
113-133
423-499
Particle Size (µm)
Time (minutes, normalized)
Volume Concentration (µL/L)

Figure 12. Downstream LISST DSD and VMD (left panels) and time series of concentration and particle size (right panels) for ANS and Finasol OSR 52 warm water treatments. From top to bottom, DOR = 1:200, 1:100, 1:20. Refer back to Figure 6 for ANS DOR = 0.

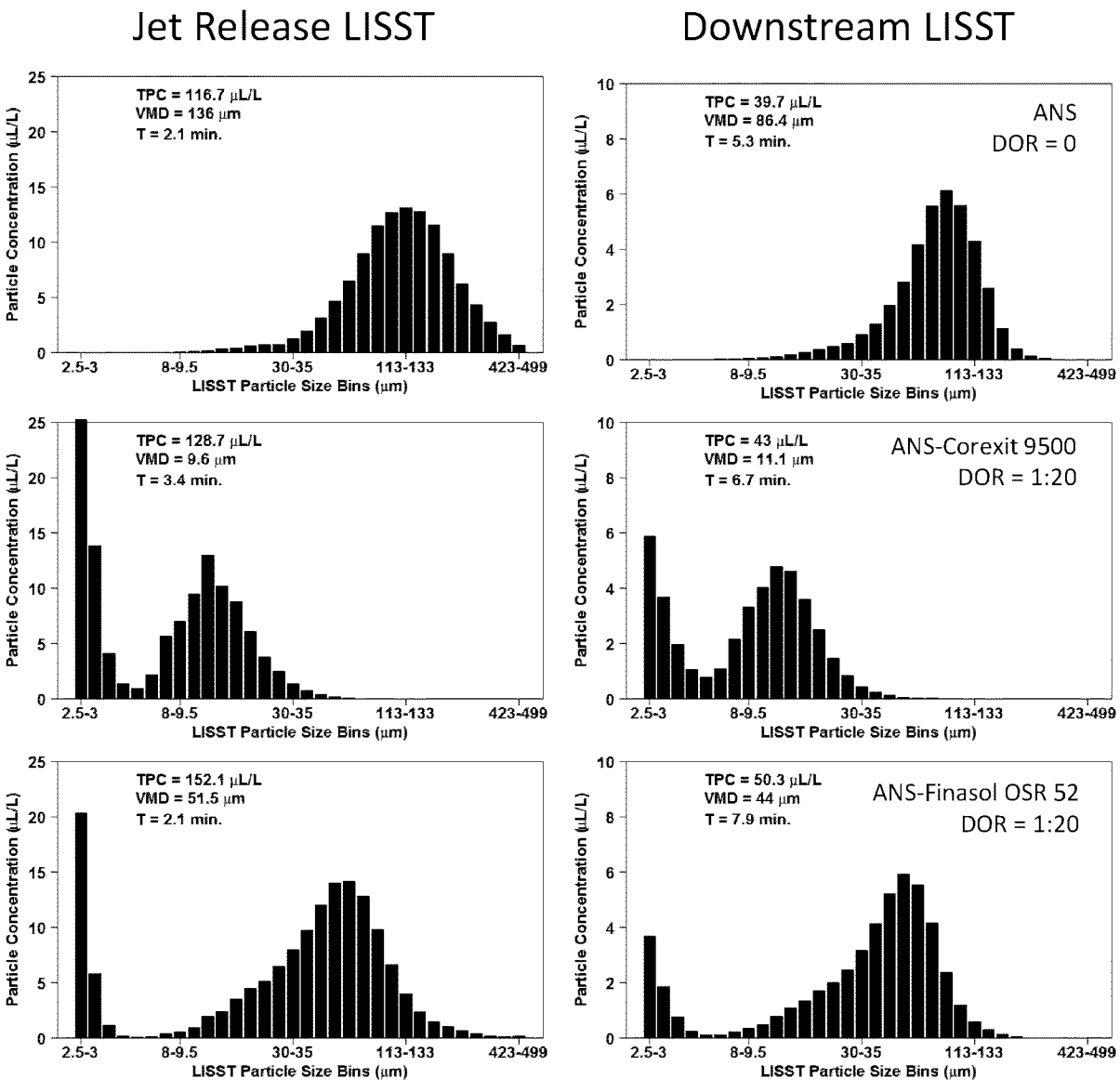

Figure 13. LISST DSD with TPC for ANS with Corexit 9500 and Finasol OSR 52 warm water treatments. DOR = 0 (top panel); DOR = 1:20 experiments are middle and bottom panels.

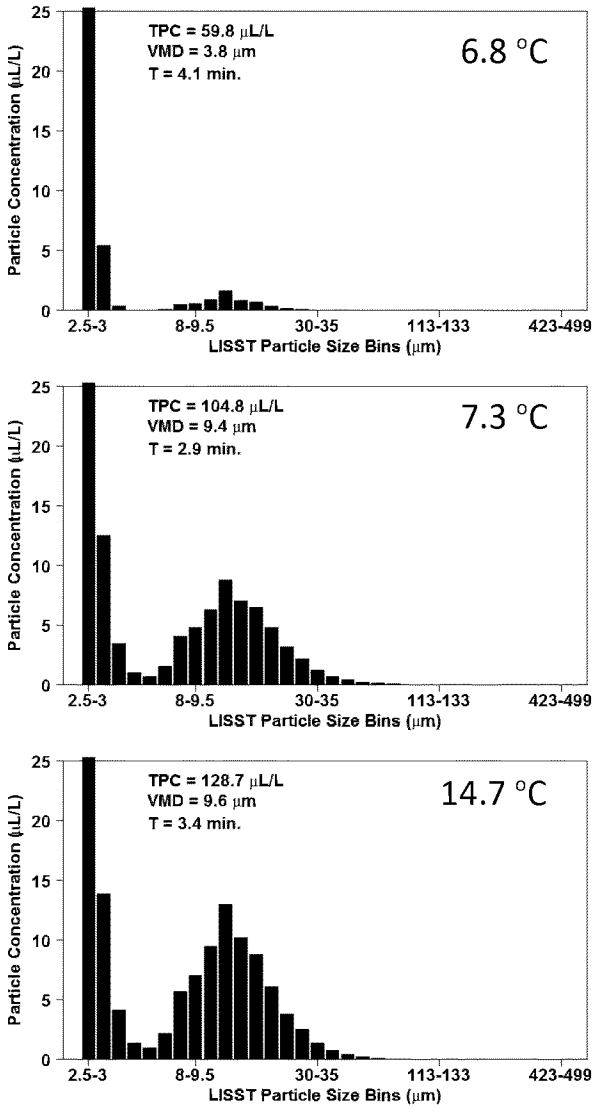

Figure 14. LISST DSD with TPC (Total Particle Concentration) for DOR = 1:20 experiments of ANS and Corexit 9500 treatments. Water temperatures increase from top to bottom panels.

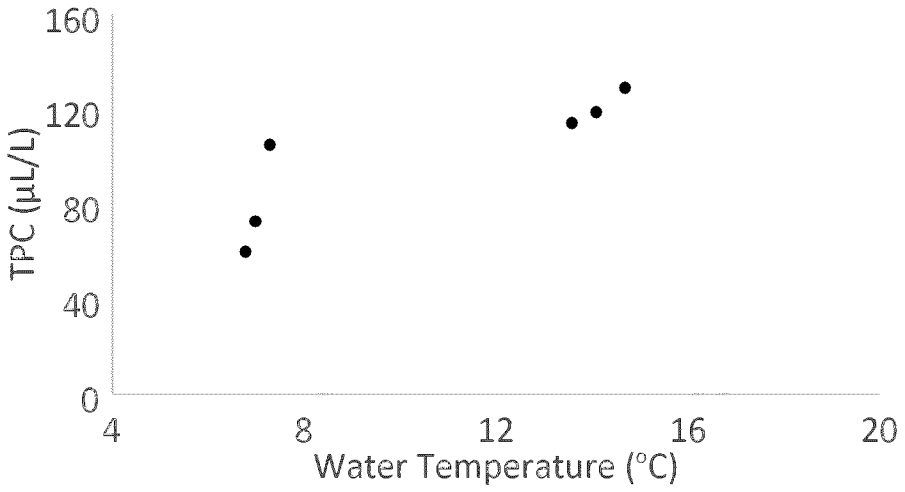

Figure 15. LISST TPC (Total Particle Concentration) for DOR = 1:20 experiments of ANS and Corexit 9500 treatments as a function of water temperature.

A.3.2 IFO 120 Dispersion Effectiveness

Injection experiments were conducted using Intermediate Fuel Oil (IFO 120), chemically dispersed with Corexit 9500 and Finasol OSR 52. For warm water experiments, temperatures ranged between 13.5 – 16 °C for treatments with Corexit 9500 and between 17.5 – 20.3 °C for treatments with Finasol OSR 52. In the DOR = 0, 1:200 and 1:100 treatments using Corexit 9500, VMD typically remained > 200 µm (Figure 16). VMD values were smaller for DOR = 1:20 treatments (~66-120 µm), indicating a shift in DSD, but to a lesser extent than the shift observed for ANS experiments. Fluorescence data exhibited scatter and noise in the signal for all but the DOR = 1:20 treatments (Appendix E). A similar trend in DSD, VMD and fluorescence signal was observed for IFO 120 exposed to Finasol OSR 52 at warm temperatures (Figure 17), where DOR = 1:200, 1:100 and 1:20 exhibited VMD values of 376.5, 209.5 and 125.8 µm, respectively. Unlike experiments with ANS, which is less viscous and dense, IFO 120 exposed to dispersant tended to result in larger oil droplets for a given amount of dispersant added. Comparing the results of IFO 120 with the two dispersants is challenging because no triplicate experiments were conducted for Finasol OSR 52 treatments, as the latter treatments were add-on experiments and not central to the project. In general, from the data collected, Finasol OSR 52 yielded higher VMD for a given DOR compared to Corexit 9500 at warm temperatures. As with ANS, the Downstream LISST measured a decrease in TPC and shift to smaller droplet sizes as the plume moved through the tank for all treatments, but to a lesser extent with DOR = 1:20 (Figures 18, 19 and 20).

For cold water experiments using IFO 120 exposed to Corexit 9500, temperatures ranged between (4.9 – 7.5 °C). At these colder temperatures a shift in DSD and VMD was not as apparent (Figure 21). For DOR = 0, 1:200 and 1:100 VMD typically remained > 223 µm but was as high as 344 µm. The DOR = 1:20 treatment exhibited VMD of 178-327 µm, suggesting that this oil was not well dispersed at cold temperatures. Fluorescence time series data were noisy for all experiments except the DOR = 1:20 (Appendix E). The Downstream LISST recorded extremely low particle concentrations, further suggesting poor dispersion (Figure 22). During the IFO 120 cold water treatments, one experiment resulted

in an anomalous DSD histogram that was similar to an anomalous one observed during one of the ANS experiments (Figure 23). In both cases, the experiments were conducted at the coldest temperatures during the course of this study (4.9 and 5 °C). Suspected as a possible cause may be the LISST instrument itself. The manual reports that the lower operating temperature for the LISTT-100X is -10 °C. However, the data suggests that our particular unit may have experienced some complications at low temperatures. This is supported by the fact that the fluorescence signal and chemistry data for these experiments indicate no anomalies. Further testing would be needed to confirm the effect of low temperatures on particle size analysis results using our instrument to rule out any potential issues with operating at temperatures between 5 and -10 °C.

One aspect to note with the IFO 120 cold water experiments is that a few of the treatments were conducted at water temperatures of ~12 °C, which overlaps with the temperatures of the warm water group. This was the result of erratic weather patterns that at times were difficult to work around. Thus, when interpreting the temperature data, caution must be exercised for these particular experiments (refer to Appendix A for temperature log), and for the interpretation in this section, they were excluded as they do not represent cold conditions.

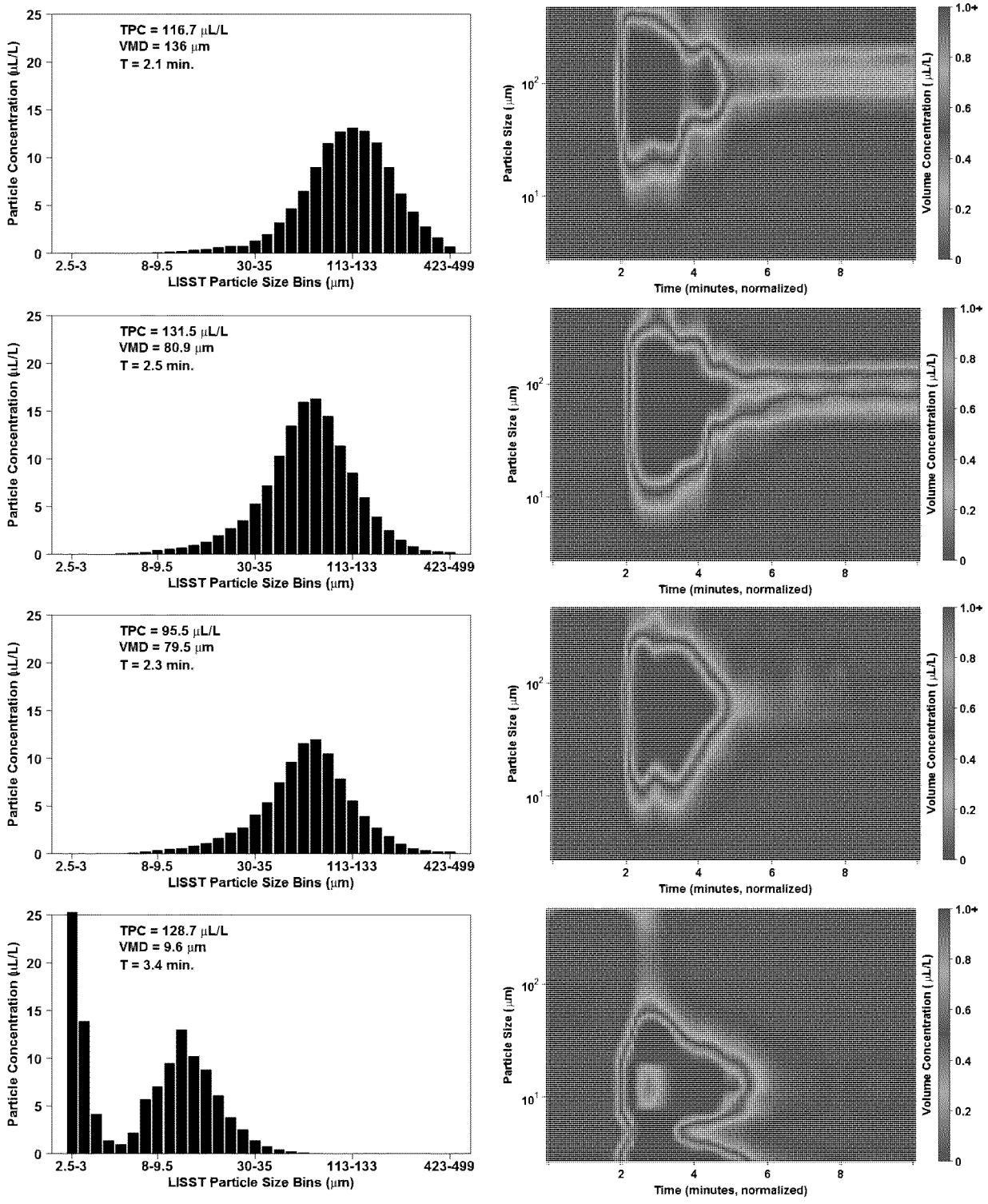

Figure 16. LISST DSD and VMD (left panels) and time series of concentration and particle size (right panels) for IFO 120 and Corexit 9500 warm water treatments. From top to bottom, DOR = 0, 1:200, 1:100, 1:20.

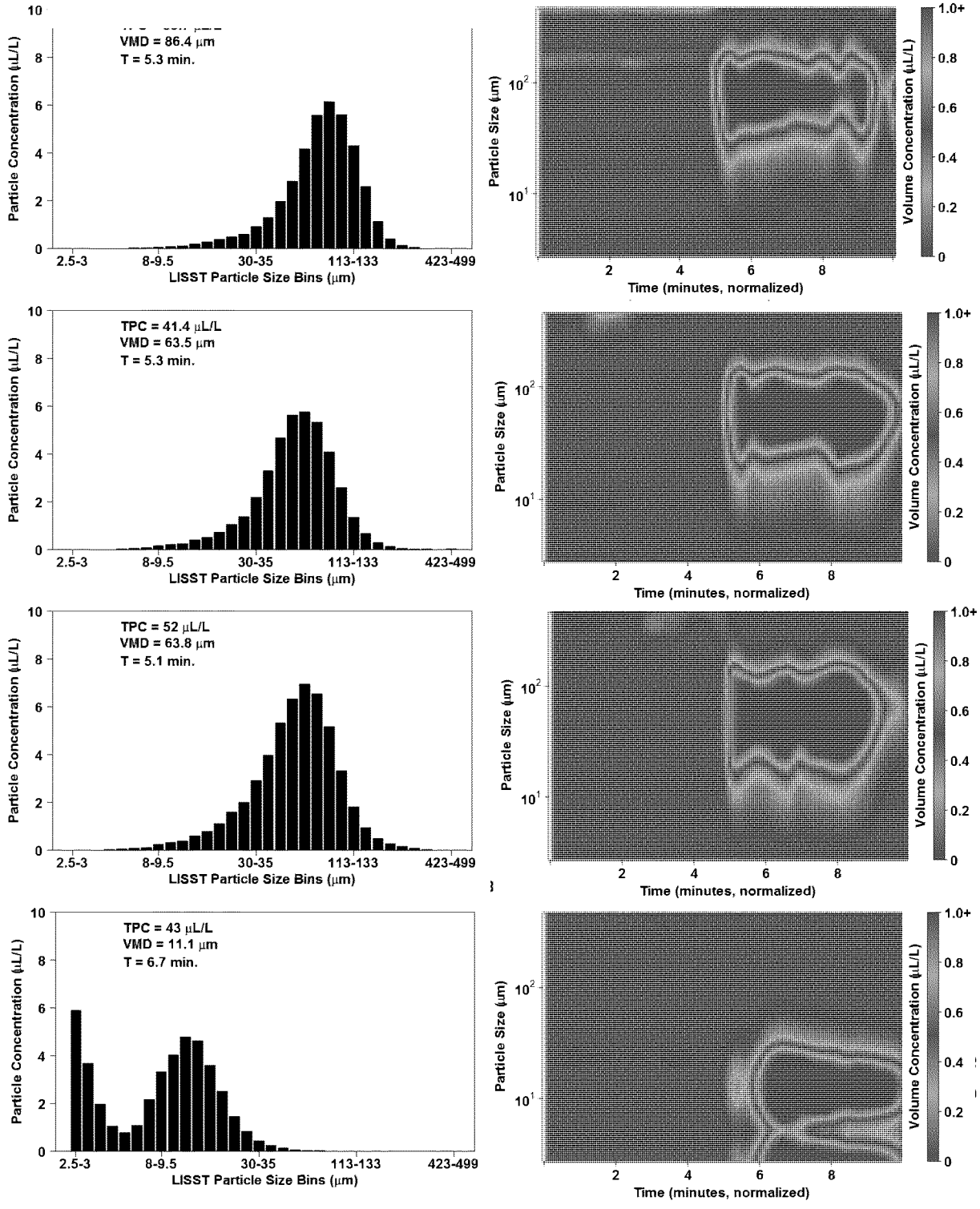
VMD = 86.4 µm
T = 5.3 min.
TPC = 41.4 µL/L
VMD = 63.5 µm
T = 5.3 min.
TPC = 52 µL/L
VMD = 63.8 µm
T = 5.1 min.
TPC = 43 µL/L
VMD = 11.1 µm
T = 6.7 min.
Particle Concentration (µL/L)
LISST Particle Size Bins (µm)
2.5-3
8-9.5
30-35
113-133
423-499
Particle Size (µm)
Time (minutes, normalized)
Volume Concentration (µL/L)

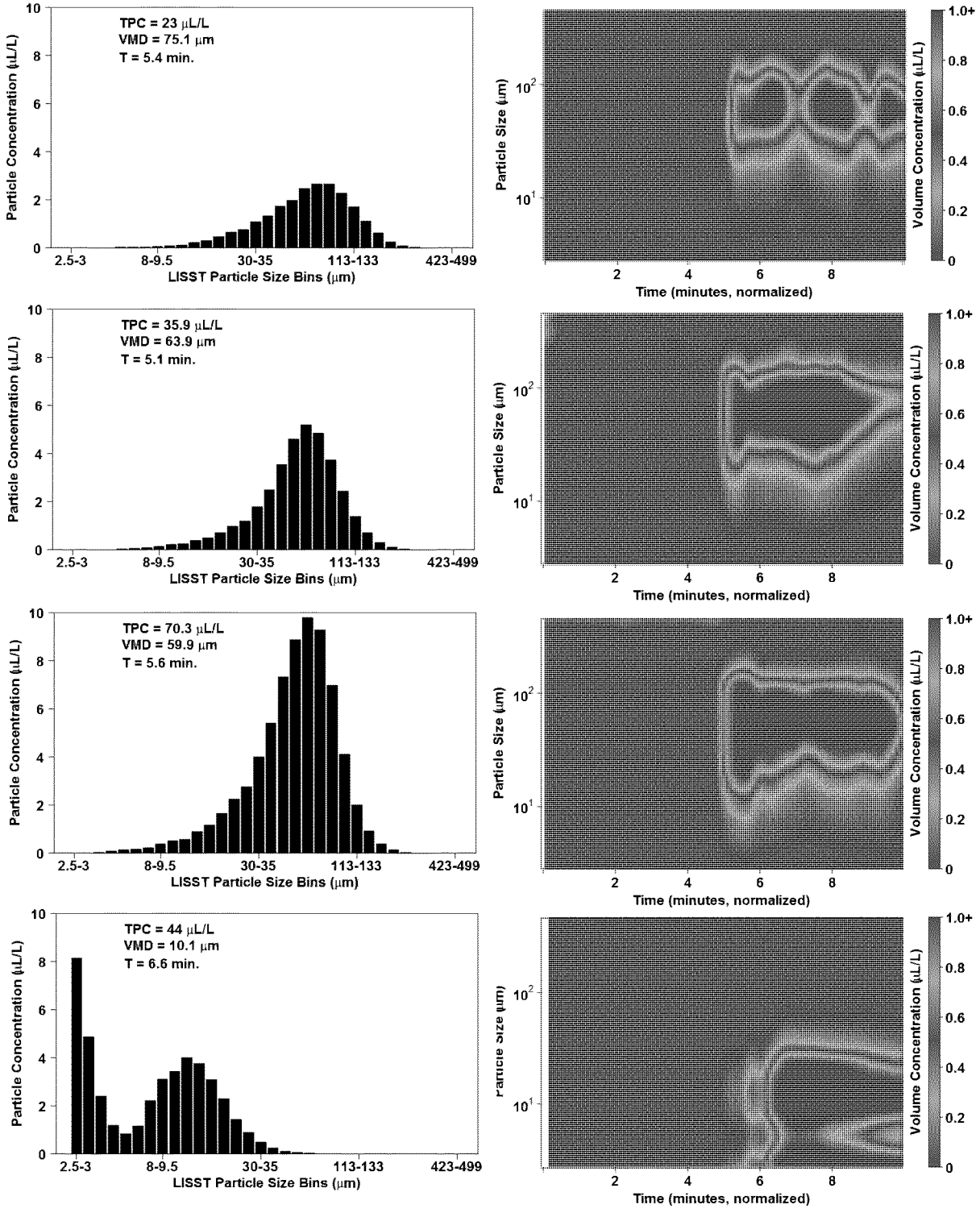

Figure 18. Downstream LISST DSD and VMD (left panels) and time series of concentration

and particle size (right panels) for IFO 120 and Corexit 9500 warm water treatments. From top to bottom, DOR = 0, 1:200, 1:100, 1:20.

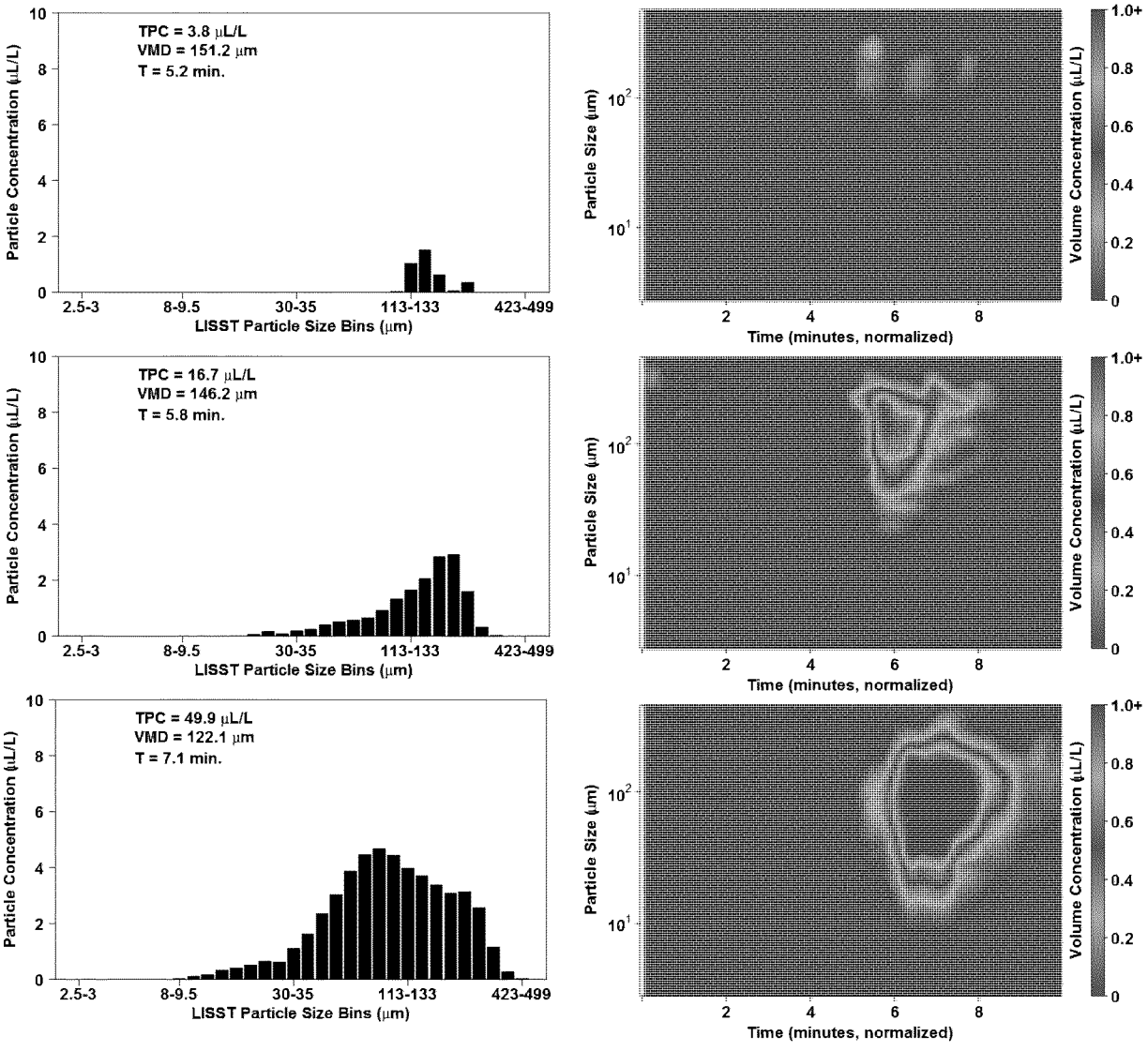

Figure 19. Downstream LISST DSD and VMD (left panels) and time series of concentration and particle size (right panels) for IFO 120 and Finasol OSR 52 warm water treatments. From top to bottom, DOR = 0, 1:200, 1:100, 1:20. Refer to Figure 18 for ANS DOR = 0.

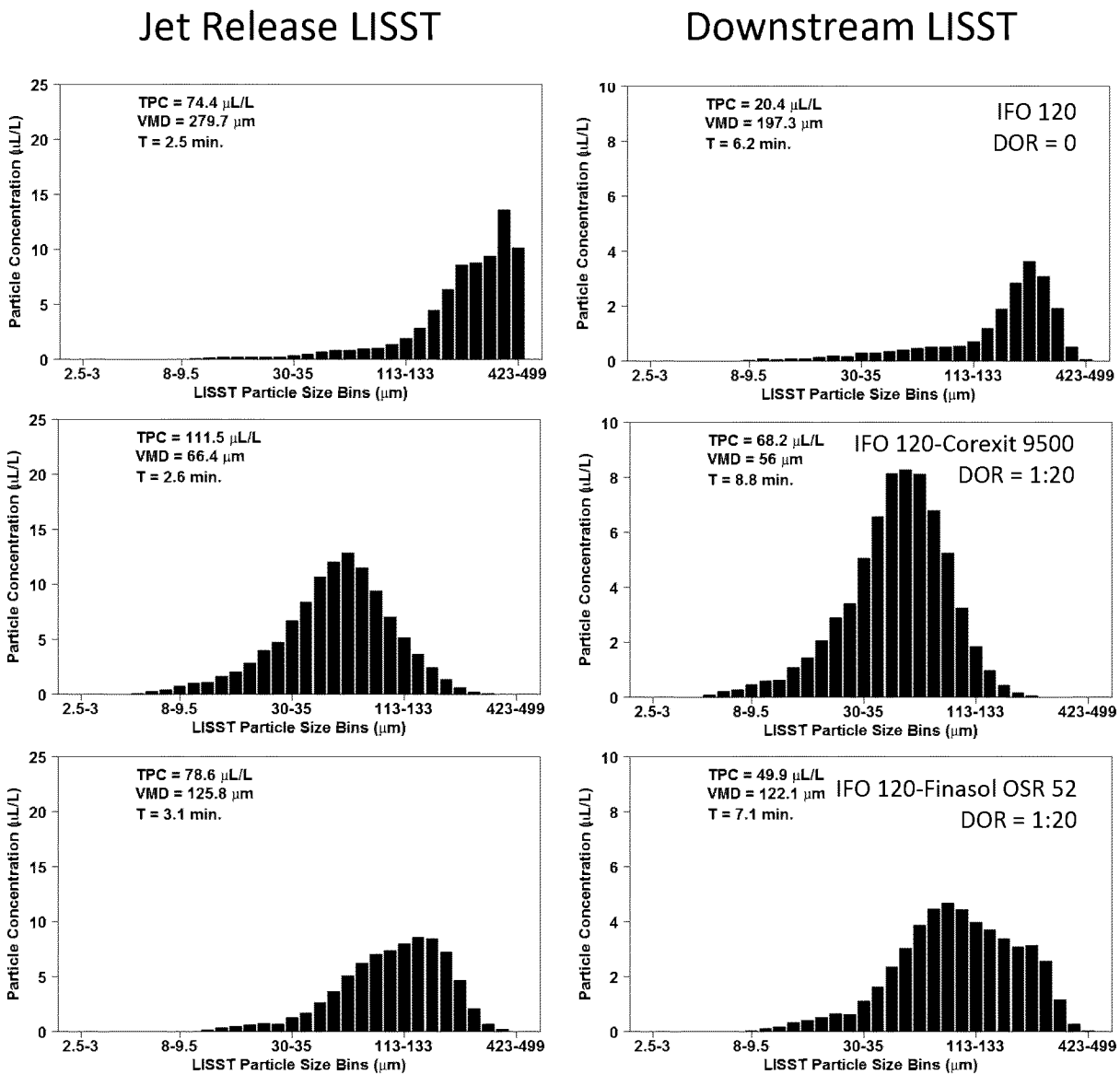

Figure 20. LISST DSD with TPC for IFO 120 with Corexit 9500 and Finasol OSR 52 treatments at warm temperatures. DOR = 0 (top panel); DOR = 1:20 experiments are middle and bottom panels.

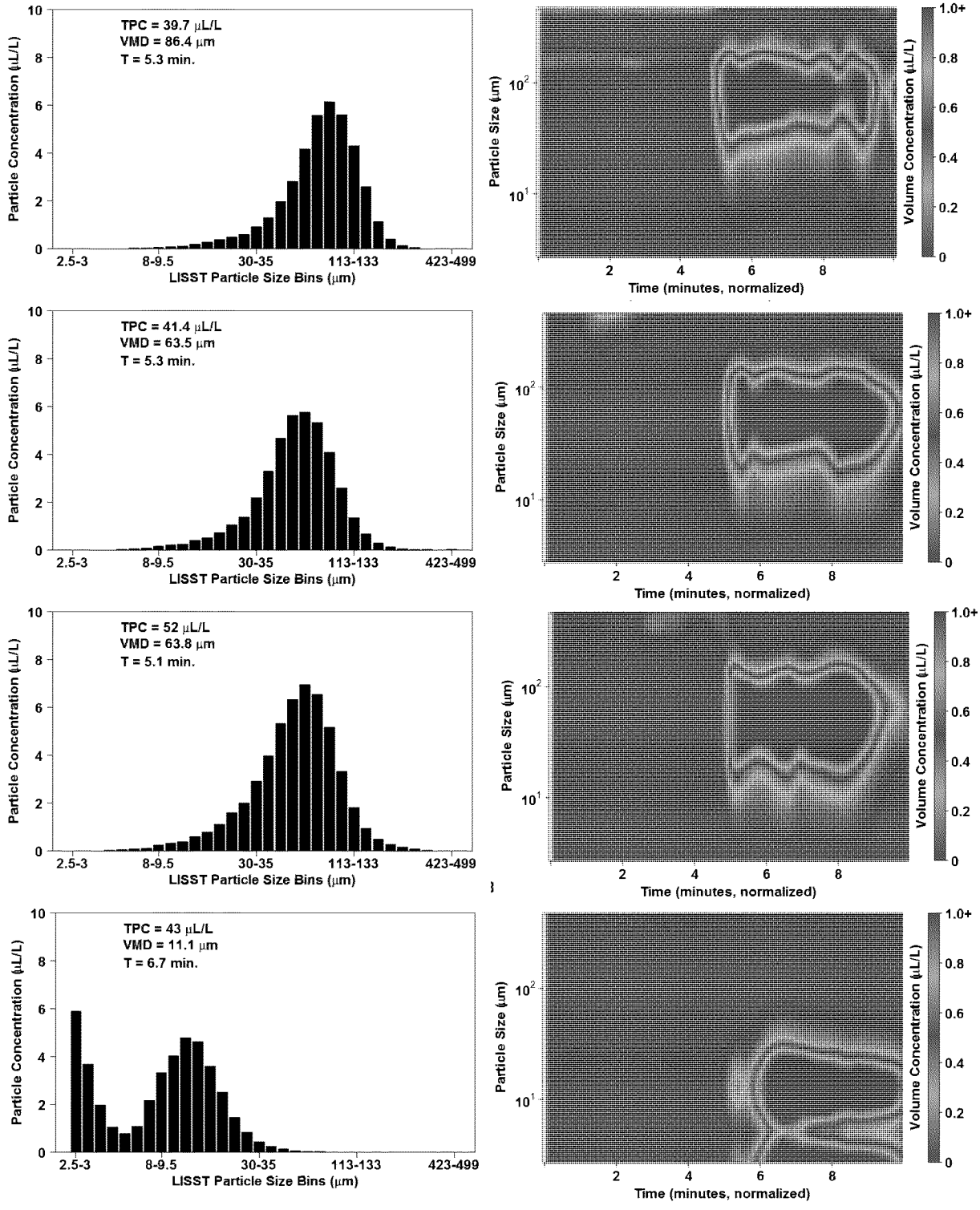

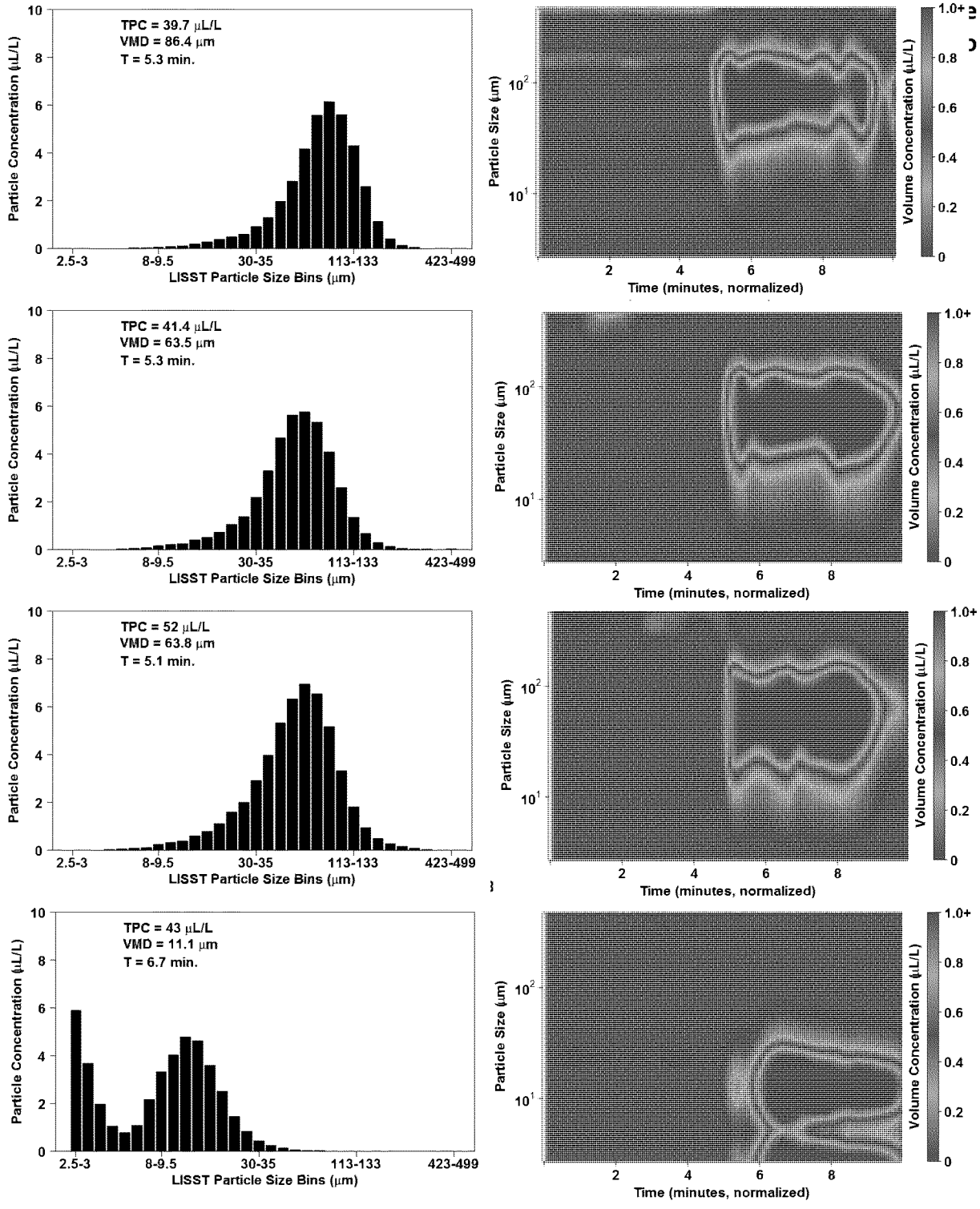

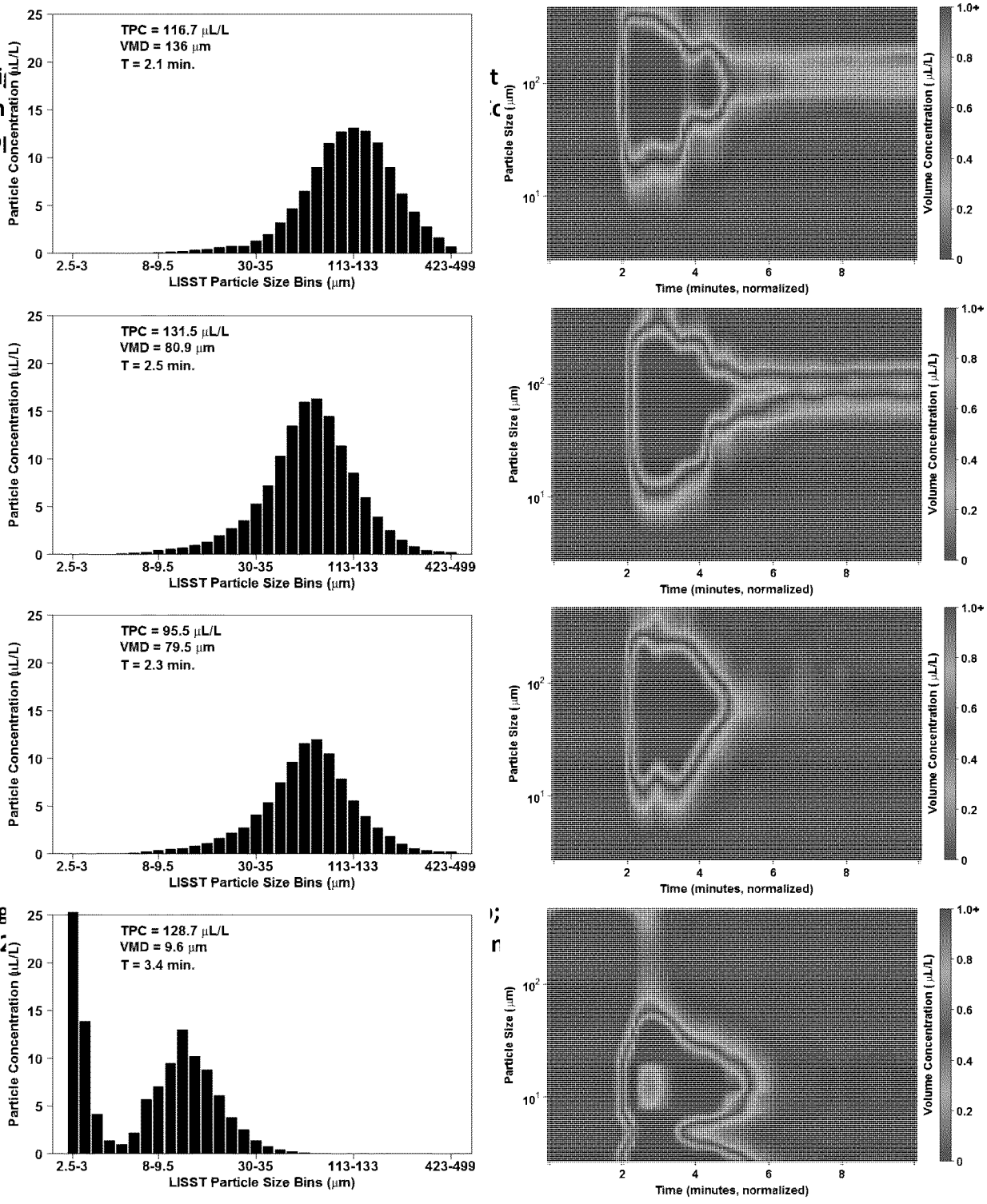

A.3.3 SLC Dispersion Effectiveness

Experiments involving South Louisiana Crude (SLC) oil treated with Corexit 9500 were conducted for warm water conditions (16.6 – 19.6 °C) to compare dispersion between ANS and SLC. Experiments with SLC yielded higher TPC values compared to ANS results, most likely the result of slightly larger amounts of oil added to the pressure canister (~25-50 g) due to the lower viscosity of SLC resulting in more oil injected by the injector, so comparisons shouldn't be made regarding TPC. The observed VMD of physically-dispersed SLC oil (neat; DOR = 0; ~123-148 µm) was found to be less than that of ANS (>200 µm). The addition of dispersant yielded a shift in DSD and VMD to smaller particles, where DOR = 1:200 and 1:100 exhibited diameters of ~91-108 µm, and DOR = 1:20 ranged between ~15 - 21 µm, as depicted in Figure 24. The Downstream LISST results indicate smaller droplet size as the plume moves through the tank (size fractionation) and a decrease in TPC (plume dilution), further demonstrating this trend for all oils (Figures 25 and 26). The fluorescence data indicates a strong signal with little scatter for up to 4 min in these treatments (Figure 27; Appendix E). Using these results, comparisons can be made to results of SLC with Corexit 9500 from surface plume simulations (oil released into tank via pour in from flask) from Conmy et al., 2014a (and unpublished data) from those experiments. No apparent differences between DSD and VMD for DOR = 0 treatments were found. For DOR = 1:20 VMD values are similar, however, the range of droplet diameters for surface simulations is larger with particles up to 200 µm. In subsurface injection jet experiments the range of diameters is narrower, where particles > 100 µm were not observed. This suggests that the combination of the chemical dispersant tested here, elevated turbulent mixing from the jet release and higher oil temperature of 80 °C yielded smaller droplets. To discern the dominant factor controlling the difference, additional testing would need to be conducted.

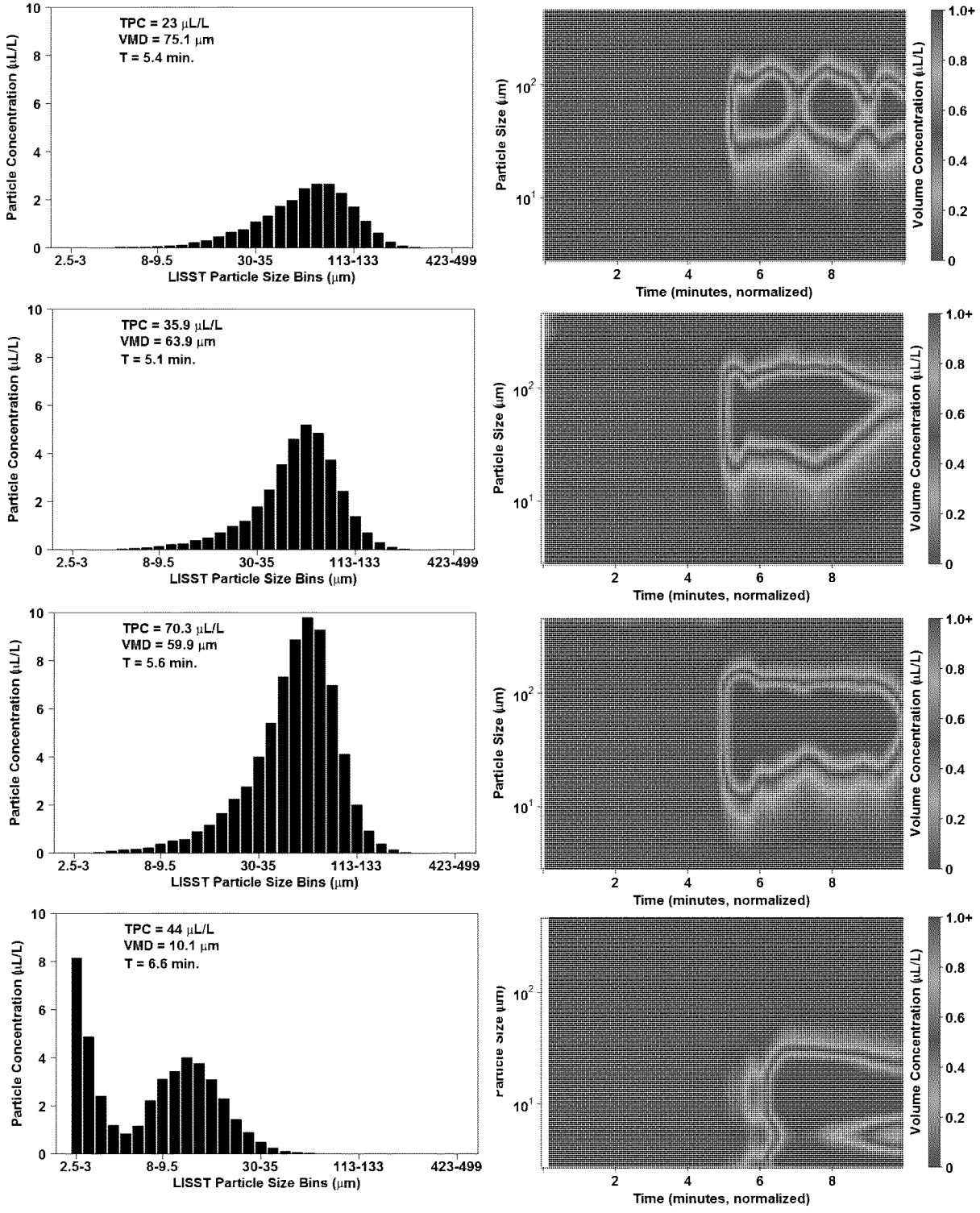
TPC = 23 µL/L
VMD = 75.1 µm
T = 5.4 min.
Particle Concentration (µL/L)
LISST Particle Size Bins (µm)
2.5-3
8-9.5
30-35
113-133
423-499
Particle Size (µm)
Time (minutes, normalized)
Volume Concentration (µL/L)
TPC = 35.9 µL/L
VMD = 63.9 µm
T = 5.1 min.
TPC = 70.3 µL/L
VMD = 59.9 µm
T = 5.6 min.
TPC = 44 µL/L
VMD = 10.1 µm
T = 6.6 min.

Fig
siz
DC

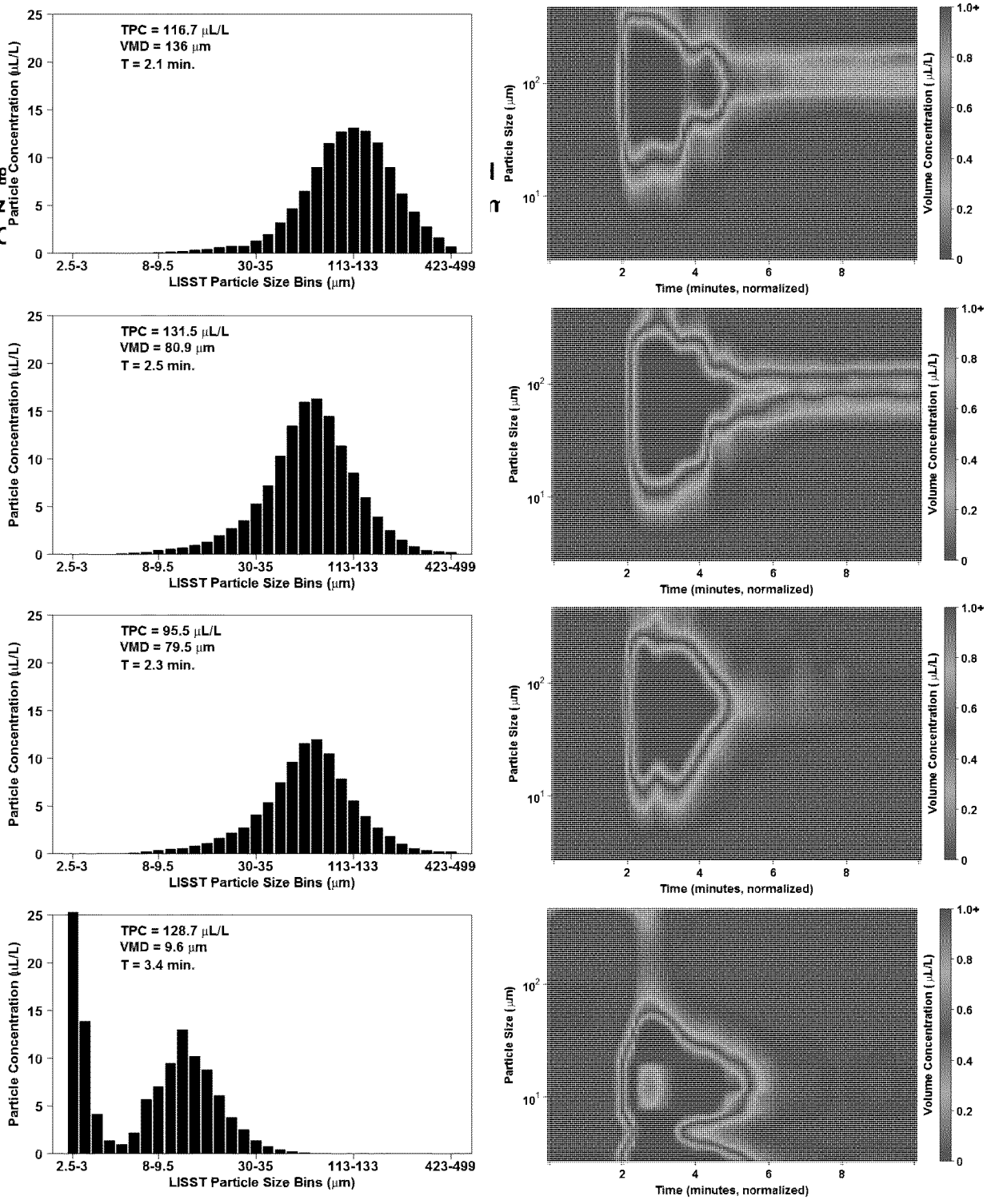
TPC = 116.7 µL/L
VMD = 136 µm
T = 2.1 min.
TPC = 131.5 µL/L
VMD = 80.9 µm
T = 2.5 min.
TPC = 95.5 µL/L
VMD = 79.5 µm
T = 2.3 min.
TPC = 128.7 µL/L
VMD = 9.6 µm
T = 3.4 min.
Particle Concentration (µL/L)
LISST Particle Size Bins (µm)
2.5-3
8-9.5
30-35
113-133
423-499
Particle Size (µm)
Time (minutes, normalized)
Volume Concentration (µL/L)

Figure 25. Downstream LISST DSD and VMD (left panels) and time series of concentration and particle size (right panels) for SLC and Corexit 9500 warm water treatments. From top to bottom, DOR = 0, 1:200, 1:100, 1:20.

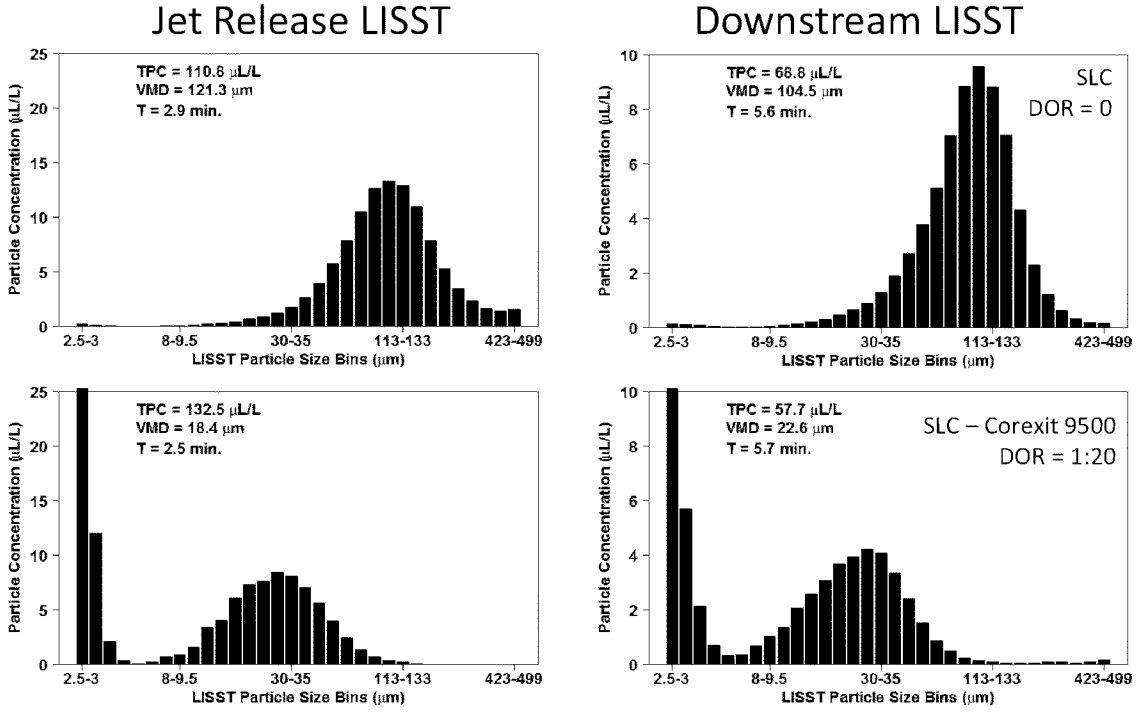

Figure 26. LISST DSD with TPC for SLC with Corexit 9500 treatments at warm temperatures. DOR = 0 (top panel); DOR = 1:20 experiments are bottom panels.

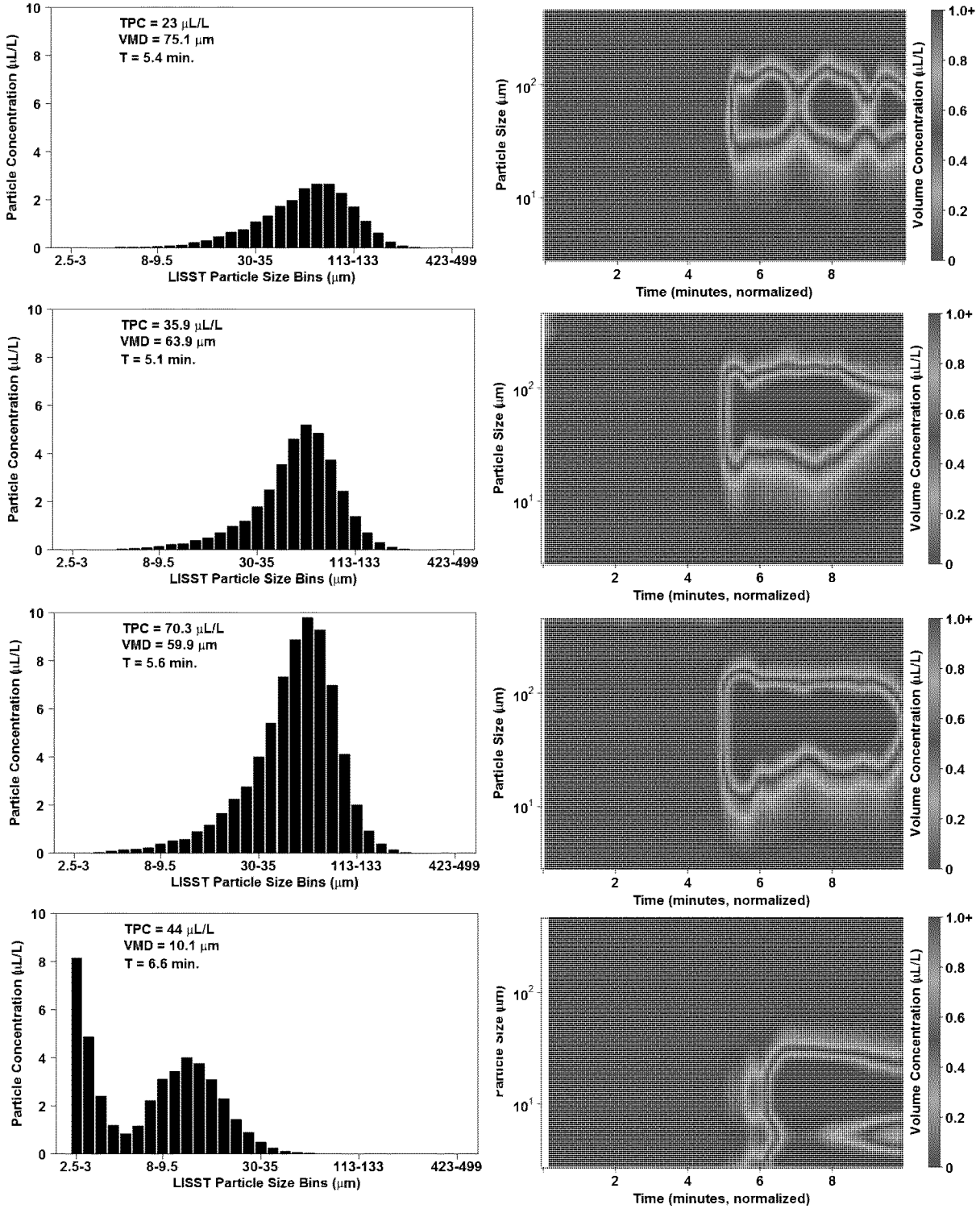

Figure 27. *In situ* submersible fluorescence time series of sub-injection plume of SLC and Corexit 9500 warm water treatments. From top to bottom, DOR = 0, 1:200, 1:100, 1:20.

A.3.4 Gas Condensate Dispersion Effectiveness

Injection experiments were conducted with Gas Condensate and Corexit 9500 for warm water conditions (10 – 12 °C temperature range) and DOR = 0 and 1:20 only. The Gas Condensate consisted of mostly C15 alkanes and lower PAHs (napthalene and alkylated derivatives. The VMD for Gas Condensate with no dispersant added ranged between ~150 – 215 µm (Figure 28). With the addition of dispersant, VMD for the triplicates were 60.4, 68.2 and 170.4 µm suggesting that dispersant at DOR = 1:20 shifts the DSD to smaller particles for most experiments. Large variability in the triplicates was observed, however at this time there is no clear explanation as to the cause. The corresponding fluorescence data for these treatments indicate a strong signal with little scatter for up to 3 min in both treatments (Figure 28; Appendix E).

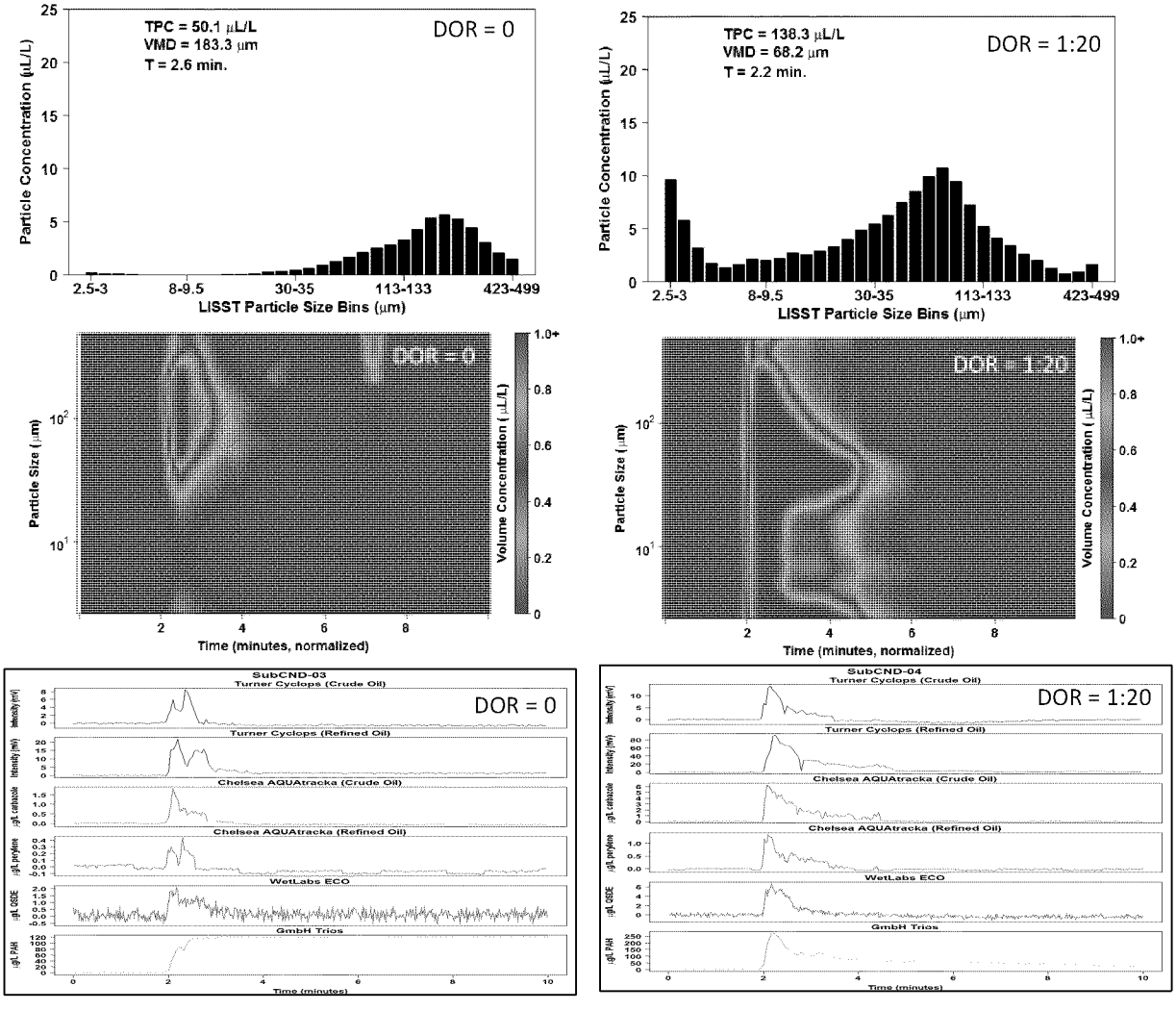

Figure 28. LISST DSD and VMD (top panels),time series of concentration and particle size

(middle panels), and fluorescence time series (bottom panels) for Gas Condensate and Corexit 9500 warm water treatments. Left panels are DOR = 0 and right panels are DOR = 1:20.

A.3.5 Tank Dilution Series Fluorescence Measurements

Submersible fluorescence results are presented in units recommended by manufacturers and using calibration factors provided by the manufacturers. Efforts were made to correlate the fluorescence intensity with TPH and / or BTEX concentration but were not possible due to issues inherent with the discrete sample collection. In order to fill bottles for chemical analysis, a 30 second time period was needed. Due to the short time period of the experiments and the heterogeneity of the plume concentration through time (evident from the fluorescence time series), oil concentrations within the bottles represent an average over a 30 second time period that cannot be aligned with the time series data, which are generated on the time scale of seconds. Given this fact, a dilution series within the tank using ANS was conducted to provide a calibration curve for fluorometers to a known concentration of oil in a homogeneous tank akin to Conmy et al., 2014a. Calibration regression results for all submersible fluorometers can be found in Figures 29 and 30 for TPH and BTEX, respectively and regression equations are tabulated in Table 5. Strong correlations between oil concentration and fluorescence intensity were observed, suggesting that fluorescence signal may serve as a proxy for TPH or BTEX at specific time points within the tank. This is an advantage as fluorescence intensity and oil droplet concentrations time series can therefore be calibrated and employed to provide for chemistry estimates that can be correlated with particle / oil droplet concentrations at fine time scales within the tank during experiments. For example, comparing the TPC and fluorescence signature for ANS with and without dispersant illustrates the differences in the oil droplet concentration and dissolved oil during injection experiments and the utility of monitoring both to understanding

plume dynamics (Figure 31).

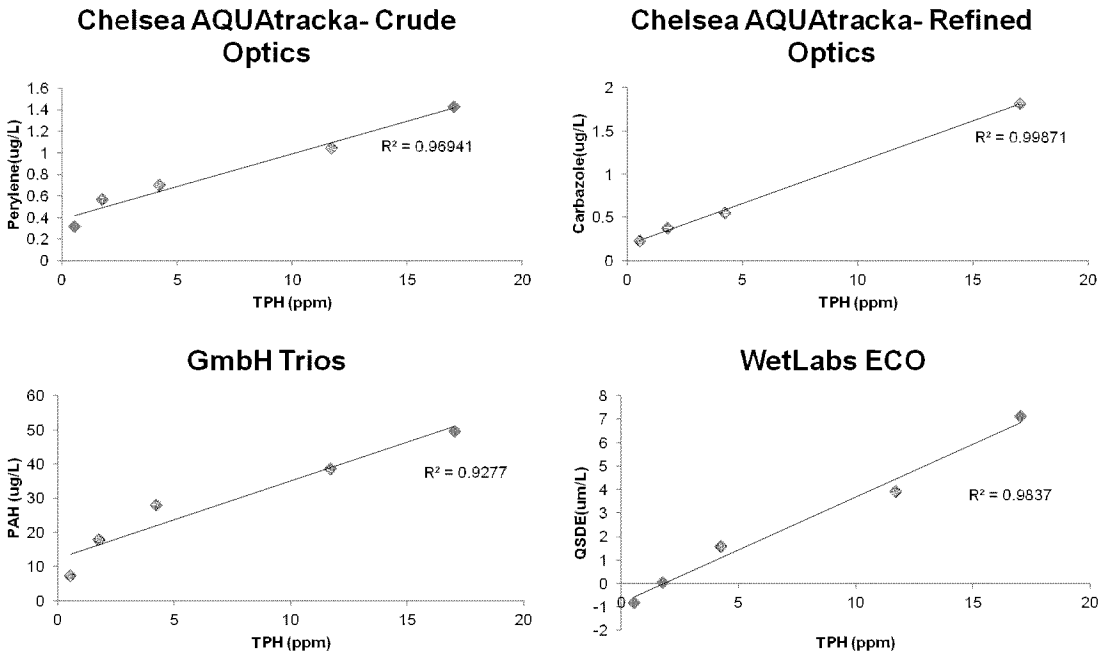

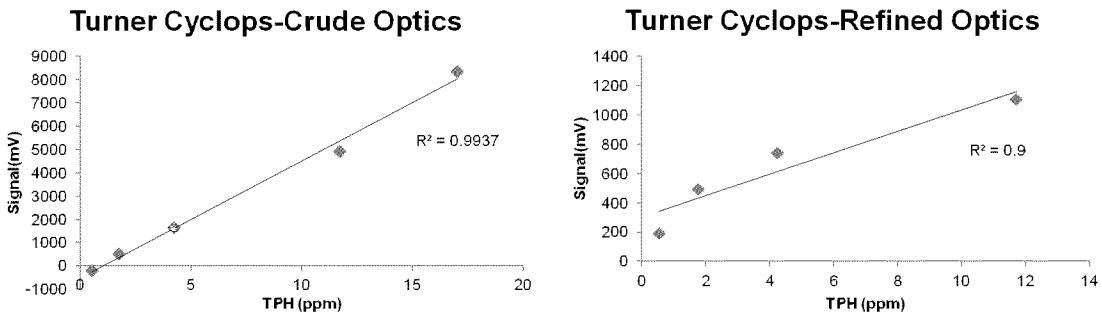

Figure 29. Calibration lines for fluorometer response vs TPH concentrations.

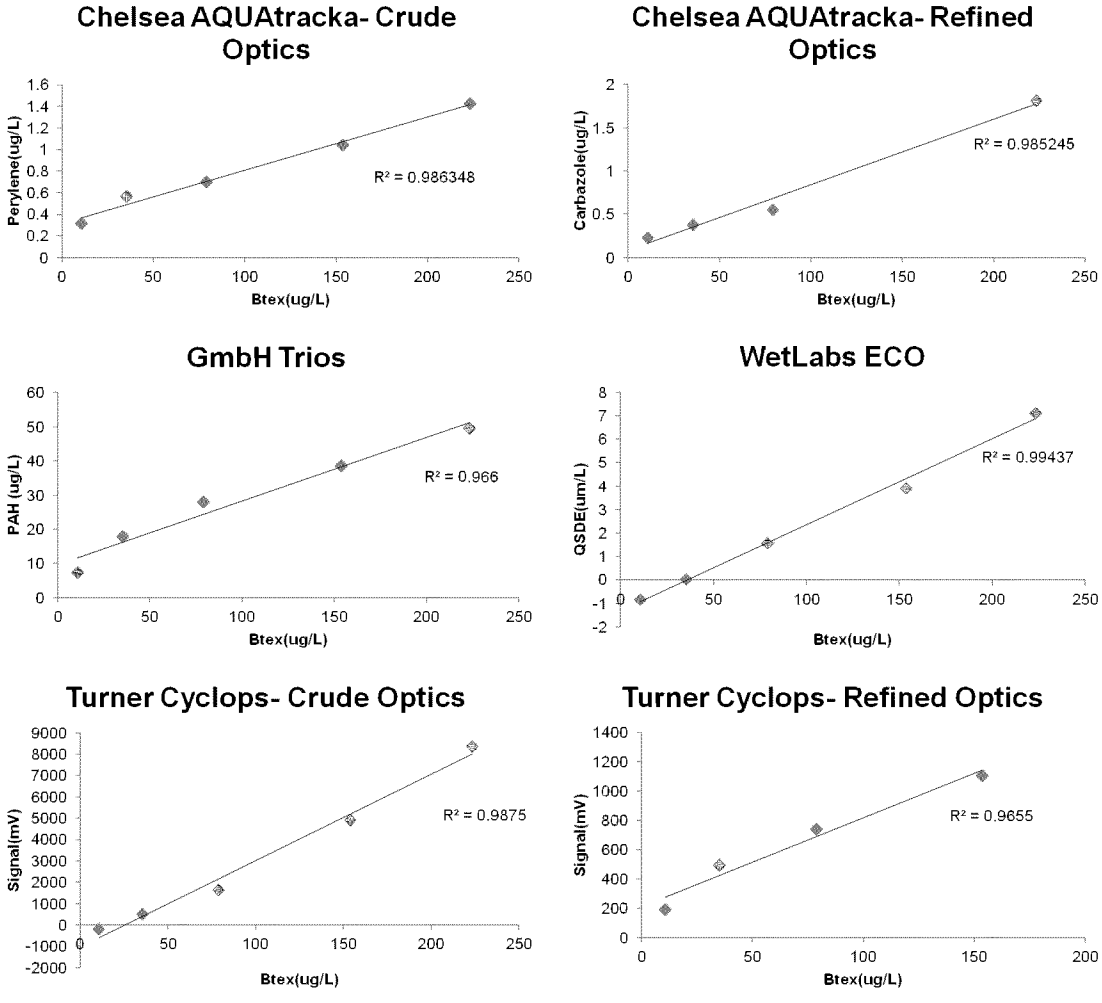

Figure 30. Calibration lines for fluorometer response vs BTEX concentrations.

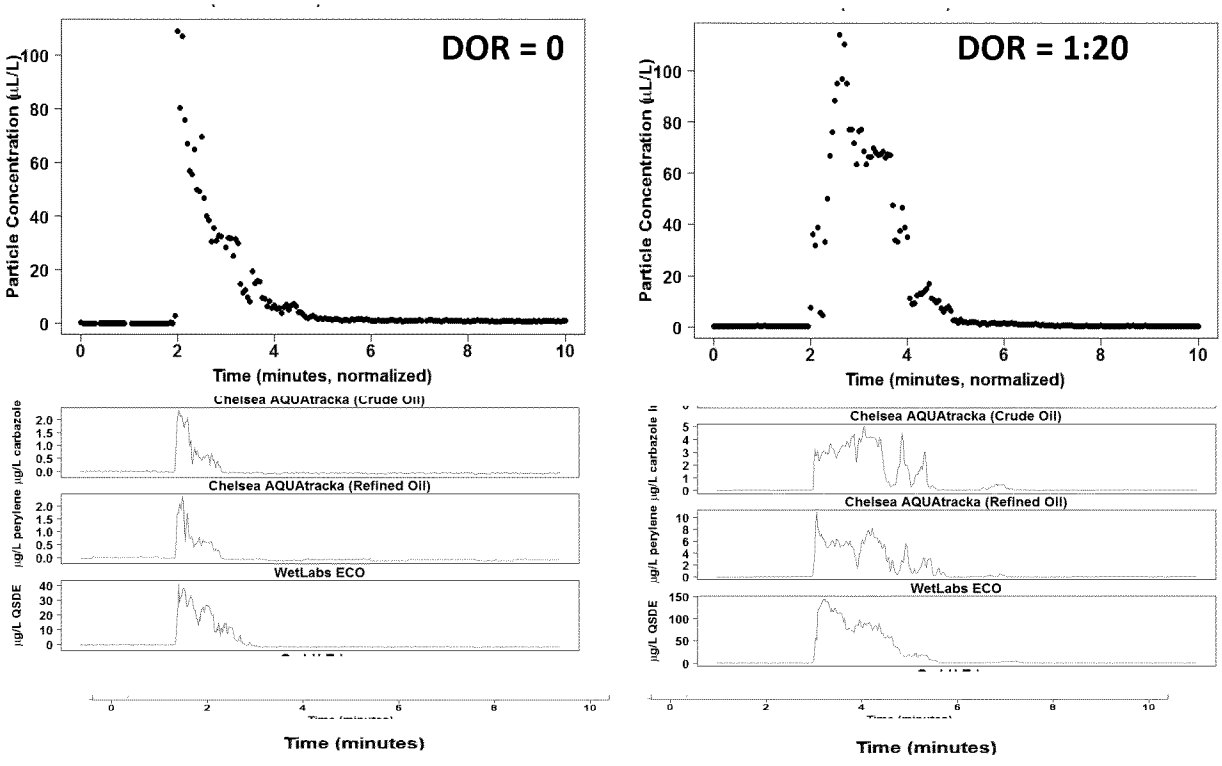
DOR = 0
Particle Concentration (µL/L)
Time (minutes, normalized)
Chelsea AQUAtracka (Crude Oil)
µg/L carbazole
Chelsea AQUAtracka (Refined Oil)
µg/L perylene
WetLabs ECO
µg/L QSDE
Time (minutes)
DOR = 1:20
Particle Concentration (µL/L)
Time (minutes, normalized)
Chelsea AQUAtracka (Crude Oil)
µg/L carbazole
Chelsea AQUAtracka (Refined Oil)
µg/L perylene
WetLabs ECO
µg/L QSDE
Time (minutes)

Figure 31. Total Particle Concentration and fluorescence time series for ANS crude oil with Corexit 9500 dispersant.

Table 5. Calibration equations for the submersible fluorometers. Data in this report have fluorescence signal in the manufacturer recommended units.

Instrument	Factory Calibration Standard (units)	TPH Calibration Equation	BTEX Calibration Equation
Chelsea Aquatracka (Crude Optics)	Perylene (ug/L)	[TPH] = ([Perylene]-0.3834)/0.06051	[BTEX] = ([Perylene]-0.3165)/0.004922
Chelsea Aquatracka (Refined Optics)	Carbazole (ug/L)	[TPH] = ([Carbazole]-0.1804)/0.09575	[BTEX] = ([Carbazole]-0.08487)/0.007584
GmbH Trios	PAH (ug/L)	[TPH] = ([PAH]-12.288)/2.2733	[BTEX] = ([PAH]-9.559)/0.1871
Turner Cyclops (Crude Optics)	Signal (mV)	[TPH] = (Signal+320.26)/503.94	[BTEX] = (Signal+1152.2)/42.429
Turner Cyclops (Refined Optics)	Signal (mV)	[TPH] = (Signal-299.29)/73.339	[BTEX] = (Signal-212.05)/6.0593
Wetlabs ECO	QSDE (uM/L)	[TPH] = (QSDE-0.2102)/0.4362	[BTEX] = (QSDE+0.5403)/0.03697

A.3.6 VOC Air Monitoring

For all experiments, the Volatile Organic Compounds (VOC) measurements exhibited higher variability compared to the in water sensor measurements. The installation of a wind curtain along the western side of the tank helped to reduce the prevailing winds coming directly off

the water, however the effects of wind were not completely eliminated. The observed variability is likely caused by differences in wind speed and direction both among the triplicate experiments (typically run on the same day), and among the different treatments (which were run over days/weeks). The VOC meters were installed with the air intakes pointing down and were 0.4 m above the water surface at the top edge of the tank. This positioning helped to reduce the effects of wind, given that the tank walls acted as an additional wind blocker.

Two VOC meters were deployed above the tank, but only results from the VOC meter closest to the oil release are presented here (Jet Release VOC meter; the VOC meter directly above the fluorometer rack). Results from the second VOC meter (Downstream VOC meter) installed 11.8 m farther downstream are more variable, both in concentrations between triplicate runs and in the time it takes for airborne VOC concentrations to reach the meter. In general, readings from the second meter showed a broader plume with a lower peak VOC concentration. Due to an instrument malfunction, approximately 17 experiments are missing data from the Downstream VOC meter. All results from the Jet Release VOC meter are presented in Figures 32-39. Note that the Y-axis scale differs depending on the oil type (20 ppm for IFO, 45 ppm for ANS & SLC, 250 ppm for Gas Condensate).

Of the four different hydrocarbon products tested, experiments using the gas condensate exhibited the highest surface VOC concentrations, followed by ANS and SLC which exhibited similar values. The lowest concentrations were observed for IFO 120 experiments. Higher concentrations of VOC in the air were usually accompanied by lower BTEX concentrations in the water for each oil type (analytical chemistry results in Appendix B). Chemistry results from the water column (effluent, listed in Appendix B tables) samples help to verify the findings from the VOC meters. In general, the measured concentrations of BTEX in the effluent water samples were higher for experiments using dispersant compared to the untreated experiments. The effluent port in the flume tank during normal operation produces a depth integrated water sample which does not draw off the water surface. Therefore, oil that rises to the surface is not drawn into the effluent, and so the tank effluent

can be used as a measure of how much oil was dispersed into the water column. Regardless of the oil product tested, the use of chemical dispersants resulted in a reduction in VOC concentrations in the air above the water compared to corresponding experiments without dispersant. These results comparing the mean maximum VOC concentrations (30 second before/after peak readings) measured during each experiment are summarized in Table 6. A general trend was also observed where increasing the DOR resulted in lower surface VOC concentrations near the jet release location. Statistical analysis using ANOVA followed by confidence interval test (Tukey's test) to compare the means found that there were significant differences between VOC readings for ANS at a DOR of 1:20 versus no dispersant (both Corexit and Finasol), as well as significant differences for SLC at a DOR of 1:20 versus no dispersant and DOR 1:100 and 1:200. Caution should be used when extrapolating these results to other spill scenarios, given that this was a shallow water tank so the effects of dissolution of VOCs from oil droplets in a deepwater blowout would not be accounted for in these experiments. Due to wind effects mentioned previously, trends in VOC concentrations above the plume further down the tank could not be established. Further, wind conditions may have contributed to the observed variability in the measurements. The effects of wind on the dilution and transport of VOCs should also be considered during a real world spill scenario, and so the absolute values of VOC concentrations measured in this study should only be used to compare the relative differences between treatments, and should not be used as a guide for worker exposure. Caution must be exercised however in that these results merely represent VOCs that make it to the air-sea interface from a very shallow wave tank. They cannot simulate the dissolution of VOCs into water that would be expected in a deep water column.

Table 6. Summary of maximum VOC concentrations at the various treatment conditions tested in this study. Results are for only for warm water experiments.

	Avg. Peak VOC Concentration (ppm), n = 3				ANOVA
Oil Type	No Dispersant	DOR 1:200	DOR 1:100	DOR 1:20	p-value, α = 0.05
ANS (Corexit 9500)	23.07	13.27	12.43	0.13	0.023
ANS (Finasol OSR 52)	23.07	16.56	7.17	2.9	0.024
IFO 120	1.00	0.90	7.37	0.17	0.133
Condensate	121.23	--	--	19.73	0.152
SLC	28.53	27.5	16.75	1.53	0.001

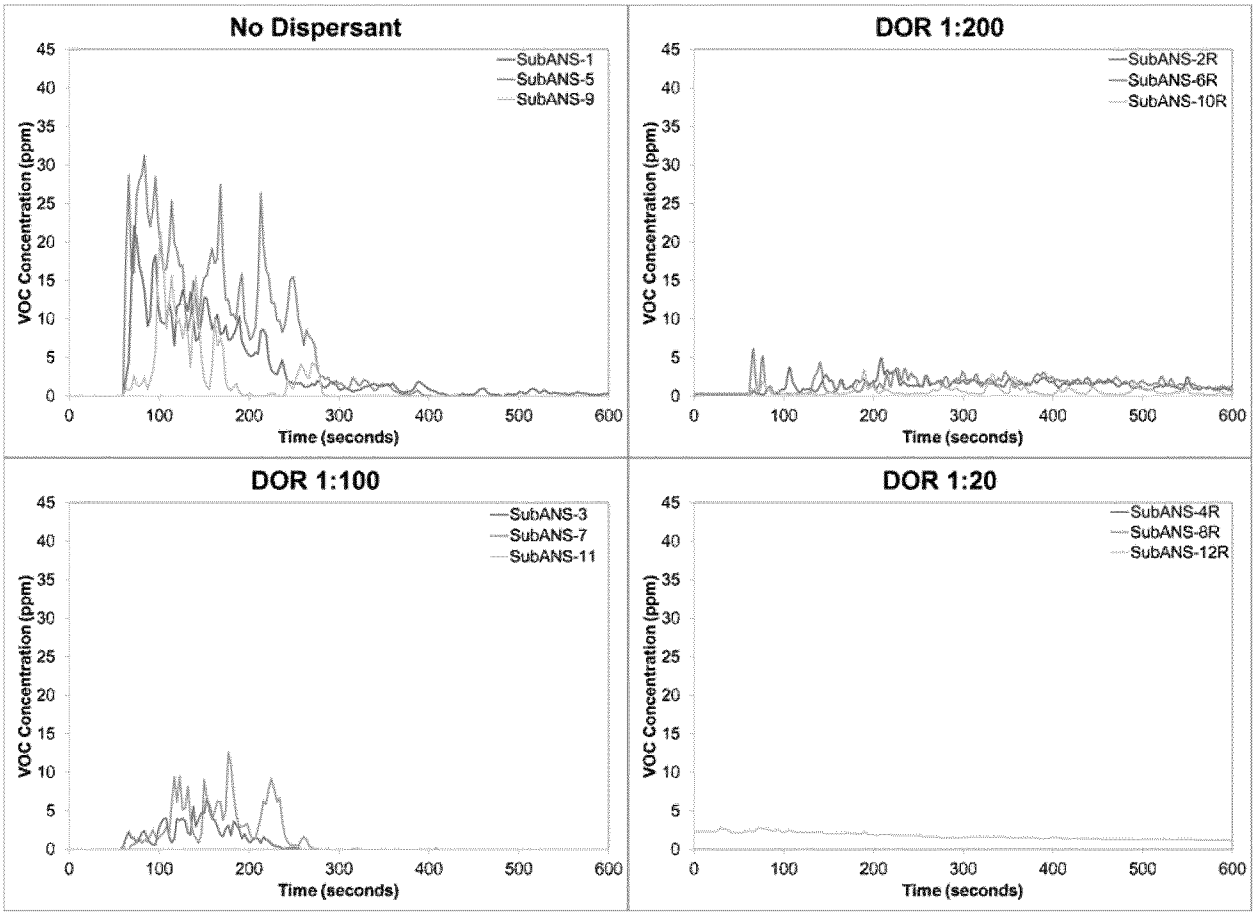

Figure 32. VOC results for subsurface injection experiments (cold water season) using Alaska North Slope crude oil and four treatment conditions (no dispersant, DOR 1:200, DOR 1:100, DOR 1:20). Replicate treatments represented by light blue, dark blue and green colored lines.

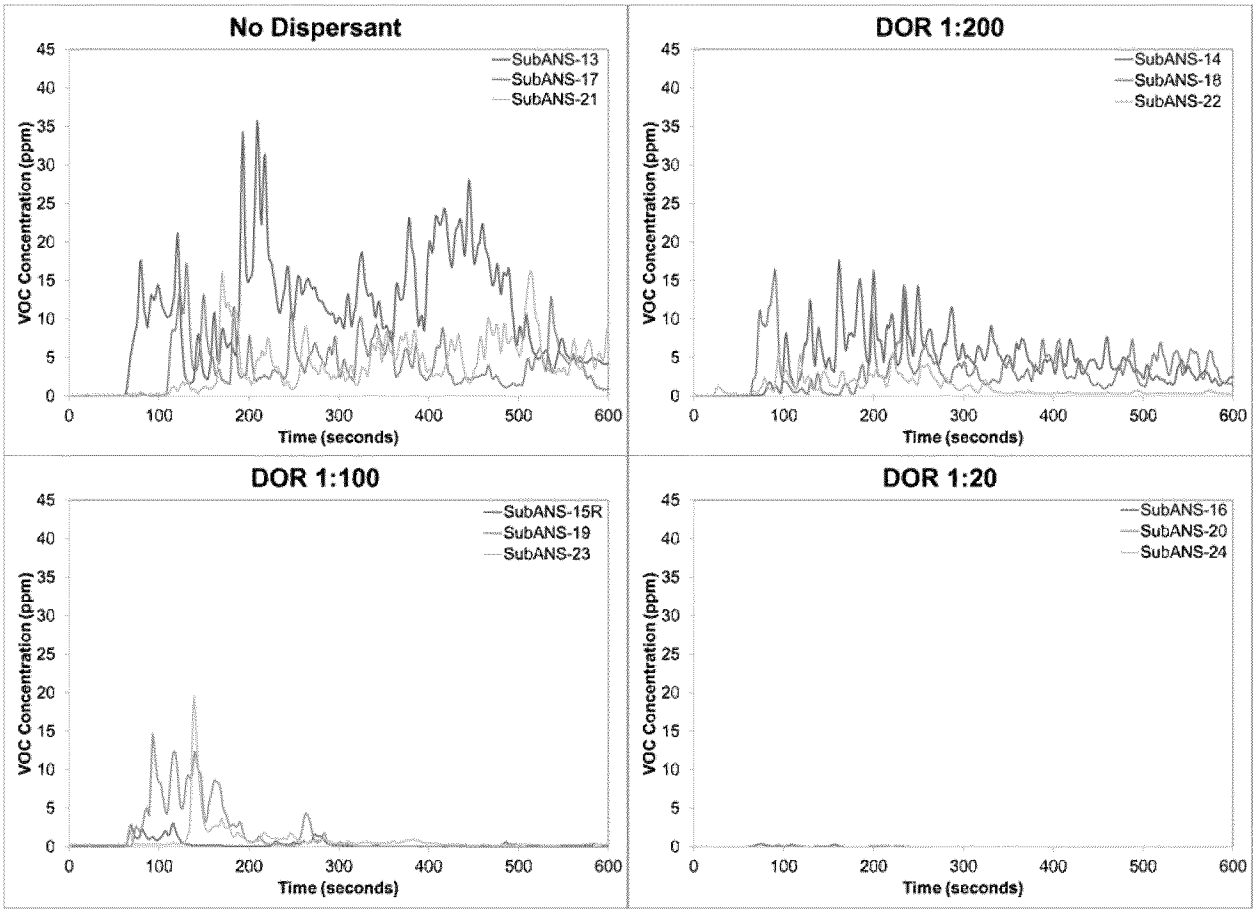

Figure 33. VOC results for subsurface injection experiments (warm water season) using Alaska North Slope crude oil and four treatment conditions (no dispersant, DOR 1:200, DOR 1:100, DOR 1:20). Corexit 9500 was used as the treating agent. Replicate treatments represented by light blue, dark blue and green colored lines.

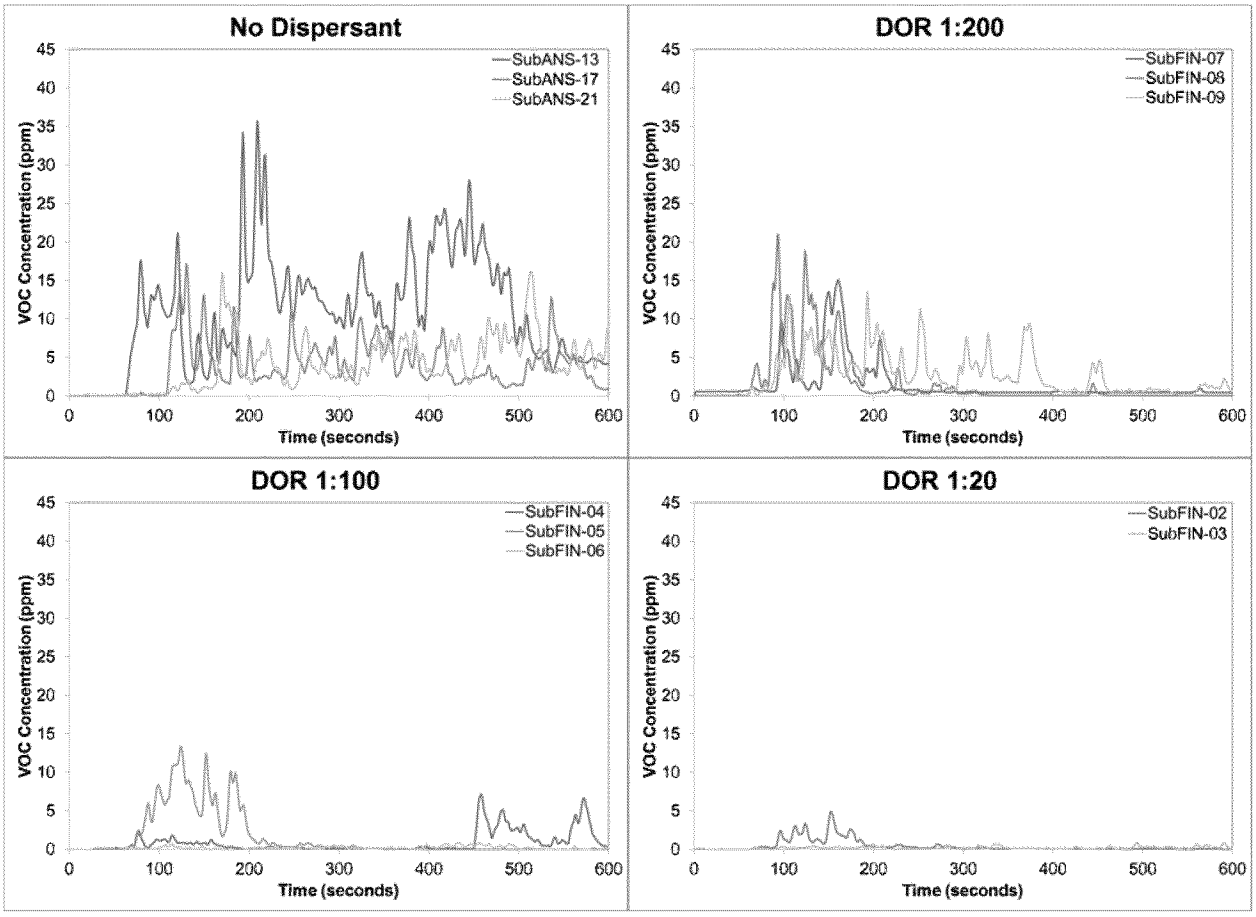

Figure 34. VOC results for subsurface injection experiments (warm water season) using Alaska North Slope crude oil and four treatment conditions (no dispersant, DOR 1:200, DOR 1:100, DOR 1:20). Finasol OSR 52 was used as the treating agent. Replicate treatments represented by light blue, dark blue and green colored lines.

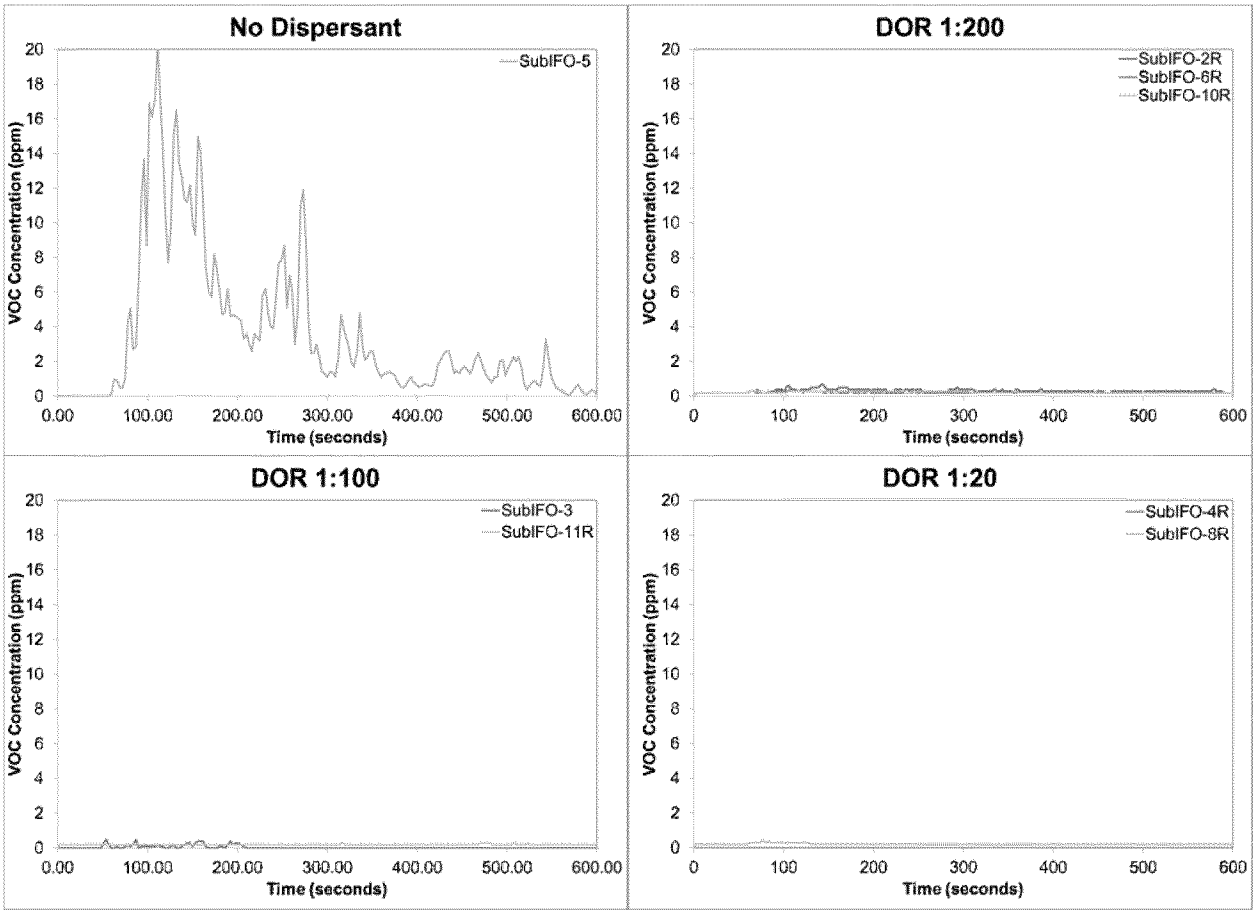

Figure 35. VOC results for subsurface injection experiments (cold water season) using IFO 120 and four treatment conditions (no dispersant, DOR 1:200, DOR 1:100, DOR 1:20). Corexit 9500 was used as the treating agent. Replicate treatments represented by light blue, dark blue and green colored lines.

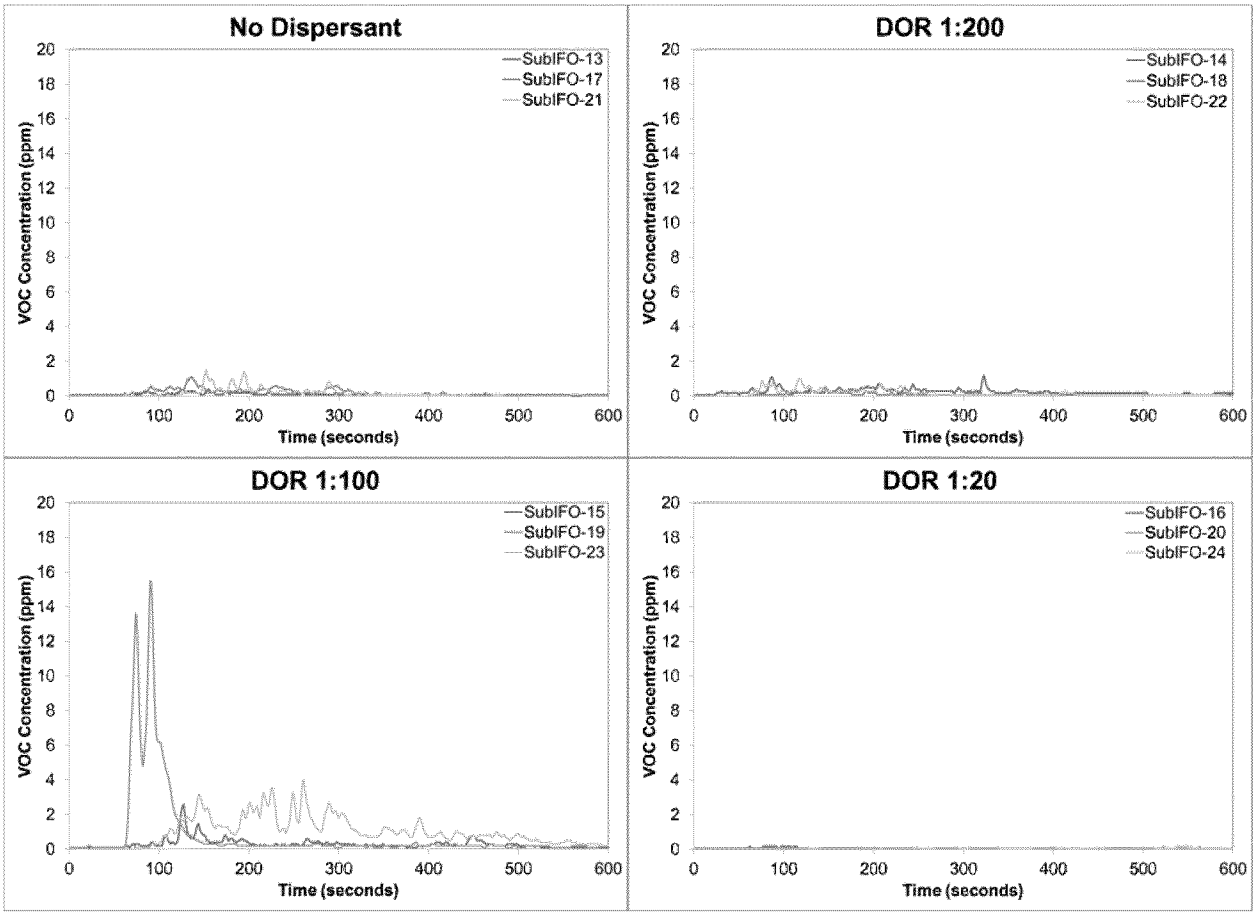

Figure 36. VOC results for subsurface injection experiments (warm water season) using IFO 120 and four treatment conditions (no dispersant, DOR 1:200, DOR 1:100, DOR 1:20). Corexit 9500 was used as the treating agent. Replicate treatments represented by light blue, dark blue and green colored lines.

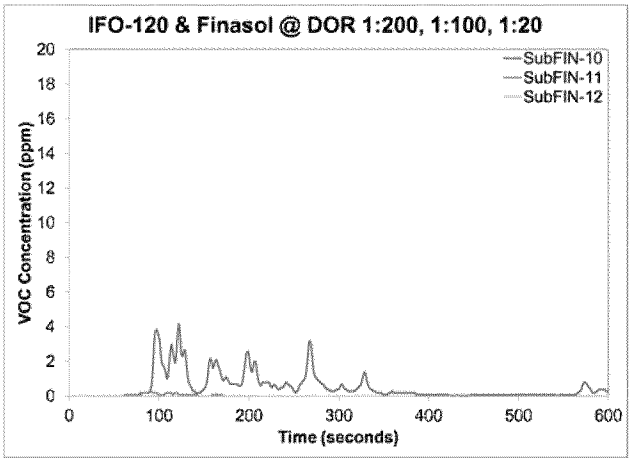

Figure 37. VOC results for subsurface injection experiments (warm water season) using IFO 120 and three treatment conditions (DOR 1:200, DOR 1:100, DOR 1:20). Finasol OSR 52 was used as the treating agent (note – these treatments were not tested in triplicate).

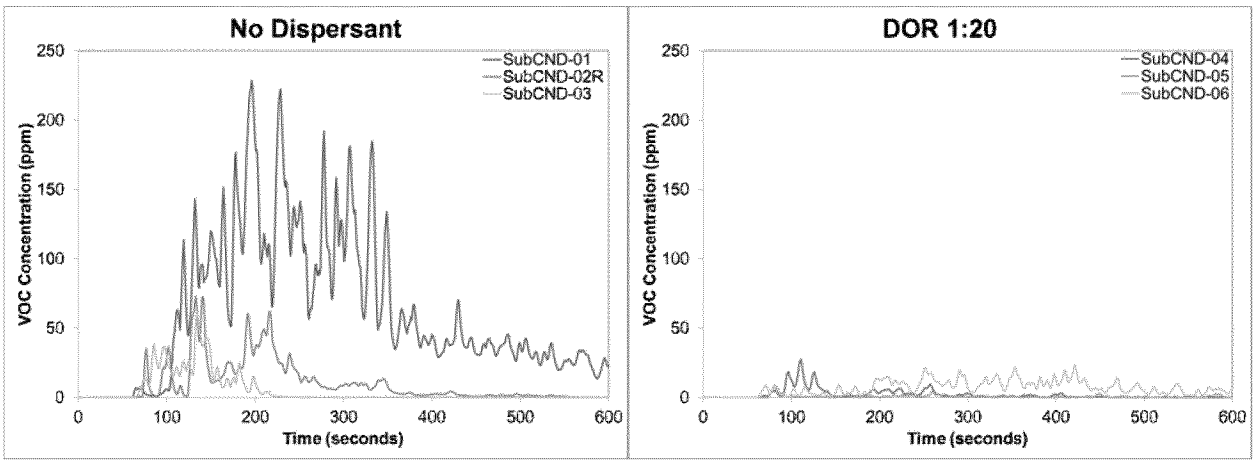

Figure 38. VOC results for subsurface injection experiments using gas condensate and two treatment conditions (no dispersant, DOR 1:20). Corexit 9500 was used as the treating agent.

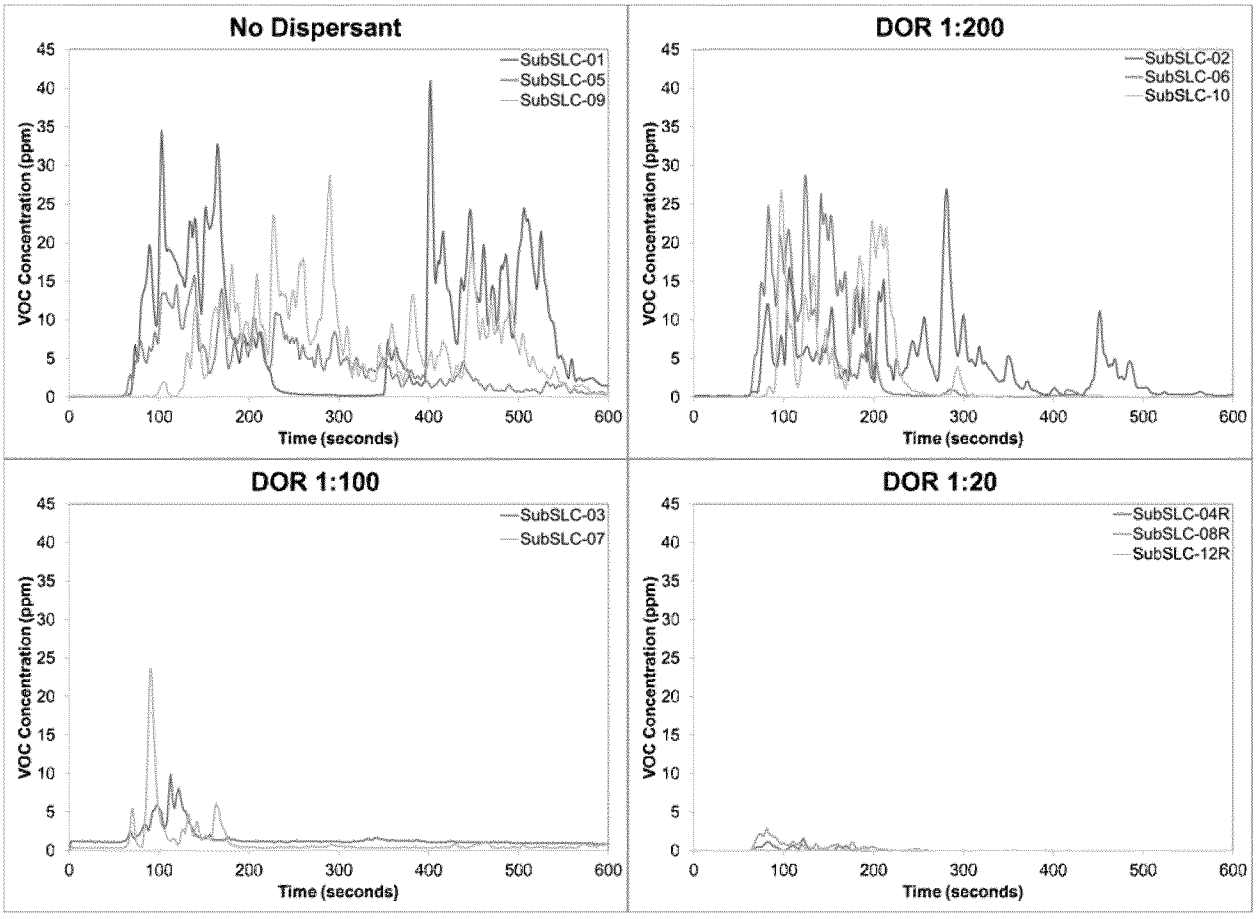

Figure 39. VOC results for subsurface injection experiments using Sweet Louisiana Crude oil and four treatment conditions (no dispersant, DOR 1:200, DOR 1:100, DOR 1:20). Corexit 9500 was used as the treating agent.

A.3.7 VDROP-J and JETLAG Numerical Plume Modeling

Refer to Appendix G for detailed summary of the VROP-J and JETLAG numerical modeling component along with figures. Modeling the movement of oil released underwater is a challenging task due to limitations in measuring hydrodynamics in an oil-water system. Computational Fluid Dynamics (CFD) models are capable of reproducing the hydrodynamics provided they have sufficient resolution. However, current CFD models cannot predict the droplet size distribution. For this reason, we used a suite of programs to understand jet hydrodynamics, the droplet size distribution, and the movement of oil droplets within the jet/plume. The developed models were calibrated to experimental data of oil jet released underwater in the BIO tank. Based on the properties of the jet (mass flow rate 3.8 L/min through a 2.4 mm orifice), the regime of the jet is atomization, which indicates that the jet would break into small droplets. The models VDROP-J and JETLAG were used to predict the streamwise centerline velocity and the holdup (volume of oil divided by the total volume of fluids in a control volume) along the centerline of the plume, where both models were in agreement. This implies that VDROP-J is adequate to predict the average droplet size distribution in the plume. In the absence of dispersant, the model VDROP-J predicted oil DSD that is very close to that measured by the LISST instrument. However, In the presence of dispersant premixed with the oil, the VDROP-J model captured the overall trend of the DSD, but could not capture the peak in droplet concentration observed at 5 μm. The observed peak is most likely due to tip-streaming (when at high DORs, oil droplets shed filaments from their edges resulting in smaller droplets), and VDROP-J does not have such a module at this time but is considered for future development.

The computational fluid dynamics (CFD) program Fluent (www.ansys.com) was used to model the hydrodynamics of the horizontal jet experiments. The standard $k-\varepsilon$ model was used to model turbulence, and the Volume of Fluid (VOF) was used to model the two phases (oil and water). The profiles of the holdup (ratio of oil volume to total volume), velocity magnitude, eddy diffusivity and turbulent dissipation rate were presented. Findings indicate that the holdup drops sharply with distance from the source to a few percent within 0.50 m from the source, suggesting the occurrence of water entrainment into the plume. A

significant reduction in the energy dissipation rate was also observed, by orders of magnitude along the centerline, starting from 10^4 watt/kg to 10^{-4} watt/kg. Both holdup and energy dissipation values have important consequences on oil droplet breakup and coalescence. The plume exhibited a core of high velocity and high mixing, while the edge of the plume had more or less violent conditions, which is probably due to the entrained water squishing the edges of the plume. The velocity and eddy diffusivity are needed to predict the movement of individual oil droplets. The shape of the plume was circular near the orifice, but became oblate horizontally at a centerline distance of 2.0 m, which is due to both the buoyancy of the whole plume and its inertia. This suggests that the narrow width of the tank (0.60 m) did not affect the jet hydrodynamics (otherwise the jet would be elongated in the vertical). The width of the tank had an effect on the jet dynamics only near the surface as the plume became elongated along the tank near the surface.

The CFD approach has its limitations as it smooths out the edge of the oil jet/plume, and thus does not allow for the formation of large eddies around the plume. Here, large eddy simulations (LES) were used to capture the large eddies where the movement of individual oil droplets employed a lagrangian approach. Water velocity and the eddy diffusivity were used to transport oil droplets, and the effect of individual oil droplet buoyancy and inertia were accounted for. Accounting for the inertia of oil droplets has not been done previously in the oil spill literature. Neglecting the inertia of the droplets results in overestimates of their rise rate as the inertia from a horizontal jet tends to propel the droplet more horizontally, and thus their rise gets delayed also by turbulent mixing. Results suggest that oil droplets with a diameter less than 100 µm would mix uniformly in the plume, while those close to 500 µm would tend to be above the centerline of the plume. This indicates that, when measuring the droplet size distribution using the LISST, the placement of the LISST would not affect the reading of droplets that are less than 100 microns. But the LISST needs to be placed judicially to capture particles that are 300 to 500 µm, otherwise LISST placement below the centerline would underestimate the actual droplets in that range. In contrast, LISST placement above the centerline does not allow for determining that the concentration values represent the whole cross section of the plume.

A.3.8 Weber Number Scaling Numerical Plume Modeling

Refer to Appendix H for detailed summary of the Weber Number Scaling numerical modeling component. During the Deepwater Horizon oil spill, modeling activities for predicting oil droplet size distribution formed in subsea oil blowouts was critical given their direct influence on the fate and transport of oil in the marine environment. The scientific community's knowledge on droplet size distributions and our capability to predict the distributions are still limited. A recent and promising approach for predicting DSD is the Modified Weber Number approach developed by SINTEF. Thus far, this method has been based on experimental results, validated by a light crude oil (Oseberg Blend crude oil). Here, this approach is validated over a range of oil types (IFO 120 and ANS) using a series of experiments conducted with a subsurface release of oil within the DFO horizontal flow tank.

Based on the measured droplet sizes obtained from the tank experiments, corresponding median droplet diameters (d_{50}) and the relative droplet size (d_{50}/D) were calculated, where D is the nozzle diameter. Accordingly, the relations between d_{50}/D and modified Weber number, Reynolds number, and oil concentration were quantified. With regression analyses, the empirical coefficients for the prediction of droplets size distribution based on the modified Weber number were determined for a certain type of oil (e.g., IFO 120 and ANS). The results indicated that chemical dispersants play an important role in reducing the droplet size of ANS in both cold and warm temperatures. The effectiveness of dispersant in reducing droplet size is higher for ANS compared to IFO 120. There may be thresholds for the dose of chemical dispersant to some oils (e.g., IFO 120) but further data analyses are needed to confirm this. There may also be over dose of dispersant to some oils (e.g., ANS) when the DOR is high, eventually affecting the droplet size distribution. Furthermore, the data indicate that the distributions of the data with $d/d_{50} <= 1$ and $d/d_{50} > 1$ are significantly varied. Therefore, a two-step Rosin-Rammler approach was introduced to more accurately predict the droplet size distribution. The regression coefficients for the two-step Rosin-Rammler are higher compared to the single step in most cases (Appendix H), indicating the advantage of the proposed two-step Rosin-Rammler approach. It should also be noted that the measured

interfacial tension (IFT) for the IFO 120 and ANS with different DORs appear to be significantly different compared to the measured results from SINTEF for the modified Weber number approach, possibly due to the characteristics of different oils.

Task B.1 Introduction & Relevance

BSEE's *Remote Sensing & Surveillance of Oil Spills* broad agency announcement that funded this work states that "In remote sensing, a sensor other than human vision or conventional photography is used to detect or map oil spills." Thus, although certain remote sensing of oil spills is traditionally linked to detection of oil on the sea surface from above, the scope of the technology can be extended to include the detection of oil in the deep-sea and/or under-the-ice conditions using various sensors, as responders cannot use vision within the water column. As demonstrated during the 2010 Gulf of Mexico Deepwater Horizon (DWH) oil spill, oil detection by fluorescence can enable responders to discern trajectory of plumes and assess effectiveness of dispersant countermeasures (ACT, 2008; Joint Analysis Group Report, 2010). The information gained from such technologies was used to track oil in the water column and inform response strategies to protect natural resources potentially at risk; thus supporting both Net Environmental Benefit Analyses (NEBA) and Natural Resource Damage Assessments (NRDA). To advance the application of this methodology, this project evaluated fluorescence characteristics of various oils with and without dispersants to aid in the selection and refinement of *in situ* sensors for use in oil spill response operations.

The overall objective of this work was to translate oil fluorescence R&D into operational tools for oil spill response. Tabulating information on the optimum fluorescence wavelengths for oil detection as a function of oil type and DOR assists responders selecting sensors and establishing Best Practices for rapid decision making during spill response. The results of this project are timely and can be used in conjunction with the National Response Team (NRT) guidance document, Environmental Monitoring for Atypical Dispersant Operations: Including Guidance for Subsea Application and Prolonged Surface Application, for incident-specific decisions concerning monitoring subsea dispersant use (www.nrt.org). It specifically calls upon using oil-specific submersible fluorometers with laboratory and on-board ship analyses using fixed wavelength and scanning spectrofluorometers to enable improvements to monitoring sampling during dispersant application. Findings from this project provide additional scientific

information in support of implementing guidance recommendations.

Fluorescence characteristics - All fluorophores (molecules that fluoresce) have characteristic wavelengths for maximum absorption of light and characteristic wavelengths at which they emit light as fluorescence. Absorption and fluorescence can occur at either narrow or wide wavelength ranges depending on the chemistry and complexity of the fluorophores. A variety of naturally occurring fluorescent compounds occur in the ocean, from ones with narrow wavelength ranges with sharp fluorescence peak maxima (pigments, proteins) to complex compounds with wide diffuse peaks over long wavelength ranges, such as the ubiquitous Colored Dissolved Organic Matter (CDOM) or petroleum oils.

Fluorescence characteristics of complex mixtures can overlap if structurally similar compounds are shared. Such is the case with CDOM and the aromatic fraction of crude oils. Both are comprised of a variety of organic molecules and both exhibit complex, three-dimensional EEM spectra. In general, crude oils have a broad excitation peak centered in the ultraviolet spectrum (< 300 nm) and two emission peaks, one centered in the ultraviolet spectrum around 340 nm and a much larger and broader peak in the visible around 445 nm (Bugden et al., 2008). These peaks result from the single ring benzene derivatives and the "polynuclear aromatic" fraction that are particularly susceptible to UV excitation wavelengths. EEMs exhibit distinct fingerprints for different oils as illustrated by previous studies (Bugden et al., 2008; Kepkay et al., 2008).

DWH in situ oil fluorescence - Deployment of submersible fluorometers during the DWH oil spill response illustrated the utility of this forensic tool that enabled large-scale monitoring of oil concentrations to a depth of approximately 1600 m. Co-deployment of the fluorometers alongside other response sensors [Conductivity-Temperature-Depth (CTD), Dissolved Oxygen (DO), Laser *In-Situ* Scattering and Transmissometry (LISST)] from multiple platforms (e.g. profilers) with real-time capabilities improved our understanding of the processes influencing the fate and behavior of the oil in the presence and absence of chemical dispersants. Added to this, extensive water column sampling also involved discrete sample collection for oil particle concentration and size, Total Petroleum Hydrocarbons (TPH), Volatile Organic Carbon (VOC)

and other physical, chemical, biological factors. To date, the in-depth reviews by the Joint Analysis Group (JAG) charged with data analysis have found that of all the variables measured, the most highly correlated in the subsea plume are *in situ* DO and oil fluorescence intensity (Joint Analysis Group Report, 2010). Such a correlation is not unexpected as laboratory tests show that enhanced oxygen utilization can result from microbial respiration in the presence of oil compounds (Venosa et al., 2002b). Beyond the underlying biochemical mechanisms however, likelihood of correlation is increased based on the fact that variables measured *in situ* at high sampling rates are better to capture plume heterogeneity. Hence, the utility of *in situ* fluorescence as a tool was ascertained early in the response due to such correlations, the high temporal and spatial resolution provided by the sensors, and also the advantages afforded by real-time capability compared to discrete analyses.

However, the multitude of submersible fluorometers used in the DWH response called to attention differences in the sensitivity and analytical capability of the instruments used due to differences in configuration of excitation and emission wavelengths, methods of calibration, sensitivity, and correlation to oil concentration (Figure 40, Table7). Many are not customized to capture oil fluorescence peak maxima, rather only a fraction of the signal (Fuller et al., 2003; Conmy et al., 2004 Conmy et al., 2014b). Furthermore, the ability of any fluorescence sensor (laboratory or field submersible) to detect oil is a function of (1) how well the sensor matches the excitation and emission wavelengths of the oil (including bandwidth of the wavelength filters or bandpasses from gratings, (2) the power of the light source, and (3) the sensitivity of the detector.

When tracking in the subsea became necessary early in the response, fluorometers used for detection of CDOM (i.e., WET Labs ECO series) were deployed on the vertical profilers as they were widely available, were capable of full ocean depth deployment and had been previously shown to detect oil in water (Wet Labs, Inc. website, www.wetlabs.com). These sensors typically have light sources that excite at wavelengths slightly longer than peak absorption by hydrocarbons and detect emission in the visible. They employ filters centered on excitation (Ex) and emission (Em) wavelengths at 370 and 460 nm ($ExEm_{370/460nm}$). Although the center

wavelength of the filters does not capture the peak of the oil fluorescence signal, the wide bandwidth of the emission filters (120 nm Full Width at Half Max) and the broad nature of the fluorescence peaks means that CDOM sensors are capable of detecting a large portion of the visible fluorescence signal. CDOM fluorometers were used to detect oil during the response in part because of their accessibility, but also because these sensors capture some portion of the oil fluorescence peak that occurs at the longer UV wavelengths where CDOM peaks also exist.

To quell questions regarding the ability of the ECO CDOM fluorometer to detect oil in the subsea plume, calibration tests were conducted at Louisiana State University (LSU) using Mississippi Canyon 252 (MC252) source oil. They provided a means to convert raw fluorescence data to Quinine Sulfate Dihydrate Equivalents (QSDE, the standard typically used for CDOM) to ppm of oil (JAG report, 2010). The calibrations were conducted in flasks on orbital shakers at 90 revolutions per minute (rpm), where oil concentrations ranged between 1-50 ppm. Dispersant (Corexit 9500) was added at a DOR of 1:2.5 and 1:25. The response of the fluorometer was linear with respect to oil but varied as a function of DOR, with a quenching of fluorescence in the presence of more dispersant per unit oil. Results of this test indicated that the ECO sensor was a sufficient proxy for oil concentrations greater than 1 ppm (NOAA, 2010). However, as the response continued and after the well was capped, oil concentrations in the subsea plume decreased as well as the magnitude of the fluorescence anomaly due to dilution and degradation of the oil, particularly at further distances from the wellhead. Concern was raised that a fluorometer with higher sensitivity for oil (one with a hydrocarbon-specific configuration) was needed. At that time, Chelsea UV Aquatrackas ($ExEm_{239/360nm}$) were deployed to track the plume in the far field of the response geographic region with the expectation (and subsequent confirmation) that it would detect fluorescence signal at lower oil concentrations.

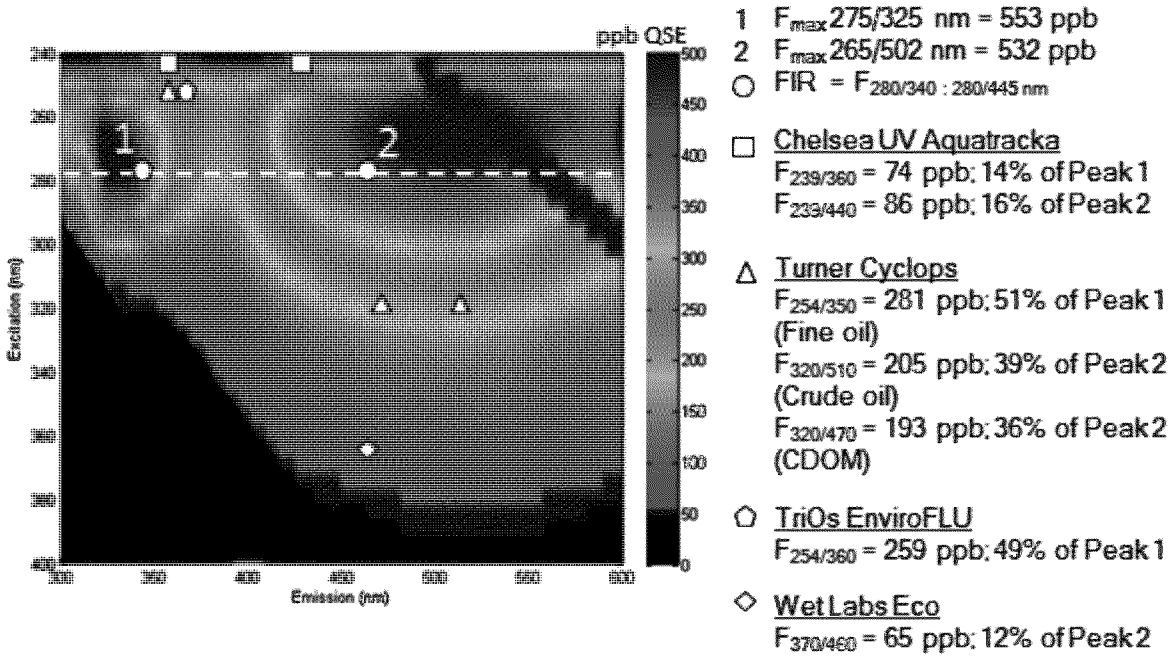

Figure 40. Fluorescence peaks of S. Louisiana sweet crude dispersed in ppb QSE (Quinine Sulfate Equivalents). Symbols represent Fluorescence Intensity Ratio (FIR) locations and the Center Wavelength (CWL) reported by sensor manufacturers. Bandwidths (BW) are not shown.

Table 7. Sensor specifications as listed from manufacturers. Wavelengths listed as Center Wavelengths (CWL) with Full Width at Half Max (FWHM) and Bandpass (BP). Standards used are QS (Quinine Sulfate Dihydrate), NDD Salt (Napthalene Disulfonic Disodium) and PTSA Salt (Pyrenetetrasulfonic Acid Tetrasodium) (From Conmy et al., 2014b).

Manufacturer	Instrument	Light source	Excitation λ (nm)	Emission λ (nm)	Detector	Dynamic Range
Chelsea Technologies Group	UV AQUAtracka	Xenon lamp	239 CWL	360 CWL	PMT	0.001- 10 µg/L Carbazole
	UV AQUAtracka	Xenon lamp	239 CWL	440 CWL	PMT	0.001 - 10 µg/L Perylene
Seapoint Sensors	SUVF	LED	370, 12 FWHM	440, 40 FWHM	Photodiode	0.1 - 1500 µg/L QS
TriOS, GmbH	EnviroFLU-HC, DS	Xenon lamp	254, 25 FWHM	360, 50 FWHM	Photodiode	0 - 5000 ppb Phenanthren
Turner Designs	Cyclops (Fine oil)	LED	254, 40 nm BP	350, 50 nm BP	Photodiode	0 - 10,000 ppb NDD Salt
	Cyclops (Crude oil)	LED	320, 130 nm BP	510, 180 nm BP	Photodiode	0 - 2700 ppb PTSA Salt
	Cyclops (CDOM)	LED	320, 130 nm BP	470, 60 nm BP	Photodiode	0 - 2500 ppb QS
WetLabs	WetStar	LED	370, 10 FWHM	460, 120 FWHM	Photodiode	0.100 - 1000 ppb QS
	ECO-FLU, triplet, puck	LED	370, 10 FWHM	460, 120 FWHM	Photodiode	0.01 - 500 ppb QS

Post-DWH response sensor tank testing -To address persisting uncertainties regarding sensor performance in the subsea, a team of scientists conducted experiments in May 2011 to study the dynamic range, sensitivity, and response *of in situ* fluorometers to changing excitation or emission properties of fresh and weathered MC252 oil (NOAA Science Box Award, PI: Michelle Wood; Co-PI's from EPA, NOAA, University of South Florida). The experiment was conducted within the flow-through flume tank at the BIO in Dartmouth, Nova Scotia, taking into consideration environmental factors such as wave energy and ocean currents. Experiments included the stepwise addition of oil and dispersant (DOR of 1:25; 0.3 - 12 ppm of MC252 SLC oil) to the flume tank while collecting *in situ* fluorescence and droplet-size distribution data, as well as coincident discrete samples for chemistry and EEM analyses. The flume tank was operated in static mode and each addition of oil and dispersant was allowed to homogenize prior to collecting discrete samples and coincident sensor measurements to calculate the least linear squares regressions. Results indicated that all sensors tested were responsive to changes in MC252 oil concentration regardless of wavelength configuration. Linear response of the WET

Labs ECO, Turner Designs Cyclops and the Chelsea Technologies Group AQUAtrackas sensors as a function of oil concentration was observed, where lowest concentrations were not below the detection limit of any sensor tested (Conmy et al., 2014a). Results demonstrated that all sensors exhibited a wide dynamic range of detection for MC 252 oil and were capable of detecting oil at the lowest concentration (approximately 300 ppb oil), which is significantly lower than the LSU calibration study (1 ppm) and a common misconception during the response (Conmy et al., 2014a). Differences in the detection limit between the studies may be explained by differences in the design, scale and the amount of physical dispersion of the tests, where the tank can provide mixing energies similar to those found in the field.

The 2011 study findings answered critical questions about sensor performance to detecting MC252 oil. However, the experiment highlighted the need for future studies to evaluate sensor performance using a variety of DORs and for multiple oil types. Evident from the DWH spill and post-spill research was that further R&D is needed to transfer knowledge gained through laboratory 3-D Excitation Emission Matrix (EEM) Spectroscopy into practical information for fluorescence tools used during spill response. Fluorescent properties are oil specific and investigating variations in EEMs as function of oil type and dispersant-to-oil ratios better prepares the community in identifying sensors for response options. To that end, the objectives of this project were to:

I. Generate a comprehensive EEMs database, building upon existing data at the Department of Fisheries and Oceans Canada, to provide fluorescence peak information as a function of oil type, weathering state, concentration and Dispersant-to-Oil Ratios (DORs).
II. Critically examine the database using advanced statistical methods and models to identify wavelengths best suited for oil monitoring during dispersant application and degradation.
III. Conduct flume tank experiments to determine submersible sensors capable of providing data comparable to scanning and/or fixed wavelength laboratory fluorometers for rapid deployment during response efforts.

Through this project, a comprehensive EEMs library database was generated covering a wide variety of oils from light to heavy fuel and crude oils and diluted bitumen. Varying DORs (1:20, 1:100, 1:200, 0) and oil concentrations were evaluated as the presence of dispersant alters EEM fingerprints. EEMs were subjected to advanced statistical analyses and models to identify wavelengths best suited for oil monitoring during dispersant application and subsequent tracking. Fluorescence is a non-destructive characterization tool that is routinely used to examine complex organic mixtures (foods, wine, medical compounds, aquatic organic matter, oils). Unlike single compound solutions, they exhibit broad, diffuse peaks that result from overlapping smaller peaks with similar chemistry. Although EEMs can be a substantial source of information on chemical composition and variability amongst samples, the high-dimensionality (intensity by emission by excitation) and nonlinearity of the data equates to difficulties in data interpretation and extraction of practical information as a characterization tool (Bieroza et al., 2010). Therefore, it is difficult to determine which underlying chemical components are responsible for which portion of the fluorescence fingerprint. Combining standard techniques for EEM analysis such as assessment of particular fluorescence peak features including peak height and wavelength position via 'peak picking' with Parallel Factor Analysis (PARAFAC) modeling results in a more comprehensive understanding of the chemical constituents. The use of advanced multivariate analyses such as PARAFAC has gained popularity as an effective means to deconvolve complex, broad peaks into their underlying smaller components (Stedmon et al., 2003; Boehme et al., 2004; Christensen et al., 2005; Stedmon and Bro, 2008). Here, we processed EEMs data with scripts in the N-way toolbox for Matlab (Andersen and Bro, 2000) and SOLO software (Eigenvector, Inc) and used the algorithms to isolate wavelengths to best characterize an oil type. An excellent review of these chemometric techniques and applications is provided in Bieroza et al., 2010. This approach will allow for comparing oil in water mixtures for similarities and contrasting features.

Results were evaluated for the Fluorescence Intensity Ratio (FIR) technique (Bugden et al. 2008; Kepkay et al. 2008). The latter calculates the ratio at $ExEm_{280/340nm}$ to $ExEm_{280/445nm}$ as an

indicator of oil dispersion. Previous studies at DFO COOGER have shown that dispersed oil fluoresces over two peaks centered on emission wavelengths of 340 nm and 445 nm, at excitation wavelength 280 nm, and that chemical dispersion enhances the emission intensity at 445 nm (Bugden et al. 2008; Kepkay et al. 2008). Postulated is that the fluorescence intensity at $ExEm_{280/340nm}$ represents the dispersion of lower molecular weight aromatic hydrocarbons, while intensity at $ExEm_{280/445nm}$ corresponds to higher molecular weight aromatic compounds.

Finally our work addresses the disconnect that exists between fluorescence research conducted in laboratories and the collection of fluorescence data from submersible sensors. By conducting laboratory-based and tank-based experiments on the same oil type and DOR, comparisons between EEMs can be made across scales. This helps to determine how well the *in situ* sensors are aligned in detecting dispersed oil.

Task B.2 Experimental Methods

B.2.1 Sample Preparation - Twenty-five oil samples from the DFO and EPA stockpiles (covering a wide range of viscosity and oil type) were used for spectrofluorometric testing, where oil characteristics were tabulated for the test oils based on an extensive literature search (Table 8; Supplemental Material A). All glassware used in this study was cleaned to ensure highest analytical integrity including solvent rinsing, deionized water rinsing and baking in a muffle furnace at 450˚C where appropriate. Samples were stored in 125mL amber glass bottles with PTFE-lined caps (Figure 41).

B.2.2 Artificial Seawater Protocol - Artificial seawater was used for DOR mixing to avoid interference of fluorophores found in natural seawater with oil fluorescence signal. Fresh artificial seawater was made to salinity of 28 ppt and was prepared in 1 L quantity at the beginning of each experiment by adding Tropic Marin® salts (Appendix A) to 1 L ultrapure water dispensed from a Millipore Milli-Q unit (≤ 4 ppb DOM) into a 1.5 L glass beaker, covering the beaker with aluminum foil, and stirring with a magnetic stir-bar on electric stir plate for 20 minutes at room temperature (~24°C).

B.2.3 Dispersed Oil in Seawater Protocol - A series of dispersed-oil-in-seawater experiments were performed using baffled trypsinizing flasks (baffled flasks) with artificial seawater, MC252 oil and Corexit 9500 chemical dispersant (Venosa et al., 2002a). Four petroleum oil / dispersant solutions were prepared for each oil type at the following DORs: 0, 1:20, 1:100, and 1:200. Oil was pipetted into an 8.6 ml amber vial, followed by addition of the appropriate amount of Corexit 9500 chemical dispersant into the vial. Teflon-lined capped vials were shaken by hand for 60 seconds and 10 µL of dispersant / oil mixture was pipetted (Eppendorf positive displacement micropipettes, 1-20 µL) into 100 mL artificial seawater contained in each of three replicate flasks. Flasks were covered with parafilm and placed on a New Brunswick Scientific Innova 2100 platform shaker (orbit = 1.9 cm) for 12 minutes at 200 rpm. Approximately 3.5mL of the resulting dispersed-oil-in-seawater was immediately dispensed through a spigot near the bottom of each flask into three 4.0-mL UV-grade quartz cuvettes, which were immediately

covered with Teflon stoppers to prevent evasion of volatile components during fluorescence analyses (Figure 42). After removal of spectrophotometric samples, additional volumes of sample were removed from the baffled flasks for extraction of total petroleum hydrocarbons (TPH) by dimethylene chloride (DCM). TPH analysis follows the same Gas Chromatography-Mass Spectrometry (GC-MS) method as in Task A of this project.

B.2.4 Spectrophotometric Analysis - A Horiba Scientific AquaLog spectrofluorometer was used to analyze the 25 oil types with varying DOR. A series of analyses were initially performed while varying the instrument's settings (excitation and emission increments, gain setting, integration time) in order to determine optimal settings for the entire experimental protocol. Excitation-Emission Matrices (EEMs) were generated using the following instrument parameters: 200 – 800 nm excitation (3 nm increments), 249 – 828 nm emission range (CCD detector at 534 nm 8 pixel increments), medium gain setting and integration time of 0.1 sec. A quinine sulfate dihydrate dilution series was created consisting of: 0.5N H_2SO_4 solvent; 100 ppm 1° (primary stock) solution; 100 ppb 2° (secondary stock) solution; 1,3,5,10 and 20ppb quinine sulfate solutions. Dilutions were analyzed for fluorescence and used for cross-calibration with instrument software built-in quinine sulfate tool to convert results into Quinine Sulfate Equivalents (QSE) and demonstrate linearity of fluorescence in a dilution series. All data processing and spectral corrections follow the manufacturer's manual. Dilution series with oil concentrations between 1 – 500 ppb were also generated to determine lower detection limits for oils. EEMs are presented in Raman Units (RU).

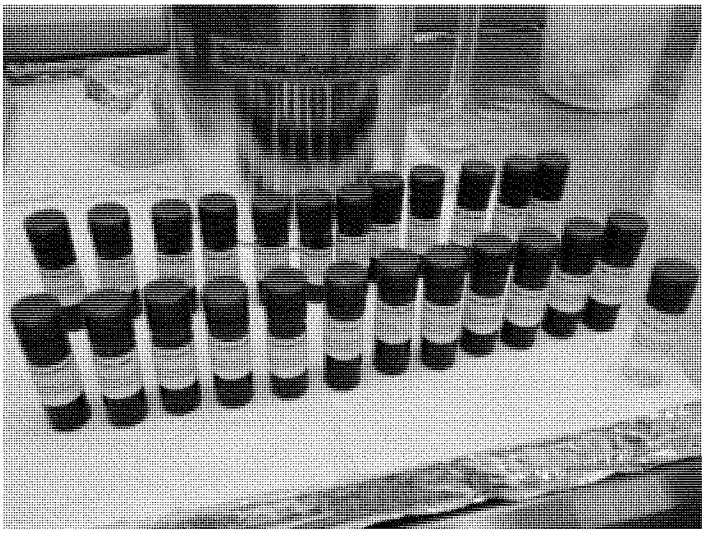

Figure 41. Twenty-five oil samples stored in glass bottles.

Table 8. List of oil samples used for EEM analyses. Oils separated by API (American Petroleum Institute) gravity.

Light (API >31.1°)	Medium (API 22.3 – 31.1°)	Heavy (API <22.3°)
Arabian Light (32.2°)	Alaska North Slope (29.7°)	Access Western Blend Dilbit (21.3°)
Brent (38.2°)	Alaskan North Slope (10% weathered)	Belridge Heavy (13.6°)
Federated (39.4°)	Heidrun (28.6°)	Cold Lake Dilbit (21.5°)
Gullfaks (32.7°)	Lago (25.0°)	Hondo (19.5°)
Hibernia (35.6°)	Mesa (30.3°)	IFO 40 (21.9°)
MC252—Discoverer Enterprise (37.2°)	Sea Rose (29.8°)	IFO 120 (18.4°)
MC252—generic (35.2°)	Vasconia (26.3°)	IFO 180 (14.1°)
Scotian Shelf Condensate (53.2°)		IFO 300
Terra Nova (33.8°)		Santa Clara(22.1°)

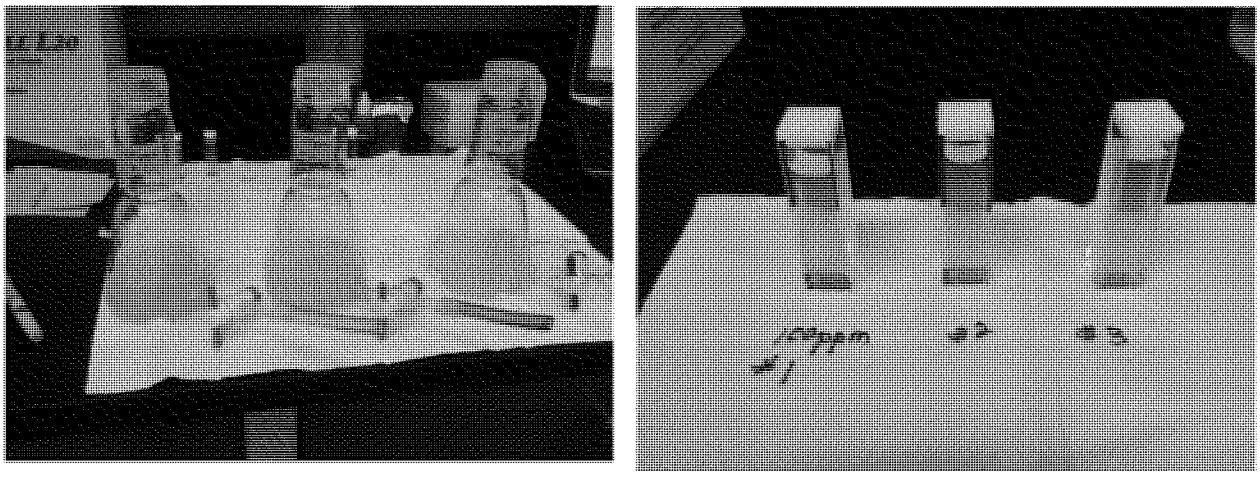

Figure 42. Trypsinizing baffled flasks containing dispersed oil in artificial seawater (top) and corresponding samples removed from each flask, ready for spectrofluorometric analysis.

Task B.3 Results & Discussion

B.3.1 Oil Fluorescence Properties

Four characteristic excitation/emission (Ex/Em) peak locations were identified: F_{max1} – F_{max4} (Figure 43) for all 25 oil types at four DORs (Figure 43). The highest intensity peak (F_{max1}) occurred, without exception, at Ex 221-239 nm/Em 335-344 nm and was paired with a blue-shifted, lower intensity peak (F_{max2}) at Ex 215-221 nm/Em 285-308 nm in all oil types. A third broad, low-intensity peak (F_{max3}) was observed at Ex 215-305 nm/Em 418-571 nm, to varying degrees across oil types, corresponding with oil categories determined by API gravity (Table 8). Light crude oils exhibited F_{max3} fluorescence at all DORs with the exception of Scotian Shelf

Condensate. Of note is that Scotian Shelf Condensate appeared physically unlike any of the other light oils: clear in color with apparent very low viscosity. Since viscosity is largely determined by the size and relative weight of component hydrocarbons (Fingas 2011), fewer complex fluorophores would likely be present in this oil type. Fluorescence in the F_{max3} region was identified at all DORs in only one medium weight oil (Heidrun), and was not present at any DOR in one medium oil (Vasconia). Two medium-weight oils emitted measurable fluorescence in the F_{max3} region only with full dispersion (Lago and Mesa), while Sea Rose showed fluorescence at DORs 1:100 and 1:20. One medium weight oil, Alaska North Slope (both fresh and 10% weathered), exhibited unusual F_{max3} behavior, with measureable fluorescence at DOR 0, 1:100 and 1:20, but not at DOR 1:200. Finally, for the heavy weight oils, F_{max3} was almost completely absent at all DORs, with the exception of fluorescence at DOR 1:20 for Cold Lake Dilbit (Diluted Bitumen) and IFO 40, and across all DORs for one anomalous member of this group—Access Western Blend Dilbit. Dilbit is a mixture of bitumen—essentially a heavy crude oil with API gravity < 10.0°—and a diluent—either a light condensate or naptha (Priaro 2016). The combination of characteristics from both oil types may account for the unusual F_{max3} fluorescence observed in this oil type. Additionally, Intermediate Fuel Oils (IFOs) are not true crude oils, but marine fuels consisting of a mixture of post-refinery heavy residual oil and refined diesel fuel, which may also help to explain the appearance of F_{max3} fluorescence in IFO 40. Clearly, the presence of fluorescence in the F_{max3} region, especially at DOR 1:20, appears to be related to API gravity, and thus to density as well as kinematic viscosity since API gravity = (141.5/Specific Gravity) – 131.5 (Fingas, 2011). The absence of F_{max3} region fluorescence in heavy weight oils may be due to retention of energy within the large, complex hydrocarbons which make up the highest density oils. Additionally, the appearance of fluorescence in the F_{max3} region at highest DORs for the medium weight oils (Lago, Mesa, and Sea Rose) suggests that smaller droplet sizes were created via the dispersion which could lead to a decrease in reabsorption of fluorescence within the oil – water mixture. A fourth region of broad, low-intensity fluorescence (F_{max4}) was identified at Ex 269-291 nm/Em 326-353 nm for all oil types at all DORs. F_{max1} and F_{max4} oil-in-water fluorescence regions appear to be analogous to the characteristic colored dissolved organic matter (CDOM) fluorescence regions 'A_C' at Ex 260/Em

400-460 and 'C' at Ex 320-365/Em 420-470 (Coble, 2014).

In addition to maximum intensity for each fluorescence peak (in RU), full width at half maximum (FWHM) was also recorded. Further, fluorescence intensity at Ex/Em 281/340 and 281/456 nm was recorded to enable calculation of the FIR for all samples. Optimum settings for signal collection on the HORIBA AquaLog necessitated excitation at 3 nm intervals, which accounts for the 1 nm discrepancy from the published FIR wavelengths (Bugden, et al. 2008). Fluorescence intensity at the specified Ex/Em wavelength settings of five off-the-shelf *in situ* fluorometers (Conmy et al., 2014a & b), which were all employed in the response to the DWH spill, was recorded. Those wavelengths were also adjusted slightly to compensate for signal collection intervals on the HORIBA AquaLog. Selected results are presented in Table 9 along with results of chemical analyses, and complete fluorescence results are included as a Supplemental Table A. EEM contour 'fingerprint' plots for all oils, which characterize each oil type and illustrate the effect of dispersant on the fluorescence properties, are presented in Appendix F. The ability to identify oil source can be useful in the prevention and abatement of oil spill pollution. To that end, efforts to determine characteristic fluorescence fingerprints have existed since the 1970s (Frank, 1978) and have received renewed attention with the advent of improved fluorescence detection systems (Bugden, 2008).

Intensity of F_{max1} was consistently strong across oil types, with no ambiguity in peak location. The observed Ex/Em range of significant fluorescence intensity was fairly narrow with FWHM of only 37-50 nm, and little to no change in peak location with increasing DOR. However, Six of the nine light oil types, but just one of the seven medium oil types and one of the nine heavy oil types[1] displayed this slight increase (approximately 4.5 nm) in FWHM with maximum dispersion (DOR 1:20). One medium weight oil (Lago) and one heavy oil (Access Western Blend Dilbit) showed the same slight increase in FWHM at both DORs 1:100 and 1:20. The impact of applying the Inner Filter Effect correction tool (IFE) to fluorescence intensity was also calculated for F_{max1}. This correction utilizes the measured absorbance of the sample to correct for fluorescence emitted by fluorophores within the sample, but re-absorbed within the sample itself. Of note is

[1] Increase of approximately 4.5 nm in FWHM in F_{max1} seen in light oils Arabian Light, Brent, Federated, Gullfaks, Hibernia, and Terra Nova; in medium oil Mesa; and in heavy oil IFO 120 at DOR 1:20.

that application of the IFE resulted in only a small magnification of the fluorescence signal at DORs 0, 1:200 and 1:100 for all oil types; however, there was a clear delineation between two categories of oil types at DOR 1:20: Oil Type I, with IFE effect > 2.5 and Oil Type II, with IFE effect < 2.5 (Table 9). This appears to be due to the increase in optical density, and thus absorbance, possibly caused by interaction between Corexit 9500 and well dispersed Type I oils. Photographs of four representative pre-analysis samples, along with the resulting EEMs of oil type are shown in Figure 44 to illustrate the difference in fluorescence between the types regardless of being a light, medium or heavy crude oil.

Due to variation from laboratory to laboratory, and even differences in instrument to instrument performance from the same manufacturer, it is necessary to convert fluorescence intensity "raw counts" to a standardized unit for useful reporting purposes. Traditionally, the fluorescence community has utilized a dilution series of quinine sulfate dihydrate in weak acid to convert instrument output to Quinine Sulfate Equivalents (QSE) (Coble, 1996). However, in recent years the alternate method of reporting in Raman Units (RU) has gained favor (Murphy et al., 2010). Due to inherent properties of water molecules, the Raman scatter peak is a reliable feature which can be used through collecting a scan of ultra-pure water at the beginning of each day, and then using the ratio of raw counts to the area under the curve of the Raman peak (approximately 381-426 nm) to convert fluorescence to RU. As the Quinine Sulfate SRM is no longer available from NIST (National Institute of Standards and Technology), we have reported results in RU and offer a conversion factor to QSE using the highest quality quinine sulfate dihydrate readily available.

Overall, F_{max1} intensity ranged from a minimum of 39.58 RU (Access Western Blend Dilbit DOR 0) to 3090.23 RU (IFO 120 DOR 1:100). Since all of the Intermediate Fuel Oils and the Scotian Shelf Condensates showed unusual fluorescence profiles which tended to skew the results for the aforementioned reasons (Figures 45 and 46), these will be eliminated from the remaining discussion. F_{max1} intensity within Type I oils ranged from 357.62 RU (Arabian Light DOR 1:200) to 1998.60 RU (MC252 Discoverer Enterprise DOR 1:20), while the range in Type II Oils was the overall low of 39.58 previously mentioned to a high of 1098.90 (Heidrun DOR 1:20).

While the excitation wavelength of maximum intensity for F_{max2} remained relatively consistent, the emission wavelength varied within, as well as among, oil types. The occurrence of double and triple peaks, as well as minor sub-peaks, within the F_{max2} region was fairly common. It was sometimes difficult to distinguish the F_{max2} peak from the shoulder of a very strong F_{max1} peak, especially at higher DORs. For this reason, determination of the true FWHM was sometimes problematic. For F_{max2} intensity, Type I Oils ranged from 63.95 RU (Brent DOR 1:200) to 437.32 RU (MC252 Discoverer Enterprise DOR 1:20), and Type II Oils ranged from 25.07 RU (Belridge Heavy DOR 0) to 164.07 RU (Heidrun DOR 1:20).

For oil types exhibiting an F_{max3} peak, it was most apparent at the highest DOR (1:20) and some oils exhibited a strong F_{max3} peak across all DORs (e.g., Brent, Federated). However, for those oils the F_{max3} peak at DOR 1:20 was significantly blue shifted (peak moved to lower wavelengths) from the F_{max3} location observed at lower DORs. FWHM of the F_{max3} peak was much greater than that of any other peak (145-283 nm), with the exception of the three lower DORs of Access Western Blend Dilbit (52-56 nm). Identification of highest F_{max3} intensity proved somewhat problematic as it tended to lay within the second order Rayleigh region, a band of high intensity light resulting from scattering by water molecules. The edge of highest intensity could also lie in this region, so determination of the true FWHM was also problematic for many oil types. Traditionally, second order Rayleigh is eliminated by simply masking this region (10-12 nm). Although algorithms have been developed to model the character of fluorescence peaks lying within (Zepp, et al. 2004; Bahram, et al. 2006), assumptions about the linearity of fluorescence must be made, and the true signal behavior cannot be known. For this reason, as our goal was to identify signals which could also be detected by *in situ* instruments, the decision was made to identify the maximum fluorescence intensity lying outside of the second order Rayleigh region rather than to try to interpolate the data.

As previously mentioned, F_{max3} intensity was not always present, and it was observed far more often in Type I Oils with a range of 2.64 RU (Arabian Light DOR 1:200) to 744.69 (MC252 Discoverer Enterprise DOR 1:20). Only four of the Type II Oils exhibited F_{max3} peaks and these ranged from 2.45 RU (Access Western Blend Dilbit DOR 0) to 174.93 RU (Heidrun DOR 1:20).

As with F_{max2}, the F_{max4} region sometimes contained double peaks. Unique spectral shapes for this region were also observed, especially in higher-density oils such as Access Western Blend Dilbit, Belridge Heavy, and Cold Lake Dilbit. FWHM ranged from 27 nm to 73 nm, for all oil types but one. The exception was Access Western Blend Dilbit, with FWHM of 77-110. Intensity at F_{max4} ranged from 33.53 RU (Arabian Light DOR 1:200) to 231.86 RU (MC252 Discoverer Enterprise DOR 1:20) in Type I Oils and from 4.93 RU (Access Western Blend Dilbit DOR 0) to 116.97 RU (Heidrun DOR 1:20) in Type II Oils.

Results of the concentration dilution series showed that the HORIBA AquaLog was consistently capable of detecting dispersed oil in artificial seawater in the three oil types tested (Alaska North Slope, IFO 120, and MC252 Discoverer Enterprise) at all four DORs down to at least 50 ppb. However, detecting dispersed oil below 100 ppb necessitated increasing the integration time to 10 sec. per scan in order to collect sufficient data, which resulted in a total analysis time of approximately 30 minutes for each sample. Since the HORIBA AquaLog scans from high to low wavelengths and much of the fluorescence signal from petroleum resides in the UV region, photobleaching of the sample as well as temperature effects certainly may have impacted these results.

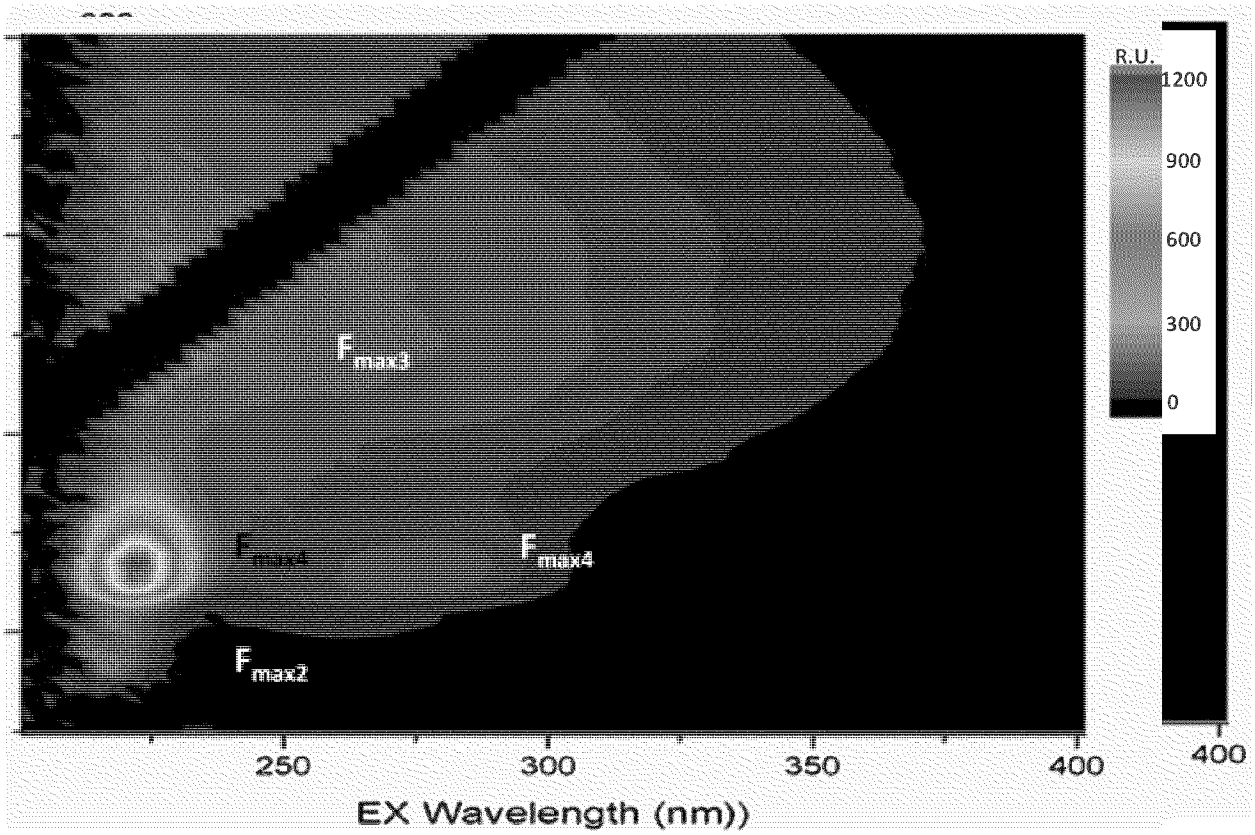

Figure 43. Alaska North Slope dispersed oil in artificial seawater at DOR 1:20 with locations of F_{max1}, F_{max2}, F_{max3} and F_{max4} indicated. Note that maximum fluorescence intensity at F_{max3} is mostly obscured by masking of second order Rayleigh scattering.

Table 9. EEM fluorescence and chemical characteristics. Refer to Supplemental Table A for full table.

Type I Oils	DOR	F_{max}[1] (RU)	IFE	FIR	Alkanes (µg/L)	2-ring PAHs (µg/L)	3-ring PAHs (µg/L)	4-ring PAHs (µg/L)
Alaska North Slope	0	697.07	1.16	21.59	375	145	15	8
	1:200	715.01	1.15	35.41				
	1:100	839.60	1.32	6.59				
	1:20	1171.63	3.33	0.88	3019	477	89	65
Alaska North Slope (10% weathered)	0	812.97	1.19	21.70	545	182	19	14
	1:200	831.70	1.21	21.70				
	1:100	828.06	1.28	9.08				
	1:20	1109.51	3.01	0.91	3312	499	99	74
Arabian Light	0	400.42	1.18	7.29	733	113	11	12
	1:200	357.62	1.07	11.61				
	1:100	426.82	1.26	2.70				
	1:20	701.75	4.19	0.39	6004	571	71	103
Brent	0	646.18	1.15	7.59	1068	162	21	12
	1:200	660.37	1.16	6.65				
	1:100	708.16	1.37	1.97				
	1:20	1098.42	3.05	0.68	5954	456	97	58
Federated	0	574.35	1.14	3.70	1921	197	41	30
	1:200	607.97	1.21	2.01				
	1:100	645.28	1.37	0.94				
	1:20	1223.17	4.37	0.36	6501	488	129	87
Gullfaks	0	937.00	1.24	5.79	762	326	47	26
	1:200	934.42	1.27	5.57				
	1:100	933.08	1.35	3.24				

	1:20	1524.21	3.73	0.71	1943	642	107	60
Hibernia	0	938.08	1.24	6.91	2289	296	39	24
	1:200	951.49	1.34	3.22				
	1:100	978.62	1.47	1.69				
	1:20	1812.41	4.02	0.49	6095	541	94	59
MC252 (Discoverer Enterprise)	0	998.50	1.27	5.01	1578	300	50	30
	1:200	1009.18	1.37	3.06				
	1:100	1085.54	1.48	1.22				
	1:20	1998.60	4.76	0.39	3992	482	101	68
MC252 (generic)	0	857.35	1.24	4.42	1468	231	36	21
	1:200	877.78	1.25	3.56				
	1:100	964.02	1.57	0.95				
	1:20	1795.13	4.73	0.40	5093	511	113	67
MESA	0	757.84	1.19	18.14	1388	234	34	24
	1:200	806.76	1.22	11.97				
	1:100	745.17	1.26	6.44				
	1:20	1107.09	2.77	1.04	4088	439	85	62
Sea Rose	0	1145.29	1.28	9.80	1583	285	35	19
	1:200	1223.98	1.33	7.59				
	1:100	1236.63	1.55	2.18				
	1:20	1973.55	3.56	0.71	5903	601	120	70
Terra Nova	0	665.50	1.16	6.93	1038	168	18	11
	1:200	719.72	1.22	3.79				
	1:100	821.24	1.37	1.47				
	1:20	1380.34	3.76	0.40	5608	463	77	50

Type II Oils	DOR	F_{max}[1] (RU)	IFE	FIR	Alkanes (µg/L)	2-ring PAHs (µg/L)	3-ring PAHs (µg/L)	4-ring PAHs (µg/L)
Access Western Blend Dilbit	0	39.58	1.02	11.41	93	15	4	10
	1:20 0	46.52	1.02	11.62				
	1:10 0	49.84	1.03	8.54				
	1:20	60.19	1.08	1.13	258	40	17	37
Belridge Heavy	0	118.69	1.07	4.90	42	31	21	30
	1:20 0	161.75	1.08	5.22				
	1:10 0	140.96	1.07	4.62				
	1:20	147.09	1.12	3.30	44	49	35	52
Cold Lake Dilbit	0	120.61	1.05	18.92	155	74	20	22
	1:20 0	120.65	1.05	17.33				
	1:10 0	125.85	1.06	11.50				
	1:20	133.15	1.17	1.92	368	160	50	57
Heidrun	0	902.69	1.28	4.50	382	337	55	43
	1:20 0	909.47	1.26	6.22				
	1:10 0	964.31	1.33	3.74				
	1:20	1098.90	2.19	0.77	684	524	96	79
Hondo	0	283.04	1.09	18.38	412	76	8	2
	1:20 0	312.27	1.08	15.38				
	1:10 0	274.80	1.07	17.44				
	1:20	288.01	1.07	16.33	319	67	7	1
IFO-40	0	1173.91	1.20	27.94	1324	408	152	168
	1:20 0	1246.63	1.22	47.73				
	1:10 0	1338.56	1.25	35.74				
	1:20	1458.79	2.29	4.57	4354	1033	475	561
IFO-120	0	3030.69	1.68	109.67	343	607	88	49
	1:20 0	2903.21	1.61	101.83				
	1:10							

	0							
	1:20	2527.73	1.67	34.32	840	885	212	118
IFO-180	0	1263.05	1.22	33.67	866	410	235	320
	1:20 0	1394.42	1.23	36.08				
	1:10 0	1703.55	2.37	36.31				
	1:20	1532.99	1.63	12.19	2933	1189	797	1095
IFO-300	0	720.55	1.11	61.26	446	216	79	188
	1:20 0	443.51	1.14	25.85				
	1:10 0	465.91	1.07	45.70				
	1:20	661.50	1.10	39.81	366	183	65	157
Lago	0	352.22	1.07	12.13	1289	114	32	18
	1:20 0	398.40	1.13	11.73				
	1:10 0	367.75	1.12	8.88				
	1:20	453.10	1.75	0.92	4221	258	88	51
Santa Clara	0	157.30	1.05	25.93	209	27	1	0
	1:20 0	147.55	1.05	22.73				
	1:10 0	154.98	1.08	18.26				
	1:20	169.39	1.12	6.97	1196	72	9	3
Scotian Shelf Condensat e	0	946.52	1.15	40.62	447	125	2	0
	1:20 0	1408.59	1.44	53.68				
	1:10 0	1487.16	1.53	58.06				
	1:20	1337.98	1.50	47.65	1057	216	4	0
Vasconia	0	844.93	1.15	34.56	2550	317	98	59
	1:20 0	828.37	1.16	44.43				
	1:10 0	835.62	1.17	34.09				
	1:20	935.79	1.67	3.41	4402	467	164	95

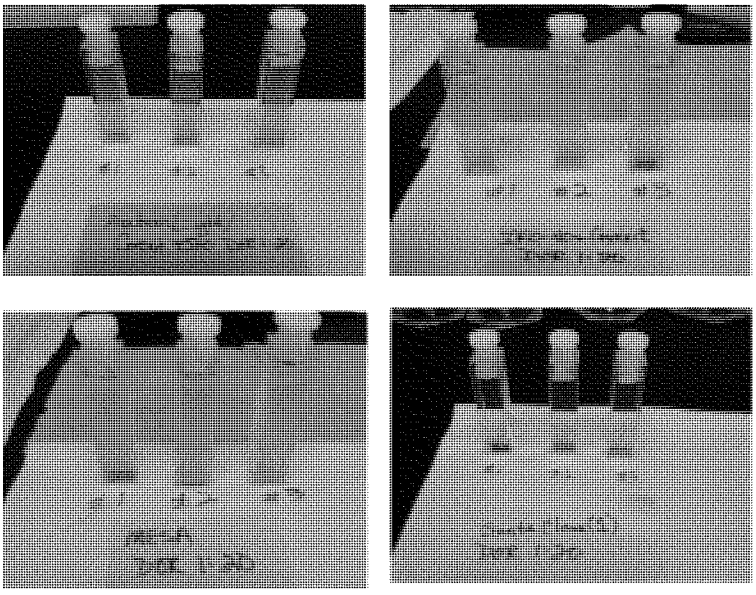

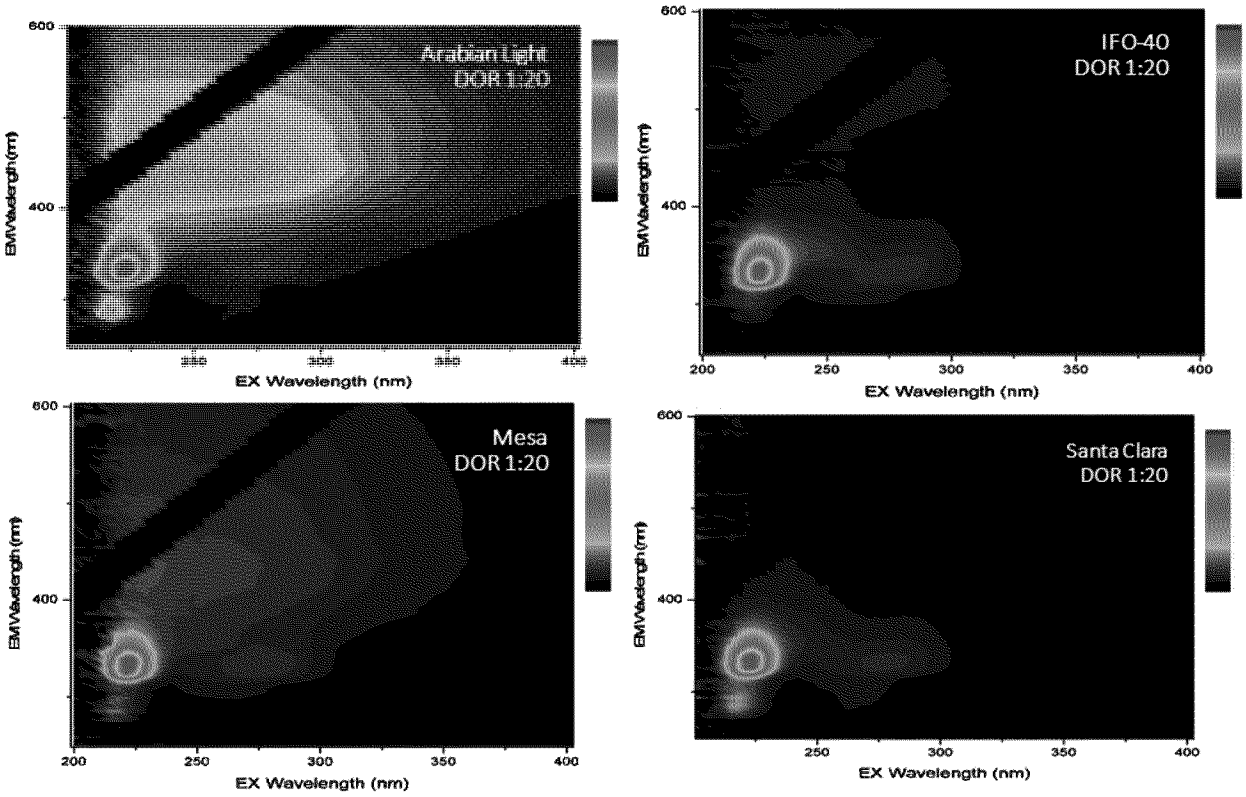

Figure 44. Photographs of pre-analysis samples and corresponding example EEMs of Type I (left) and II (right) oils; DOR = 1:20 for Arabian Light (light oil, API gravity > 31.1°), Mesa (medium oil, API gravity 22.3 – 31.1°) and heavy oils (IFO 40 and Santa Clara, API gravity < 22.3°).

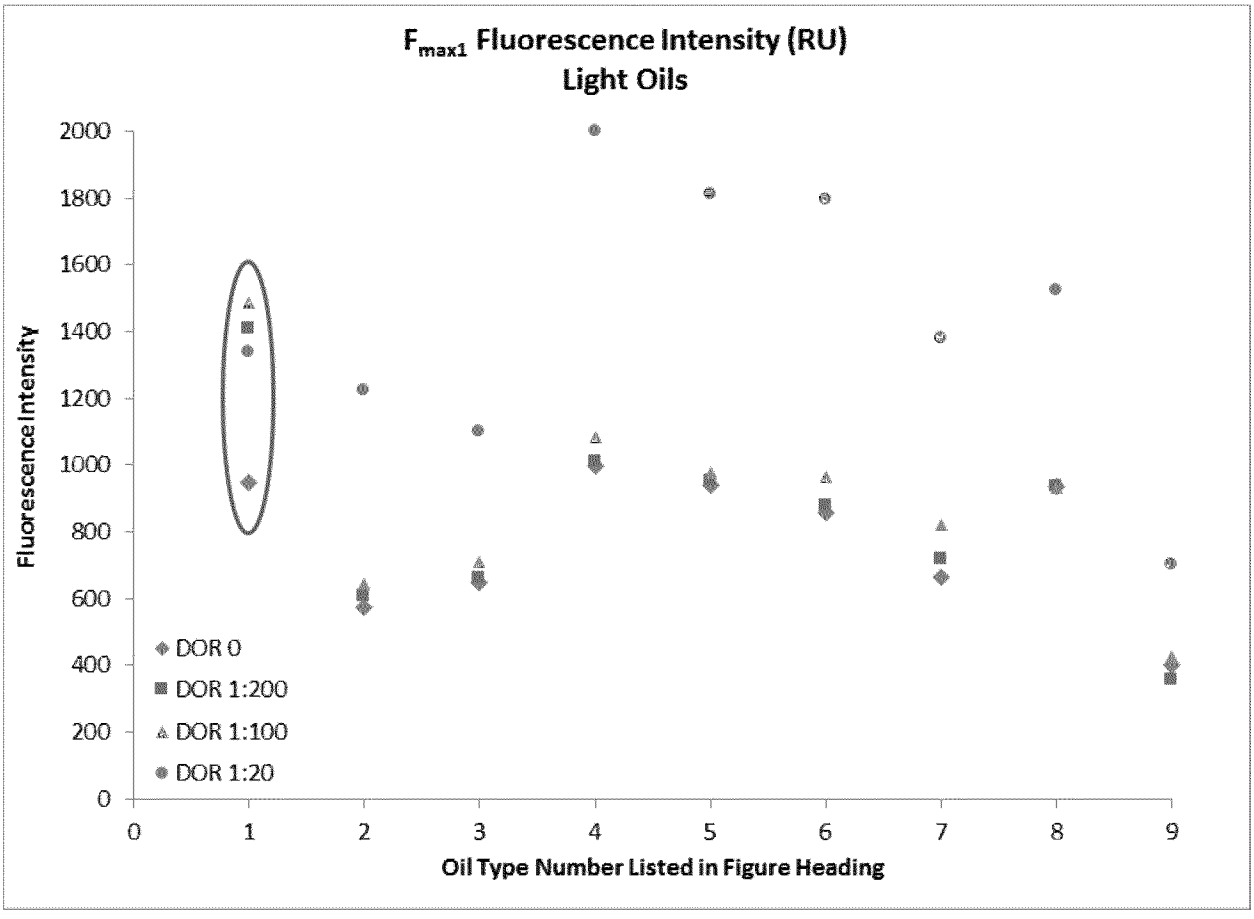

Figure 45. F_{max1} fluorescence for Light Oils (API gravity > 31°), in order of increasing density: 1. Scotian Shelf Condensate, 2. Federated, 3. Brent, 4. MC252—Discoverer Enterprise, 5. Hibernia, 6. MC252—generic, 7. Terra Nova, 8. Gullfaks, 9. Arabian Light. Note discrepancy in Scotian Shelf Condensate fluorescence pattern (circled) from that of all other Light Oils. It's particularly unusual that fluorescence intensity at highest DOR is lower than that at DORs 1:200 and 1:100.

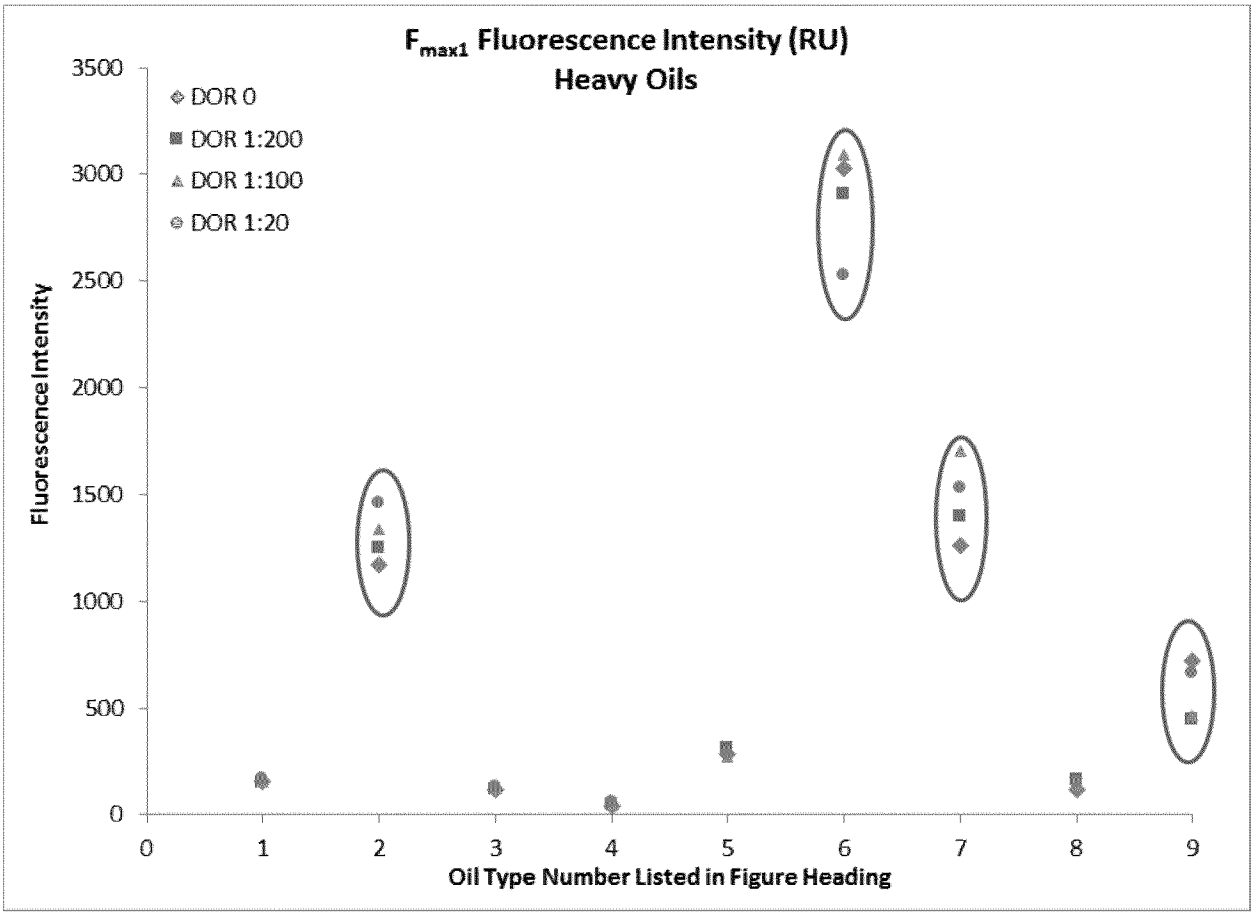

Figure 46. F_{max1} fluorescence for Heavy Oils (API gravity < 22.3°), in order of increasing density: 1. Santa Clara, 2. IFO 40, 3. Cold Lake Dilbit, 4. Access Western Blend Dilbit, 5. Hondo, 6. IFO 120, 7. IFO 180, 8. Belridge Heavy, 9. IFO 300. Note discrepancy in Intermediate Fuel Oils (circled) from that of all other Heavy Oils.

B.3.2 Fluorescence as a Function of Chemistry

Samples of dispersed oil in artificial seawater (DOR 0 and DOR 1:20 for each oil type), extracted into methylene chloride were analyzed via GC-MS. Total alkanes, 2-ring, 3-ring, and 4-ring PAHs (see Table 10 for list of hydrocarbons in each class) were each plotted against F_{max1}, F_{max2}, F_{max3}, and F_{max4} (Figures 47-50). Results showed highest correlation at DOR 0 between total 3-ring PAHs and fluorescence intensity at F_{max3} and F_{max4} (Figure 48) followed by that of 2-ring PAHs and fluorescence intensity at F_{max1} and F_{max2} (Figure 47) and between 4-ring PAHs and fluorescence intensity at F_{max3} and F_{max4} (Figure 48). It is important to note, however, that only 12 of the 25 oil types exhibited any F_{max3} fluorescence at DOR 0.[2] These correlations support the fact that larger, more complex PAHs fluoresce at longer emission wavelengths.

For all oils at DOR 1:20, logarithmic relationships rather than linear relationships best modeled all correlations; however, overall these were weaker than those found at DOR 0. Highest correlation was observed between 2-ring PAHs and F_{max3} intensity (Figure 50), with moderate correlations observed between 2-ring PAHs and fluorescence at F_{max1} and between 2-ring PAHs and F_{max2} fluorescence (Figure 49), and between 3-ring PAHs and F_{max3} fluorescence (Figure 50). Only weak correlations were observed between 2-ring PAHs and fluorescence at F_{max2} (Figure 49) and between 4-ring PAHs and F_{max3} fluorescence (Figure 50). Clearly, full dispersion at DOR 1:20 results in widely varying changes in fluorescence intensity across all oil types.

[2] Oil types exhibiting Fmax3 fluorescence at DOR 0: Access Western Blend Dilbit, Alaska North Slope (both fresh and 10% weathered), Arabian Light, Brent, Federated, Gullfaks, Heidrun, Hibernia, MC252 (both Discoverer Enterprise and generic), and Terra Nova.

Table 10. Individual hydrocarbon compounds reported as Total Alkanes, Total 2-ring, 3-ring and 4-ring PAHs.

Total Alkanes:	Total 2-ring PAHs:	Total 3-ring PAHs	Total 4-ring PAHs:
n-decane	Naphthalene	phenanthrene	pyrene
undecane	Methylnaphthalene	anthracene	methylpyrene
dodecane	Dimethylnaphthalene	methylphenanthrene	dimethylpyrene
tridecane	Trimethylnaphthalene	dimethylphenanthrene	trimethylpyrene
tetradecane	tetramethylnaphthalene	trimethylphenanthrene	tetramethylpyrene
pentadecane	Acenaphthene	tetramethylphenanthrene	naphthobenzothiophene
hexadecane	Acenaphthylene	fluoranthene	methylnaphthobenzothiophene
heptadecane	Fluorene		dimethylNBenzothiophene
2,6,10,14-TMPdecane (pristine)	Methylfluorene		trimethylNbenzothiophene
octadecane	Dimethylfluorene		tetramethylNbenzothiophene
2,6,10,14-TMHdecane (phytane)	Trimethylfluorene		benz[a]anthracene
nonadecane	Dibenzothiophene		chrysene
eicosane	methyldibenzothiophene		methylchrysene
heneicosane	dimethyldibenzothiophene		dimethylchrysene
docosane	trimethyldibenzothiophene		trimethylchrysene
tricosane	tetramethyldibenzothiophene		tetramethylchrysene
tetracosane			benzo[b]fluoranthene
pentacosane			benzo[k]fluoranthene

hexacosane			benzo[e]pyrene
heptacosane			perylene
octacosane			
n-nonacosane			
tricontane			
n-heneicontane			
dotriacontane			
tritriacontane			
tetratriacontane			
n-pentatriacontane			
17α(H), 21β (H)-hopane			
17β(H), 21α(H)-hopane			

The effect of DOR 1:20 on dissolved hydrocarbons can also be investigated by taking the ratio of total alkanes + PAHs at DOR 1:20 to total alkanes + PAHs at DOR 0 to yield the Chemical Dispersibility Ratio (CDR). The ratio ranges from between 0.8 for two heavy oils (Hondo and IFO 300) and 7.8 for Arabian Light. Although heavy oils tended to have lower CDRs and light oils tended to have higher ratios, oil density was not correlated with chemical dispersion For example, the heavy oil Santa Clara (API Gravity 22.1°) had the third highest CDR (5.4), while Scotian Shelf Condensate, by far the lightest oil (API Gravity 46.6°), had a CDR of only 2.2 (Figure 51 The effect of dispersion on fluorescence intensity can be similarly investigated by taking the ratio of F_{max1} fluorescence intensity at DOR 1:20 to that at DOR 0, resulting in the Fluorescence Dispersibility Ratio (FDR). The FDR also shows a general increasing trend with increasing API Gravity, but only a moderate linear correlation (R^2 = 0.55). The relationship between CDR and FDR exhibited weak linear correlation (R2 = 0.17) (Figure 52).

All four Intermediate Fuel Oils (IFO 40, IFO 120, IFO 180, and IFO 300) as well as Scotian Shelf Condensate (SSC), showed fluorescence and chemistry anomalies that tended to skew overall results. With respect to SSC, all other light oils (API Gravity < 22.3°) exhibited increasing fluorescence intensity with increasing DOR, culminating in an increase at DOR 1:20; however, SSC showed a decrease in fluorescence intensity at DOR 1:20, dropping to below the level exhibited at DOR 1:200 (Figure 45). Additionally, SSC was the only light oil which exhibited no F_{max3} fluorescence at any DOR. Chemically, SSC is unique, containing a high proportion of 2-ring to 3-ring PAHs—52.2 for DOR 0 and 58.6 for DOR 1:20. With the exception of Santa Clara, with a 2-ring to 3-ring ratio of 31.9 at DOR 0, all other oil types had a ratio of 10 or less at both DOR 0 and DOR 1:20. SSC also contained no 4-ring or 5-ring PAHs, unlike all other oils with the exception of DOR 0 Santa Clara. All Intermediate Fuel Oils fell into the heavy oil group (API Gravity > 31°), in which all other oils showed little to no increase in fluorescence intensity with increasing DOR as well as maximum F_{max1} intensity of just 60-288 RU. The IFOs, however, showed far greater F_{max1} intensity across the board (721-3031 RU) along with clear separation with increasing DOR. Like Scotian Shelf Condensate, IFO 120, IFO 180, and IFO 300 also exhibited a drop in F_{max1} intensity at DOR 1:20; in fact, IFO 120 F_{max1} at DOR 1:20 was

actually 17% lower than at DOR 0. These same three IFOs also had the highest overall concentration of PAHs, and all four IFOs were the only oils to contain any anthracene. For all oil types, total alkanes as a function of fluorescence intensity was found to be only loosely correlated, as total concentration increased overall in relation to fluorescence intensity with no clear relationship.

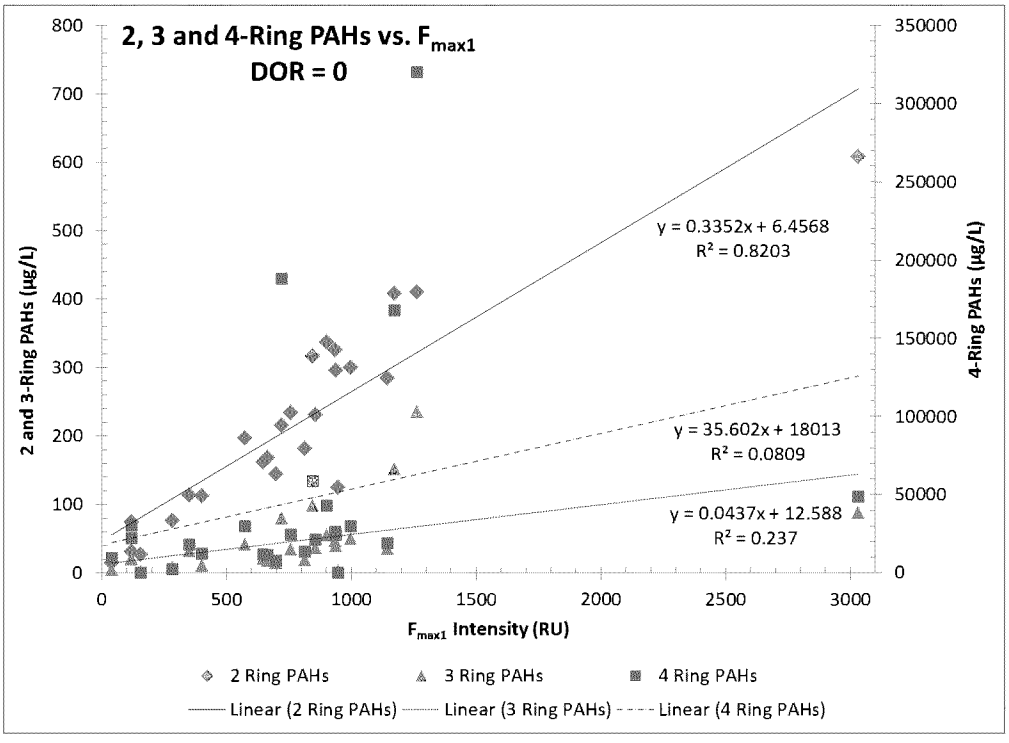

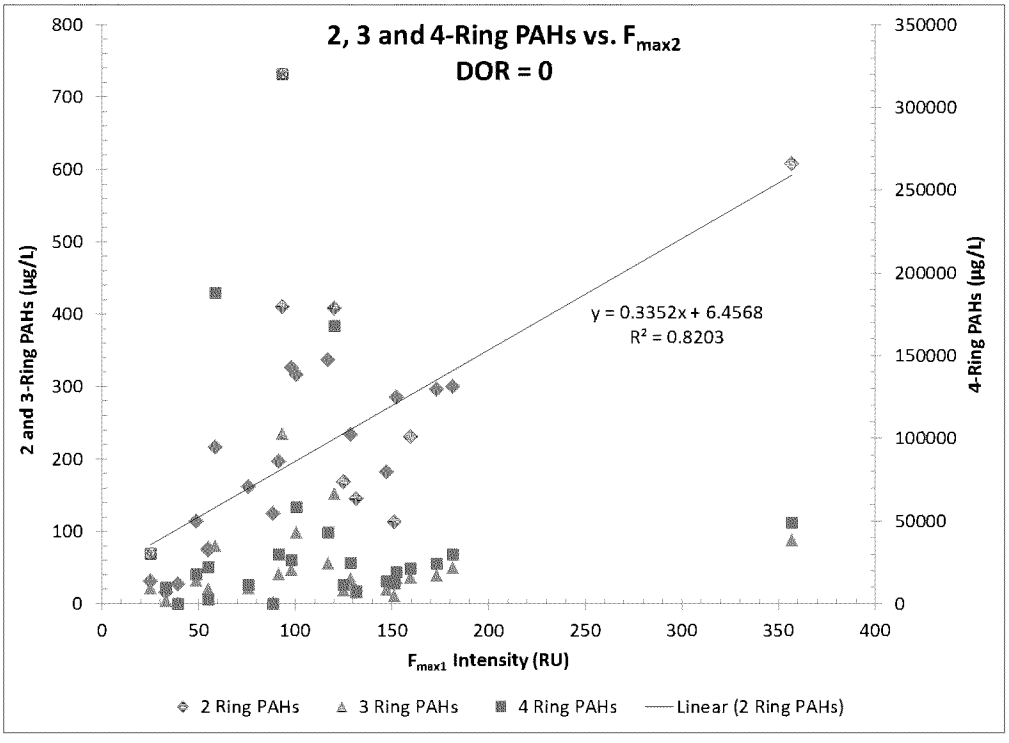

Figure 47. For all oil types at DOR 0, total concentration of 2-ring, 3-ring, and 4-ring PAHs (µg/L) against fluorescence intensity (RU) at F_{max1} (top), and against F_{max2} (bottom). Strong linear correlation exists between 2-ring PAHs and F_{max1} fluorescence, but little to no correlation between 3-ring or 4-ring PAHs and F_{max1} fluorescence intensity (top). Strong linear correlation also exists between 2-ring PAHs and F_{max2}, but no correlation between 3-ring PAHs or 4-ring PAHs and F_{max2} (bottom).

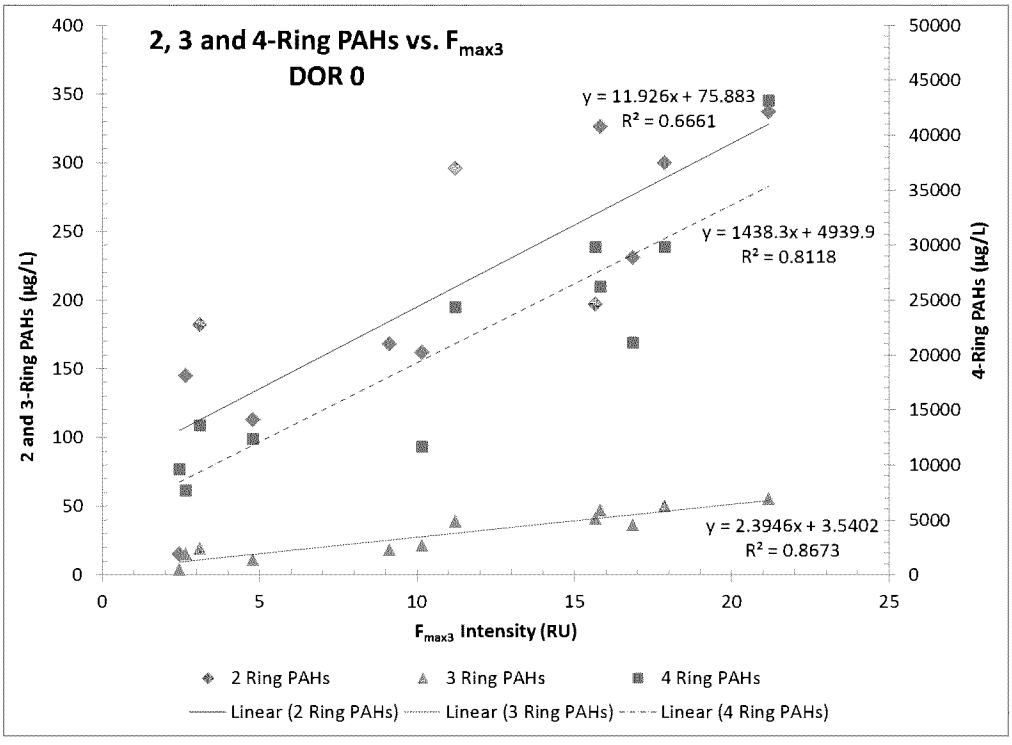

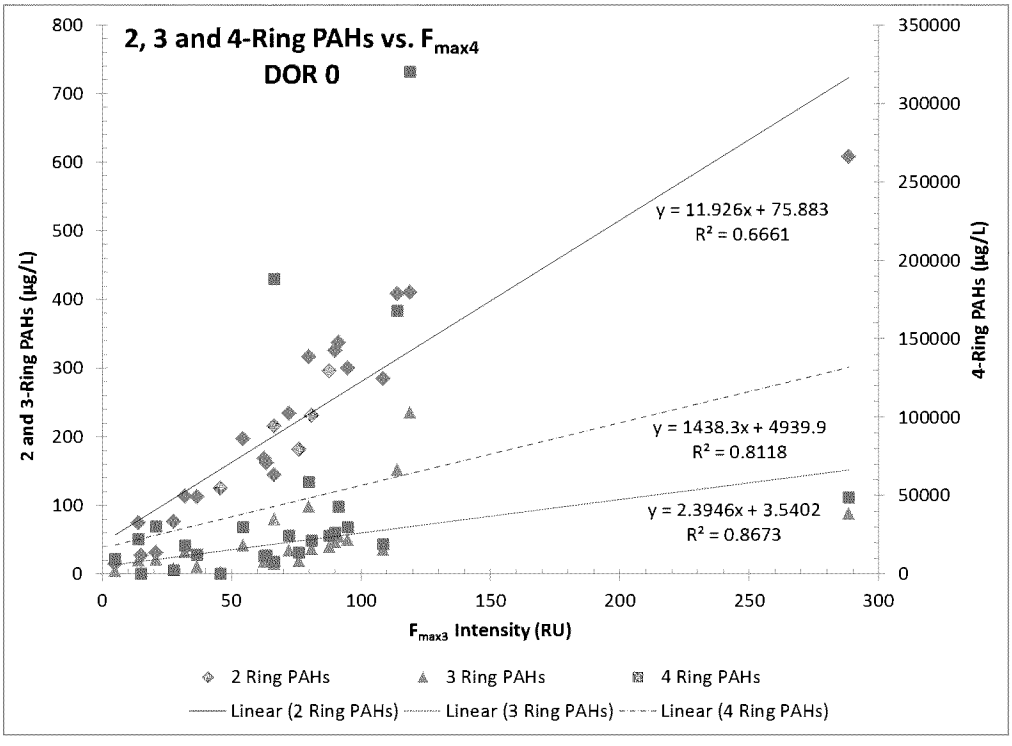

Figure 48. For all oil types at DOR 0, total concentration of 2-ring, 3-ring, and 4-ring PAHs (µg/L) against fluorescence intensity (RU) at F_{max3} (top), and against F_{max4} (bottom). Strong linear correlation exists between 3-ring and 4-ring PAHs and both F_{max3} and F_{max4} fluorescence; however, only moderate correlation exists between 2-ring PAHs and F_{max3} and F_{max4} fluorescence intensity.

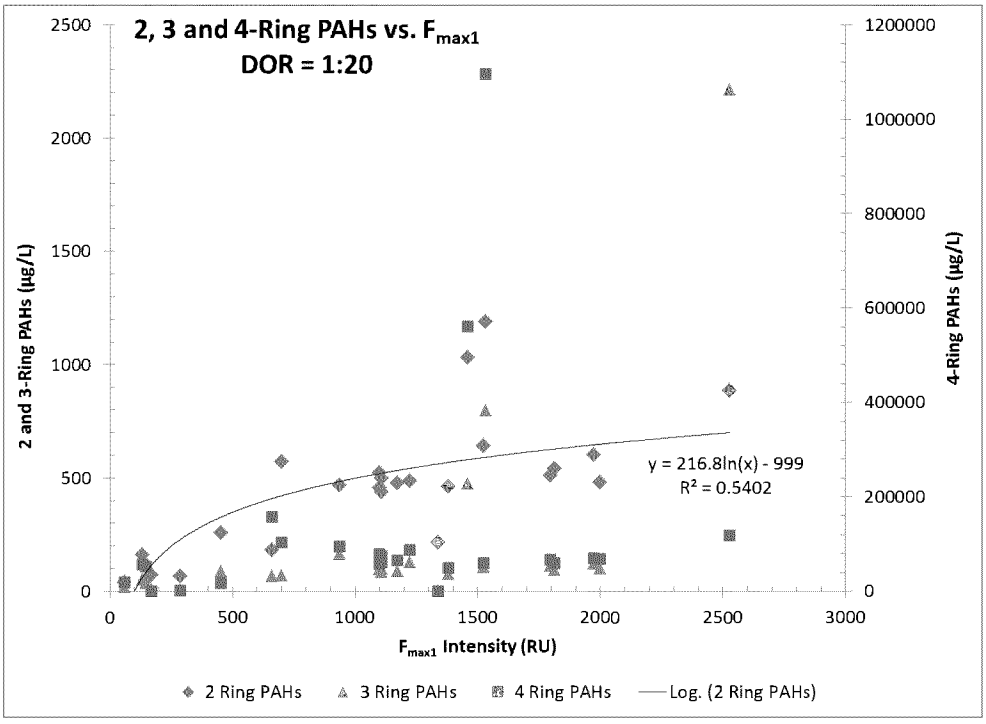

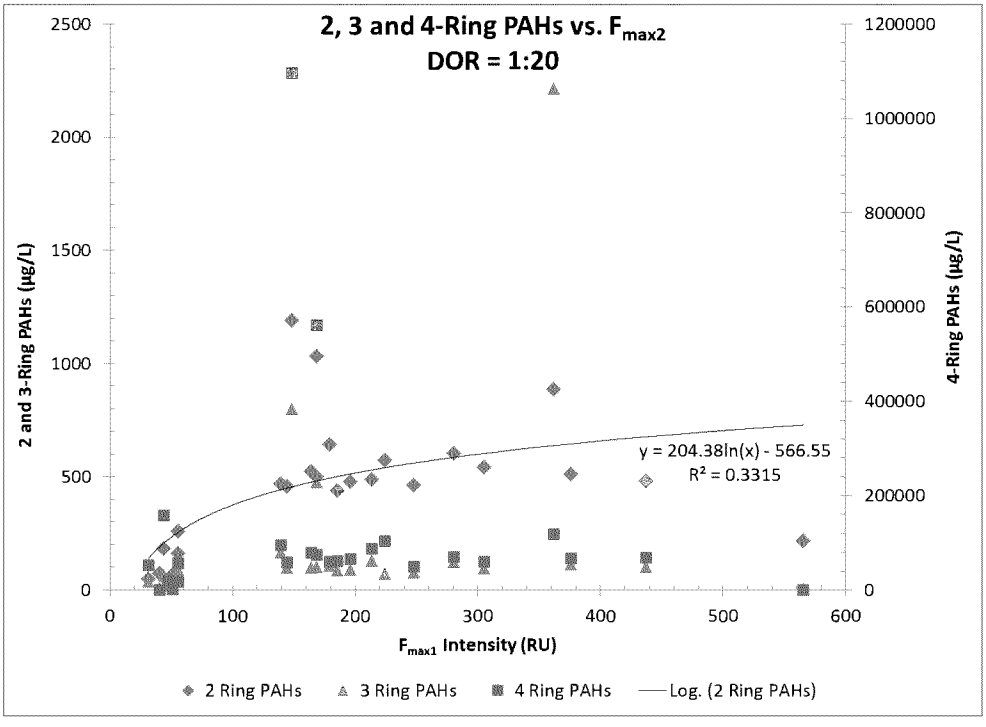

Figure 49. For all oil types at DOR 1:20, total concentration of 2-ring, 3-ring, and 4-ring PAHs (µg/L) against fluorescence intensity (RU) at F_{max1} (top), and against F_{max2} (bottom). A moderate logarithmic correlation is exhibited between 2-ring PAHs and fluorescence intensity (RU) at F_{max1} and a weaker correlation between 2-ring PAHs and F_{max2}, but no correlation exists between 3-ring or 4-ring PAHs and fluorescence intensity at either F_{max1} or F_{max2}.

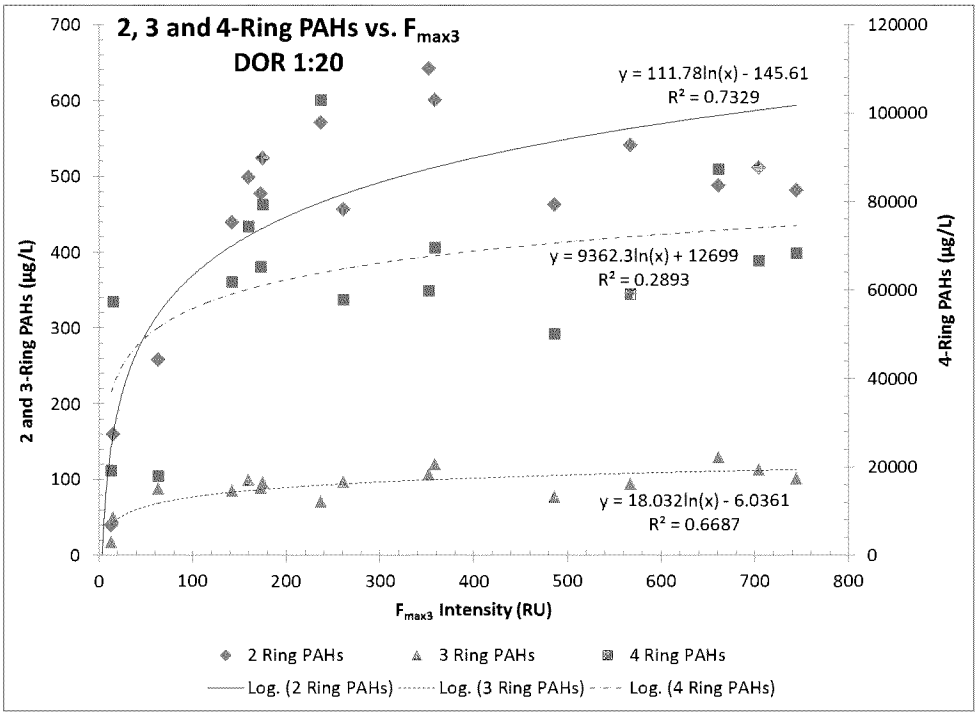

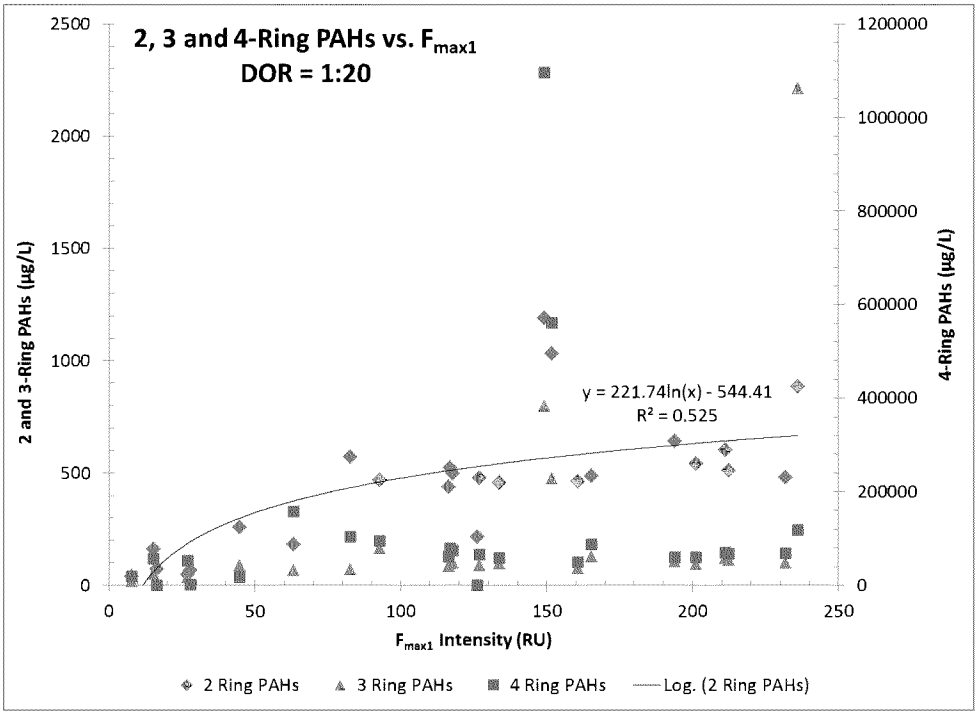

Figure 50. For all oil types at DOR 1:20, total concentration of 2-ring, 3-ring, and 4-ring PAHs (µg/L) against fluorescence intensity (RU) at F_{max3} (top), and against F_{max4} (bottom). A strong logarithmic correlation is exhibited between 2-ring PAHs and fluorescence intensity at F_{max3}. Moderate correlations exist between 3-ring PAHs and F_{max3} as well as between 2-ring PAHs and F_{max4}. However, only a weak logarithmic correlation exists between 4-ring PAHs and fluorescence intensity at F_{max3}, and there is no correlation between 3-ring or 4-ring PAHs and F_{max4}.

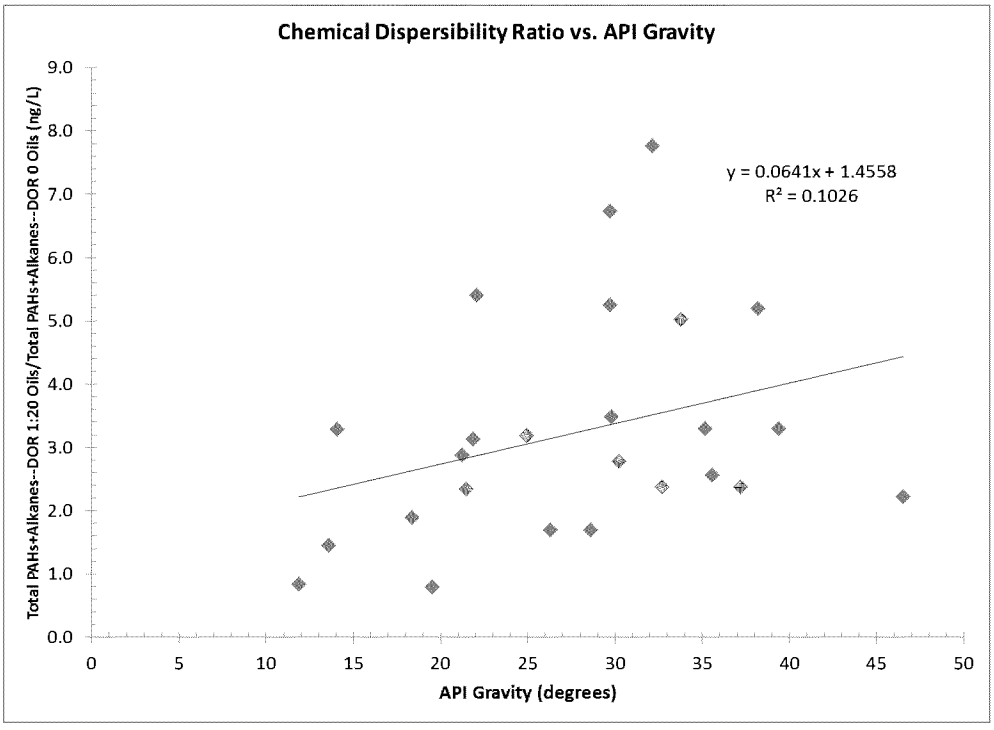

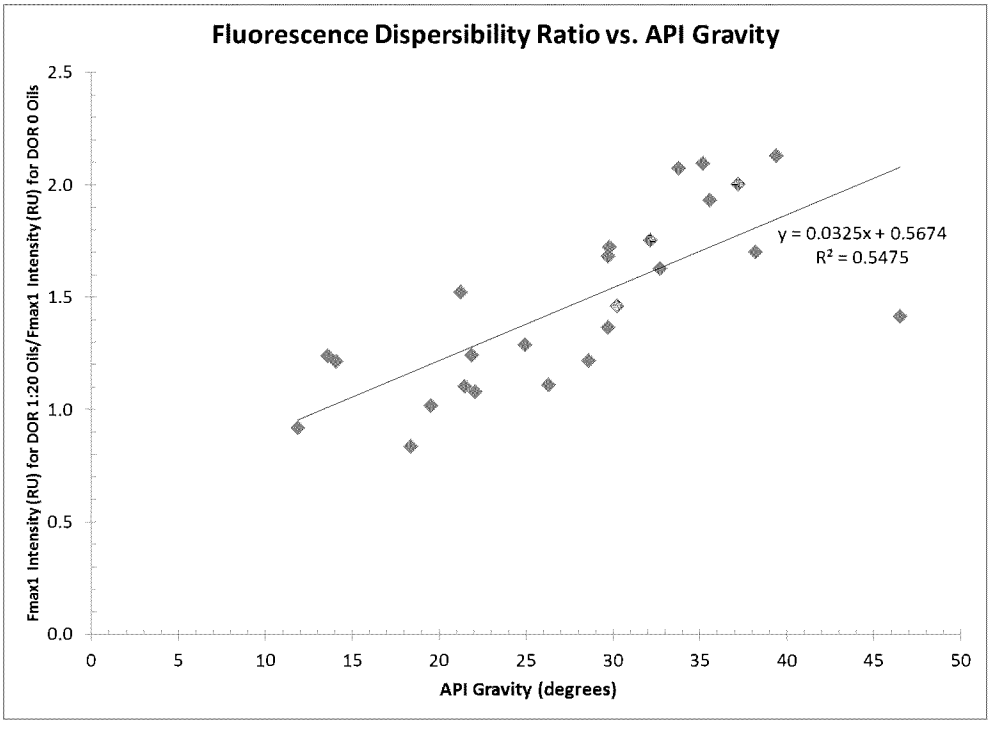

Figure 51. Chemical Dispersibility Ratio (CDR) vs. decreasing oil density (top) and Fluorescence Dispersibility Ratio (FDR) vs. decreasing oil density (bottom) show only a weak correlation between chemistry and oil density, and a moderate correlation between fluorescence and oil density. With the removal of the data point for Scotian Shelf Condensation, correlation between fluorescence and oil density improves to $R^2 = 0.71$.

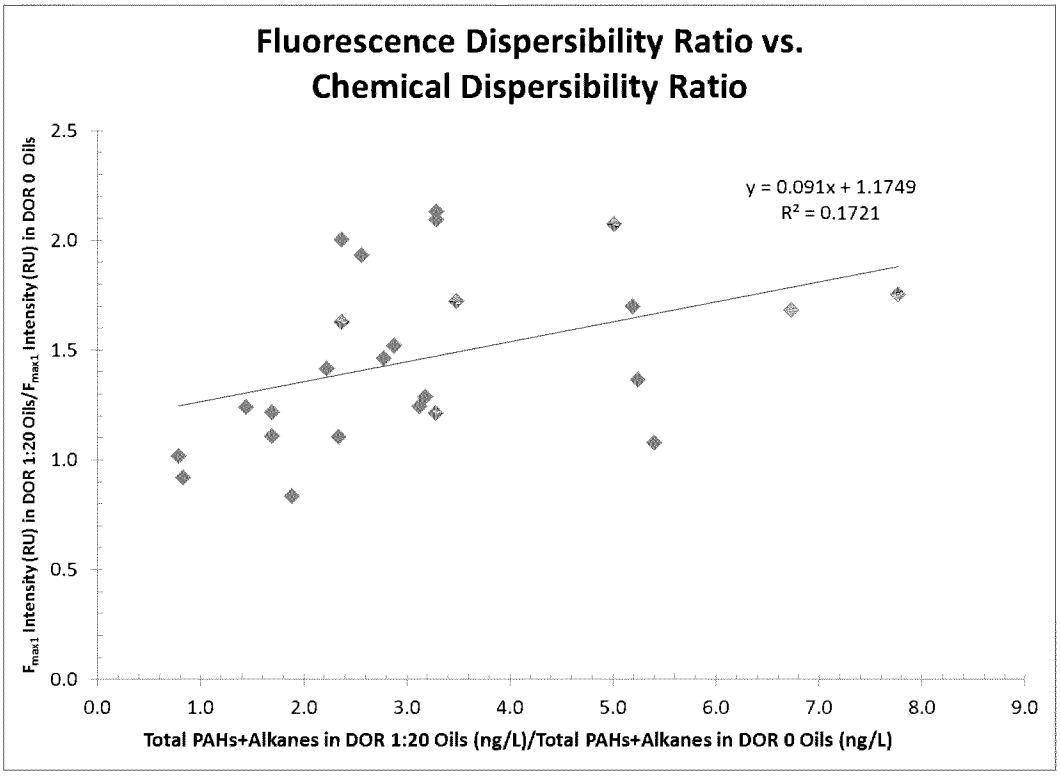

Figure 52. Fluorescence Dispersibility Ratio (FDR) vs. Chemical Dispersibility Ratio (CDR) shows weak correlation between these two ratios.

B.3.3 Flume Tank and Baffled Flask EEM Comparison

In addition to the EEMs generated from the BFT of 25 oil types, EEMS were also generated from the discrete sample collection during the flume tank experiments using South Louisiana Crude oil (SLC) in Task A of this project report. Samples for EEM analysis were collected and immediately analyzed on the same Horiba Aqualog at DFO using identical analysis protocols and data processing. A comparison of SLC MC252 EEMs for varying DOR from the BFT (left) and the flume tank (right) experiments are illustrated in Figure 53. Note that that the contour coloring for the peaks is identical between experiments, but the baseline color varied, where black was used for the BFT EEMs and blue used for tank EEMs, but the appearance of the blue color this is not to be confused with the presence of higher fluorescence in regions away from the peak fluorescence. Fluorescence Intensity Ratios (FIR) were calculated for the tank EEMs and found to be between 7.1 and 9.1 for DOR = 0, 1.3 and 4.3 for DOR = 1:100 and 0.6 and 0.8 for DOR = 1:20. This is follows the findings of Bugden et al., 2008 where a decrease in FIR is observed with the addition of dispersant. It is also consistent with the BFT EEMs which show a 4.9 for DOR = 0 and 0.4 for DOR = 1:20 (Supplemental Table A). These results indicate that FIR can be an indicator of dispersion effectiveness for SLC oil.

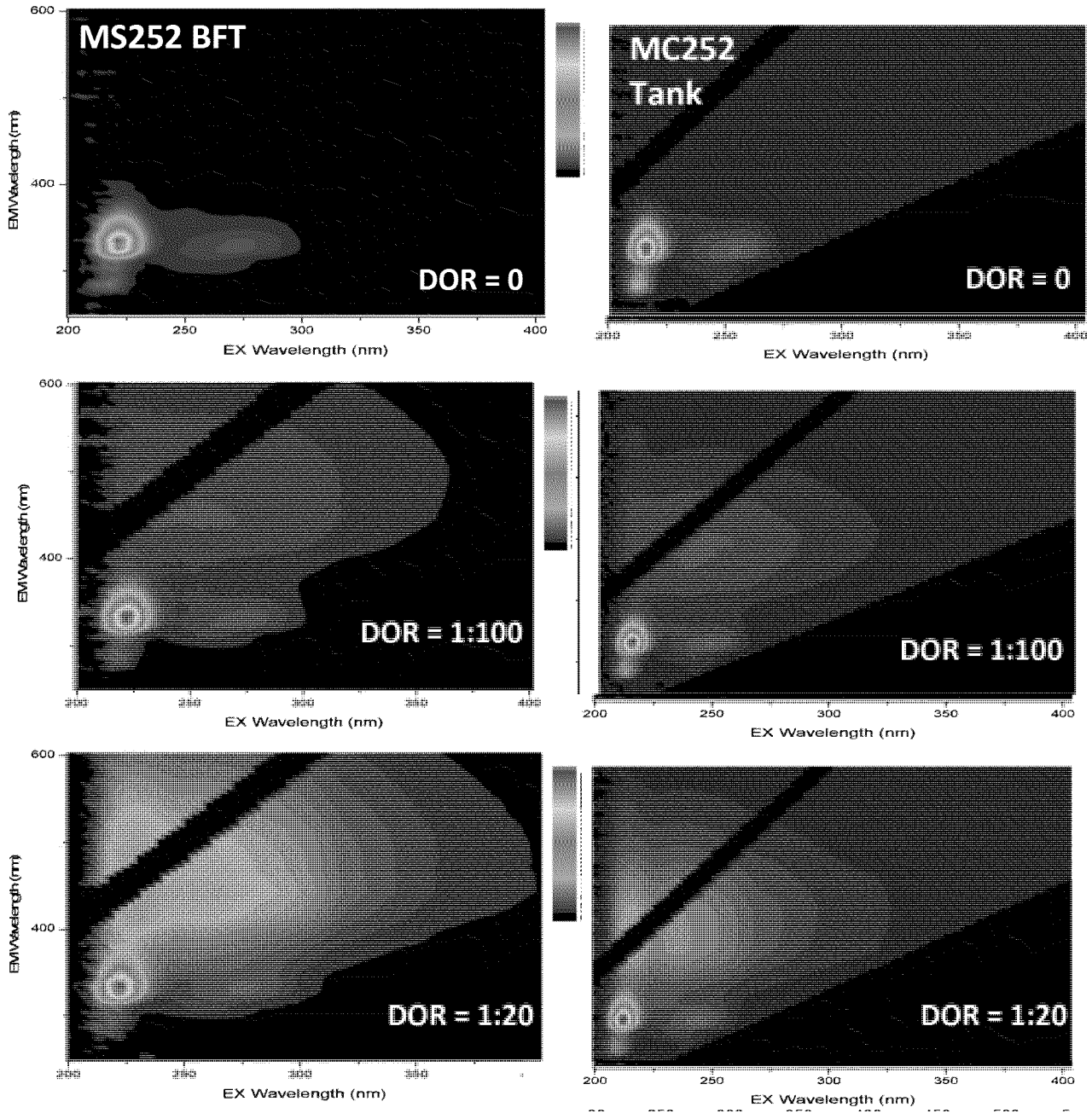

Figure 53. South Louisiana Crude MC252 EEMS from BFT (left panels) and tank experiments (right Panels) for DOR = 0, 1:100 and 1:20.

B.3.4 PARAFAC Modeling

Originally designed to model complexity in the field of psychometrics (Carroll and Chang, 1970; Harshman, 1970), parallel factor analysis (PARAFAC, also known as canonical decomposition or CANDECOMP) was first employed in the analysis of fluorescence data within the next ten years (Appellof and Davidson, 1981). Over the past twenty years, PARAFAC has been widely embraced by chemometricians and used to tease apart the overlapping fluorescence components of complex chemical mixtures containing fluorescent substances ranging from proteins and pigments to pesticides and PAHs (Andersen and Bro, 2003). More recently, PARAFAC analysis has been used in the analysis of the fate and transport of dispersed oil from the Deepwater Horizon Oil Spill (Mendoza, et al., 2013; Zhou, et al., 2003).

Presented with hundreds of complex fluorescence EEM data sets containing samples, excitation, and emissions; PARAFAC analysis can reduce this to data sets containing samples and intensity at a few important wavelength pairs (Murphy et al., 2014). In the past, this information gathering was often done via time-consuming "peak-picking" whereby EEMs were visually inspected for apparent F_{max} location, then fluorescence intensity data at that excitation/emission point was copied and pasted into a spreadsheet for further analysis. PARAFAC provides the capability to turn that somewhat qualitative task into a more quantitative exercise; however, careful preparation of the data is critical in order to obtain a meaningful outcome. PARAFAC analysis also allows the consideration of minor fluorescence peaks, which may have been overwhelmed by high-intensity major peaks, but may be no less important in the analysis of EEM results. More importantly, PARAFAC analysis allows for direct comparison to chemical composition upon successful modelling of an EEM data set (Murphy, et al., 2014). The steps that must be undertaken for successful PARAFAC analysis are: (1) assembling the dataset; (2) preprocessing to correct biases, remove scatter and normalize; (3) exploring the dataset to remove possible outliers and develop preliminary models; (4) validating the model by determining the proper number of components and evaluating model fit; (5) interpreting results (Murphy, et al., 2013).

In order to identify connections between the fluorescence profiles and underlying chemical

complexity of the 25 oil types in the BFT analysis (Figure 53), PARAFAC analysis was performed on the fluorescence data. The PLS Toolbox (Eigenvector, Inc.) was used within MATLAB (MathWorks, Inc. 2014b) to accomplish this task. After importing raw data and assembling datasets, three constraints were applied to all samples: normalization, EEM filtering, and non-negativity. Normalization was conducted to compensate for the wide variation in fluorescence intensity across oil types (F_{max1} = 39.6 RU for Access Western Blend Dilbit to F_{max1} = 3090.2 RU for IFO 120) in order to prevent samples with high fluorescence intensity values from skewing the model. Further, normalization of maximum intensity to 1 (inf-Norm) was chosen rather than normalization of the entire area of fluorescence (1-Norm) to preserve differences in spectral shape. EEM filtering was applied in order to remove artifacts of the fluorescence analysis process known as first and second order Rayleigh scatter. This was accomplished by interpolating data across those regions (12 nm for first order Rayleigh and 24 nm for second order Rayleigh); zero values were also assigned to sub-Rayleigh wavelengths since fluorescence emission takes place at wavelengths above excitation due to Stokes shift. Raman scatter, the other light-related artifact which must be removed before PARAFAC analysis can be performed, was accomplished as sample analysis was done by subtracting that day's sample blank from each sample. Upon running several PARAFAC test models using 4, 5, 6 and 7-components on a dataset containing the DOR 0 sample from flask #1 of all 25 oil types, data between excitation at 200 nm and 212 nm was excluded. The inherent "noise" typically found at excitation < 240 nm, related to the low intensity of xenon lamps in that region, led to this decision. Excluding data at excitation and emission wavelengths above 680 nm was also employed in order to improve processing results since no fluorescence information of value was contained in that region.

The biggest challenge in PARAFAC modelling is in determining the most appropriate number of component factors. While it is important to ensure separation of all individual factors, it is also critical not to select too many components in order to avoid over-fitting the data. Several ways of doing this are suggested in the PARAFAC tutorial (Bro, 1997): comparison of the resulting factor profiles with background knowledge of expected components, consideration of the

residuals, and split half validation of the model. The latter has also been recommended by other researchers (Harshman and Lundy, 1994; Murphy, et al., 2013). Split half analysis is accomplished by dividing the data into two independent subsets and applying the model to each of the subsets. In theory, if the correct number of components has been selected, the two halves of the data should each fit the model well; however, Murphy cautions that a relatively large data set is necessary in order for this to hold true (2013). Smilde, et al., (2004) also caution that some phenomenon observed within a subset of data may not match the overall model, but instead may just be present in that particular random half of the dataset. Thus, it could be anticipated that split half validation will work better with samples within oil weight subdivisions than with the dataset containing all 25 oil types as a whole. Bro and Kiers (2003) have also advised using core consistency of the model to validate that the correct number of components have been selected. All of these methods were employed for the following analyses by first noting the percentage of data fit by the model, next checking the core consistency of the model, then inspecting residuals, inspecting the loadings for Mode 3 (excitation) and Mode 2 (emission), and inspecting EEMs of each component. Finally, split half analysis was done. In all cases, several models were run with different numbers of components to ensure selection of the most appropriate model.

DOR 0

Initially, a five-component model was fit to the dataset, followed by 4-, 6- and 7-component models. Best overall fit was obtained with the six-component model, which explained 99.504% of the data. Core consistency was 52%, and split half validation was 56.4% (Figure 54). Review of residuals showed they were minimal with random distribution, inspection of plots of Mode 2 and Mode 3 loadings (Figure 55), variation per component (Figure 56), as well as EEMs of individual components (Figure 57) all supported choice of the 6-factor model for best fit.

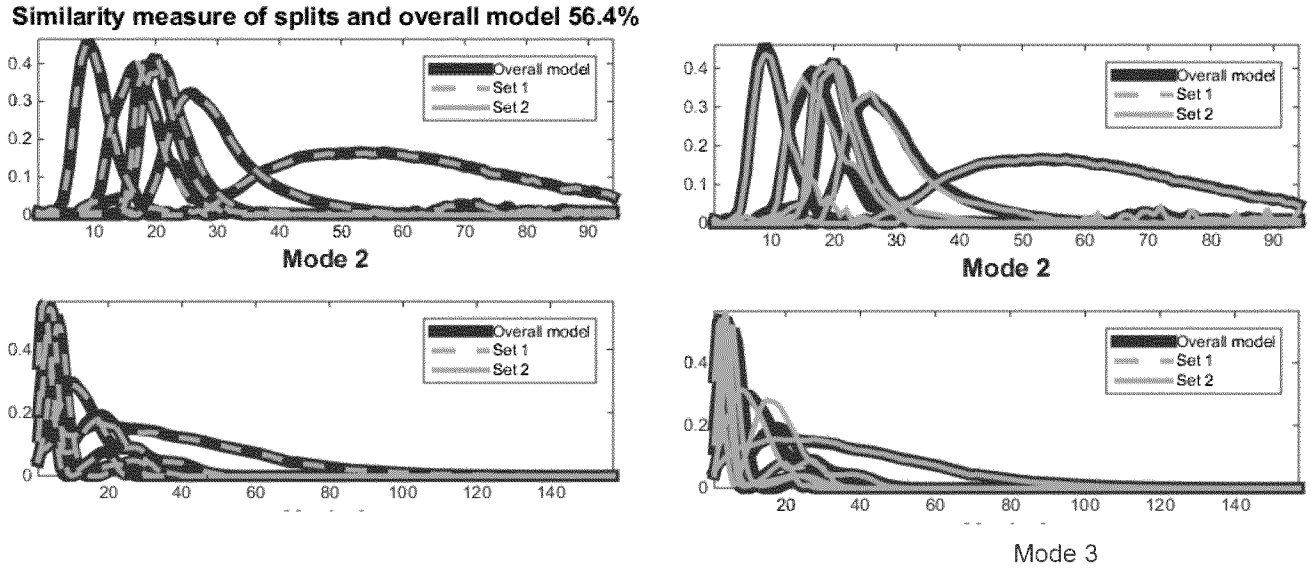

Figure 54. Example of split half validation for the 6-component model of 25 oil types at DOR 0 showing individual fit of data splits (Set 1, left; and Set 2, right) compared to overall model for Mode 2 (top) and Mode 3 (bottom) loadings.

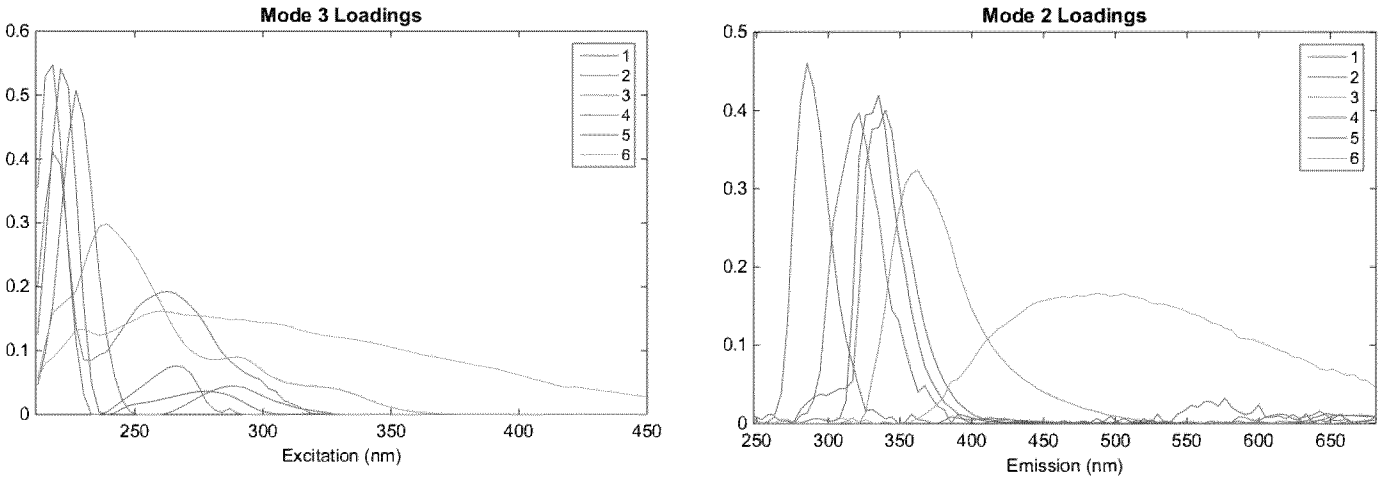

Figure 55. Mode 3 Loadings (Excitation) and Mode 2 Loadings (Emission) for all 25 oil types—DOR0 using 6-component model. Note difference in x-axis scales. Although components are tightly spaced, all appear as separate and distinct peaks.

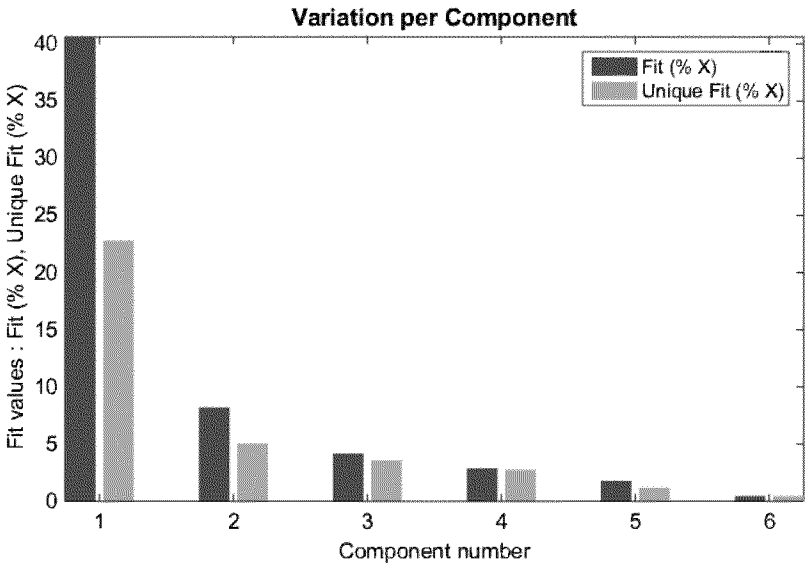

Figure 56. Variation per Component shows Component 1 accounted for >20% to 40% (unique fit and fit) of the data, while Component 2-contributed 5-10% (unique fit and fit) and Components 3-6 accounted for 5% or less of the data, respectively. While Component 6 accounted for a very low percentage of the data, the 6-component model was still a better fit to the data than the 5-component model.

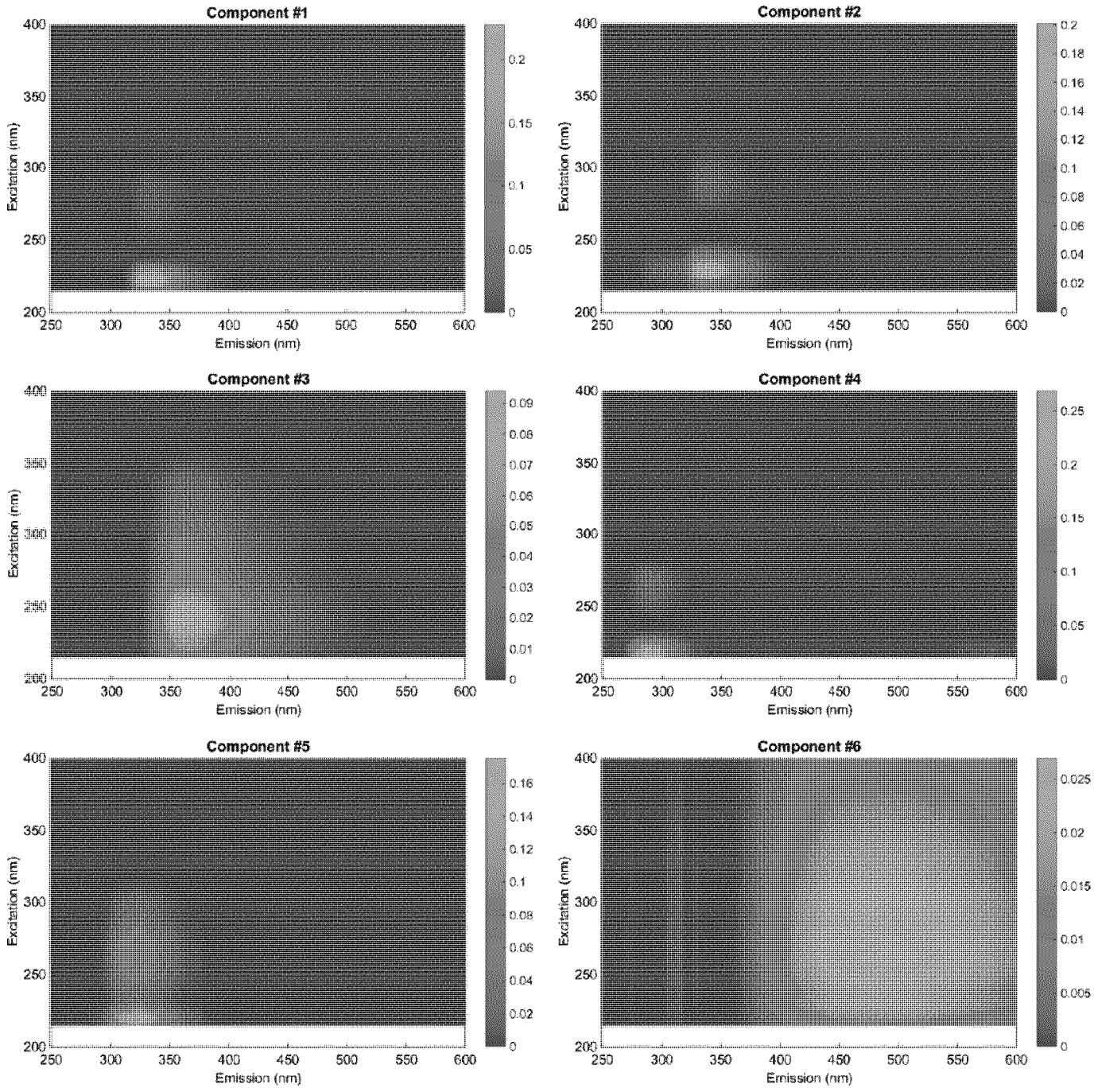

Figure 57. EEM views of the six components of PARAFAC model for 25 oil types at DOR 0. Component #1: F_{max} = Ex 224nm/Em 335nm; Component #2: F_{max} = Ex 230nm/Em 340nm; Component #3: Fmax = Ex 239nm/Em 363nm; Component #4: Fmax = Ex 218nm/Em 290 nm; Component #5: Fmax = Ex 221nm/Em 322nm; Component #6: Fmax = Ex 260nm/Em 474-511nm.

DOR 1:100

A six-component model was fit to the dataset containing all 25 oil types at DOR 1:00 since that was the best fit for the DOR 0 dataset, followed by a 7-component model, which returned an error warning that two or more components may be fitting the same feature, as well as core consistency <0%. Finally, a 5-component model was fit to the dataset. Interestingly, for the DOR 1:100 dataset, the 5-component model proved to be the best fit, explaining 99.353% of the data with core consistency of 72% and split half validation of 75.8%. Residuals were minimal and randomly distributed, and visual inspection of loadings (Figure 58), variation per component (Figure 59) and component EEMs (Figure 60) led to acceptance of the 5-component model.

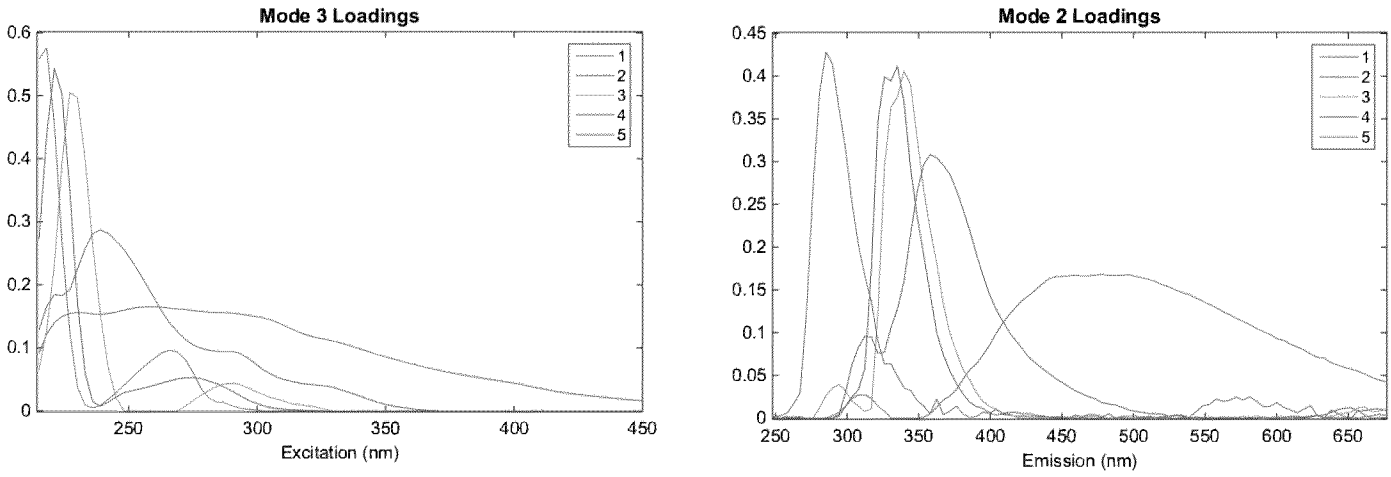

Figure 58. Mode 3 Loadings (Excitation) and Mode 2 Loadings (Emission) for all 25 oil types—DOR 1:100 using 5-component model. Note difference in x-axis scales. Although components are tightly spaced, all appear as separate and distinct peaks.

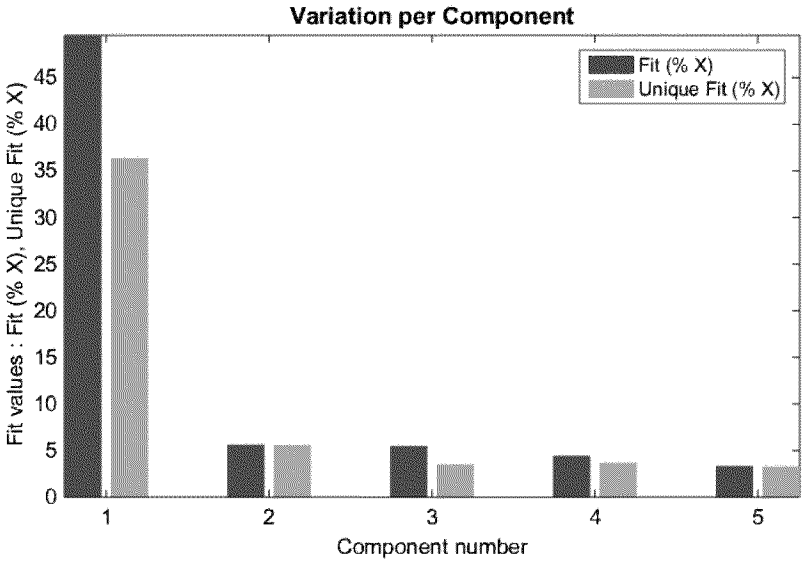

Figure 59. Variation per Component shows Component 1 accounted for >35% to almost 50% (unique fit and fit) of the data, while Components 2-5 accounted for 5% or less of the data, respectively.

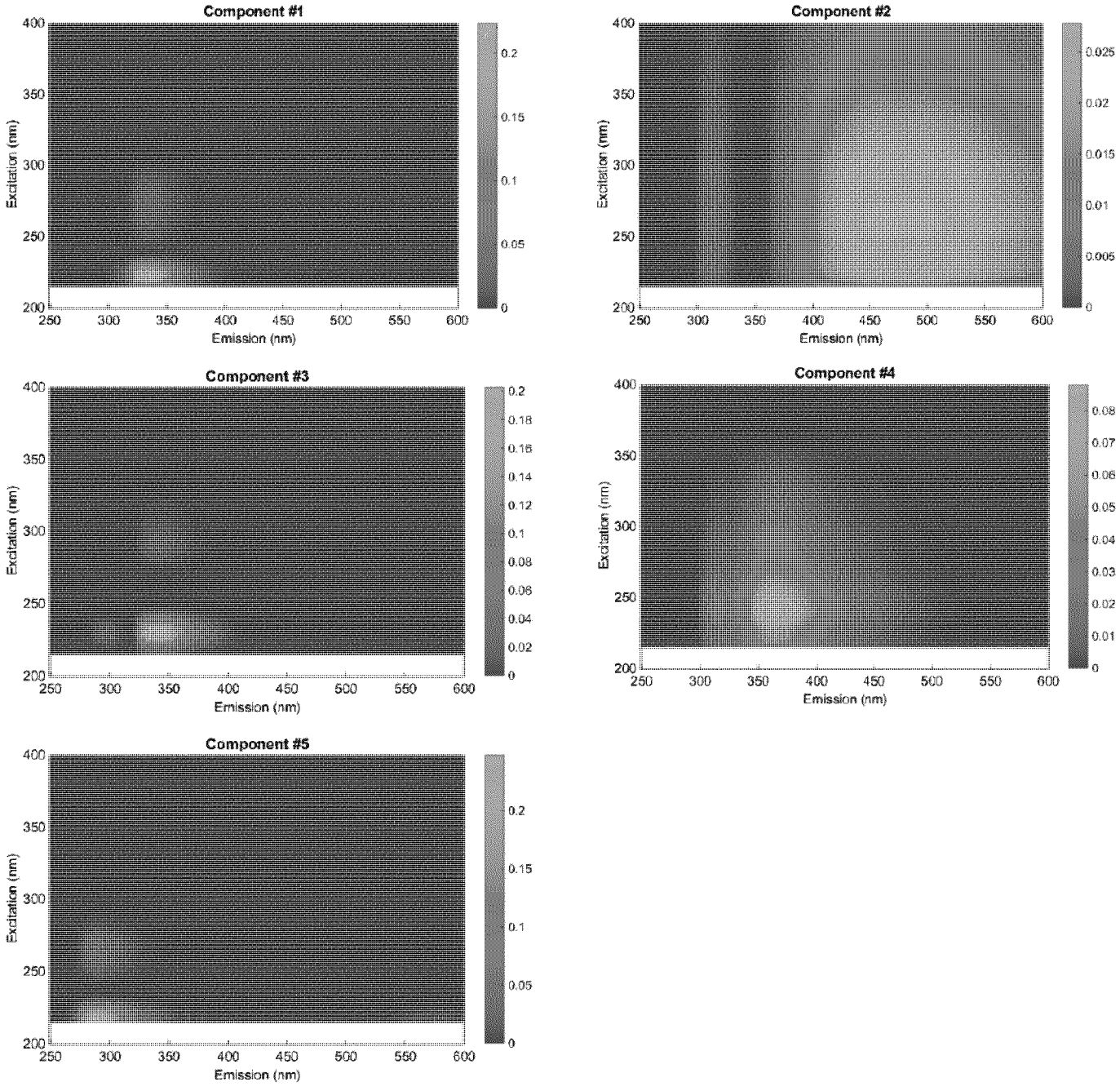

Figure 60. EEM views of the five components of PARAFAC model for 25 oil types at DOR 1:100. Component #1: F_{max} = Ex 224nm/Em 335nm; Component #2: F_{max} = Ex 254-266nm/Em 455-501nm; Component #3: F_{max} = Ex 230nm/Em 344nm; Component #4: F_{max} = Ex 242nm/Em 363 nm; Component #5: F_{max} = Ex 218nm/Em 290nm.

DOR 1:20

Once again, a six-component was fit to the dataset containing all 25 oil types at DOR 1:20; however, an error message warning that two or more components may be fitting the same data was displayed, and the core consistency was <0%. Fitting a 5-component model to the data, however, resulted in 98.891% of the data explained by the model as well as core consistency of 84% and a split half validation of 84%. Overall, residuals were minimal and randomly distributed; however, residuals appeared to occur at somewhat higher wavelengths than at other DORs. Visual inspection of loadings (Figure 60), variation per component (Figure 62), and component EEMS (Figure 63) led to final acceptance of the 5-component model.

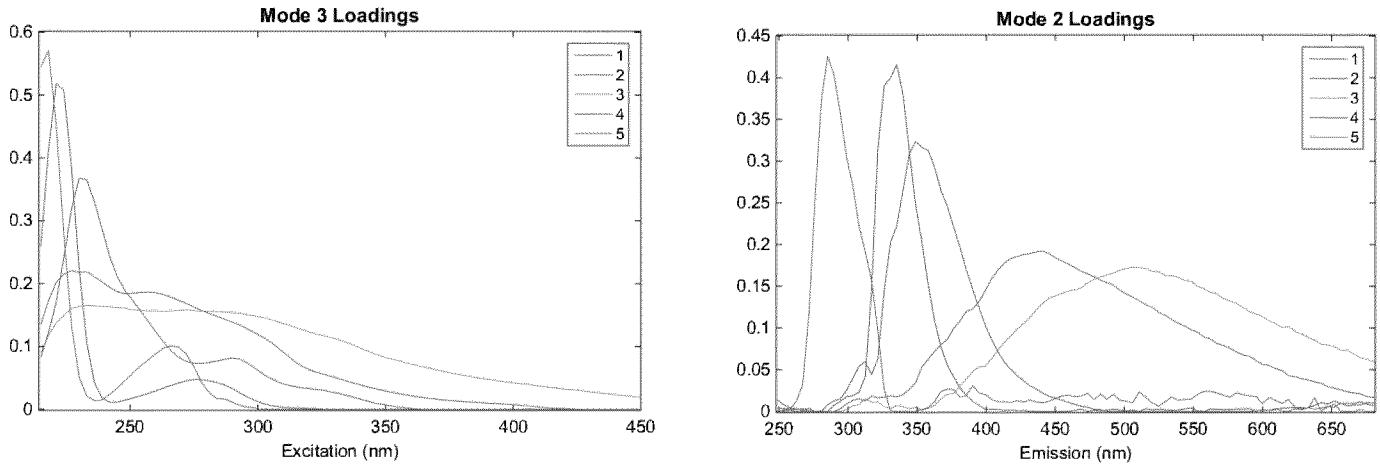

Figure 61. Mode 3 Loadings (Excitation) and Mode 2 Loadings (Emission) for all 25 oil types—DOR 1:20 using 5-component model. Note difference in x-axis scales. Effect of full dispersion appears to broaden and shift emission peaks to longer wavelengths.

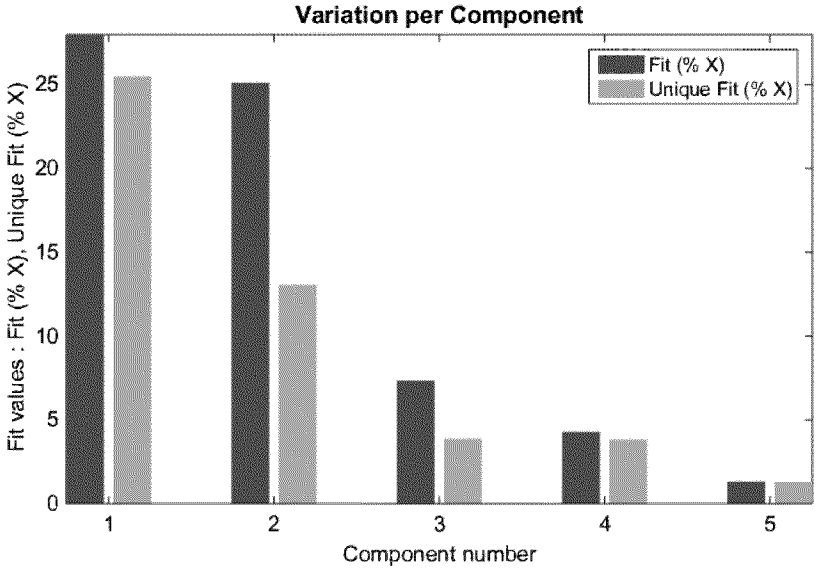

Figure 62. Variation per Component shows Component 1 accounted for 25 to 30% of the data (unique fit and fit) while Component 2 has increased to >10% to 25% (unique fit and fit) of the data. Contribution from Component 3 and 4 have increased, as well.

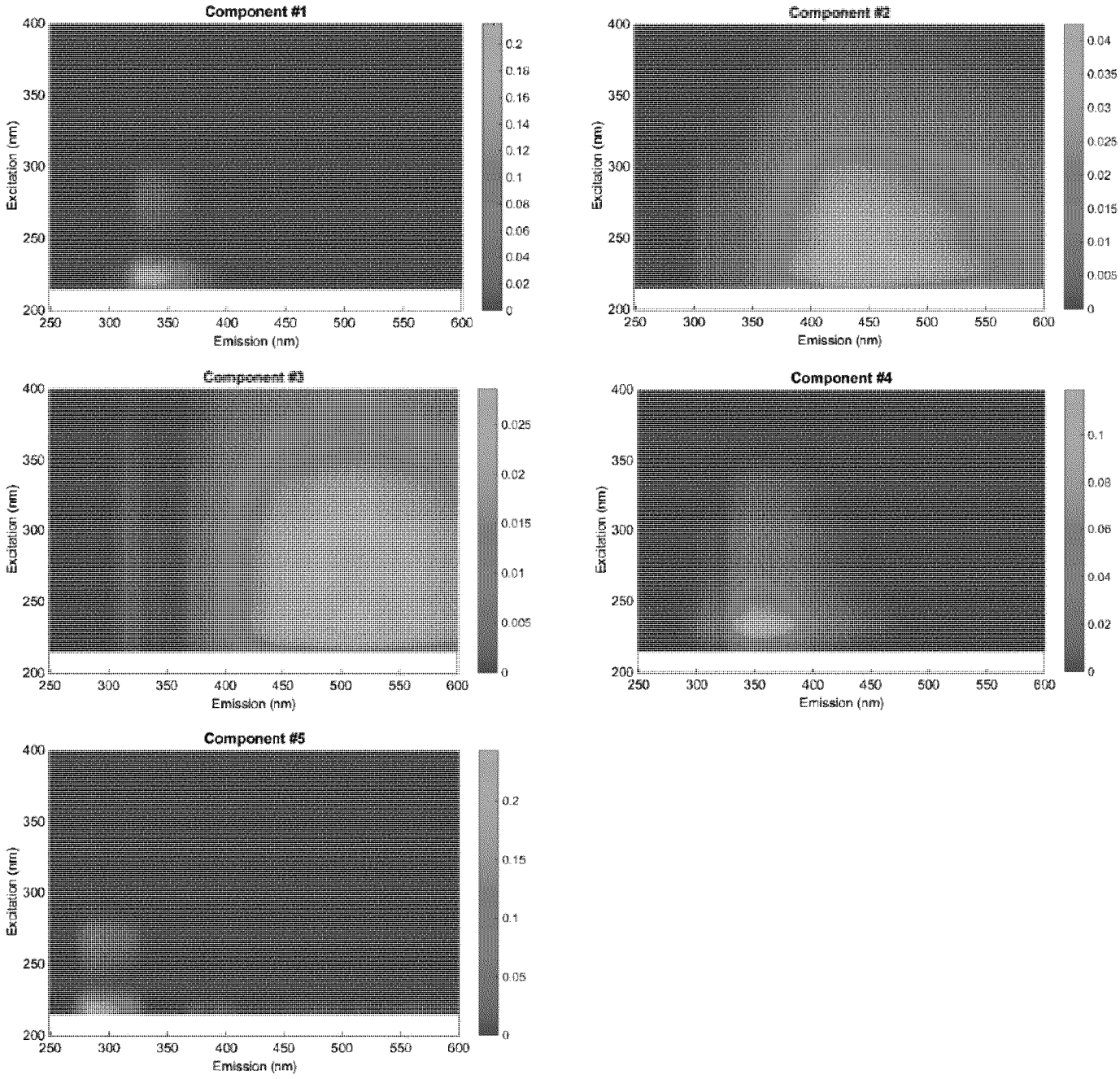

Figure 63. EEM views of the five components of PARAFAC model for 25 oil types at DOR 1:20. Component #1: F_{max} = Ex 224nm/Em 335nm; Component #2: F_{max} = Ex 233-266nm/Em 432-450nm; Component #3: F_{max} = Ex 230-242nm/Em 501-520nm; Component #4: F_{max} = Ex 233nm/Em 349nm; Component #5: F_{max} = Ex 218nm/Em 290nm.

PARAFAC Summary

PARAFAC analysis of EEM datasets for the 25 oil types at DOR 0, DOR 1:100 and DOR 1:20 show interesting changes in fluorescence intensity with increasing dispersion. However, we see a decrease in distinct components from six at DOR 0 to five at DOR 1:100 and 1:20. From analysis of plots of Mode 3 (Excitation) and Mode 2 (Emission) Loadings, it appears that increased dispersion results in a broadening and shift to longer emission wavelengths as well as in a larger contribution of fluorescence intensity at higher wavelengths. Upon examination of the EEMs of each component, several other patterns emerge. Even with the minimal dispersion at DOR 1:100, contribution to the overall model from a broad fluorescence peak which provided the least contribution to the overall model at DOR 0--Component #6—became second in importance at DOR 1:100, albeit with a contribution to the model of only about 5%. Upon full dispersion at DOR 1:20, this broad, high-wavelength peak retained importance to the model of approximately 5-7%; however, another broad, but slightly lower wavelength peak appeared as Component #2 with 12-25% contribution to the overall model. Throughout the entire analysis, Component #1 at Ex 224nm/Em 335nm remained the most important contribution to the model, which confirms this fluorescence region as the best target for detecting oil in the marine environment. However, since the region represented by Component #2 in the DOR 1:20 dataset becomes a major contribution to the model only upon effective dispersion, the FIR ratio (Bugden et al., 2008) can be used to track this important parameter.

The MC252 oil samples used for these analyses, both ones collected onboard the Discoverer Enterprise during DWH and the generic version provided by BP, are classified as light, sweet crude based on density and sulfur content. Overall, oil types range from light to heavy due to the proportion of n-alkanes and cyclo-alkanes vs. aromatic hydrocarbon compounds, while sulfur content determines the rank of sweet (<1%) vs. sour (>1%). These characteristics arise from kerogen source and reservoir maturity (Tissot and Welty, 1978). The 25 oils analyzed in the BFT cover a wide range of light to heavy oil types, as well as a range of sulfur content. Oil fluorescence phenomena arise from the presence of π-bonding in C=C bonds, leading to highest fluorescence intensity from polycyclic aromatic hydrocarbons (Ryder, 2005), with fluorescence

intensity tending to increase with increasing molecular weight (Mendoza, et al., 2013). However, the presence of fluorescence quenching species, as well as energy transfer between complex molecules, complicates the isolation of compound-specific fluorescence in crude oil analysis. Fluorescence research has shown that heavy oils generally have broad, weak fluorescence while lighter oils have narrower, more intense emission bands (Steffens and Landulfo, 2010). Due to the hundreds, if not thousands, of complex hydrocarbons present in crude oils, characterization of fluorescence arising from specific PAH molecules would not be useful. However, PARAFAC analysis of these 25 oil types has shown that it is possible to use fluorescence characterization in specific wavelength regions for detect ion of non-dispersed vs. dispersed oil across a wide variety of oil types.

The well depth of the MC252 oil source is by far the deepest of all our 25 oil type sources (approximately 1600 m); however, a number of other oil types were sourced from offshore well locations. These include the light oils Brent and Gullfaks from the North Sea (140-230 m water depth) as well as Hibernia, Scotian Shelf Condensate and Terra Nova from offshore eastern Canada (12-100 m water depth). Intermediate weight oils Heidrun from the Norwegian Sea (350 m water depth) and Sea Rose from off the coast of Newfoundland, Canada (100 m water depth) as well as the heavy oil Hondo from offshore California (260 m water depth) were also included in this study. The intermediate weight Alaskan North Shore, both fresh and 10% weathered, would be representative of oil which may be sourced from offshore Alaska in the future. Additionally, with the presence of approximately 3,000 platforms in the U.S. Gulf of Mexico (BOEM, 2016), understanding the characterization of non-dispersed and dispersed MC252 oil will certainly aid in preparedness for the possibility of future oil spill events in that region.

References

Alliance for Coastal Technologies Report (2008) Hydrocarbon sensors for oil spill prevention and response. Ref # [UMCES]CBL08-095, 28 pp.

Andersen, C. M., R. Bro (2003) Practical aspects of PARAFAC modeling of fluorescence excitation-emission data. J. Chemom., 17:200-217.

Appellof, C.J., and E.R. Davidson (1981) Strategies for Analyzing Data from Video Fluorometric Monitoring of Liquid Chromatographic Effluents. J. Anal. Chem. 53:2053-2056.

Bahram, M., et al. (2006). "Handling of Rayleigh and Raman scatter for PARAFAC modeling of fluorescence data using interpolation." Journal of Chemometrics 20(3-4): 99-105.

Bieroza, M., A. Baker, J. Bridgeman (2010) Classification and calibration of organic matter fluorescence data with multiway analysis methods and artificial neural networks: an operational tool for improved drinking water treatment. Envirometrics, 22: 256-270.

Boehme, J.R., PG. Coble, R.N. Conmy (2004) Examining CDOM fluorescence variability using principal component analysis: seasonal and regional modeling of three-dimensional fluorescence in the Gulf of Mexico. Marine Chemistry, 89:3-14.

Bro, R. (1997) PARAFAC. Tutorial and applications. Chemometrics and Intelligent Laboratory Systems. 38:149-171.

Bro, R., and H.A.L. Kiers (2003) A new efficient method for determining the number of components in PARAFAC models. J. Chemometrics 17:274-286.

Bugden, J.B.C., C.W. Yeung, P.E. Kepkay, K. Lee (2008) Application of ultraviolet fluorometry and EEMS to fingerprint oil and chemically dispersed oil in seawater. Marine Pollution Bulletin, 56(4): 677-85.

CRRC Report (2010) Coastal Response Research Center Deepwater Horizon Dispersant USE Meeting Report, May 26-27, 2010, 108 pp.

Carroll, J.D. and J.-J. Chang (1970) Analysis of Individual Differences in Multidimensional Scaling via an N-Way Generalization of "Eckart-Young" Decomposition. Psychometrika 35:283-319.

Christensen, A.B. Hansen, J. Mortensen, O. Andersen (2005) Characterization and matching of oil samples using fluorescence and PARAFAC. Anal. Chem., 77:2210-17.

Coble, P.G. (1996) Characterization of marine and terrestrial DOM in seawater using EEM spectroscopy. Mar. Chem., 51: 325-346.

Coble, P.G. (2014) Aquatic Organic Matter Fluorescence. In Aquatic Organic Matter Fluorescence. Coble, P.G., Lead, L., Baker, A., Reynolds, D.M. and Spencer, R.G.M., Eds., Cambridge University Press, pp. 75-122.

Cole, M.G., T. King, K. Lee (2007) Analytical technique for extracting hydrocarbons from water using sample container as extraction vessel in combination with a roller apparatus. Anal. Chem., 77: 2210-17.

Conmy, R.N., P.G. Coble and C.E. Del Castillo (2004) Calibration and performance of the WetLabs' SAFIre

in situ fluorometer using seawater. Contin. Shelf Res., 24: 431-42.

Conmy, R. N., et al. (2014a) Submersible Optical Sensors Exposed to Chemically Dispersed Crude Oil: Wave Tank Simulations for Improved Oil Spill Monitoring. Environ Sci Technol 48(3): 1803-1810.

Conmy, R.N., C.E. Del Castillo, B. Downing, R.F. Chen (2014b) Calibrations and Quality Control of *In situ* Sensors. In: Fluorescence Applications in Aquatic Science. Eds: A. Baker & P.G. Coble, Cambridge Univ. Press, 31 pp.

Fingas, M. (2011) Introduction to Oil Chemistry and Properties. In Oil Spill Science and Technology; Fingas, M., Eds; Elsevier. pp. 51-59.

Frank, U. (1978) A Review of Fluorescence Spectroscopic Methods for Oil Spill Source Identification. Toxicological and Environment Chemistry Rev., 2:163-185.

Fuller, C.B., J.S. Bonner, C.A. Page, G. Arrambide, M.C. Sterling, Jr., T. Ojo (2003) Field instruments for real time in-situ crude oil concentration measurements. A Conrad Blucher Institute, Texas A&M Corpus Christi Report, 10 pp.

Harshman, R.A. (1970) Foundations of the PARAFAC procedure: Models and conditions for an "explanatory" multimodal factor analysis. UCLA Working Papers in Phonetics 16:1-84.

Harshman, R.A. and M.E. Lundy (1994) PARAFAC: Parallel factor analysis. Computational Statistics & Data Analysis 18:39-72.

Johansen, O., et al. (2013) Droplet breakup in subsea oil releases - Part 2: Predictions of droplet size distributions with and without injection of chemical dispersants. Marine Pollution Bulletin 73(1): 327-335.

Joint Analysis Group Report (2010) Review of Data to Examine Subsurface Oil in the Vicinity of DWH MC-252, May 19-June 19, 2010; 29 pp.

Kepkay, P., W. Young, J.B.C. Bugden, Z. Li, K. Lee (2008) Ultraviolet fluorescence spectroscopy (UVFS): A new means of determining the effectiveness of chemical dispersants on oil spills. International Oil Spill Conference. API, Washington D.C., Savannah, GA, pp. 639-44.

King, T.L., B. Robinson, C. McIntyre, P. Toole, S. Ryan, F. Saleh, M.C. Boufadel, K. Lee (2015) Fate of surface spills of cold lake blend diluted bitumen treated with dispersant and mineral fines in a wave tank. In: Environmental Engineering Science, Vol. 32, No. 3, 01.03.2015, p. 250-261.

Lee, K., Li, Z., Boufadel, M.C., Venosa, A.D. and Scott Miles, M. (2009) Wave tank studies on dispersant effectiveness as a function of energy dissipation rate and particle size distribution. Final report submitted to NOAA/CRRC/UNH. Pp67+ appendix.

Li, Z., Lee, K., King, T., Boufadel, M.C. and Venosa, A.D., (2008) Oil droplet size distribution as a function of energy dissipation rate in an experimental wave tank 2008 International Oil Spill Conference. American Petroleum Institute, Washington D.C., Savannah, GA, pp. 621-626.

Li, Z., Lee, K., King, T., Boufadel, M.C. and Venosa, A.D., (2009a) Evaluating Chemical Dispersant Efficacy in an Experimental Wave Tank: 2, Significant Factors Determining *In Situ* Oil Droplet Size Distribution. Environmental Engineering Science, 26(9): 1407-1418.

Li, Z., Lee, K., King, T., Boufadel, M.C. and Venosa, A.D., (2009b) Evaluating crude oil chemical dispersion efficacy in a flow-through wave tank under regular non-breaking wave and breaking wave conditions. Marine Pollution Bulletin, 58: 735-744.

Li, Z., Lee, K., King, T., Boufadel, M.C. and Venosa, A.D., (2010) Effects of temperature and wave conditions on chemical dispersion efficacy of heavy fuel oil in an experimental flow-through wave tank. Marine Pollution Bulletin, In Press, Corrected Proof.

Li, Z., K. Lee, T. King, P.E. Kepkay, O. Mikkelsen, C. Pottsmith (2011) Monitoring dispersed oil droplet size distribution at the GOM Deepwater Horizon spill site. International Oil spill Conference Proceedings, March 2011.

Masutani, S.M., E.E. Adams (2000) Experimental Study of Multiphase Plumes with Application to Deep Ocean Oil Spills," Final Report to U.S. Dept. of the Interior, Minerals Management Service, Contract No., 1435-01-98-CT-30946.

Mendoza, W.G., D.D. Riemer, R.G. Zika (2013) Application of fluorescence and PARAFAC to assess vertical distribution of subsurface hydrocarbons and dispersant during the Deepwater Horizon oil spill. Environmental Science Processes & Impacts 15:1017-1030.

Murphy, K. R., et al. (2010). "Measurement of Dissolved Organic Matter Fluorescence in Aquatic Environments: An Interlaboratory Comparison." Environ Sci Technol 44(24): 9405-9412.

Murphy, K. R., C.A. Stedmon, D. Graeber, R. Bro (2013) Fluorescence Spectroscopy and mutli-way techniques, PARAFAC. Anal. Methods, 5: 6557-6566.

Murphy, K.R., Bro, R., Stedmon, C.A. (2014) Chemometric Analysis of Organic Matter Fluorescence. In: Aquatic Organic Matter Fluorescence. Eds: Coble, P.G., Lead, J., Baker, A., Reynolds, D.M., Spencer, R.G.M. Cambridge University Press, pp.339-375.

NOAA Technical Report NOS OR&R 25 (2010): Joint Analysis Group, Deepwater Horizon Oil Spill: Review of Preliminary Data to Examine Subsurface Oil in the Vicinity of MC252, May 19 – June 19, 2010, 168 pp.

Oil Budget Calculator (2010) NOAA Report Oil Budget Calculator: Deepwater Horizon, Federal Interagency Solutions Group, 217 pp.

NRC Report (2005) National Research Council Oil Spill Dispersants: Efficacy and Effects, Washington, DC, 400 pp.

Priaro, M. (2014) A Bitumen and Dilbit Primer. https://www.behance.net/gallery/16654901/A-BITUMEN-AND-DILBIT-PRIMER (accessed June 10, 2016).

Rosin, P., E. Rammler (1933) The Laws Governing the Fineness of Powdered Coal. J. Institute of Fuel, 7, 29-36.

Ryder, A.G. (2005) Analysis of Crude Petroleum Oils Using Fluorescence Spectroscopy. Reviews in Fluorescence 2005 pp. 169-198.

Smilde, A., Bro, R., Geladi, P. (2004) Validation and Diagnostics. In: Multi-way Analysis with Applications in the Chemical Sciences. John Wiley & Sons, Ltd. Pp. 145-173

Stedmon, C.A., S. Markager, R. Bro (2003) Tracing dissolved organic matter in aquatic environments using a new approach to fluorescence spectroscopy. Mar. Chem., 82: 239-54.

Stedmon, C.A., R. Bro (2003) Characterizing dissolved organic matter fluorescence with parallel factor analysis: a tutorial. Limnol. Oceanogr. Methods, 6: 572-579.

Steffens, J., Landulfo, E., Courrol, L.C., Guardani, R. (2011) Application of Fluorescence to the Study of Crude Petroleum. J. Fluoresc. 21:859-864.

Tissot, B.P. and D.H. Welty (1978) Classification of Crude Oils. In: Petroleum Formation and Occurrence. Springer-Verlag, pp. 369-377.

Venosa, A.D., D.W. King, G.A. Sorial (2002a) The Baffled Flask Test for Dispersant Effectiveness: A Round Robin Evaluation of Reproducibility and Repeatability. Spill Science &Technology Bulletin, 7(5-6): 299-308.

Venosa, A.D., K. Lee, M.T. Suidan, S. Garcia-Blanco, S. Cobanli, M. Moteleb, J.R. Haines, G. Tremblay, M. Hazelwood (2002b) Bioremediation and Biorestoration of a Crude Oil-Contaminated Freshwater Wetland on the St. Lawrence River. Bioremediation Journal,6(3):261-281.

Wickley-Olsen, E., Boufadel, M.C., King, T., Li, Z., Lee, K., Venosa, A.D. (2007) Regular and breaking waves in wave tank for dispersion effectiveness testing. In: Proceedings of the 30th Arctic and Marine Oil spill Program (AMOP) Technical Seminar, Edmonton, AB, Canada. Environment Canada, Ottawa, Ontario, Canada, pp. 161–187.

Zepp, R. G., et al. (2004). "Dissolved organic fluorophores in southeastern US coastal waters: correction method for eliminating Rayleigh and Raman scattering peaks in excitation-emission matrices." Marine Chemistry 89(1-4): 15-3.

Zhao, L., et al. (2014). "Evolution of droplets in subsea oil and gas blowouts: Development and validation of the numerical model VDROP-J." Marine Pollution Bulletin 83(1): 58-69.

Zhou, Z, Guo, L., Shiller, A.M., Lohrenz, S.E., Asper, V.L., Osburn, C.L. (2003) Characterization of oil components from the Deepwater Horizon oil spill in the Gulf of Mexico using fluorescence EEM and PARAFAC techniques. Marine Chemistry 148:10-21.

Appendices (Separate Document)

APPENDIX A – Experiment Logs

APPENDIX B – Analytical Chemistry Results

APPENDIX C – Jet Release LISST Oil Droplet Size Distribution Histograms

APPENDIX D – Jet Release LISST Oil Droplet Size Distribution Time Series Contours

APPENDIX E – Submersible Fluorescence Time Series

APPENDIX F – Excitation Emission Matrix Contours

APPENDIX G – VDROP-J and JETLAG Numerical Plume Modeling Report

APPENDIX H – Weber Number Scaling Numerical Plume Modeling Report